This thesis was composed by me and consists entirely of my own work.

January, 1978

PHOTOELECTRIC SPECTROPHOTOMETRY OF EARLY-TYPE STARS

Evangelos Tzanni Kontizas
B.Sc. (GREECE, Athens)

Presented for the Degree of Doctor of Philosophy
at the University of Edinburgh

1978 January

A B S T R A C T

A photoelectric spectrum scanner has been built in Edinburgh University Department of Astronomy by Dr. M.J. Smyth and the author. A feature of the spectrum scanner is the use of a small fraction of the undispersed starlight to provide a reference beam for compensating changes in atmospheric transparency, seeing and guiding errors. Using the ratiometric spectrum scanner Nova Cygni 1975 has been observed (Kontizas, Kontizas & Smyth 1976).

Photoelectric spectra of 72 early type stars have been studied for two purposes: a) to investigate the luminosity effect; and b) to establish a temperature scale for stars from BO to early A spectral type.

The ultraviolet part of the spectra has been observed with a 27-cm ultraviolet telescope which gave low dispersion spectra over the wavelength range 1350 A - 2550 A and a broad band measurement centred at 2740 A. This telescope was installed in the TD-1A satellite (Boksenberg et al. 1973).

The visible part of the spectra has been observed by E. Kontizas using the spectrum scanner mentioned earlier or by K. Nandy using a single channel, low resolution, spectrum scanner.

Real/

Real spectra have been compared with synthetic spectra from the models of Kurucz, Peytremann & Avrett (1974) for the estimation of Teff. The used data cover a wide wavelength range (5556 A - 1350 A) and the models include a very large number of lines (1 760 000 lines) in order to compute a statistical representation of the line opacity in terms of distribution functions.

It has been found that for early B stars the supergiants are cooler than the main sequence stars of the same spectral type but become hotter around B9.

The gravity, multiple systems, non-LTE, convection, rotation, opacity, and line blanketing effects have been considered for their possible influence on the ovserved flux deficiency of B supergiants and giants compared with main sequence stars of the same spectral type.

C O N T E N T S

==========

To the Astronomy Department and the Royal Observatory of Edinburgh staff, for being so helpful.

I INTRODUCTION

During the last few years ultraviolet stellar astronomy has made enormous progress. The various experiments organised to take place in balloons, rockets or satellites provided a large number of high quality data from which new scientific results were reported.

The first major stellar observatory in space, OAO-2, was launched at the beginning of 1973. The ultraviolet observations were made with two objective grating spectrometers, the first for the spectral range ~2000 - 3800 Å and the second from ~1100 - 2000 Å with spectral resolutions of about 20 Å and 10 Å respectively (Code et al. 1970).

The ultraviolet Copernicus satellite (OAO - 3) gave high dispersion spectra and many important scientific results were reported on interstellar matter and O and B stellar spectra. (York 1976).

The Orion-2 Space Observatory aboard the Russian Soyuz-13 provided over a thousand stellar spectra in the region of 2000 - 5000 Å with a resolution of 8 - 28 Å. Ultraviolet spectrograms were also obtained shortward of 3000 Å for faint stars (12 - 13^m). (Gurzadyn 1976).

The Netherlands Astronomical Satellite (ANS) provided ultraviolet photometric data in 5 bands centred at 1550, 1800, 2200, 2500 and 3295 Å with a passband of ~200 Å. Up to October 1975, 16000 observations were performed for the study of 25 various astronomical problems. (Duinen et al. 1976).

Additional results were obtained by the Skylab S183 program, the French satellite AURA, TD-1A, ESRO satellite etc.

The ESRO TD1-A satellite carried in addition to other experiments a 27cm diameter telescope-spectrometer combination which provided over 20 000 spectra with a 35 Å resolution in the wavelength range between 1350 and 2550 Å, and a single channel photometer for broad band measurements (400 Å passband) centred on 2740 Å for 30 000 stars (Boksenberg et al. 1973).

Ultraviolet spectra obtained by TD1-A were available in Edinburgh Observatory, at the beginning of this project. It was therefore considered to combine the ultraviolet data with ground based observations and study the energy distribution of early type stars for a wide spectral range (1350 to 5556 Å).

For the observations in the visible, a two channel photoelectric spectrometer was built in Edinburgh University by Dr. M.J. Smyth and the author.

The type of spectrometer that has to be chosen for a project depends on several factors, some of which are uncontrollable. Technically the instrument must be adequate for its particular purpose, like measurement of bright sources with high resolution or measurement of faint sources with lower resolution, but the final choice of an instrument is restricted to those which can collect enough information in a given time in the most economical way.

The dispersing element and kind of detection determine

the different types of spectrometers.

Prisms were first used as dispersing elements. The absence of overlapping spectral orders and the freedom from "ghosts" made it very useful for the detection of faint spectral lines.

Gratings were used as dispersing elements next. It was found that the spectrometers with a large prism have luminosity-resolution product (LR) far below that of a grating spectrometer of modest size. The consequent overlapping of orders and their inefficiency for large telescopes are the main disadvantages of grating spectrometers.

The Fabry-Perot spectrometer usually consists of two parallel discs of glass or quartz which have the inner faces at a constant distance between them over the whole area to better than 1/100 of the wavelength of visible light. These flat faces are coated with a special material so that most of the light incident upon them is reflected and only a small fraction is transmitted. The transmitted intensity is given by the so-called "Airy Formula"; and by cutting a circular hole in the screen, some wavelengths can be selected for transmission whereas all the others are rejected. These dispersing elements have the disadvantage of having a small spectral range and consequent overlapping of orders. Fabry-Perots are constructed in such a way that they become very useful for the study of extended faint sources.

A way of detection is conventional photography which has the multiplex advantage (all spectral ranges simultaneously), but the low quantum efficiency, low photon storage, low

dynamic range and non-linearity are its main disadvantages.

Another way of detection is photoelectrically. The advantage of this technique is that the response is linear over a large range of intensity and therefore absolute intensities may be derived more easily than from photographic recording.

Electronic imaging devices have been developed recently and have become an efficient way of detection. They combine some of the best features of conventional photography and photoelectric photometry. The electronic imaging devices integrate simultaneously the input information at each point in a two dimensional field of view.

However as in photoelectric photometry, the recorded signal can be linear with respect to the total input photon flux. The most important advantage of electronic imaging devices over conventional photography is due to the very high efficiency with which photoemissive surfaces or photoconductive material emit electrons when irradiated with photons. They can be used with film recording and two primary methods are used to produce the image:
i) electronography in which high-energy electrons from the photocathode cause the blanketing of the grains directly; and ii) the use of a phosphor screen intensifier to convert the electron energy into visible light, which is then recorded on ordinary, light sensitive photographic film.

The electronic imaging devices can also be used with television readout image tubes. These differ from other types of image tubes and conventional photography because their output is an electrical signal, which can be processed

directly to provide quantitative measurements of intensity, spectral distribution etc. whereas film records must be scanned with a densitometer in order to transform the information into quantitative form. An additional advantage of television technique is that of remote readout. But the total information content in a television frame is generally much less than can be obtained in a similar frame using high resolution electronographic techniques (Carruthers 1971; Livingston 1973).

When this project started, there was only one way (to us) available for obtaining stellar spectra, conventional photoelectric spectrometry. But when spectral elements are not observed simultaneously, scintillation becomes an important source of noise. Different researchers have tried to face this problem and they developed specially designed spectrometers.

One way to compensate scintillation is the use of multichannel spectrometers. The idea is to measure the light of a reference beam as well. Guerin (1959) monitored the output of a photomultiplier located behind a slot with that from a second photocell which measures the white light reflected off the quartz-prizm face.

Dobronravin and Nikonov (1955) have used a thin uncoated glass-plate located behind the camera lens to divert a smallportion of the dispersed but unfocused radiation to the monitoring photomultiplier.

Geake and Wilcock (1956) have used a flint glass prism that reflects a portion of the white light into the monitoring photocell.

Tull (Code & Liller 1962) at the University of Michigan used a chopping mirror behind the entrance slot allowing the light to enter the scanner for one third of the time. During the next third of a cycle light passes undispersed via a second optical system onto the cathode of a single photomultiplier. For the last third of the cycle no radiation reaches the photocell. These signals are then fed into an a.c. amplifier which produces the ratio of the intensities of the two signals.

Grainger & Ring (1963) have used a small plane mirror intercepting a small area of the undispersed collimated beam in order to produce a reference beam and provide compensation for scintillation. The current from the main multiplier through an identical channel was fed to a second recorder whereas the other recorder was receiving the signal from the undispersed light.

A two channel spectrometer has been developed by M.J. Smyth and the author in Edinburgh University. The problem of scintillation was faced with a commercial ratiometer, used for the first time in astronomy as far as is known. A glass splitter was used to provide a reference beam of undispersed light. A grating was the dispersion element and the novelty of the scanner is that the two signals from the two photomultipliers (monochromatic and undispersed light) were ratioed by a commercial d.c. ratiometer (Brookdeal) and the output was fed to a pen recorder. Thus the ratio $\frac{A}{B}$ of the two signals was recorded.

Rapid scanners have also been used to avoid scintillation. These scanners have been designed so that each scan of the spectrum takes a short period of time and many such

scans are summed until the desired signal/noise ratio is achieved. By rapid scanning the effects of seeing and variable haze are almost eliminated (Walker 1976; Haupt et al. 1976).

The description and performance of the ratiometric spectrum scanner is given in Chapter II, followed by a brief description of the S2/68 experiment installed in the ESRO - TD 1A satelitte.

The observed stars were chosen on the basis of their spectral type. All of them are O, B and early A spectral type stars that are the main members of the family of early type stars. The early type stars are important astronomical objects and have been studied extensively in recent years. They are relatively few in number and few of them are apparently bright. Their distribution is not uniform and they are mainly detected very close to the galactic plane where interstellar gas and dust are concentrated. In their spectra a few lines are strong and the remainder are very shallow and weak. They are also convenient objects to treat model atmospheres because convection is not important.

The spectra of O and B stars show a large number of metallic lines in the ultraviolet range of the spectrum, that is between the Lyman limit and approximately 2000 Å. In the spectra of A type stars the Balmer lines reach their maximum strength and at the same time the major part of the radiation emerges in the region where these lines overlap and coalesce into the Balmer continuum. A large fraction of the radiation is affected by the presence of these lines.

It has been suggested that all these lines have an influence on the observed luminosity effect.

In chapter III the list of the observed stars is given and in the same chapter the reduction, errors and comparison with other workers are discussed.

The effect of luminosity by comparing the energy distribution of stars with the same spectral type but different luminosity class has been studied and discussed in chapter IV.

Differences between the ultraviolet energy distributions of early type supergiants and dwarfs of the same spectral type has been noted earlier (Carruthers 1969; Weber, Henry & Carruthers 1971; Bless & Savage 1972; Laget 1972).

The appearance of the spectrum in the neighbourhood of the Balmer Jump (D) is used to define spectral type and luminosity class (Chalonge & Divan 1952). The parameter D is a measure of spectral type (temperature in the outer layer of the stellar atmosphere) and its position λ is a measure of the luminosity (pressure in the outer layer of the stellar atmospheres). These two parameters (D, λ) are the basis of two dimensional classification by Barbier and Chalonge.

It has been shown that shortward of the Balmer Jump the fluxes of luminous stars become fainter with decreasing wavelength as compared to the fluxes of the corresponding less luminous stars. This applies to all spectral types from BO to B8.

It has also been found that B-type giants and supergiants show stronger absorption near 1920 Å than the

corresponding main sequence stars. The 1720 Å feature is present only in giants and supergiants and seems to be weaker than the 1920 Å feature. In the visible the observations allow us to suggest that there is no luminosity effect or it is not strong enough compared to that in the ultraviolet part of the spectra.

The magnitude difference (Δw_λ) for pairs of main sequence stars and pairs of supergiant stars has been plotted for different wavelengths. The slopes of the curves for the main sequence pairs are approximately the same as for the corresponding supergiant pairs. In other words the decrements in effective temperature in passing from B1 through B3 and B5 are similar for main sequence and supergiant stars.

The luminosity effect is described and discussed in chapter IV. It is examined how gravity, multiplicity, departures from LTE, convection, rotation, opacity and blanketing could influence the continuum and how the observed deficiencies for early type supergiants and giants in their fluxes with respect to main sequence stars could be caused by one or a combination of these effects.

In chapter V, a temperature scale for early type stars in the spectral range from O9 to A3 has been established from comparison of the observed stellar spectra with theoretical spectra. The ATLAS computer program (Kurucz 1970) has been used to provide the necessary synthetic spectra (Kurucz,Peytremann & Avrett 1974, and Kurucz 1976, private communication). The models used here range in temperature from 5500K to 50 000K and in log g

from 0.5 to 5. The line opacity was included in the form of distribution functions based on a list of 1 700 000 lines. No models have been used so far with such an enormous list of lines for the treatment of blanketing. Solar abundances and microturbulent velocity of 2 km/sec have been assumed.

The synthetic spectra have been superimposed on the observed spectra, corrected for the interstellar extinction, in order to derive the temperature scale.

For the very hot stars the visible portion of the spectrum lies on the long wavelength side of the Planck maximum and so the relative energy distribution is essentially independent of effective temperature. The derived temperatures for O type stars are much lower than expected for their spectral type (Stecher 1970; Boksenberg et al. 1973).

For B and A stars effective temperatures were found to be in very good agreement with previous workers (Hanbury Brown et al. 1967; Morton et al. 1968; Hyland 1969; Henize 1969; Schild et al. 1971; Nandy et al. 1975; Code et al. 1976; Lesh 1976).

Finally it has been found that supergiants are cooler than the main sequence stars of the same spectral type and become hotter near B9.

II INSTRUMENTS

II 1. PHOTOELECTRIC SPECTRUM SCANNER

a) Description and specifications.

When spectral elements are not observed simultaneously scintillation becomes an important source of noise. For this reason astronomical spectrometers must be provided with some means of compensating such variations. A technique applied for elimination of source variations is the use of compensating spectrometers and the idea is to measure the light of a reference beam (Dobronravin et al. 1955; Geake et al. 1956; Guerin et al.1959; Meinel et al. 1959;Grainger et al.1963).

The spectrum scanner described here is a two channel photoelectric spectrometer developed in Edinburgh University (Smyth & Kontizas). For the elimination of stellar scintillation, changes in atmospheric transparency and guiding errors, a commercial d.c. ratiometer (by Brookdeal) was used for the first time in astronomy and gave very good results as is shown below.

The main part of the scanner is a "SPEX" Minimate monochromator with a digital read-out wavelength in nm. A glass splitter was used to provide a reference beam of undispersed light. The dispersing element (grating) rotates with a synchronous motor-drive in order to provide successive monochromatic light beams for channel A (Fig. 1). The motor has interchangeable gears to provide speeds of 125, 250, 500, 1000, 2000, 4000 Å/min. The two available

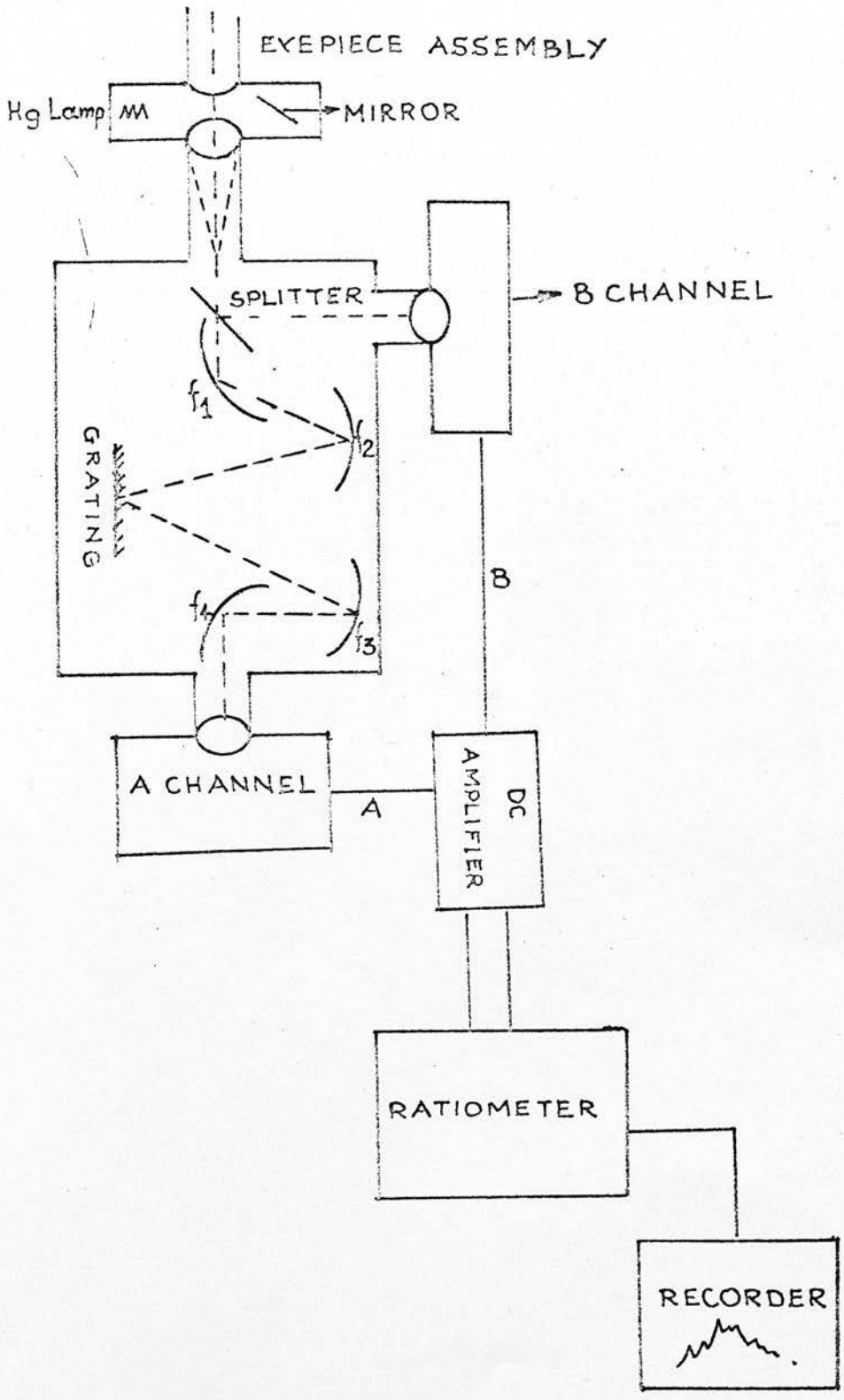

Fig. 1. Schematic diagram of the photoelectric spectrum scanner.

gratings (1200, 600 grooves/mm) are blazed at 5000 Å and 10 000 Å respectively.

The two signals, main beam (A) and reference beam (B) through two identical d.c. amplifiers are led to the ratiometer that produces their ratio R = A/B in a pen recorder.

R is equal to:

$$R = \frac{\int_{\lambda_1}^{\lambda_2} S_\lambda I_\lambda d\lambda}{\int_{c}^{d} S_\lambda' I_\lambda d\lambda}$$

where S_λ, S_λ' are the sensitivities of the A and B channel respectively, $(\lambda_2 - \lambda_1)$ is equal to the resolution of the scanner and (d-c) are the limits of the wavelength range response of the B photomultiplier.

The interior of the "SPEX" Minimate monochromator, the spectrum scanner on the Newall refractor and the electronics used are shown on Figs. 2, 3 and 4.

The main channel tube (which receives the monochromatic beam) is an EMI photomultiplier type 9558B with a 44 mm cathode and 11 venetian blind dynodes having stable secondary emitting surfaces. The cathode is of S-20 (trialkali) type which provides very high quantum efficiency in the blue as well as extremely good response in the red extending out to approximately 8500 Å. The wide range response, its very low dark current and a gain of 2×10^6 make this photomultiplier very useful. This type can be cooled to -180°C but thermionic emission can be reduced to negligible proportions at -40°C. The normalized response curve of this photomultiplier is illustrated in

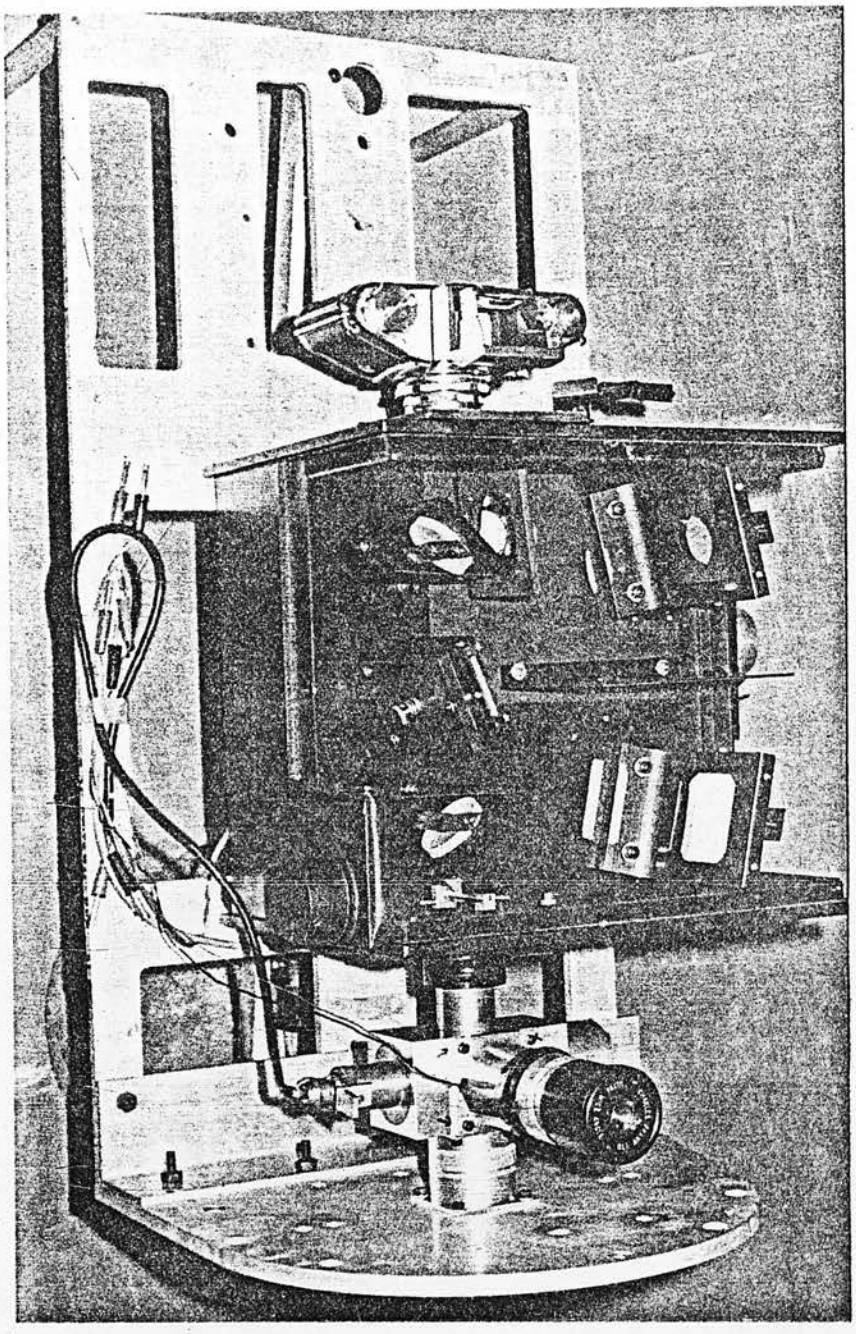

Fig. 2 The interior of the "SPEX" Minimate monochromator.

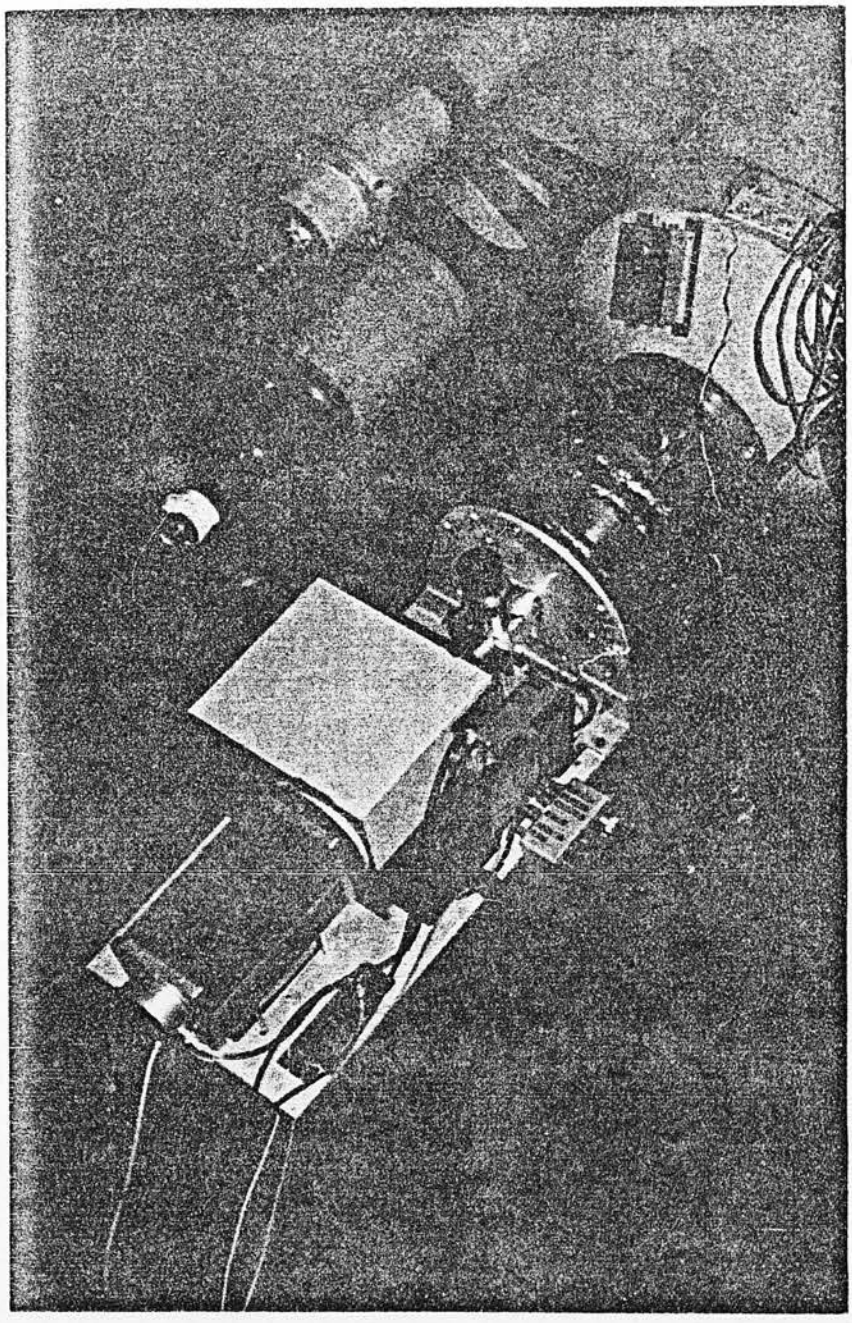

Fig. 3. The spectrum scanner on the Newall refractor.

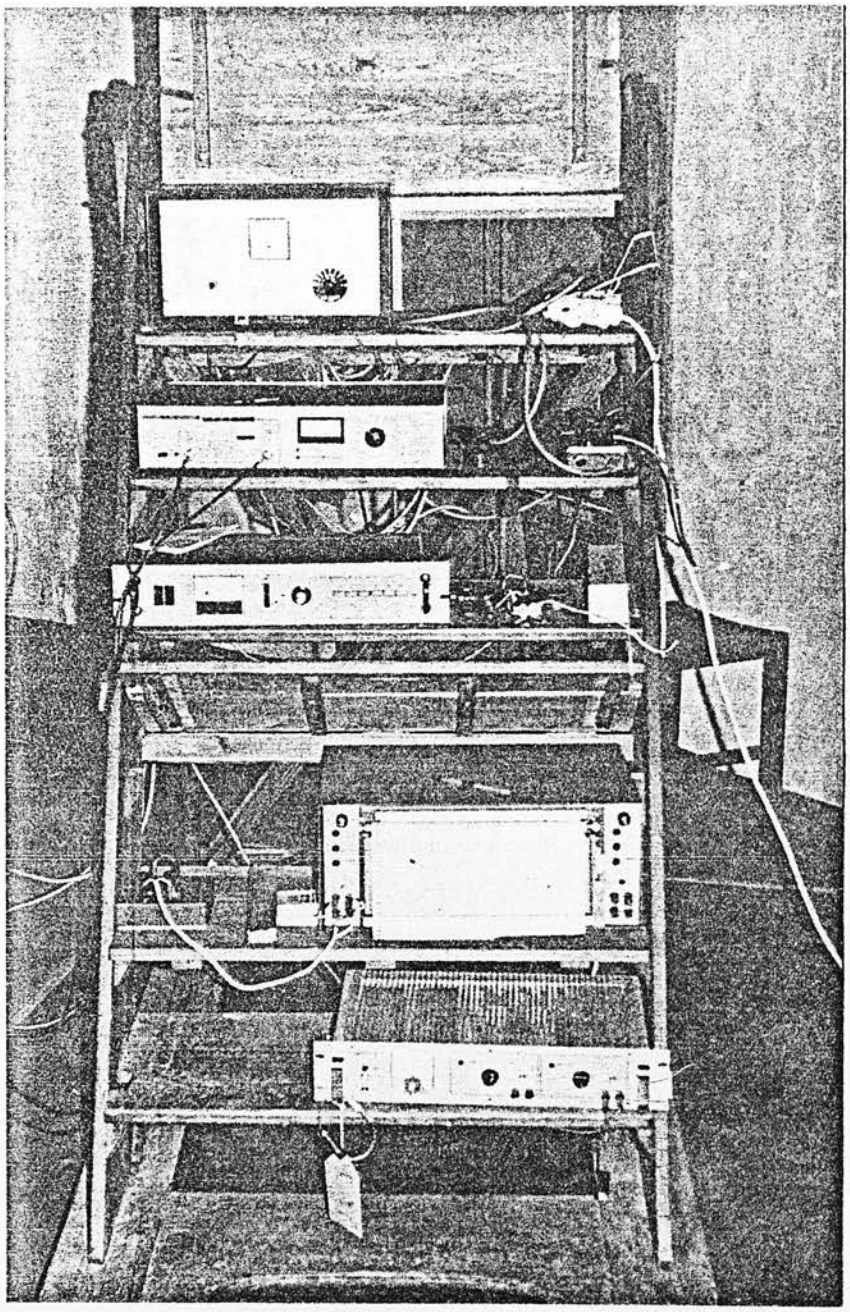

Fig. 4. The electronics used with the spectrum scanner.

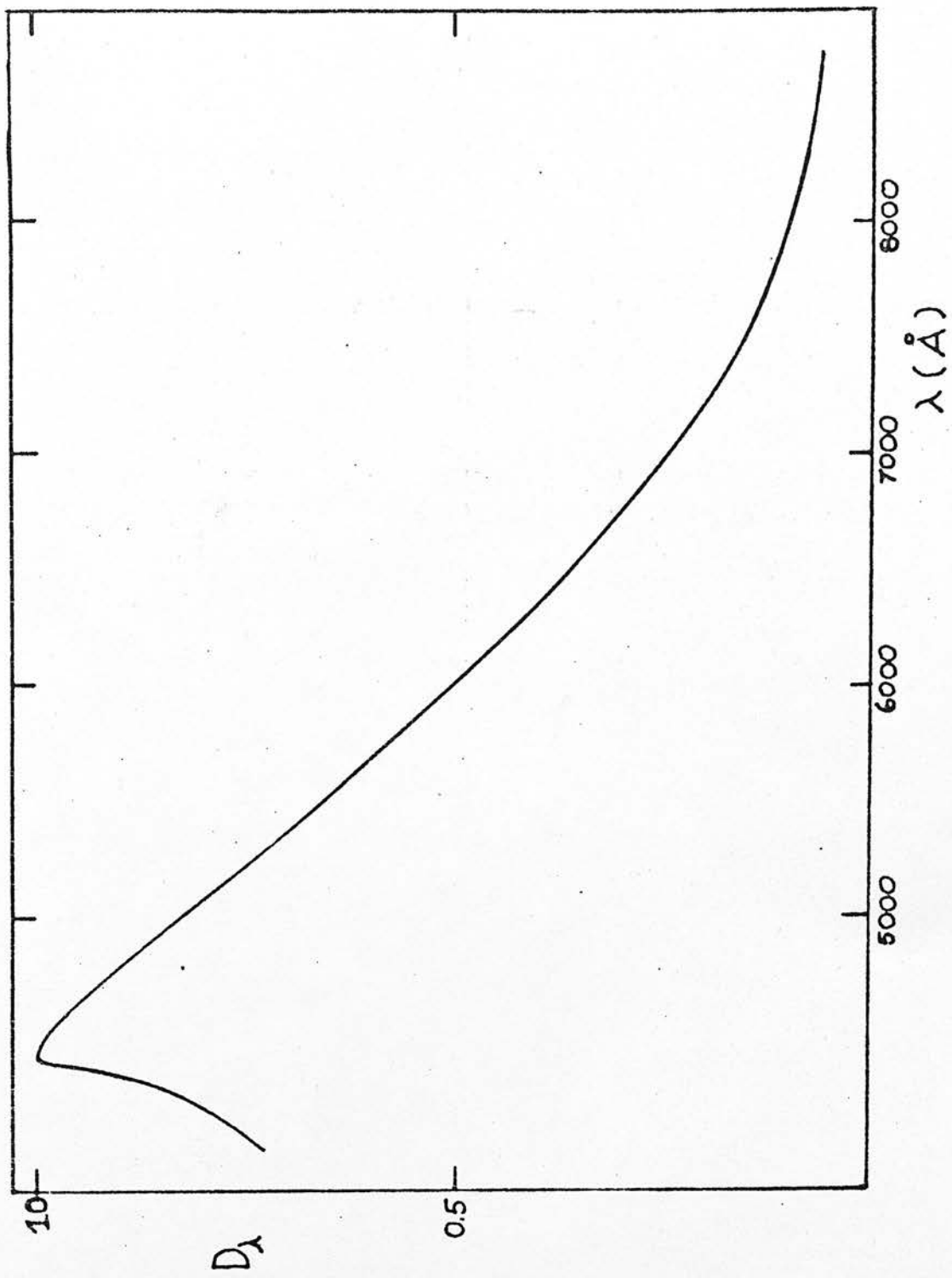

Fig. 5. Normalized Response of the 9558 EMI photomultiplier for the wavelength range 4000 A to 8500 A.

Fig. 5, showing that it is very useful for the wavelength range 4000 Å to 8500 Å.

The undispersed light goes to an EMI 9781 A photomultiplier with S.5 response. Its dark current reaches ~0.1 nA at dome temperature. The normalised response of this photomultiplier is illustrated in Fig. 6 and it extends from 4000 Å to 6000 Å.

The main photomultiplier is cooled by a temperature regulated chamber (by Products for Research Inc., TE-104 TS) that has been designed to cover completely the tube during its operation. This unique design is arranged to allow quick interchange of tubes in a few minutes.

Operation is completely automatic. A mu-metal shield, operating at cathode potential, provides the optimum in electrostatic/magnetic shielding for the tube while the hermetically closed inner chamber prevents the tube or chamber from becoming frosted. There is a double plane insulating window which remains completely dew free and ensures a clear light signal path to the photocathode at all times.

The thermoelectric heat exchanger is cooled very easily using tap water. Table 1 gives the measured cooling speed of the main photomultiplier and the dark current at each temperature.

TABLE 1

Time (min)	Temperature (°C)	Dark curr (nA)
0	+ 20	3.200
20	+ 00	0.180
35	- 10	0.050
60	- 16	0.025
100	- 20	0.020

The Brookdeal 9547 ratiometer which receives the signal from the two photomultipliers gives ratiometric measurements; it compensates the source fluctuations automatically; and it can be used also as an automatic gain control d.c. amplifier. A front panel meter indicates either the output voltage or % ratio. Offset voltages in the source may be measured and suppressed by the front panel control. When the ratiometer is used as a low frequency d.c. amplifier it gives gains of 10 or 100.

The two photomultipliers deliver their signals (from now on called A and B channels for the main and the compensating one respectively) to the ratiometer with the following input levels as given by Brookdeal:

High ratio mode	A : $\pm$ 10V	B : 0.1V to 10V
Low ratio mode	A : $\pm$ 1V	B : 0.01 to 1V

The linearity of the A channel is 0.05% and the output ratio (A/B) is $\pm$ 10V for $\pm$ 100%. By a rear panel switch the instrument can alternatively give $\frac{A - |B|}{B}$

The use of a small fraction of light abstracted behind

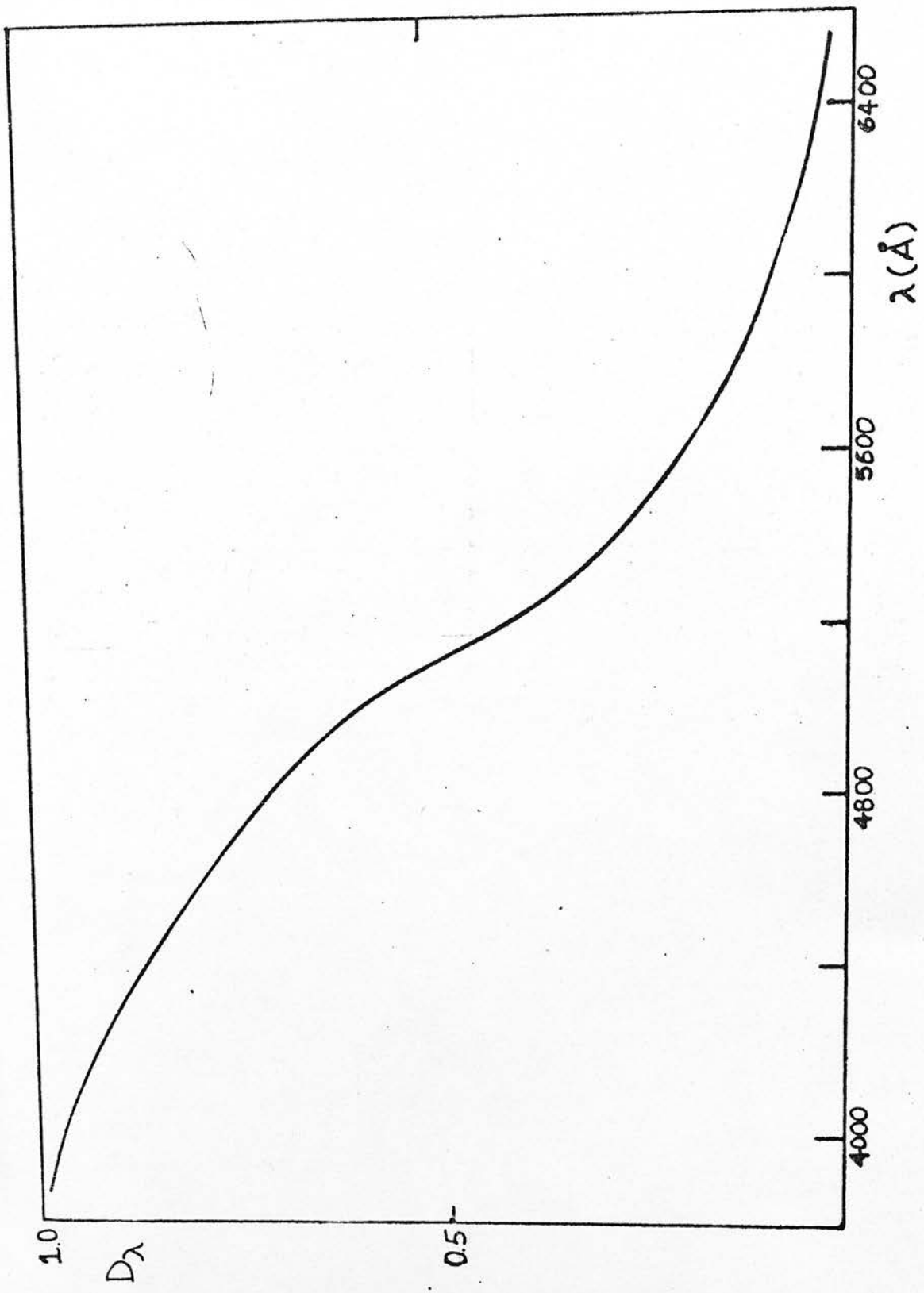

Fig. 6. Normalized Response of the 9781A EMI photomultiplier for the wavelength range 4000 Å to 6500 Å.

the entrance slit, to provide a reference beam, lowers the faint limit of star magnitudes which can be observed with the scanner. So a d.c. amplifier has been made at Edinburgh University (Smyth & Kontizas 1978) in order to increase the efficiency of the scanner. This amplifier consists actually of two identical d.c. amplifiers (their schematic diagram is illustrated in Fig. 7) to receive the signals from the two photomultipliers. The properties desired for a good amplifier are the following: 1) very stable gain 2) low output drift after warm-up 3) low noise 4) stable calibration 5) wide range of gain 6) variety of output time constants and 7) short warm-up time.

Each amplifier has a stable gain of 10^8 V/Amp. The integration circuit used is a FET-OPA and some of its operational data given by the manufacturer are: the max input voltage (either input) with respect to zero reference level 15V, the operating temperature range 0° - 70°C, the output short-circuit duration indefinite, and the minimum load 1kΩ.

The limiting magnitude that can be observed without this d.c. amplifier is 5.0 - 6.0 mag. using the 0.5m reflector of Edinburgh University and this can be improved up to 9 mag. interconnecting the d.c. amplifier between the output of the photomultipliers and the input of the ratiometer. This proves the usefulness of the new amplifier.

In Table 2, the A output and B output of the d.c. amplifier for a given input are listed and were tested by Smyth and Kontizas. It is obvious that there is not

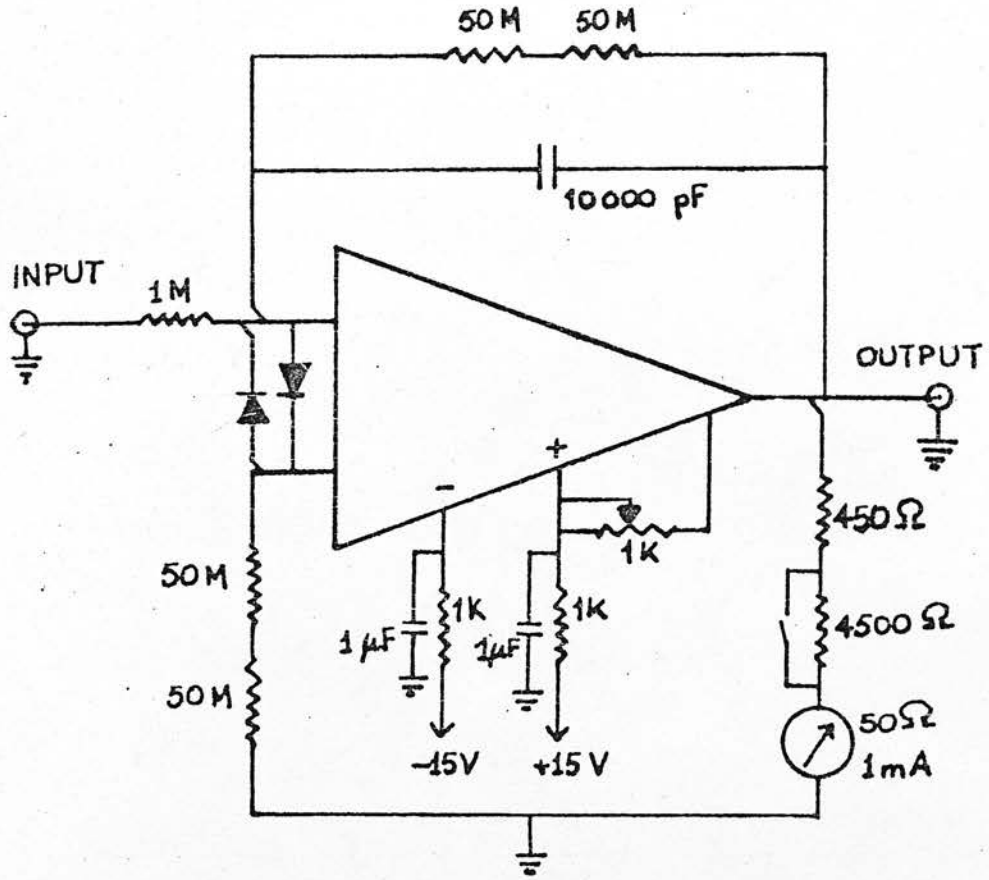

Fig. 7. The schematic circuit diagram of the dc amplifier.

TABLE 2

V_{in} (Volt)	A_{out} (Volt)	B_{out} (Volt)
- 5.00	+ 5.06	+ 4.96
- 4.00	+ 4.05	+ 3.97
- 3.00	+ 3.03	+ 2.98
- 2.00	+ 2.03	+ 2.00
- 1.00	+ 1.01	+ 1.00
- 0.50	+ 0.51	+ 0.50
- 0.00	+ 0.00	+ 0.00

The described spectrometer is a low dispersion ~ 36 Å/mm (grating 1200 grooves/mm) and its spectral resolution for the different exit apertures is given in table 3.

TABLE 3

RESOLUTION

slit	grating 1200 grooves/mm	grating 600 grooves/mm
0.25 mm	9 Å	18 Å
0.50 mm	18 Å	36 Å
1.25 mm	45 Å	90 Å
2.50 mm	90 Å	180 Å
5.00 mm	180 Å	360 Å

A typical set of parameters using the 1200 grooves/mm grating are

Entrance slit: 1.25 mm
Integration time: 0.24 sec/Å
Chart speed: 30 mm/min
Time constant: 1 sec

For faint stars a time constant of 2 sec has been used to smooth the noise.

any significant change of the ratio A/B using the d.c. amplifier. The spectral purity (resolved spectral element) is

$$\Delta_\lambda = \cos\alpha \frac{Wd}{f_{coll} n}$$

where W is the width of the entrance slit, α is the incidence angle, f_{coll} is the focal length of the collimator, d is the ruling spacing of the grating, and n the order of the spectrum. This is an important relation because it ties together the grating parameters d and n with the scanner parameters W and f_{coll}. For $\cos\alpha = 1$, $n = 1$, the spectral purity of the prescribed scanner is 46 Å.

A very simple way of describing the overall performance of a detection system is to give the noise equivalent quantum efficiency. If the detection system yields a signal with 'noise' (standard deviation of the unwanted fluctuations of the signal), and with signal/noise ratio R, then this is equivalent to the ideal detection of R^2 photons, and if the number of photons actually received during the measurement is N, the noise-equivalent quantum efficiency is $\varepsilon = R^2/N$. For this scanner it has been estimated that ε is $\sim 8.10^{-2}$ at $\lambda = 5550$ Å.

Measurements of the instrumental profile tell us how much degradation occurs and allow the reconstruction of the original spectrum prior to distortion. Suppose we have a light source giving an infinitely narrow spectral emission line and such a line can be denoted by $\delta(\lambda - \lambda_o)$. The measured spectrum with an instrument for $\delta(\lambda - \lambda_o)$ source is the instrumental profile (also called

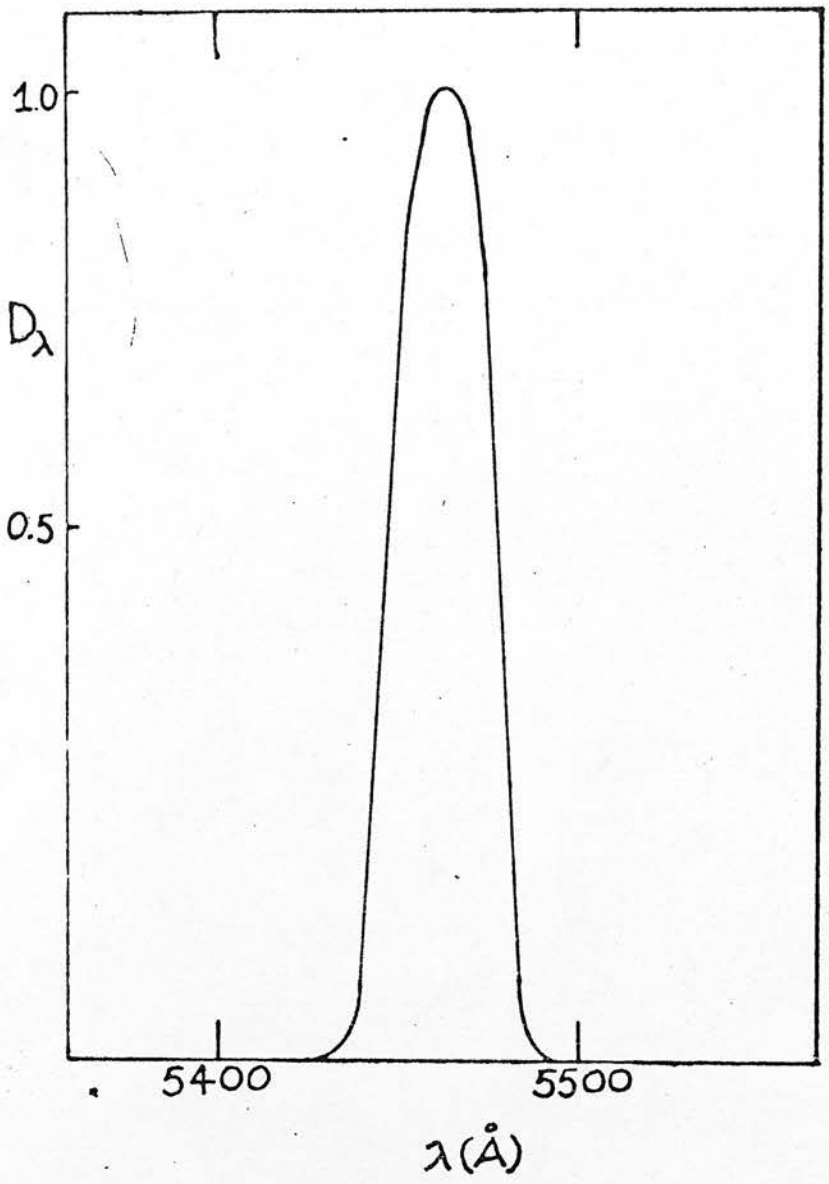

Fig. 8. Instrumental profile of the scanner working as a two-channel photometer for the Hg emission line λ=5461 Å (normalized to unit peak height). Exit slit 0.25 mm.

the delta function response). The instrumental profile of the scanner working as a two channel photometer, for the Hg emission line λ = 5461 Å is shown in Fig. 8. The half width at half height of this profile is $\sim$15.6 Å (normalized to unit peak height), with exit slit 0.25 mm.

b) Scientific mission and performance.

The described spectrum scanner can be used for narrow band photometry pass-band up to 360 Å or wide band spectrophotometry up to 9 Å spectral resolution as a single or two-channel spectrometer for the spectral range 3500 Å to 8000 Å (using a GC495(V) filter for λ>6500 Å to cut the second order blue spectrum). This scanner provides information about the stellar continuum and spectral lines. As a by-product, flux variation, atmospheric extinction, interstellar extinction, slope of the continuum, Balmer Jump, chemical abundances, and much other information about the stellar structure can be studied. The ratiometer arrangement has proved its value (Smyth & Kontizas 1978, in preparation) on nights of doubtful transparency and on a telescope with poor guiding facilities. It does not compensate for errors due to atmospheric dispersion, but such errors are insignificant at low resolution and small zenith distances. It has the advantage that, since the monochromatic beam of each scan is ratioed to a non-dispersed light beam which is in effect a broadband measurement of the starlight, the ratio of the spectra of two stars may be obtained provided only that their broadband magnitudes are known. Thus, if the spectral energy distribution of one star is known in absolute units, that of the second is immediately obtained.

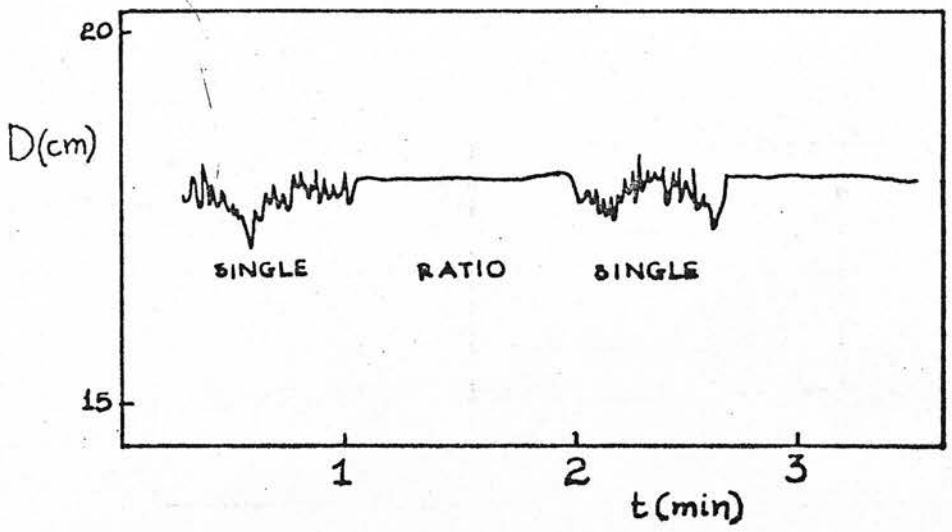

Fig. 9. Tracing taken with the spectrum scanner working as a single and as a two-channel photometer to show the effect of ratiometer in reducing scintillation and changes in sky transparency. Observed star λPer at λ= 4000 Å. Used time constant 0.5 sec.

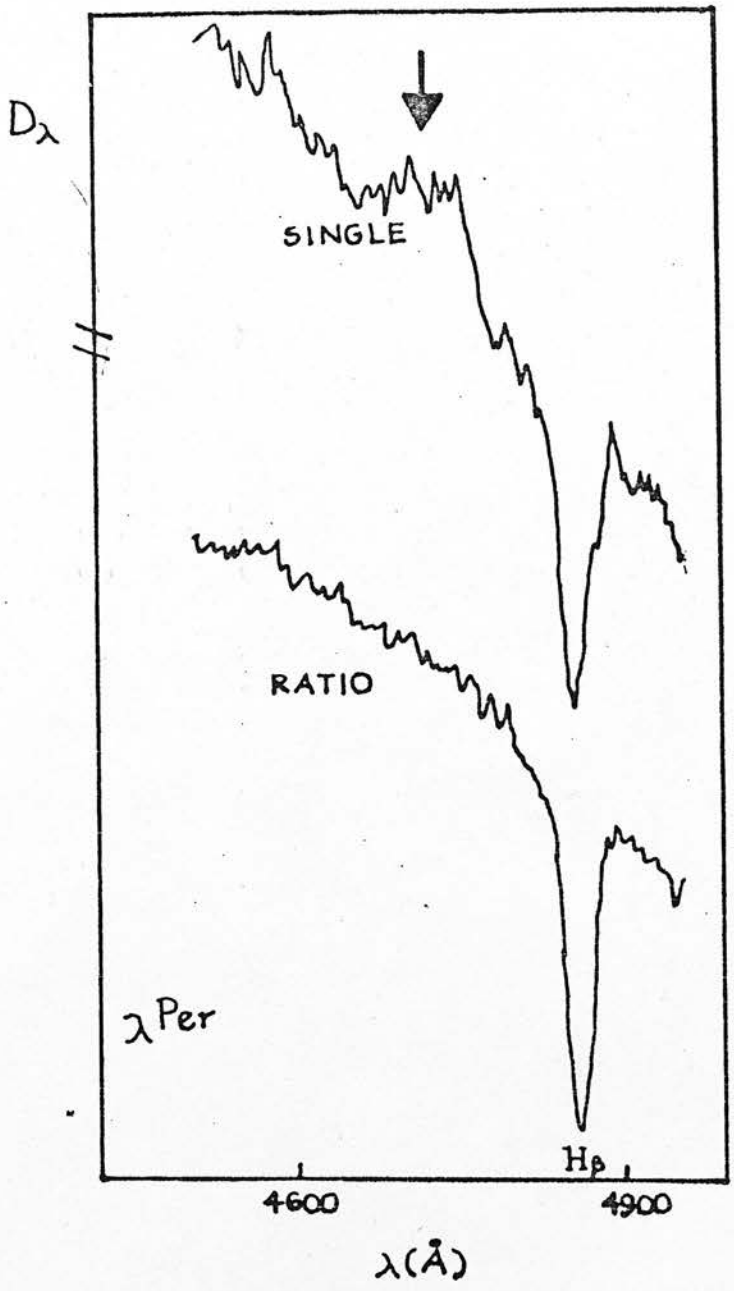

Fig. 10. The spectrum of λ Per (B9V) observed with the scanner working as a single-channel and two-channel spectrometer. Dλ deflection in an arbitrary linear scale with different zero points. The arrow indicates the distortion of the spectrum from atmospheric disturbances when the scanner is used as a single-channel spectrometer.

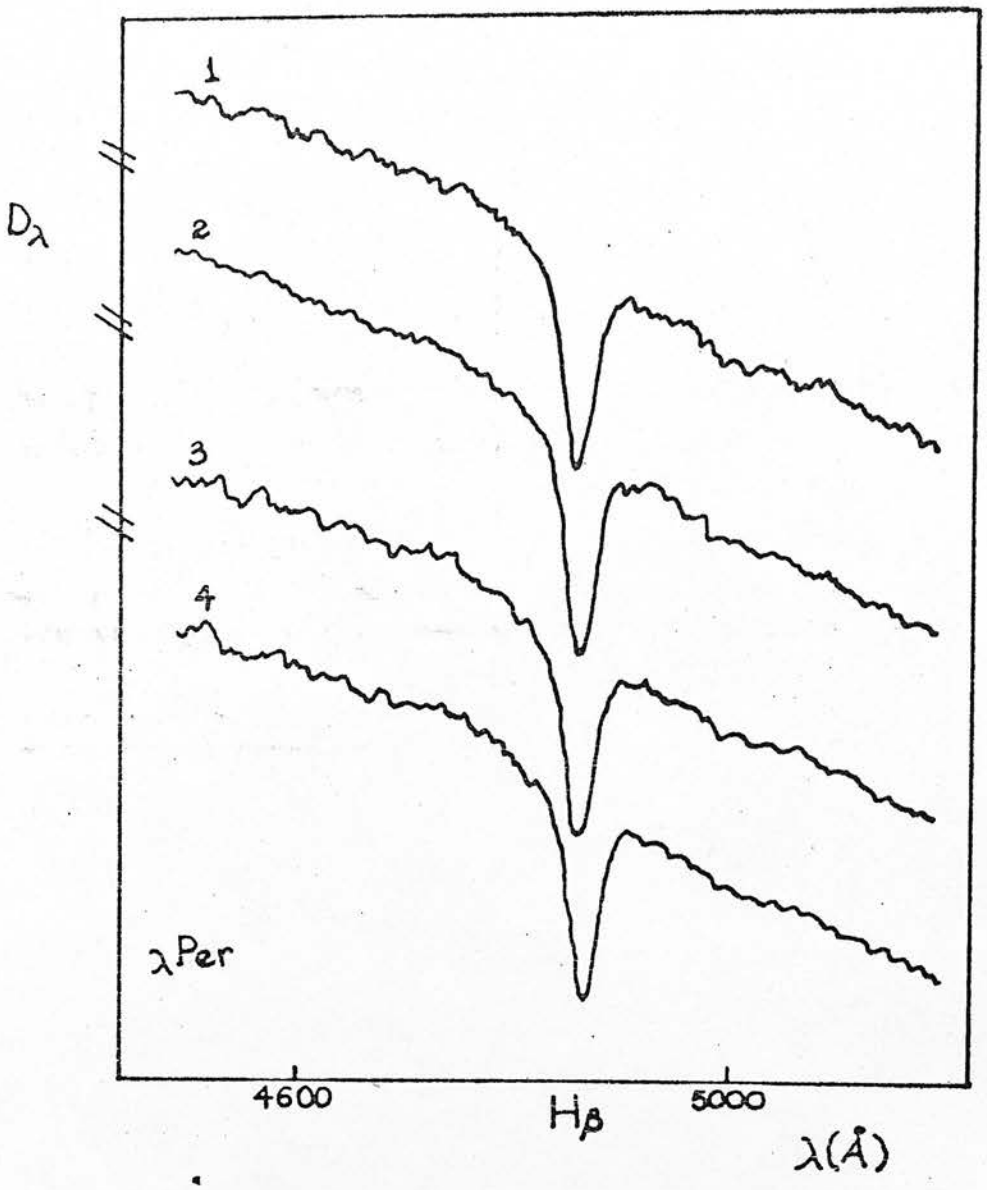

Fig. 11. H_β line profile of the λPer (B9V) observed with the scanner (two-channel photometer) on the same night. The two channels were used to show the output stability of the scanner. Resolution ~18 Å. D_λ deflection in arbitrary linear scale with different zero points for the cases 1, 2, 3, 4.

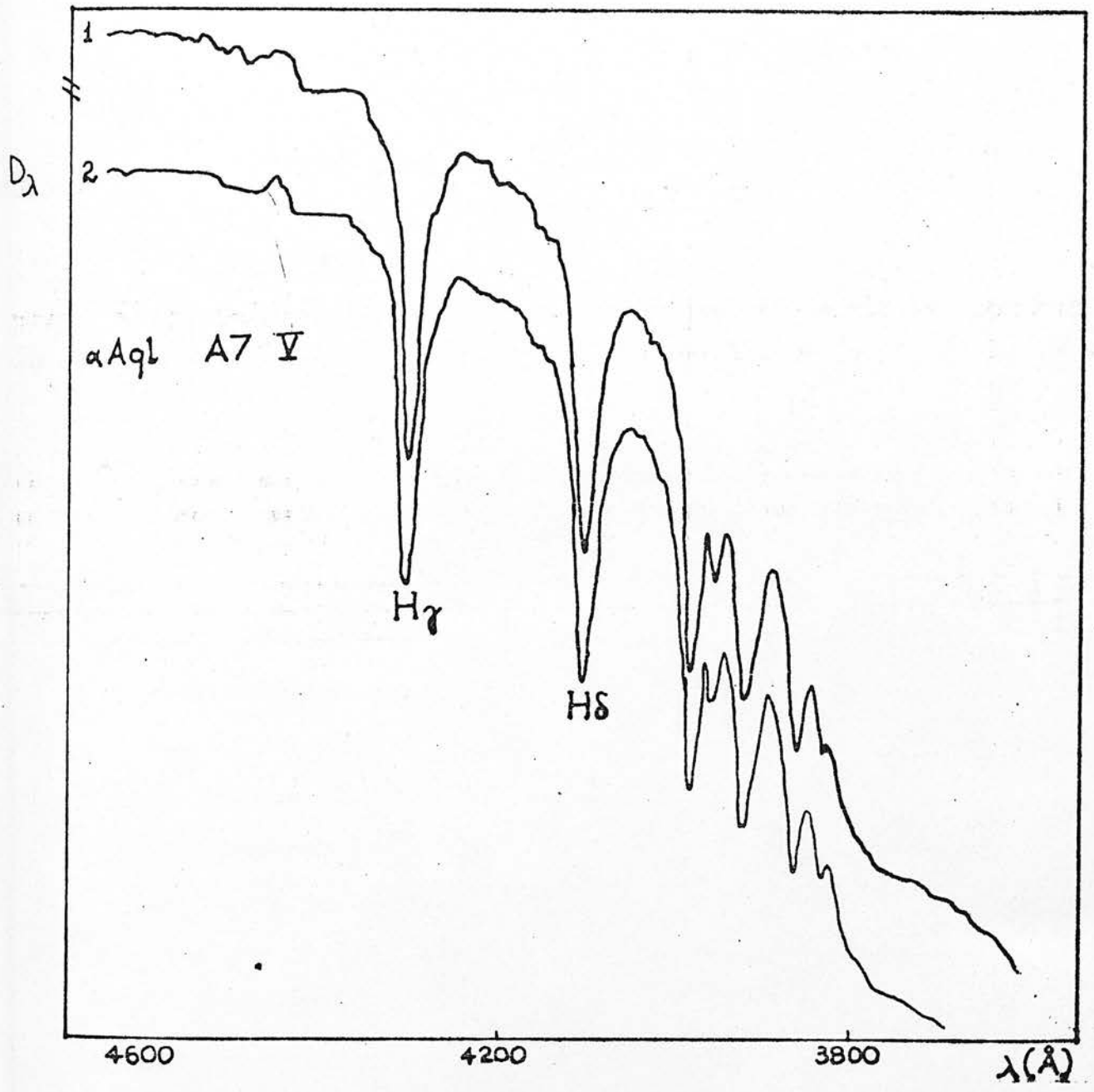

Fig. 12. Spectra of αAql (A7V) observed with the scanner (two-channel photometer) on different nights and therefore in different atmospheric conditions to show the consistency of the ratioed measurements. The deflection D_λ is in an arbitrary linear scale and with different zero points for the cases 1 and 2.

The performance of the scanner has been proved using spectra taken with it. The distortion due to noise and seeing can be minimised with the use of the ratiometer. This is shown in Figs 9 and 10. Fig 9 illustrates tracings taken with the scanner working either as a single-channel or as a two-channel photometer. The decrease in scintillation noise is obvious when the ratiometer is introduced. Another example is illustrated in Fig. 10 where the spectrum of λ Per (B9V) was taken by the scanner working as a single-channel and a two-channel photometer respectively. The arrow indicates the distortion of the spectrum by atmospheric disturbances when the scanner is used as a single-channel photometer (resolution $\sim$18 Å). The stability of the scanner is illustrated in Fig. 11, where the H_β line profile of the λ Per (B9V) is taken at different times on the same night (resolution $\sim$18 Å). The consistency of the ratioed measurements can be shown in Fig. 12 which illustrates spectra of αAql (A7V) observed on different nights and therefore in different atmospheric conditions. The spectrometer has proved its good performance during the appearance of Nova Cygni 1975, when ratiometric photoelectric spectra of the Nova were taken on 1975 August 31 and September 2,3. αLyr was used as a reference star and its absolute spectral energy distribution was used to reduce the spectrophotometry of the Nova to absolute units. On the first night, close to maximum light, the spectrum is relatively featureless, showing broad, weak Balmer lines in emission with violet-shifted absorption

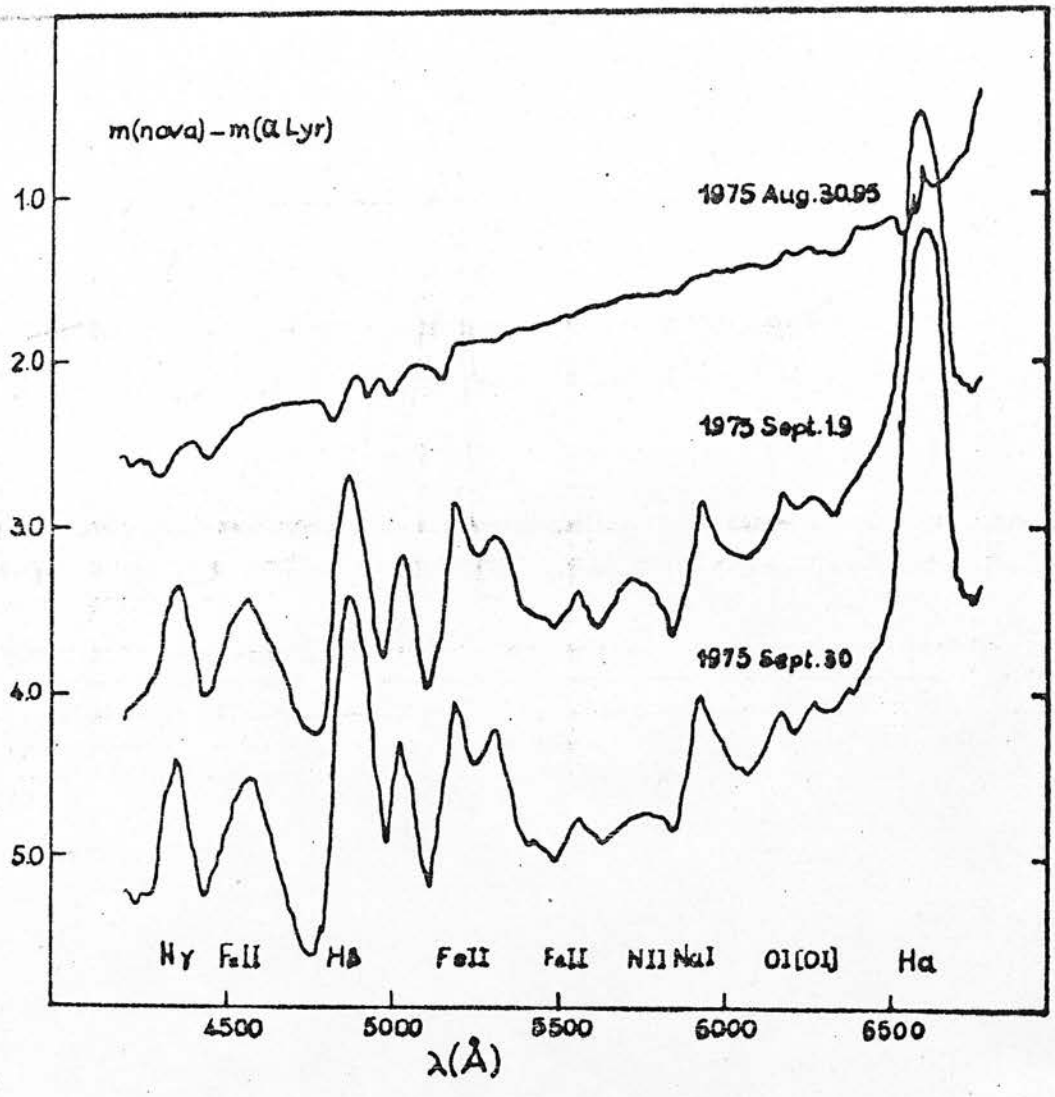

Fig. 13. Spectra of Nova Cygni 1975, relative to the smoothed continuum of a Lyr, on three nights.

components, the characteristic P Cygni profiles. On the two later nights the continuum is progressively weaker, but Hα, Hβ, Hγ and the NaI D-lines show strong P Cygni profiles, and broad blended lines of FeII and [OI] appear. These are illustrated in Fig. 13. Emission strengths of Hα, Hβ, Hγ (in Wcm^{-2}) were compared with theory, and found to deviate less than had been reported for an earlier Nova (Kontizas, Kontizas & Smyth 1976).

c) Operational instructions.

Before starting observations with the scanner it is wise to check the optical alignment. When wide entrance and exit holes are used, small vertical misalignment is not very important.

The wavelength scale is affected by lateral misalignment, which can be eliminated by calibrating the wavelength scale with a standard source every night.

In the eyepiece assembly there is a 45^{o} viewing mirror which reflects the light of the star into the square of the crosswires. This also needs checking for alignment but not very often.

The light beam partially reflected by the microcover glass behind the entrance hole must fall into the reference photomultiplier, whereas the transmitted beam analysed by the grating should be focused on the main photomultiplier. These two alignments are very important.

The "Spex" Minimate monochromator is not light-tight so the setting up has to be in the dome illuminated as little as possible. The polarity of high voltage power

supply must be negative (-). It is advised not to start the observations before the temperature of the main photomultiplier into the refrigerated chamber goes down to $\sim -15^{o}$.

The sky background is compensated in the initial setting-up by setting on sky near the program star and then zeroing the output for each channel independently isolating one at a time. If it is not possible to zero both channels, then either the dark current is very high or the sky background is abnormally high. In that case the scanner cannot be used as a two channel spectrometer. After eliminating the dark current and sky background the star is moved into the crosswire square allowing the light to reach the two photomultipliers. At first, the High Input button is pressed and if the B LOW indicator lights then clouds are passing or the star is too faint. The latter may be corrected by pressing the LOW Input button, but if the B LOW indicator is still on, the star cannot be observed. The B overload indicator shows that the star is too bright ($B < 1^{m}.5$) and it is necessary to reduce the photomultiplier voltage, or to insert a neutral filter.

If the scanner cannot be used in the ratio mode it is possible to be used in single channel mode by pressing DC AMPLIFIER (A x 10) or possibly DC AMPLIFIER A x 100 for faint stars.

For $\lambda > 6500$ Å the second order spectrum appears when the 1200 l/mm grating is used. Therefore a GG495 filter (V filter) available is inserted in order to extend the

wavelength range towards the red end. The interchangeable 600 l/mm grating halves the dispersion. It is blazed for 1000mm and so is more efficient for the red area and less affected by second order.

Although no drift has been noticed of the wavelength scale there is a Hg lamp in the eyepiece assembly which permits us to check the wavelength scale, using Hg lines. The schematic circuit diagram for the mercury lamp is used for the wavelength calibration is shown in Fig. 14.

Since the output from both channels includes a component from the sky any reasonable change in the sky background produces an error that is smaller than the error introduced when the scanner is working as a single channel photometer.

If in a single channel photometer S(star), B(background), D(dark current) are pulses per second then exposure of $\frac{1}{2}t$ seconds on star+sky gives signal $\frac{1}{2}$ (S + B + D)t and the r.m.s. noise is $\left\{\frac{1}{2}\text{ (S + B + D)t}\right\}^{\frac{1}{2}}$. Exposure of $\frac{1}{2}t$ seconds on sky gives signal $\frac{1}{2}$ (B + D)t and r.m.s. noise $\left\{\frac{1}{2}\text{ (B + D)t}\right\}^{\frac{1}{2}}$. Thus difference signal $\frac{1}{2}St$ gives r.m.s. noise $\frac{1}{2}\text{ (S + 2B + 2D)t}^{\frac{1}{2}} = \sigma$ (Smyth 1973).

In the case of the described spectrum scanner it has been assumed the detected photons are integrated with equal statistical weights (W = 1) and S_A, B_A, D_A, S_B, B_B, D_B are the signals from the star, background and dark current for channels A and B respectively. For these two channels the difference signals S_A and S_B give r.m.s. noise

$$\sigma_R = \frac{\sigma_A}{S_A} + \frac{\sigma_B}{S_B}$$

where σ_B is smaller or of the same order of σ_A, $S_B \gg S_A$, and so for stars $V \leq 7.5$ (observed for this project) $\sigma_A \ll S_A$ so $\sigma_R < \sigma_A$.

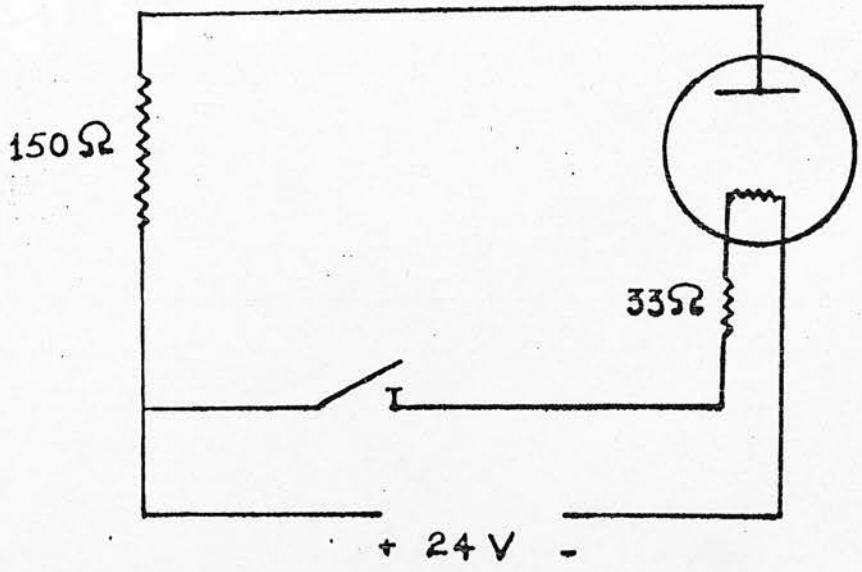

Fig. 14. Schematic circuit diagram of the Hg lamp for the wavelength calibration.

II 2 THE ULTRAVIOLET SKY SURVEY TELESCOPE IN THE TD-1A SATELLITE

The S2/68 Experiment originated from a proposal by Dr. H.E. Butler at the Royal Observatory Edinburgh (ROE) in 1961. The satellite was launched from Western Test Range California at 01 55hr G.M.T. 1972 March 12 and it is described by Boksenberg et al. (1973). The orbit of TD-1A is approximately circular in shape, of 550 km height and period 95.5min, and inclined at $97^{\circ}.55$ to the Earth's equator, to produce a precession of $360^{\circ}yr^{-1}$.

The satellite was stabilised in three axes; one of them points to the centre of the Sun and the perpendicular axes roll about the Earth-Sun line once each orbit. The optical axis of the telescope was aligned to one of the three axes with the direction of view pointing away from the Earth. As a consequence of the Earth's motion around the Sun, the celestial sphere was scanned along ecliptic meridians, each displaced by 4 arc min; and complete sky coverage was achieved in 6 months.

It carried in addition to other experiments, a 27cm ultraviolet telescope which gave low dispersion spectra over the wavelength range 1350-2550 Å and a broad band measurement centred at 2740 Å.

The instrument calibrations were carried out at the Royal Observatory Edinburgh and the Institute of Astrophysics of Liège, independently.

III OBSERVATIONS

III 1. OBSERVED STARS

A temperature scale for early type stars has been derived and the luminosity effect has been studied from spectra in the visible and ultraviolet for stars which are listed in Table 4. 36 stars were observed by Nandy with a low resolution single channel photoelectric spectrum scanner attached to the 100cm. Cassegrain reflector at Kavalur Observatory of India Institute of Astrophysics on 2/3, 3/4, 6/7, 8/9, 9/10, 10/11 of February 1975. 21 stars were observed by the author with the two channel spectrum scanner (Smyth & Kontizas, 1978) attached to the 64cm. (Newall 1896) refractor at the Penteli station near Athens on 1975 August 26 - 29 and to the 120cm. reflector at Kryonerion Observatory (Contopoulos et al. 1976) Greece on 1976 July 26 - 29. Ultraviolet data were kindly provided by the Edinburgh TD-1 team, at the beginning of this project and have now been published (Jamar et al. 1976).

In Table 4 all the stars observed in the visible and ultraviolet are listed. Column 1 gives the running number, column 2 gives the HD number of the stars and column 3 their names. In columns 4,5 and 6, the visual magnitudes, the B-V colour indices and the spectral types of the stars are given. Finally the last column refers to the sources from where the data were taken. (N refers to Nandy's observations, K to Kontizas' observations).

The observed stars were chosen to have spectral type O, B and early A.

TABLE 4

OBSERVED STARS

	H.D	Name	V	B-V	Sp.Type	Remar
1	886	γ Peg	2.83	-0.23	B2IV	K - P
2	3360	ζ Cas	3.61	-0.20	B2V	K - P
3	15318	ξ^2Cet	4.27	-0.05	B9III	N - I
4	18326	-	7.28	+0.38	08V	N - I
5	23180	σ Per	3.82	+0.06	B1III	K - KR
6	24398	ζ Per	2.83	+0.13	B1Ib	K - KR
7	24431	-	6.72	+0.37	09V	N - I
8	24760	ε Per	2.88	-0.17	B0.5V	N - I
9	30614	α Cam	4.38	+0.02	09.5Ia	N - I
10	31327	-	6.06	+0.41	B2Ia	N - I
11	32249	ψ Eri	4.80	-0.20	B2V	N - I
12	33988	-	6.88	+0.25	B2V	N - I
13	34085	β Ori	0.08	-0.03	B8Ia	N - I
14	35468	γ Ori	1.63	-0.23	B2III	N - I
15	36371	χ Aur	4.75	+0.30	B5Ia	N - I
16	36512	ν Ori	4.60	-0.26	B0V	N - I
17	36879	-	7.58	+0.20	06V	N - I
18	37128	ε Ori	1.70	-0.19	B0Ia	N - I
19	37209	-	5.70	-0.23	B1V	- -
20	38771	κ Ori	2.04	-0.18	B0Ia	N - I
21	40111	139Tau	4.82	-0.08	B1Ib	- -
22	40589	-	6.05	+0.25	B9Ia	N - I
23	42087	3 Gem	5.76	+0.20	B2.5Ia	N - I
24	43384	9 Gem	6.28	+0.44	B3Ia	N - I
25	45910	-	6.77	+0.33	B2III	N - I
26	46149	-	7.58	+0.17	08V	N - I
27	47240	-	6.15	+0.15	B1Ib	N - I
28	47839	15 Mon	4.66	-0.25	07III	N - I
29	51283	-	5.28	-0.19	B3II/III	- -
30	52089	ε CMa	1.50	-0.22	B2II	- -
31	52382	-	6.48	+0.20	B2.5Ia	N - I
32	53138	o^2CMa	3.05	-0.08	B3Ia	- -
33	53367	-	6.97	+0.43	B0IV	N - I
34	54668	-	6.21	+0.03	06V	N - I

Cont. (Table 4)

	H.D	Name	V	B-V	Sp.Type	Remarks	
35	58131	-	7.37	+0.34	B2V	N	I
36	58350	ηCMa	2.47	+0.06	B51a	N	I
37	64760	-	4.23	-0.15	B1Ib	-	-
38	66811	ζPup	2.25	-0.28	05V	N	I
39	75821	-	5.10	-0.21	BOIII	-	-
40	77581	-	6.88	+0.56	BOIa	N	I
41	79186	-	5.00	+0.20	B3Ia	N	I
42	87734	ηLeo	3.55	-0.02	AOIa	N	I
43	87901	αLeo	8.14	-0.11	B7V	N	I
44	91316	ρLeo	3.85	-0.14	B1Ib	N	I
45	94367	-	5.28	+0.15	AOIa	-	-
46	102647	βLeo	2.12	+0.09	A3V	N	I
47	120315	ηUMa	1.86	-0.20	B3V	-	-
48	122451	βCem	0.61	-0.22	B1II	-	-
49	132200	μCem	3.12	-0.22	B2V	-	-
50	149438	τSco	2.83	-0.24	B0V	N	I
51	152614	ιOph	4.37	-0.09	B8V	K	KR
52	155763	ζDra	3.17	-0.11	B7III	K	KR
53	160762	ιHer	3.80	-0.17	B3IV	K	KR
54	161868	γOph	3.76	+0.04	A0V	-	-
55	164353	67 Oph	3.97	+0.02	B5Ib	K	KR
56	175191	6 Sgr	2.10	-0.21	B2V	-	-
57	176137	γLyr	3.23	-0.04	B9III	K	KR
58	182255	3 Vül	5.18	-0.12	B6III	K	KR
59	186882	δCyg	2.92	-0.03	B9III	K	P
60	188209	-	5.63	-0.07	09.5I/III	K	KR
61	188260	13Vul	4.57	-0.06	B9III	K	KR
62	195810	εDel	4.04	-0.12	B6III	K	KR
63	197345	αCyg	1.26	+0.09	A2Ia	K	KR
64	205021	βCep	3.18	-0.25	B2III	K	P
65	209952	αCru	1.73	-0.13	B5V	-	-
66	213998	ηAgr	4.02	-0.09	B8V	-	-
67	214993	12 Lac	5.22	-0.12	B2III	K	KR
68	215789	εCru	3.48	+0.08	A2V	-	-
69	218045	αPeg	2.49	-0.05	B9V	K	P
70	218376	1Cas	4.88	-0.02	B0III	K	KR
71	222173	iAnd	4.28	-0.10	B8V	K	KR
72	224572	6Cas	4.88	-0.06	B1V	K	KR

Remarks:N(Nandy),K(Kontizas),

* I(India station),P(Pendeli station,Greece)KR(Kryonerion station Greece)

For the observations in the visible a reference star was observed a number of times during each night in order to derive the atmospheric extinction and sensitivity of the system. The reference stars were γOri (Nandy) and αLyr (Kontizas).

A complete scan of the spectrum for a star takes almost 15 minutes in both scanners.

The Nandy observations have been taken in the range of 3400 Å to 5000 Å from the second order spectrum and in the range 4500 Å to 6000 Å from the first order with a 50 Å bandwidth centred on 15 wavelengths.

The observations carried out with the Newall refractor were taken in the range (6500 to 4150 Å) centred on 27 wavelengths whereas Kryonerion observations were taken in the range (5556 Å to 3600 Å) centred on 13 wavelengths with a $\sim$48 Å bandwidth in both cases. The data are listed in Appendix I and II.

The ultraviolet data were taken with a spectrometer covering the spectral range 2550 - 1350 Å sampling at 20 Å intervals with a spectral resolution of 35 Å and a single channel photometer that gave a broad band measure-ment centred at 2740 Å (Boksenberg et al. 1973).

III 2. REDUCTIONS AND PHOTOMETRIC ERRORS

a) Reductions

The data obtained with the two channel spectrum scanner have been reduced in the following way:
If D_λ represents the deflection, for a particular wavelength λ, on the chart recorder, then the star intensity I_λ can be measured in terms of D_λ (chapter II, 1).

$$D_\lambda = \frac{\tau_\lambda I_\lambda}{\int \rho_\lambda I_\lambda d_\lambda} \qquad (1)$$

where τ, ρ, represent the sensitivities of the two channels. If D_λ is the deflection for an observed star then the deflection D_λ' for the reference star is:

$$D_\lambda' = \frac{\tau_\lambda I_\lambda'}{\int \rho_\lambda I_\lambda' d_\lambda} \qquad (2)$$

The reference star is observed a short time before or after the program star.

The normalised magnitudes, corrected for atmospheric extinction will be respectively:

$$m_\lambda - m_{5556} = -2.5 \log \frac{\tau_{5556} D_\lambda}{\tau_\lambda D_{5556}} + A + B\left(\lambda^{-4} - 0.5556^{-4}\right) \sec z \qquad (3)$$

$$\left(m_\lambda - m_{5556}\right)' = -2.5 \log \frac{\tau_{5556} D_\lambda'}{\tau_\lambda D_{5556}} + A + B\left(\lambda^{-4} - 0.5556^{-4}\right) \sec z' \qquad (4)$$

where A and B are the coefficients of atmospheric extinction. Subtracting (3) from (4) we get:

$$\left(m_\lambda - m_{5556}\right) = \left(m_\lambda - m_{5556}\right)' - 2.5 \log \frac{D_\lambda}{D_{556}} + 2.5 \log \frac{D_\lambda}{D_{5556}} + \qquad (5)$$
$$+ B\left(\lambda^{-4} - 0.5556^{-4}\right) \Big/ \left(\sec z - \sec z'\right)$$

where m'_λ is known from the literature and D_λ , D_λ' , B, z, z′ are measured.

The reductions of data obtained with the single channel spectrometer followed the same way.

If I_λ is the intensity of the incident beam at the wavelength λ , of a program star, and D_λ the deflection measured on the chart recorder then:

$I_\lambda = \sigma_\lambda D_\lambda$ where σ_λ is the sensitivity of the system

For the reference star it is

$$I'_\lambda = \sigma_\lambda D'_\lambda .$$

Therefore the normalised magnitudes (5556 Å) corrected for interstellar extinction will be respectively:

$$(m_\lambda - m_{5556}) = -2.5 \log \frac{\sigma_\lambda D_\lambda}{\sigma_{5556} D_{5556}} + A + B(\lambda^{-4} - 0.5556^{-4}) \sec z \quad (1)$$

$$(m_\lambda - m_{5556})' = -2.5 \log \frac{\sigma_\lambda D_\lambda}{\sigma_{5556} D_{5556}} + A + B(\lambda^{-4} - 0.5556^{-4}) \sec z' \quad (2)$$

and finally,

$$m_\lambda - m_{5556} = (m_\lambda - m_{5556})' - 2.5 \log \frac{D_\lambda}{D_{5556}} + 2.5 \log \frac{D'_\lambda}{D_{5556}} + B(\lambda^{-4} - 0.5556^{-4})(\sec z - \sec z')$$

where m'_λ is known from the literature and D_λ , D_λ' , B, z, z′ are measured.

A calibration curve (Fig. 15) has been produced for the single channel spectrum scanner (Nandy observations). The stars used for this purpose are listed in Table 5.

TABLE 5

HD	V	Sp. Type
35468	1.63	B2 III
37128	1.70	B0 I
15318	4.27	B9 III
34085	0.08	B8 I

For these stars the absolute magnitude m_λ at different wavelengths was known from Schild, Peterson and Oke (1971). So for these stars $m_\lambda - m_{5556}$, (known from the literature) and the values:

$$2.5\log D_\lambda/D_{5556} + B(\lambda^{-4} - 0.5556^{-4})\sec z$$

derived from the observations are plotted in the same diagram.

Each set of data has been divided into two parts, before and after the Balmer Jump. The data near the Balmer Jump have been ignored to avoid errors in this region. The difference between these two sets of data for each star at a certain wavelength λ is:

$$(m_\lambda - m_{5556}) - 2.5\log D/D_{5556} + B(\lambda^{-4} - 0.5556^{-4})\sec z = k_\lambda = 2.5\log \frac{\sigma_\lambda}{\sigma_{5556}}$$

The best fit* curve at these points derived from the stars of Table 5 is the required calibration curve

*Computer-fitted

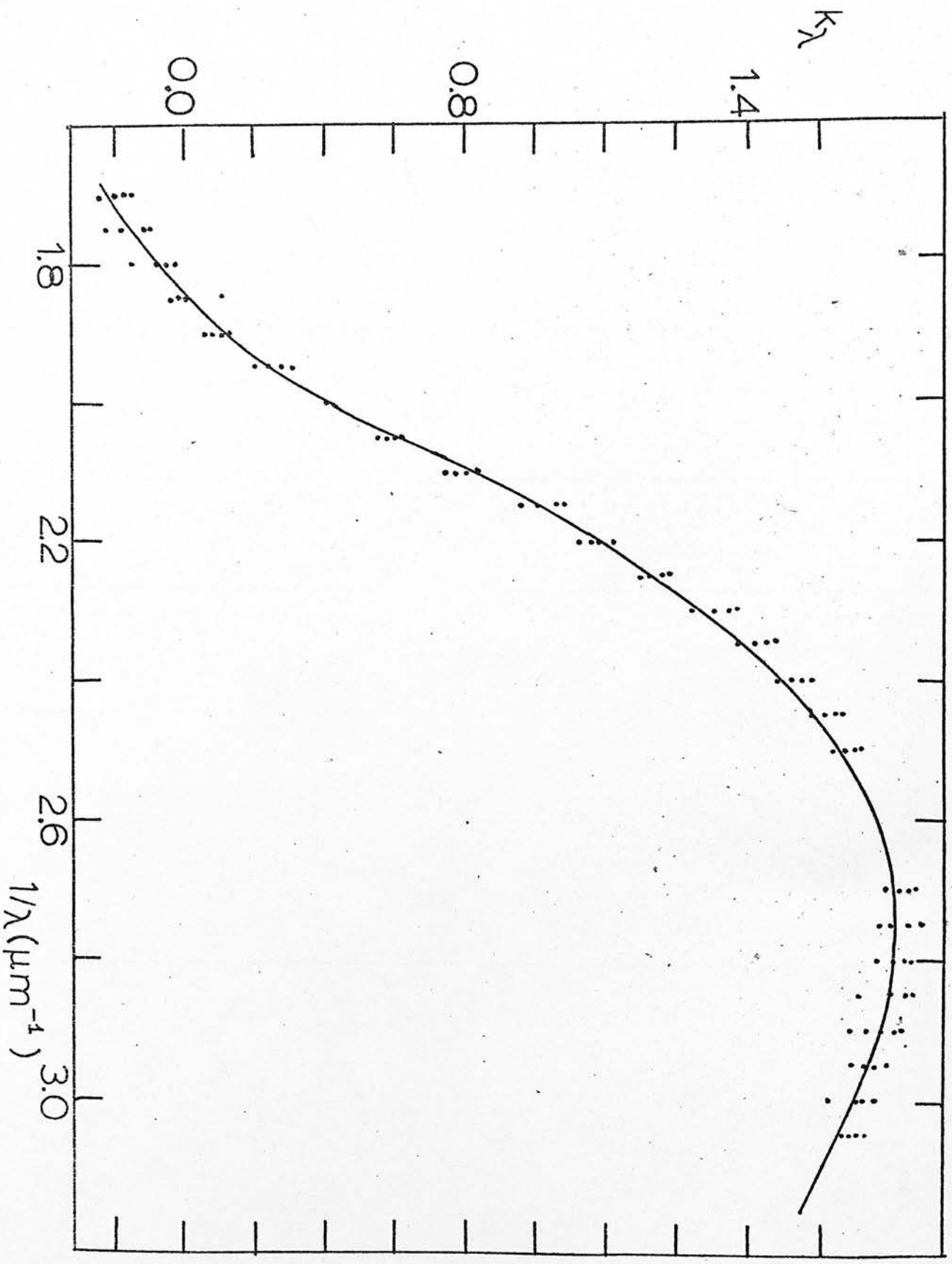

Fig. 15 Calibration curve

(Fig. 15). Assuming that D_λ is known for a star from our observations, the normalised (λ = 5556 Å) magnitude can be found from the relation:

$$m_\lambda - m_{5556} = -2.5 \log \frac{D_\lambda}{D_{5556}} + k_\lambda + B(\lambda^{-4} - 0.5556^{-4}) \sec z$$

where k_λ is the ordinate of the calibration curve at this wavelength.

Both methods have been applied for the reductions and the results have shown a very good agreement.

It is very well known that photometric data have to be corrected for atmospheric extinction because the light coming from the stars suffers an appreciable reddening. It is evident that this phenomenon is wavelength dependent and the shorter the wavelength the stronger the absorption. Primary factors which cause extinction are:

a) molecular absorption bands (not important in the visible region),

b) haze, which is fairly non-selective,

c) scattering by molecules which is roughly proportional to λ^{-4}.

The process that has been followed for calculating the atmospheric extinction coefficient has an easy application and can be used if the brightness of a star is known at different wavelengths and at different values of zenith distance. Let us suppose that m_λ and $m_{\lambda i}$ are the observed magnitudes of a star at a zenith distance z, for λ and λ_i wavelength. Then the observed values are:

$$\begin{aligned} m_{\lambda i} &= 2.5 \log D_i + \text{const} \\ m_\lambda &= 2.5 \log D + \text{const}' \end{aligned} \qquad \text{(b)}$$

where D, Di are the measured deflections.

The values corrected for atmospheric extinction will be respectively:

$$m_{\lambda i}' = -2.5\log Di + \text{const} + (A + B\lambda_i^{-4})\,\text{secz}$$
$$m_{\lambda}' = -2.5\log D + \text{const}' + (A + B\lambda^{-4})\,\text{secz} \qquad (c)$$

where A is the gray atmospheric extinction coefficient and B is the monochromatic one. The equations (b) and (c) give:

$$(m_{\lambda i}' - m_{\lambda}')\text{cor} = (m_{\lambda i} - m_{\lambda})\text{obs} + B(\lambda_i^{-4} - \lambda^{-4})\text{secz}$$

The values $(m_{\lambda i} - m_{\lambda})$obs vs. secz for a star have been plotted and using the least squares method the slope,

$$B(\lambda_i^{-4} - \lambda^{-4}) \equiv Yi$$

of the best fit line for this wavelength has been found. Finally,

$B(\lambda_i^{-4} - \lambda^{-4}) = Yi$ vs. $(\lambda_i^{-4} - \lambda^{-4})$ has been plotted for the different wavelengths and the slope of the best fit line is the B coefficient for that particular night.

This method has been applied each night and the derived values for this B coefficient are given in Table 6.

TABLE 6

India				Greece (Penteli)			
Date			$-B(\text{mag}/\mu m^{-4})$	Date			$-B(\text{mag}/\mu m^{-4})$
1975 Feb	2/3		0.0141	1975 Aug	26/27		0.0191
" "	3/4		0.0176	" "	27/28		0.0170
" "	6/7		0.0168	" "	28/29		0.0152
" "	8/9		0.0106	Greece(Kryonerion)			
" "	9/10		0.0158				
" "	10/11		0.0097	1976 July	Mean		0.0121

b) Photometric errors and wavelength scale errors.

There are many sources of error during the observations which reduce the accuracy of the data. The main categories of errors are:

1. Photometric errors

i) Fixed errors.

This kind of error can be due to variations in power supplies and amplifiers but it is very small for the sensitivity of the used system. Temperature variations can also affect the dynode gain or cathode response of the photomultiplier but this has been eliminated using the refrigerated chamber which was controlled by a thermostat.

ii) Optical errors.

Diffraction, seeing and dispersion are the main sources of optical error. Diffraction becomes important for very narrow slits. For the present project the slit was too wide (~1.25mm.) to introduce errors due to diffraction.

Seeing is the major problem of all kind of observations. It has already been discussed in detail how it was tried to eliminate this problem by using the ratiometer technique in the described spectrum scanner.

Atmospheric dispersion is insignificant at low resolution.

iii) Time-dependent errors.

The instrumental drift is one of the time dependent errors and although it was very small the adjustment of the zero point before each scan has eliminated it.

The variation of extinction is another time dependent source of error. The extinction variations for each night were suggested to be very small and only changes from night to night have been considered. Therefore the mean atmospheric extinction for each night was used for the reductions.

All the prescribed errors introduce a noise in the spectrograms which with the existence of spectral lines make the determination of the continuum uncertain. The error in the determination of the continuum has a mean value 0.2cm for a fairly good night and for a star of 4th magnitude with deflection 12 to 15cm at 4400 Å. The mean error in magnitude scale can be found from the partial derivatives of the equation:

$$m_\lambda(v=o) = 2.5 \log \sigma_\lambda D_\lambda / \sigma_v D_v$$

$$\delta m_\lambda(v=o) = \frac{\partial m_\lambda}{\partial D_\lambda}\delta D_\lambda + \frac{\partial m_v}{\partial D_v}\delta D_v$$

$$\delta m_\lambda(v=0) = \frac{2.5}{\ln 10}\left[\frac{\delta D_\lambda}{D_\lambda} + \frac{\delta D_v}{D_v}\right] \approx 0.02 \text{ mag.}$$

The photometric error in the ultraviolet has been calculated by Nandy et al. (1976). They found that the accuracy of data of the broad band measurement at 2740 Å is $\pm 0^m.02$ for stars brighter than $V = 5^m.0$ and it becomes $\pm 0^m.05$ for fainter stars.

For shorter wavelengths where the bands are narrower and particularly at the extreme ultraviolet end and that centred at 2190 Å where maximum extinction occurs the

error reaches values as high as $\pm 0^m.2$ for the fainter strongly reddened stars.

2. Internal consistency

In the visible spectral range, the internal consistency was found to be of the order of the photometric error. An example is given for the star γ Ori which was measured on different nights at λ = 3509 Å (Table 7). The standard error due to the internal consistency was found to be $\sim \pm 0^m.02$.

TABLE 7

Deflection (cm)	Date
17.40	1975 Feb 2/3
17.20	" " 6/7
16.70	" " 6/7
17.00	" " 8/9
16.90	" " 9/10
17.30	" " 10/11

3. Error in the estimation of the wavelength

The wavelength calibration has been done using a mercury lamp, with known emission lines. Although no shift has been noticed in the wavelength scale, the Hg lamp has been used to calibrate the scanners before and after the observations each night. The error in the wavelength scale is less than ± 5 Å as it has been checked in many cases for both scanners. This introduces an error of $\pm 0^m.01$.

III 3. COMPARISON WITH OTHER WORKERS

The flux distribution for some of the program stars is also known from the literature. During the first stages of this project a number of stars were compared with Schild et al. (1971) observations. The comparison has been done without involving the instrumental sensitivity to avoid any possible error introduced by this value. The instrumental sensitivity was eliminated by using the differences for two different stars, star (1) and star (2):

$$(m_\lambda - m_{5000})_{(1)} - (m_\lambda - m_{5000})_{(2)} = -2.5 \log \frac{D_\lambda(1)}{D_{5000(1)}} +$$

$$+ 2.5 \log \frac{D_{\lambda(2)}}{D_{5000(2)}} + B\left(\lambda^{-4} - 0.5^{-4}\right)\left(\sec z(1) - \sec z(2)\right)$$

The first term of this equation has been plotted vs. $1/\lambda$ using Schild's et al. (1971) values, while the second term was plotted in the same diagram from the observations presented here (Figs. 16,17,18,19). The differences of these two sets of data have standard deviation $\sim \pm 0^m.04$.

Recently, Breger (1976) has collected a considerable number of previously published stellar scans. The observations with passbands of 50 Å have been transformed to the Hayes-Lathan calibration of Vega. Fourteen stars of the present work are in common with Breger's. The energy distribution in terms of magnitude found here were compared with those of Breger for the common stars (HD: 15318, 24398,

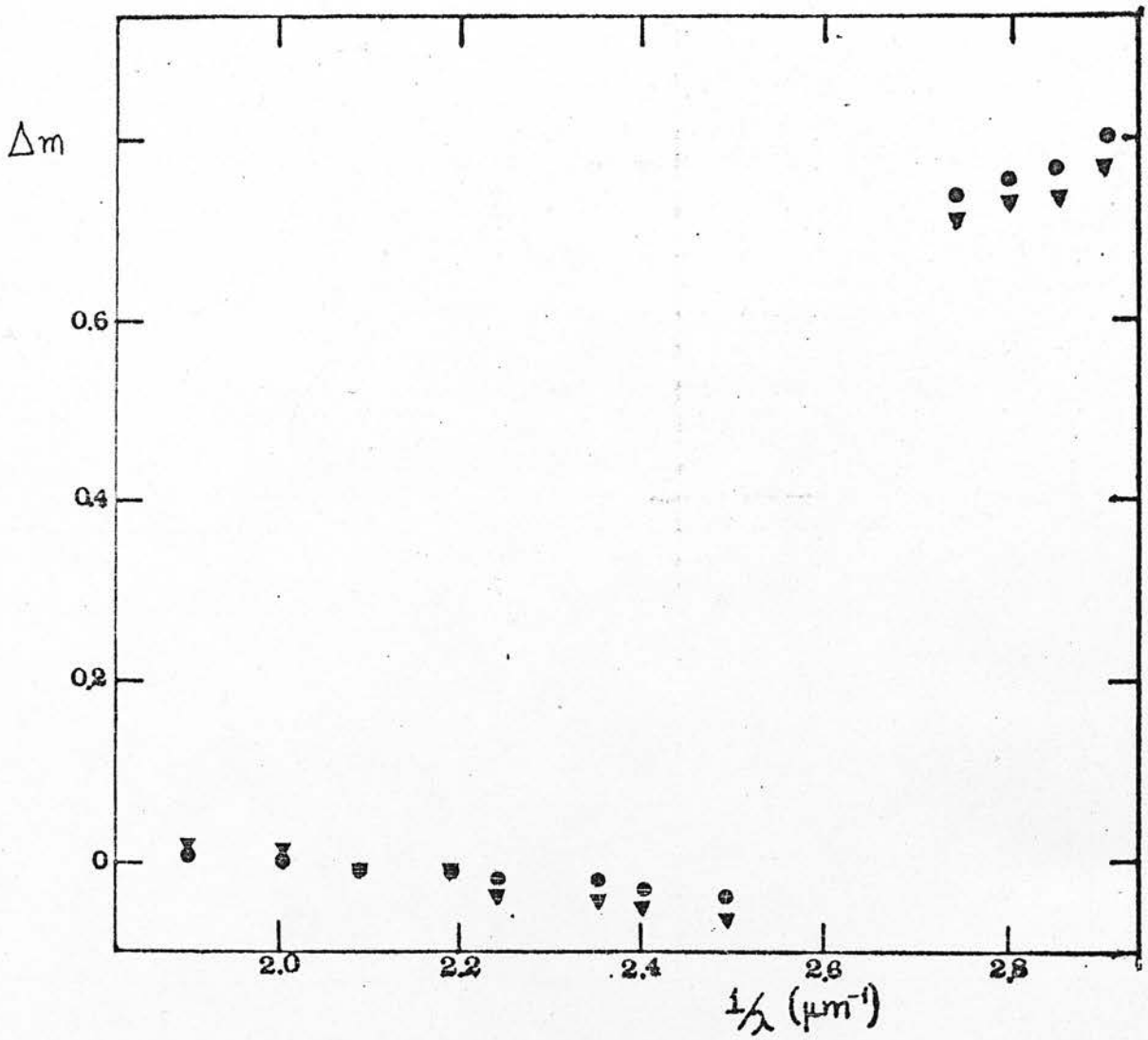

Fig. 16. Differences of the colour indices for the pair of stars HD: 15318 HD: 34085. ▼ Schild, Peterson & Oke (1971) ● Nandy observations (presented here).

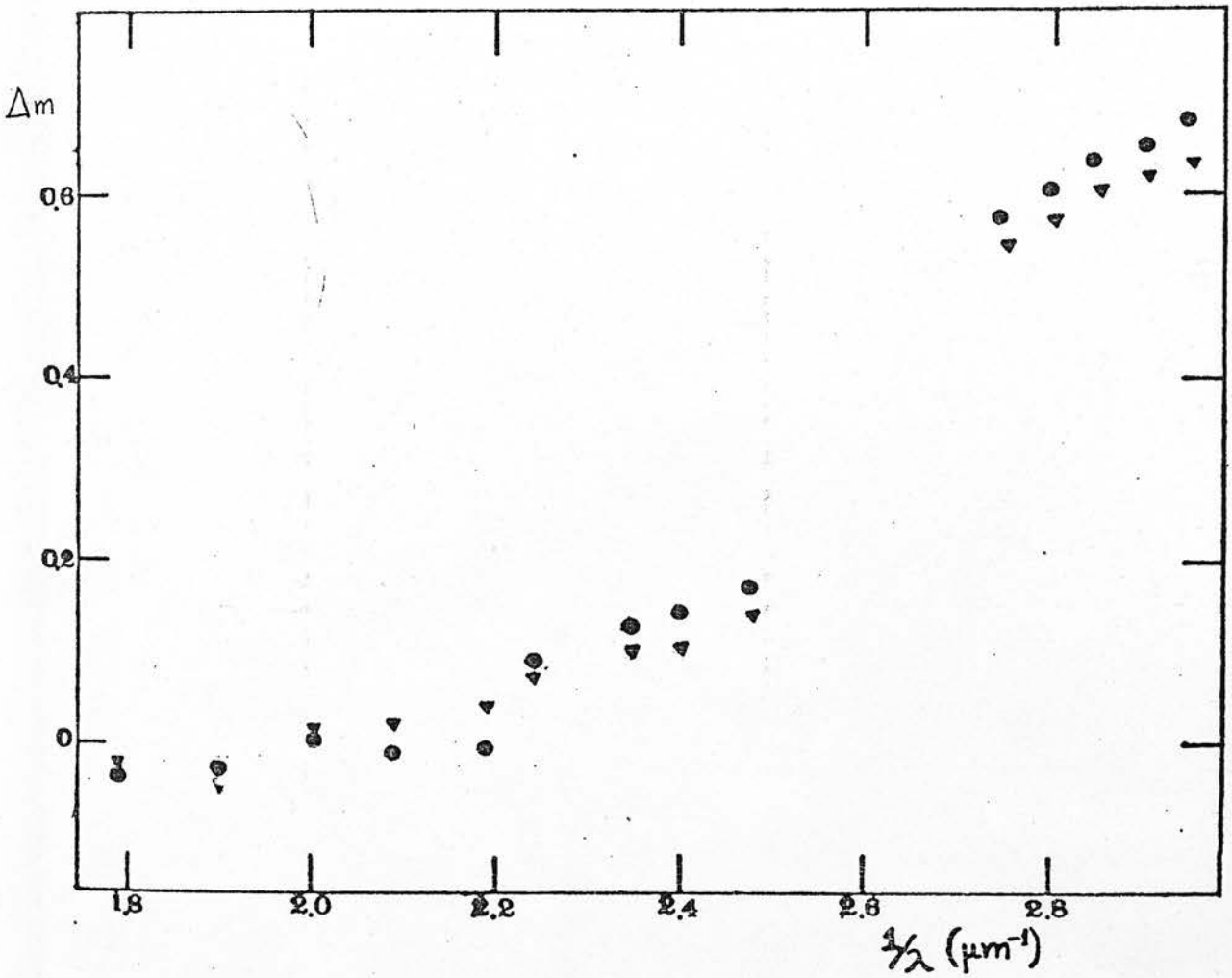

Fig. 17. Differences of the colour indices for the pair of stars HD: 34085 HD: 37128. ▼ Schild, Peterson & Oke (1971) ● Nandy observations.

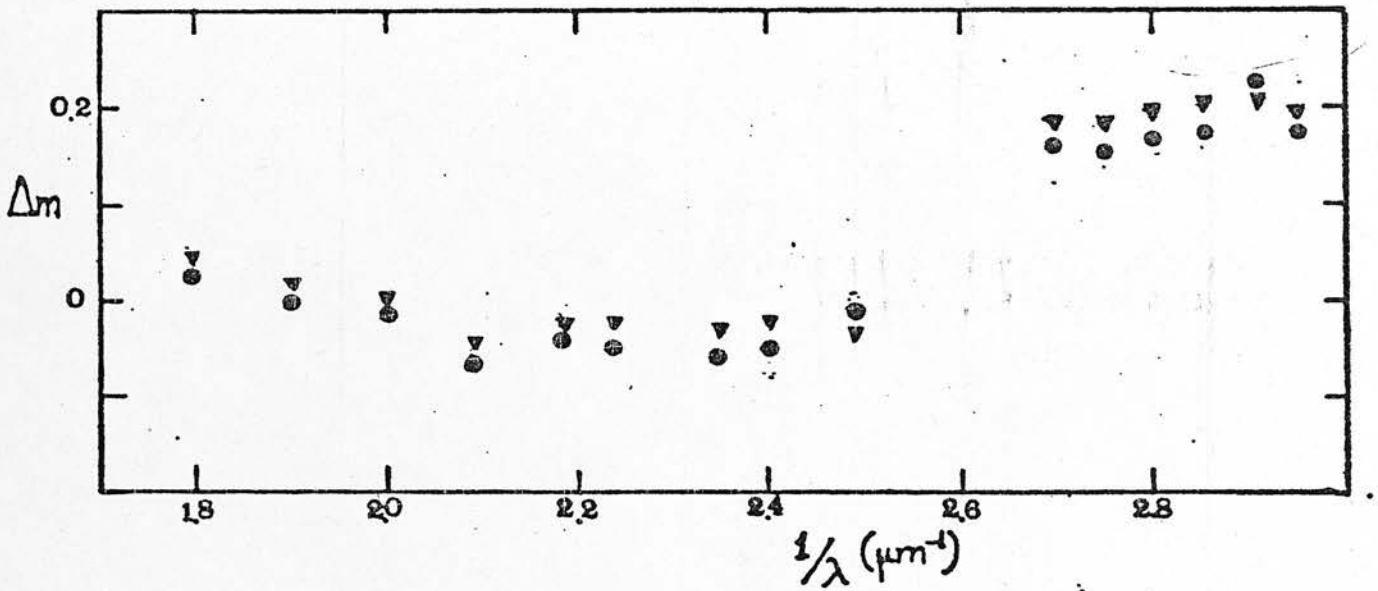

Fig. 18. Differences of the colour indices for the pair of stars HD: 35468 HD: 37128. ▼ Schild, Peterson & Oke (1971) • Nandy observations.

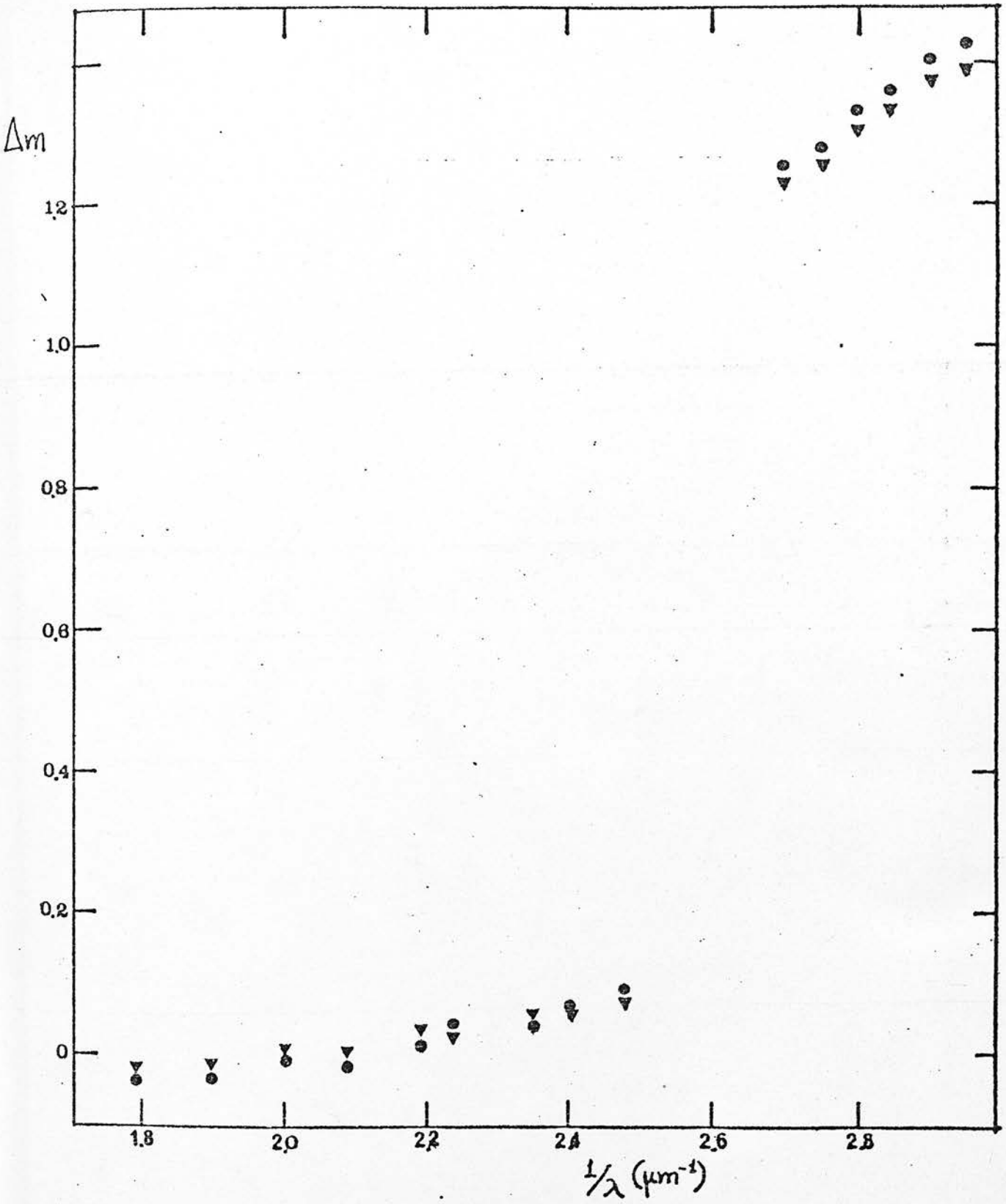

Fig. 19. Differences of the colour indices for the pair of stars HD: 15318 HD: 37128. ▼ Schild, Peterson & Oke (1971) ● Nandy observations.

TABLE 8

INDIA		GREECE	
$\lambda^{-1}(\mu m^{-1})$	Δm_λ	$\lambda^{-1}(\mu m^{-1})$	Δm_λ
1.80	0.00	1.80	0.00
1.90	0.03	1.84	0.03
2.00	0.04	1.90	0.03
2.10	0.08	1.96	0.06
2.19	0.06	2.06	0.04
2.24	0.09	2.10	0.07
2.35	0.10	2.18	0.08
2.48	0.09	2.26	0.09
2.80	0.08	2.35	0.06
2.85	0.12	2.44	0.10
2.95	0.08	2.78	0.09

Δm_λ denotes m_λ(Kontizas) - m_λ(Breger)

TABLE 9

Mean Ratio of TD1/OAO-2 for 25 stars
(Bohlin et al. 1976)

λ (Å)	Ratio	λ (Å)	Ratio
1400	.789	2050	.978
1450	.797	2100	.984
1500	.753	2150	1.005
1550	.734	2200	1.011
1600	.794	2250	1.015
1650	.907	2300	1.008
1700	.920	2350	.975
1800	.859	2400	.965
1850	.868	2450	.951
1900	.871	2500	.934
1950	.906	2540	.949
2000	.948		

24760, 35468, 37128, 58350, 91316, 102647, 149438, 155763, 160762, 197345, 222173).

The mean of differences between Breger's values and ours at the observed wavelengths are given in Table 8, for the observations taken from India and Greece. These differences can probably be accounted for by a combination of photometric errors in the two surveys together with different choices of primary standards.

For the ultraviolet data, a comparison of the TD1 data with OAO-2 (Code et al. 1972) satellite ultraviolet data has been done (Bohlin et al. 1976). Averages of the mean TD1/OAO-2 ratios for 25 stars are given in Table 9. The r.m.s. was found to be $\pm$ $0^m.14$.

It has been suggested that the differences between the two sets of data are due to uncertainties of calibration (Bohlin et al. 1976).

III 4. CORRECTION FOR INTERSTELLAR EXTINCTION

The light reaching the earth from the stars passes through vast distances in interstellar space. Gas and dust lying between the earth and stars absorb the stellar light and form interstellar absorption lines in a stellar spectrum. So the stellar spectra have to be corrected from interstellar extinction for the study of their own properties.

It is therefore necessary to give some definitions and describe how this correction has been done in the present work.

We define the absolute magnitude $M(\lambda)$ as the apparent magnitude of a star in the absence of absorption at a distance of 10 parsecs. For a given wavelength λ using observational methods we can determine a monochromatic apparent magnitude m_λ for a star, related to the absolute magnitude $M(\lambda)$ by the equation:

$$m_\lambda = M(\lambda) - 5 + 5 \log d + A(\lambda)$$

where d is the distance of the star in pcs and $A(\lambda)$ is the interstellar extinction in magnitudes.

Colour indices are defined as the difference in stellar magnitudes between the two wavelengths $(m_{\lambda i} - m_{\lambda j})$. The observed $m_{\lambda i} - m_{\lambda j}$ colour of a star is then related to the corresponding intrinsic colour by

$$(m_{\lambda i} - m_{\lambda j})_{obs} = (m_{\lambda i} - m_{\lambda j})_{int} + A(\lambda i) - A(\lambda j)$$

and the colour excesses $E_{\lambda i - \lambda j}$ are defined by

$$E_{\lambda i - \lambda j} = (m_{\lambda i} - m_{\lambda j})_o - (m_{\lambda i} - m_{\lambda j})_{int}$$ so

$$E_{\lambda i - \lambda j} = A(\lambda i) - A(\lambda j)$$

Measuring monochromatic magnitude differencesbetween a reddened and an unreddened star of the same spectral type and in the same galactic region we can find the wavelength dependence of the extinction in magnitudes. The plot of such magnitude differences against wave number represents the effect of interstellar extinction and it is usually referred as the extinction law or extinction curve.

The first reliable photometric measurement of stars in the ultraviolet wavelength made by rocket based equipment (Boggess and Borgman, 1964) gave the opportunity of extending the extinction law further towards the shorter wavelengths: Stecher (1966, 1969), Bless, Code & Houk (1968), Bless & Savage (1972).

From the extensive data available from the sky survey telescope in the TD1 satellite, Nandy et al. (1975, 1976) have investigated the wavelength dependence of interstellar extinction in the wavelength range from 2740 Å to 1350 Å for different regions throughout the galactic plane. The extinction curves derived for these regions have been extended to visible wavelengths by using available spectrophotometric data in the visible as well as the UBV data given by Blanco et al.(1968). These extinction curves do not show significant variations, although circumstellar anomalies can occur (Willis & Wilson, 1975). From all these observations incorporating UBV data, Nandy et al. (1976) have derived a mean extinction curve in terms of local extinction per unit colour excess E_{B-V}; the accuracy of A_λ/E_{B-V} is estimated to be $\pm 0^m.2$, the main source of error being the uncertainty of the adopted value of R, the

ratio of total to selective extinction.

Johnson (1965, 1968) presented evidence suggesting that R varies from a value of about 3 in some regions to values as high as 6 or 7 in other regions.

Becker (1966) treats in detail the two associations, IIICep and IAra for which Johnson has derived the values R = 5.4 and 6.6 respectively and concludes that in their cases there is no reason to assume a value of R larger than 3. In the case of IIICep Garrison (1970) has reached the same conclusions from a larger material of spectral types.

Schalén (1975) from an investigation in dark Clouds situated in widely different parts of the stellar system concludes that R is equal or a little larger than 3.

Turner (1976) has found a weighted mean value of R for 51 clusters to be 3.08 $\pm$ 0.03. His analyses led to a mean value of R for the galactic plane which is of the order of 3.1. The existence of a larger than average value of R(3.3) for the region towards the galactic anticentre and a smaller than average value (3.0) for Cygnus may be real so that extinction correction for reddened objects may depend on their direction in space.

Pottasch et al.(1977) in their paper, ultraviolet observations of planetary nebulae, have reported a value of R = 3.2 $\pm$ 0.7. This value of R lies within the limits of the generally accepted value in most regions of the interstellar medium.

Whittet (1977) has shown that there is evidence for a small but significant variation in the ratio of total to selective extinction, R, with galactic longitude. R is

TABLE 10

Scale of interstellar extinction A_λ / E_{B-V}

$\frac{1}{\lambda}(\mu m^{-1})$	A_λ / E_{B-V}	$\frac{1}{\lambda}(\mu m^{-1})$	A_λ / E_{B-V}	$\frac{1}{\lambda}(\mu m^{-1})$	A_λ / E_{B-V}
1.00	1.20	4.13	7.57	5.29	7.83
1.10	1.28	4.16	7.64	5.35	7.76
1.20	1.68	4.19	7.83	5.41	7.70
1.30	1.88	4.23	8.05	5.46	7.60
1.40	2.08	4.26	8.21	5.52	7.57
1.50	2.28	4.30	8.37	5.58	7.60
1.60	2.50	4.34	8.60	5.64	7.54
1.70	2.72	4.37	8.72	5.74	7.80
1.80	2.99	4.41	8.92	5.80	7.76
1.90	3.20	4.45	9.11	5.87	7.73
2.00	3.40	4.49	9.20	5.94	7.73
2.10	3.61	4.53	9.24	6.01	7.67
2.20	3.80	4.57	9.30	6.08	7.73
2.30	3.99	4.61	9.27	6.15	7.67
2.40	4.10	4.67	9.27	6.22	7.76
2.50	4.24	4.71	9.17	6.30	7.70
2.60	4.36	4.76	9.01	6.38	7.76
2.70	4.48	4.80	8.95	6.46	7.70
2.80	4.64	4.85	8.92	6.54	7.83
2.90	4.76	4.89	8.72	6.62	7.83
3.65	6.10	4.94	8.60	6.71	7.80
3.94	6.96	4.99	8.40	6.80	7.86
3.97	7.06	5.04	8.28	6.89	7.92
4.00	7.16	5.08	8.15	6.98	7.96
4.03	7.25	5.14	8.02	7.08	7.99
4.06	7.38	5.19	7.99	7.18	8.12
4.09	7.48	5.24	7.86	7.28	8.18

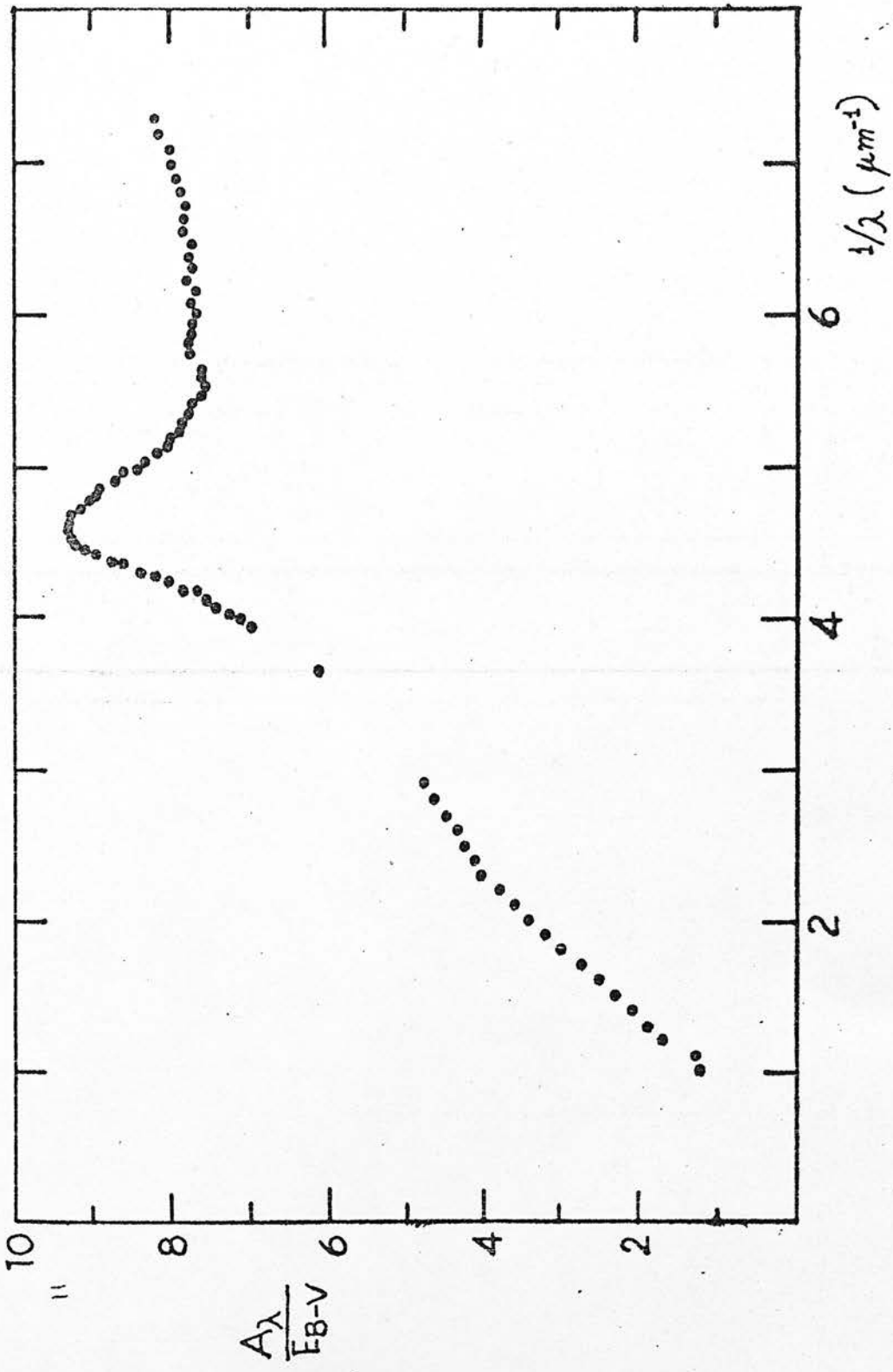

Fig. 20. The mean interstellar extinction law (Nandy et al. 1975).

found to be systematically higher by $\sim$0.3 in the Southern Milky Way than in the North. The ultraviolet observations combined with the visible data yield a scale of total extinction $A(\lambda)/E_{B-V}$ which is given in Table 10. The mean interstellar extinction law is illustrated in Fig. 20 (Nandy et al. 1975c).

The extinction law for the visible region has been derived by the author also, from the present photoelectric spectra of early type stars. Monochromatic magnitude differences have been measured between reddened and unreddened stars of the same spectral type.

Table 11 lists the pairs of reddened and comparison stars. MK spectral types are taken from Blanco et al. (1968). The difference in visual colour excess ΔE_{B-V} between reddened and comparison stars is given in column 7 of Table 11. Photometric data of these stars have been taken from observations presented in this project (Appendix I and II). The extinction A_λ was measured by taking the ratio of monochromatic fluxes between reddened and comparison star of similar spectral type. For the comparison of the extinction curves derived from different star pairs the values have been mormalised in order to have the value 0 at λ = V and the value 1 at λ = B. All the normalised extinction curves have been combined to give a mean extinction curve $\bar{k}_\lambda$.

Assuming a value of R = 3.0 the mean values of total extinction $A(\lambda)$ per unit colour excess E_{B-V} are listed in Table 12 over the wavelength range $1/\lambda$ = 1.8 to $1/\lambda$ = 2.90.

TABLE 11

Stars used for the determination of the extinction law in the visible

REDDENED STARS		COMPARISON STARS		$\Delta E(B-V)$
HD	SP-T	HD	SP-T	
77581	BOIa	38771	BOIa	+0.74
77581	BOIa	37128	BOIa	+0.75
24398	B1 Ib	91316	B1 Ib	+0.27
47240	B1 Ib	91316	B1 Ib	+0.29
36371	B5Ia	58350	B5Ia	+0.36
58131	B2V	32249	B2V	+0.54
33988	B2V	32249	B2V	+0.54
45910	B2III	35468	B2III	+0.54

Since the extinction curves in the visible derived from above data agree with that of Nandy et al.(1975c,1976) within the observational error (r.m.s. = ± 0.03mag) their mean extinction curve has been adapted as it is based on more extensive data.

The spectral distribution of the observed stars has been corrected for interstellar reddening, using the mean extinction law. The unreddened values are given by the expression:

$$m_\lambda(V=0)_{un} = m_\lambda(V=0)_{red} + C_{cor}$$

where

$$C_{cor} = -\left(A\lambda/E(B-V) - R\right) \Big/ E(B-V)$$

The accuracy of $A\lambda/E_{B-V}$ is estimated to be ± 0.2, the error arising from uncertainties in photometry, spectral mismatch between the red and the comparison star and the adopted value of R.

Schild (1977), in a new investigation of the interstellar reddening law in the range of λ 3200 Å to λ10870 Å based on new observations, has concluded that for very specific work it might be necessary to determine the interstellar extinction law for each direction of study. His results are in good agreement with those of Nandy et al. (1975c) and the differences are within the limits of accuracy of Nandy's mean extinction law.

TABLE 12

Interstellar extinction $A_\lambda/E_{(B-V)}$

$\frac{1}{\lambda}$ (μm^{-1})	$A_\lambda/E_{(B-V)}$
1.80	3.00
1.90	3.21
2.00	3.40
2.10	3.64
2.19	3.84
2.24	3.92
2.35	4.02
2.40	4.15
2.48	4.28
2.70	4.52
2.75	4.60
2.80	4.69
2.85	4.75
2.90	4.79

IV. LUMINOSITY EFFECT

IV 1. OBSERVATIONS AND DISCUSSION ON THE LUMINOSITY EFFECT

Observations obtained with the S2/62 Ultraviolet Sky Survey telescope in the European Satellite TD 1 were available at the beginning of this project. Some of them have been used for the study of the luminosity effect in the ultraviolet, comparing the energy distributions of giants and supergiants with those of main sequence stars of similar spectral type.

Differences between the ultraviolet energy distributions of early type supergiants and dwarfs of the same spectral type have been noted earlier (Carruthers 1969; Weber, Henry & Carruthers 1971; Bless & Savage 1972; Layet 1972). From model atmospheres calculation (Mihalas 1970) the normalised ultraviolet fluxes were found to be systematically lower for supergiants than for dwarfs and this has been interpreted as the result of differences in surface gravity and effective temperature.

A list of stars was produced and the chosen stars (Table 13) were selected on the basis of small interstellar reddening.

The data, taken with a spectrometer sampling at 20 Å intervals with a spectral resolution of 35 Å, cover the spectral range of 2550 - 1350 Å, together with a photometer sampling broad-band measurements centred at 2740 Å (Boksenberg et al. 1973).

TABLE 13

Observed Stars

Star	HD	MK Type	V	B-V	E_{B-V}
ε Ori	37128	B0 Ia	1.70	-0.19	0.08
	75821	B0 III	5.10	-0.21	0.09
τ Sco	149438	B0 V	2.83	-0.25	0.05
υ Ori	36512	B0 V	4.60	-0.26	0.04
	64760	B1 Ib	4.23	-0.15	0.07
139 Tau	40111	B1 Ib	4.82	-0.08	0.14
β Cen	122451	B1 II	0.61	-0.22	0.02
	37209	B1 V	5.70	-0.23	0.03
ϵ CMa	52089	B2 II	1.50	-0.22	0.00
σ Sgr	175191	B2 V	2.10	-0.21	0.03
κ Cen	132200	B2 V	3.12	-0.22	0.02
σ^2CMa	53138	B3 Ia	3.05	-0.08	0.06
	51283	B3 II-III	5.28	-0.19	0.00
ηUMa	120315	B3 V	1.86	-0.20	0.00
ηCMa	58350	B5 Ia	2.40	-0.07	0.03
α Gru	209952	B5 V	1.73	-0.13	0.03
β Ori	34085	B8 Ia	0.17	-0.03	0.00
η Aqr	213998	B8 V	4.02	-0.09	0.00
	94367	A0 Ia	5.28	+0.15	0.14
γ Oph	161868	A0 V	3.76	+0.04	0.04
α Cyg	197345	A2 Ia	1.26	+0.09	0.04
ϵ Gru	215789	A2 V	3.48	+0.08	0.02

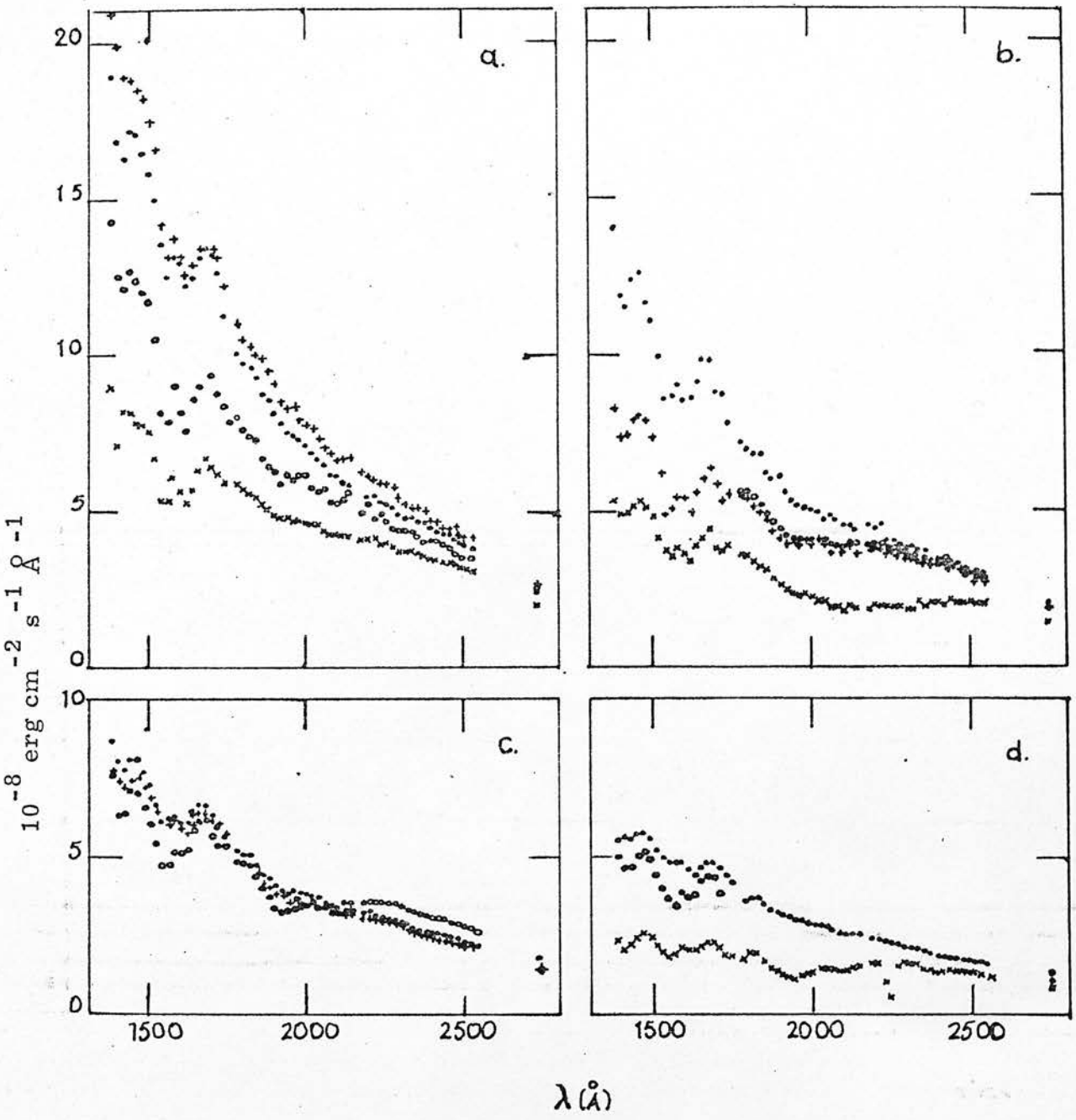

Fig. 21. Ultraviolet flux distributions normalized to V = 0 for luminous and main-sequence stars.

a) + HD 149438 B0 V; ◉ HD 36512 B0 V; ○ HD 75821 B0 III; × HD 37128 B0 I.

b) HD 37209 B1 V; HD 122451 B1 II; HD 40111 B1 Ib HD 64760 B1 Ib.

c) HD 132200 B2 V; HD 175191 B2 V; HD 52089 B2 II.

d) HD 120315 B3 V; HD 51283 B3 II-III; HD 53138 B3 Ia.

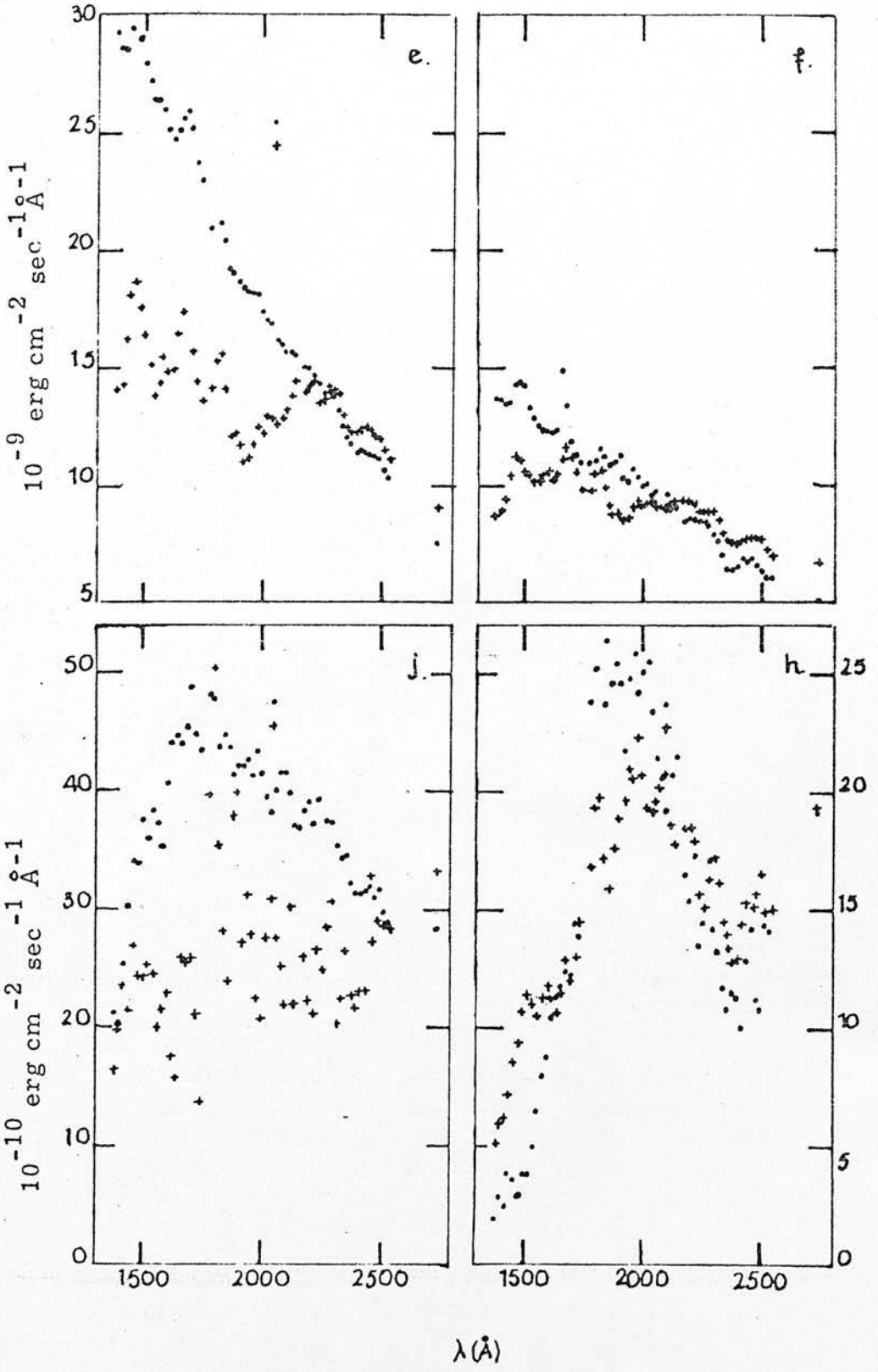

Fig. 21..

e)	HD 209952 B5 V;	HD 58350 B5 Ia.
f)	HD 213998 B8 V;	HD 34085 B8 Ia.
g)	HD 161868 A0 V;	HD 94367 A0 Ia.
h)	HD 215789 A2 V;	HD 197345 A2 Ia.

The observed ultraviolet flux distributions of these stars normalised to V = 0 are shown in Fig. 21 (a,b,c,d,e, f,g,h). Magnitude differences, defined as

$$\Delta m_\lambda = (m_\lambda - V)_{\text{luminous}} - (m_\lambda - V)_{\text{dwarf}} ,$$

have been derived for pairs of luminous and dwarf stars with similar spectral type.

Corrections for interstellar reddening were applied using the mean extinction law (chapter III). Since E_{B-V} for the stars is in most cases less than 0.05mag, the error in the corrected Δm_λ arising from uncertainties in the extinction law is very small. The corrected Δm_λ values are plotted as a function of $1/\lambda$ in Fig 22. In this diagram the corresponding magnitude differences at the wavelengths of the photometric U and B bands have been plotted as well.

Values of Δm_λ in the visible wavelength range of Fig. 22 indicate that the stars considered here have the normal UBV photometric properties characteristic of early-type stars. At ΔB, the values either are zero or take small positive values ($\sim$0.1 mag), since, in the spectral type range considered, (B-V) is not strongly dependent on luminosity. The ΔU values are approximately zero for spectral types near B0 but become progressively more negative towards later spectral types. These values are consistent with measurements of the Balmer discontinuities in early-type stars by Barbier (1952) and Chalonge (1956); the magnitude of the Balmer Jump is larger for main sequence stars than for luminous stars, and the difference in Balmer

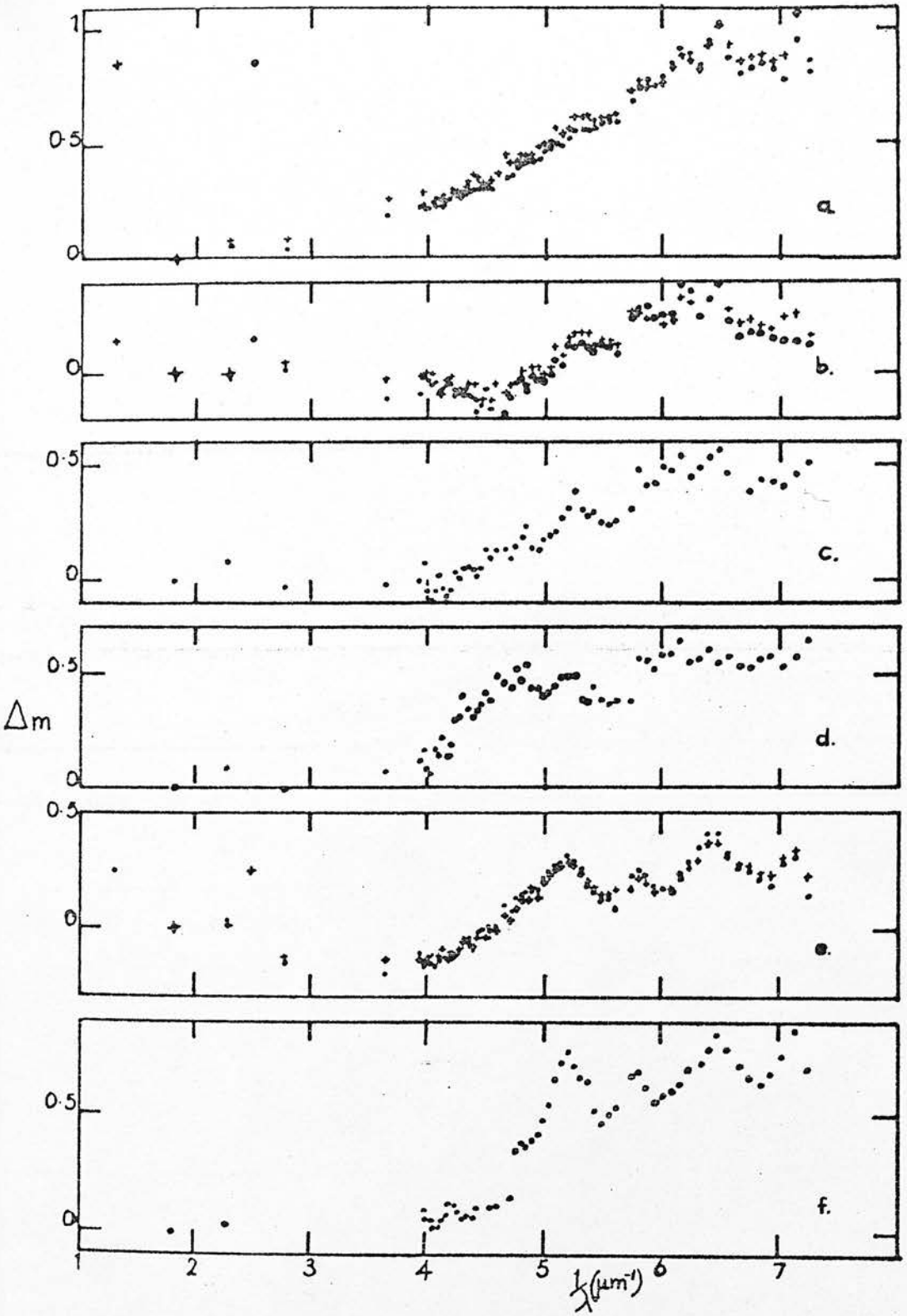

Fig. 22 Magnitude differences Δm shown as a function of $1/\lambda$ for pairs of luminous and dwarf stars of similar spectral type. For all the diagrams Δm is zero at the photometric V wavelength ($1/\lambda = 1.82\ \mu^{-1}$).

a) HD 37128 B0 Ia; HD 36512 B0 V; HD 37128 B0 Ia; HD 149438 B0 V.

b) HD 75821 B0 III; HD 36512 B0 V; HD 75821 B0 III; HD 149438 B0 V.

c) HD 64760 B1 Ib; HD 37209 B1 V.

d) HD 40111 B1 Ib; HD 37209 B1 V.

e) HD 52089 B2 II; HD 175191 B2 V; HD 52089 B2 II; HD 132200 B2 V.

f) HD 53138 B3 Ia; HD 120315 B3 V.

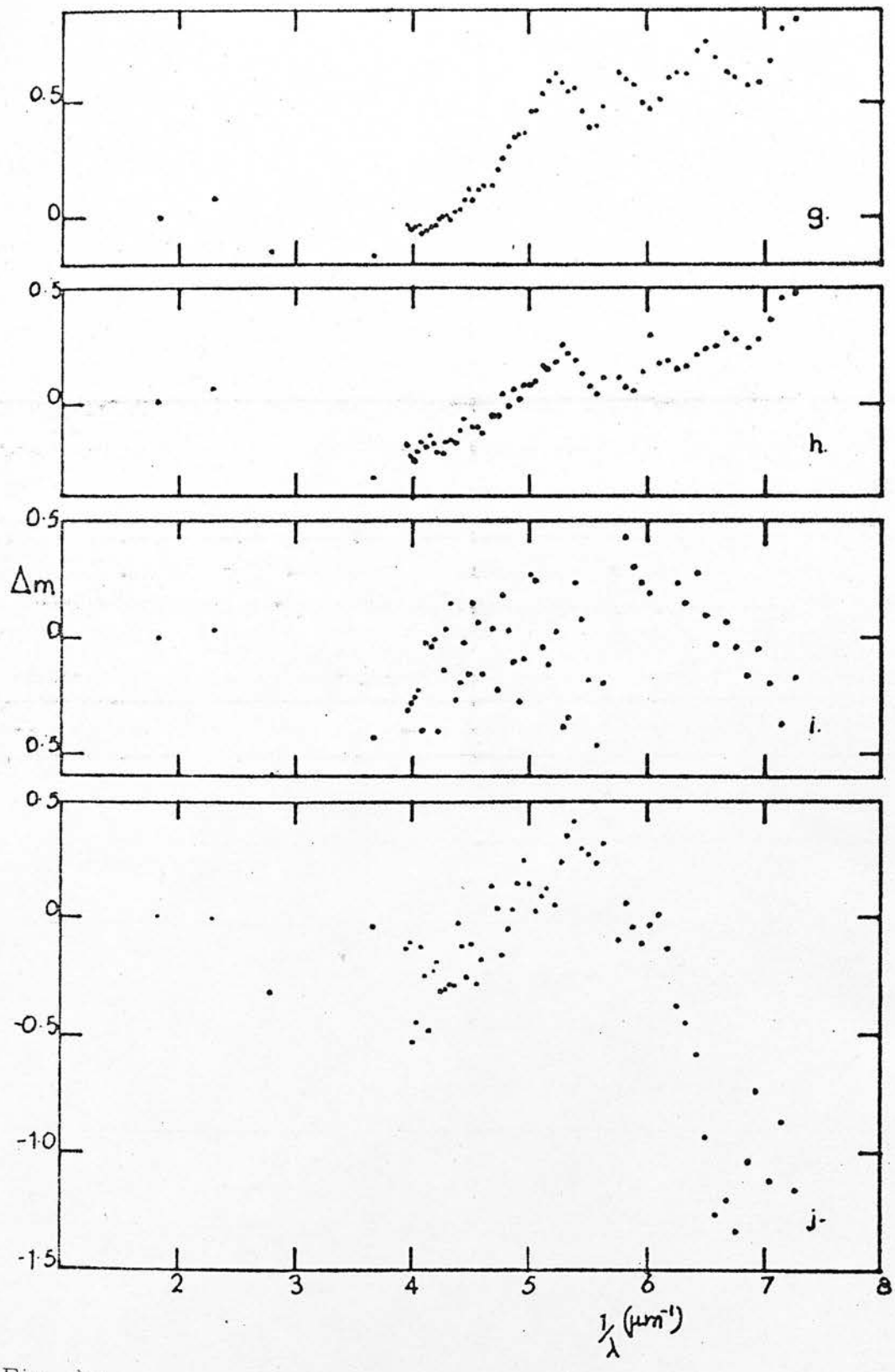

Fig. 22

g)	HD 58350 B5 Ia;	HD 209952 B5 V.
h)	HD 34085 B8 Ia;	HD 213998 B8 V.
i)	HD 94367 A0 Ia;	HD 161808 A0 V.
j)	HD 197345 A2 Ia;	HD 215789 A2 V.

Jump between main sequence and luminous stars systematically increases from early B to A2 stars.

Fig. 22 shows that shortward of the Balmer Jump increases with $1/\lambda$, indicating that the normalised fluxes of luminous stars become fainter with decreasing wavelength as compared with the fluxes of the corresponding main-sequence stars. This applies both to supergiants and giants and for all spectral types from BO to B8. In this spectral type range, the slopes of the curves in Figs. 22(a) - 22(h) are almost identical. For the pair which contain a supergiant, Δ m increases typically by 0.7 mag from λ= 2500 Å to λ = 4000 Å; for the pairs which contain a giant the corresponding increase in Δm is 0.4 mag. Fig 22(a) includes the pair consisting of ε Ori (HD 37128, BOIa) and υ Ori (HD 36512, BOV) which have also been observed photometrically at 1115 Å by Carruthers (1969). Carruthers' measurements give a normalised flux ratio for υ Ori/ε Ori of 2.4, i.e. a Δ m value of nearly 1.0 mag at this wavelength. This fits well with the present observations if the data in Fig. 22(a) are extrapolated to $1/\lambda$ = 9.0 μm^{-1}.

For the A-type stars in Fig. 22(i-j), Δ m increases with $1/\lambda$ up to λ = 1800 Å in the same way, as described before. Beyond this value however, the slope of the curve changes sign and the ultraviolet flux deficiency between the A-type supergiants and their main-sequence counterparts starts decreasing. For the AO pair shown here, the normalised flux of the supergiant becomes comparable to that of the dwarf at 1400 Å. For the A2 stars shortward of 1600 Å the normalised flux of the supergiant becomes larger than that of the dwarf.

Absorption features are also interesting to discuss in these stars. In the past, Underhill, Leckrone & West (1972) and Thompson, Humphries & Nandy (1974) have reported that these features are absent or present only weakly in main sequence stars. In Fig 22 the lines at 1550 Å and 1400 Å predominantly due to (CIV) and (Si IV) respectively, appear more strongly in giants and supergiants than in the corresponding main sequence stars in the spectral range observed. The equivalent widths of these lines have been measured previously by Code & Bless (1970) for supergiant and main sequence stars and their results support these remarks.

Another important conclusion is that the B type giants and supergiants of the present project show stronger absorption near 1920 Å than the corresponding main-sequence stars. The presence of this feature in the spectra of luminous stars was reported earlier by Thompson et al. (1974). It has also been noticed that the 1920 Å absorption is somewhat weaker for luminous BO - B1 stars than for luminous stars in the range B2 - B8. In the latter range, however, the relative strength seems to remain fairly constant. This feature has been interpreted as a photospheric line blocking effect.

The broad absorption feature at 1720 Å has been considered as originating in the extended envelopes of supergiant and shell stars (Underhill et al. 1972; Tarafdar & Vardya 1973). This feature is present in the B-type giants and supergiants studied here, and it is generally weaker than the 1920 Å feature. The ratio of the

strength of this band to that of the 1920 Å band seems to vary; for example, in η CMa the strengths of the two features are comparable whereas for β Ori the 1720 Å feature is much weaker than that at 1920 Å. It should be noted, however, that in these data 1720 Å lies in the overlap region at the extremities of the short medium wavelength spectrometer channels where vignetting of the primary image occurs. Corrections have been applied in the data reduction to compensate for this, but the measured absorption strengths here may still be affected slightly by the instrumental effect.

Δm is observed to be non-zero in the regions between the known strong bands and lines. Thus, structure in the Δm_λ versus $1/\lambda$ curve near 1920, 1720, 1550 and 1400 Å appears to be superimposed upon an additional Δm_λ component, which increased progressively towards shorter wavelengths.

It has therefore been found that the ultraviolet observations extend the spectral range of the previously given photometric and spectrophotometric data and confirm that the early type giants and supergiants are deficient in their ultraviolet fluxes with respect to main-sequence stars.

Fig. 23 shows the Δm_λ versus $1/\lambda$ curves for pairs of main sequence stars and for pairs of supergiants: A B1V star is compared with B3V, B5V and B8V stars in Fig.23(a), while a B1Ia star is compared with B3Ia, B5Ia and B8Ia stars. In Fig. 23(b) the slope of the line is proportional to the temperature difference for the pair of stars compared. It has been found that the slopes of the lines for the main

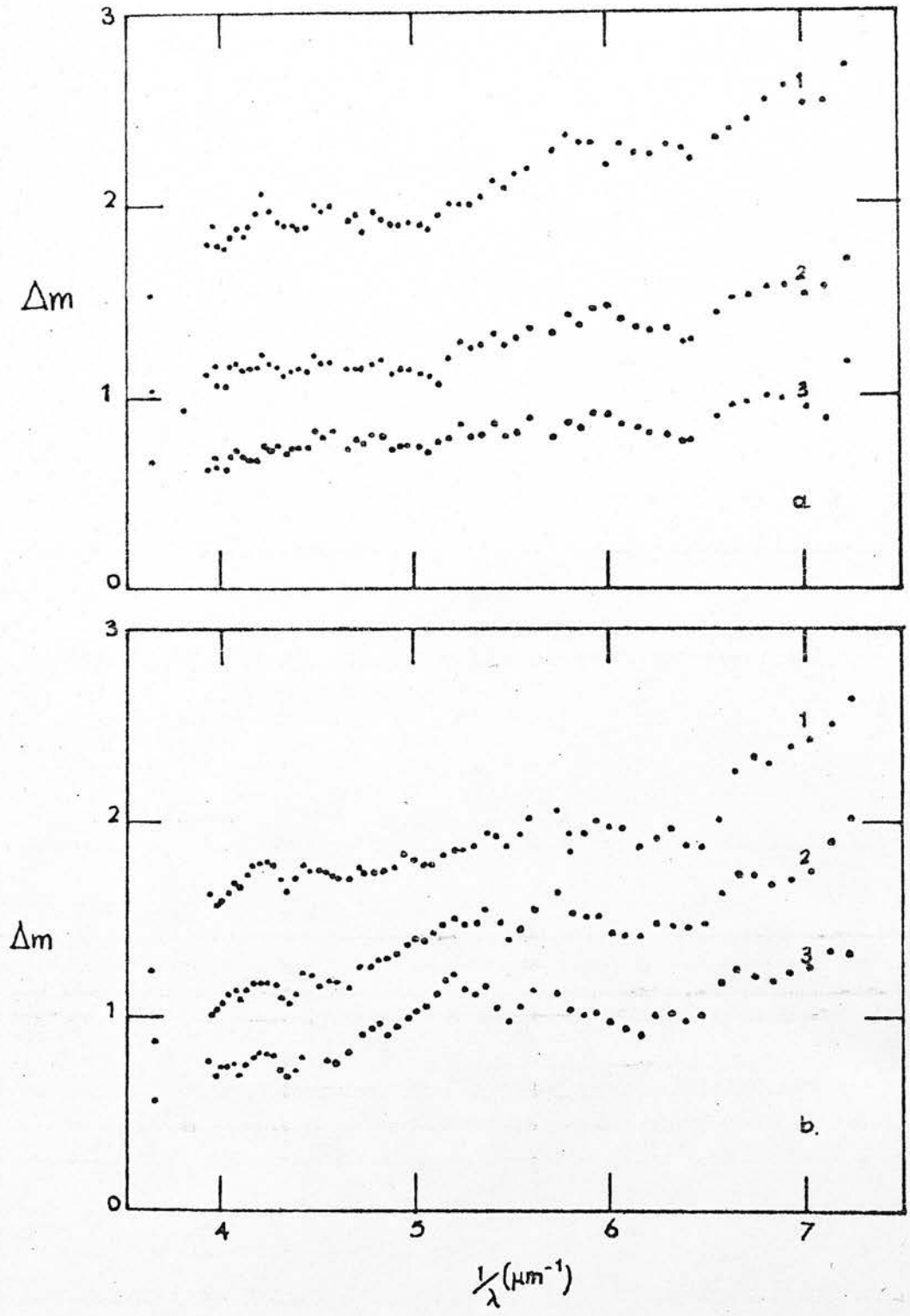

Fig. 26. Magnitude differences Δm_λ obtained by comparing ultraviolet flux distributions

a) main-sequence stars
1) HD 213998 B8 V
2) HD 209952 B5 V - HD 37209 B1 V
3) HD 120315 B3 V

b) supergiants
1) HD 34085 B8 Ia
2) HD 58350 B5 Ia - HD 64760 B1 Ia
3) HD 158408 B3 Ia

sequence pairs are approximately the same as for the corresponding supergiant pairs. In other words the decrements in effective temperature in passing from B1 through B3 and B5 to B8 are similar for main sequence and supergiant stars.

It was attempted to measure the difference in effective temperature between supergiant and dwarf stars of the same spectral type, adopting the effective temperature scale for main sequence stars given by Schild, Peterson & Oke (1971). The temperature of the main sequence stars was determined according to this scale and the supergiant's effective temperature was found in each case, assuming the blackbody energy distribution required to match the observed curves of Fig. 23. The results for spectral types B1, B3, B5 and B8 are illustrated in Fig. 24.

Thus, by assuming that the difference in colour temperature is the same as the difference in effective temperature between a supergiant and a dwarf, the effective temperature of a B1 supergiant is found to be approximately 3000K cooler than that of a B1 main sequence star; for type B5 the effective temperature of the supergiant is found to be approximately 1700K cooler than that of the main sequence star. As a further test, a comparison of the normalised energy distributions of σ^2CMa(B3Ia) and αGru(B5V) shows that the slope of Δm_λ versus $1/\lambda$ curve is close to zero, indicating that these stars have similar effective temperatures.

Stalio (1971) has also reported that luminous stars have lower effective temperatures than main sequence stars.

He establishes a temperature scale for B-type supergiants by comparing observationally determined Balmer Jumps with theoretically predicted data and his results agree closely with those given here.

From Figs. 21 a,b,c,d, where the normalised ultraviolet fluxes of a sample of B-type giants stars (included in the present set of data) are given, it can be derived that the B-type giants have effective temperatures which are intermediate between those of the corresponding supergiants and main sequence stars, and that these lie somewhat closer to the main sequence temperatures than to supergiant temperatures.

From the two pairs of A-type stars (Fig. 22i-j) the luminosity effect seems to apply only from λ1800 Å and longward whereas at the shorter wavelengths this phenomenon reverses and the luminous stars become apparently brighter than the main sequence stars. However it is not clear whether the short wavelength changes in slope (Fig. 22i-j) are caused by the supergiants or the dwarfs. Underhill (1973) has noticed that significant variations are observed between the fluxes of A-type dwarfs for $\lambda < 1800$ Å.

Data from the Tables 21 and 23 have been used to examine the luminosity effect in the visible range. The stars were selected on the basis of small interstellar reddening so there are no uncertainties in using the mean extinction law.

Within the accuracy of the observations no luminosity effect has been observed in the visible. An example is illustrated in Fig. 25(a,b) which shows the observed

energy distribution, for stars of the same spectral type and different luminosity class.

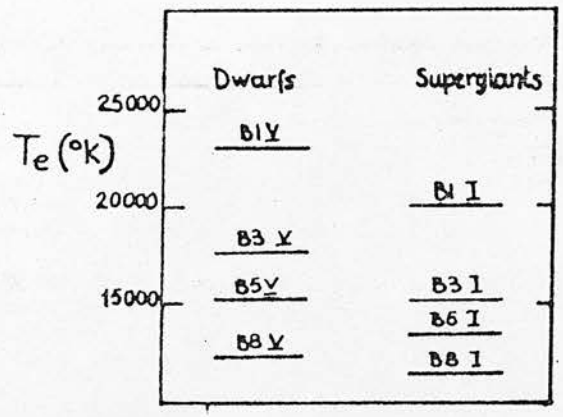

Fig. 24 Effective temperature scale for supergiants and dwarfs.

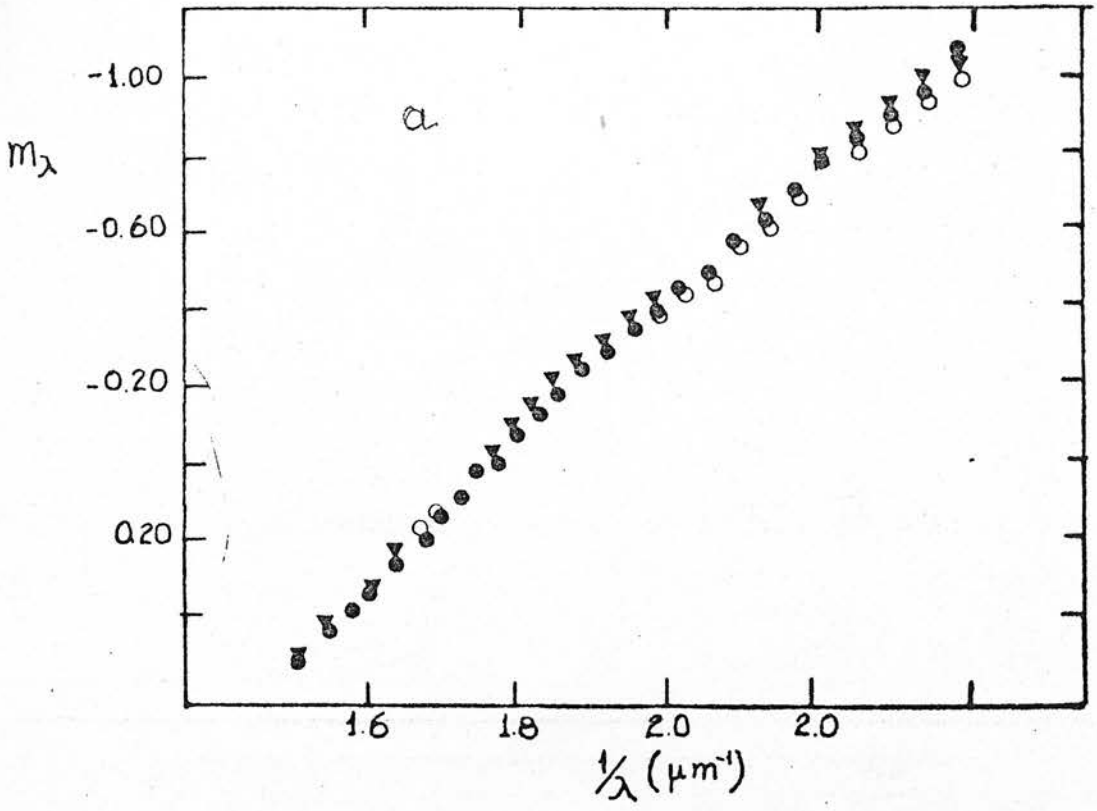

a) ● HD 205021 B2 III; ▼ HD 3360 B2 V; o HD 886 B2 IV.

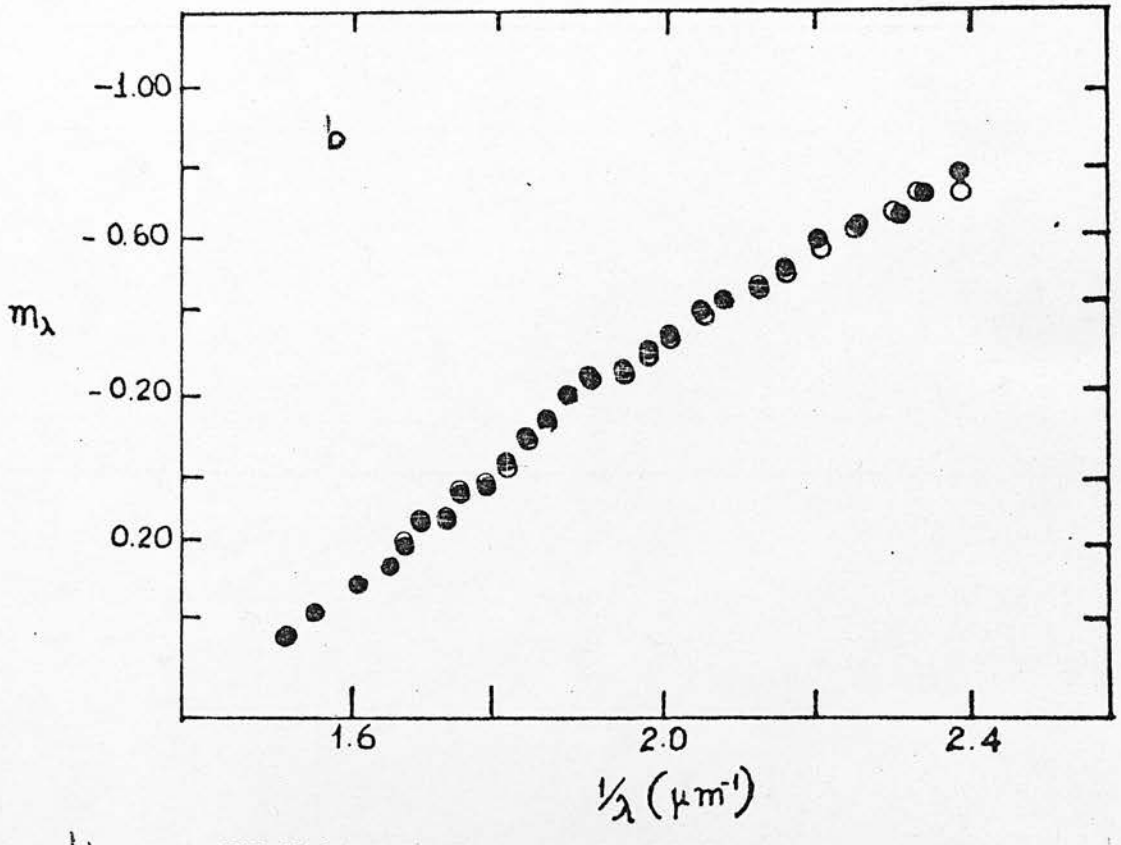

b) ● HD 218045 B9 V; o HD 186882 B9 III.

Fig. 25 Observed energy distribution in the visible for stars with the same spectral type and different luminosity.

IV 2. CONJECTURES ON THE EXPLANATION OF THE LUMINOSITY EFFECT

The purpose of this section is to examine how gravity, multiple systems, departures from LTE, convection, rotation, opacity and blanketing could influence the continuum, and how the observed deficiencies for early-type supergiants and giants in their fluxes with respect to main sequence stars of the same spectral type could be caused by one or a combination of these effects.

a) Gravity

From rocket and satellite observations Carruthers (1969) has noted that supergiants compared to dwarfs of the same spectral type are fainter by up to one magnitude in the 1050 Å - 1130 Å band. This effect is illustrated in Table 14 (Mihalas 1970) where comparison of typical pairs is given.

TABLE 14

Typical comparisons of dwarfs and supergiants of same spectral type

stars	spectral types	R
σ Ori/ζ Ori	O9.5V/O9.5Ib	1.75
υ Ori/ε Ori	BOV/BOIA	2.04
η Ori/κ Ori	BO.5V/BO.5Ia	2.70

The third column of Table 14, denotes the ratio, R, of fluxes for λ = 1115 Å, between the dwarf and the supergiant of each pair. Carruthers (1969) has suggested that this effect can be explained by gravity changes, using

Mihalas' (1965) models, although the effect predicted theoretically was much smaller. For T_{eff} = 36000K the predicted value is 1.2, (for log g = 4.0 and log g = 3.5), which is still small to explain the observed ratio. Auer & Mihalas (1970) produced additional models and for T_{eff} =35000K (for log g = 3.5 & log g = 4.0) the value R is $\sim$1.5. Thus a slight decrease in the gravity from 3.3×10^3 to 2×10^3 increases the flux deficiency appreciably. It has also been suggested that this ratio is not dependent on the spectral type. This is inadequate to explain the observed luminosity effect. It has been noticed that for pairs containing supergiants, and dwarfs, Δ m in the 1420 Å region is observed to be$\sim$0.6 mag corresponding to a value of 1.7 for the ratio R of the normalised flux of the main sequence star to that of the supergiant. Recent line blanketed model atmospheres calculations by Kurucz, Peytremann & Avrett (1974) suggest that surface-gravity differences alone are not sufficient to account for values of R as large as this. The final column in Table 15 gives the ratio of the normalised fluxes at the higher to the lower surface gravity. Comparison of the computed values of R with the observed value 1.7 indicates that, for a given effective temperature, gravity-dependent effects make only a small contribution to the observed ultraviolet flux deficiencies of supergiants. Although the Kurucz, Peytremann & Avrett (1974) models assume conditions of local thermodynamic equilibrium (LTE), the computed values of R given above are not expected to be changed significantly by inclusion of the non-LTE effects for the

TABLE 15

Computed values of F_{1422}/F_{5000} for different effective temperatures and surface gravities

	Log g			
T_{eff}	4.0	3.0	2.0	R
20 000 K	21.3	20.2	–	1.05
15 000 K	9.5	–	8.4	1.13

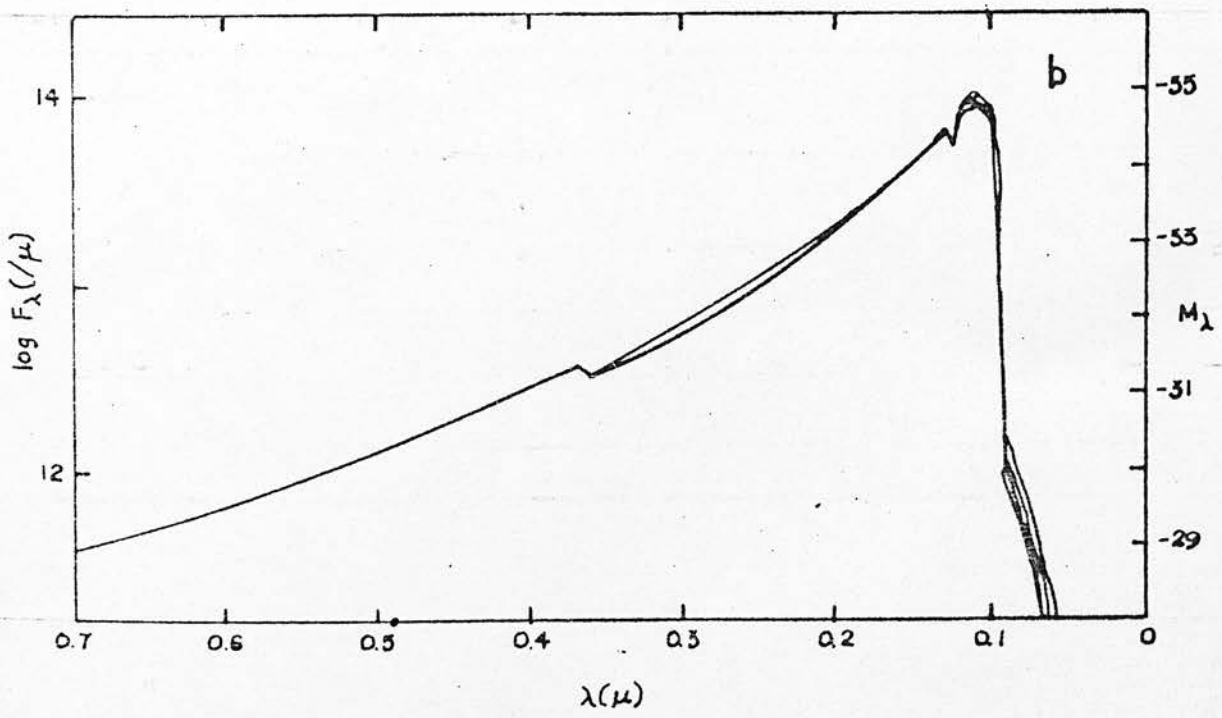

Fig. 26 The effect on the flux distributions of changing gravity (a) for effective temperature 8000 K and gravities 2, 2.5, 3, 3.5, 4, 4.5 (b) for effective temperature 2500 K and gravities 3.5, 4, 4.5, 5 (Kurucz, Peytremann & Avrett 1974).

temperature range considered here. The effect on the flux distributions of changing gravity for effective temperature 8000K and 25000K is shown in Fig. 26: Kurucz et al. (1974).

b) Multiple systems

It is well known that the vast majority of B stars belong to binary or multiple systems, and the observed spectra may be affected by the presence of a fainter companion of different spectral type. This could explain a phenomenon like the one discussed here, but the curves plotted in Fig. 25 for eight B-type pairs are extremely similar and it can not be accepted that each star has an additional unidentified companion of the required spectral type and magnitude. Therefore multiplicity seems a very improbable explanation of the luminosity effect.

c) Departures from LTE

The fact that departures from LTE occur at the depths where the Balmer and Paschen continua are formed suggests that these departures may appreciably affect the continuous energy distribution. If the observations are interpreted according to LTE models, the effective temperatures will be systematically in error. Strom & Kalkofen (1966) estimated these effects and using an approximate atomic model they have shown that the changes can be as large as 2000K. Further work by Mihalas (1967a, b, 1968) and Mihalas & Stone (1968) using improved atomic models and larger collision rates showed much smaller departures which, in fact, negligible for the main sequence stars.

An analysis (Mihalas 1972) of the effects of departures from LTE on colours measured in the uvby system, has shown that systematic errors in estimates of T_{eff} are introduced.

At log g = 4, the error ΔT_{eff} is essentially zero, at log g = 3, $\Delta T_{eff} \approx$ 200K and at log g = 2.5 $\Delta T_{eff} \approx$ 500K.

d) Convection

Convection is very unlikely to be the explanation of the luminosity effect, because it has been found that for main sequence B stars the flux carried by this mechanism is not important. Atmospheric motions in the upper parts of the photosphere of B stars may be of considerable significance in affecting the temperature, pressure, structure and abundance determination. Even for cooler main sequence A stars with temperatures greater than 8500K (Strom 1969) the effect of convection is not important.

e) Rotation

Rotation is expected to have an effect on the ultraviolet spectrum of B stars. This region is quite sensitive to the effective temperature because the Planck function peaks in the near ultraviolet. Consequently fluxes observed shortward of the peak of the Planck function corresponding to the effective temperature of the star will be very sensitive to temperature variations over the surface of the star.

It has been reported that (Collins & Harrington 1966) that calculations show the Balmer continuum region to be

weakly sensitive to the effects of rotation, in the sense that it is steeper for the higher rotational velocities.

Departures from LTE will also enter in a way to counteract the effects of rotation on the Balmer discontinuity. In the low surface gravity regions, the Balmer discontinuity will be decreased owing to departures from LTE; LTE regions would be expected to have a larger Balmer discontinuity because of their lower temperature.

Finally the changes in temperature introduced by rotational effects can be of the order of 5 to 10% (Strom 1969) which is less than the observed deficiencies. It has also been reported (Abt & Hunter 1962; Van de Heuvel 1965) that for B stars the rotational velocities are independent of their spectral subtypes, so if rotation causes this effect it should be constant for all B spectral types, but this does not happen here.

f) Opacity

It is well known that the only important sources of continuous opacity in most B stars arise from hydrogen, neutral and single ionised helium and electron scattering (Strom 1969). Recently silicon has been found as an important source of opacity and Strom (1969) has shown that silicon over-abundances of a factor of 30 result in changes in temperature of about 1000 to 1500K. The silicon discontinuity at 1527 Å ranges from 0.5 to 1.5 mag even for normal silicon-to-hydrogen ratios in the temperatures of early type stars.

Although this effect could be a possible explanation

of the effective temperature difference, the similarity of the curves plotted in Fig. 25 for the studied stars does not allow us to suggest that overabundances of silicon or another element has occurred to all stars.

g) Blanketing

The blanketing effect is very important for the appearance of the stellar spectra. The primary effect, in most cases, is to make the blanketed atmosphere to appear hotter than an unblanketed atmosphere at the same effective temperature. Therefore if unblanketed model atmospheres are used to estimate the effective temperature, the derived values will be too high. Gaustad & Spitzer (1961) were the first to study systematically the blanketing effect on the spectra of B stars. The first attempt to include the effects of a large number of lines in a model atmosphere calculation was that of Strom & Kurucz (1966) in which 30 000 lines were used to construct the distribution functions for a model of T_{eff} = 6500K. Mihalas & Morton (1965) have computed a model of a BIV star where the strong lines suggested by Gaustad & Spitzer (1961) were included in their calculations. The computed emergent flux is shown in Fig. 27. The integrated emergent flux of the blanketed model corresponds to T_{eff} = 21900K (Mihalas 1970).

The flux distribution of an unblanketed model with the same effective temperature is given and the effects of line blanketing are really very important. The flux in the continuum between the lines lies far above the unblanketed continuum, and the energy deficit in the

ultraviolet due to the line blocking is compensated by an appreciable rise in the visible continuum. Consequently if the observed flux of a star in the visible region were fitted to an unblanketed model, the error in the T_{eff} could be of the order of 2100K. It was found that many strong lines and the overlapping wings of weaker ones absorb much of the continuous radiation, particularly for $\lambda < 1410$ Å.

For stars hotter than B5, more than half of the total emergent flux comes from the Balmer continuum. At these high temperatures many elements, including the abundant light elements, are twice or three times ionised, and as a result, strong lines of many of these elements fall in the ultraviolet, especially in a region where a majority of the flux emerges. Thus, the effects of blanketing on the temperature can be very serious and the temperature estimates without taking into account the blanketing can give large errors.

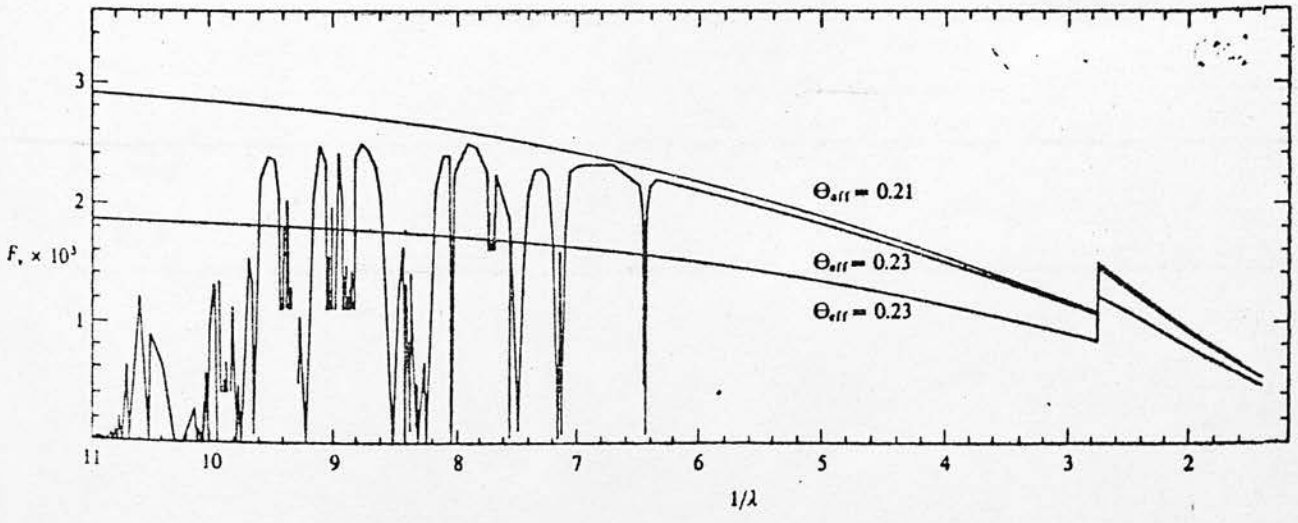

Fig. 27 Flux from blanketed and unblanketed LTE models, Blanketed model corresponds to Teff = 0.23, Abscissa; $1/\lambda$, where λ is in microns; ordinate: $F_\nu \times 10^3$ (Mihalas & Morton 1965).

Going to later B spectral types, blanketing in the range between 2000 Å to 3000 Å has been found to be very important (Strom 1969) as well.

In the spectra of A-type stars the Balmer lines reach their maximum strength and the major part of the radiation emerges in the region where these lines overlap and coalesce into the Balmer continuum. Thus a large fraction of the radiation of these stars is directly influenced by the presence of these lines. Observationally the presence of the lines completely changes the appearance of their spectra.

Blanketing in the near ultraviolet towards the visible region of the spectrum is of increasing importance since the atoms are essentially now all neutral and singly ionised at A-star effective temperatures (Strom 1969).

The blanketing effect generally is less important for the luminous B stars than for main sequence stars because of their low densities, although turbulent broadening does increase the line width in a way. The line blanketing is more significant for stars of higher surface gravities because of the increased electron and atom densities and the resulting consequences on the line broadening.

It has been reported by Morton (1969) that for a model of a spectral type the blanketing lowers the general level of the ultraviolet continuum and when lines appear within the passband of the detector there is an additional reduction of the predicted flux.

To summarise, we point out that blanketing changes temperature by about 2000K for B2 stars and less for later spectral types (Strom 1969). So blanketing effect is very important for early type stars; it gives figures appropriate to the observed deficiency; and is to some extent luminosity dependent. This effect is probably a contributor to the explanation of the observed luminosity effect, assuming that the observed band, the strong blanketed area and the band where most of the emitted flux emerges for a particular T_{eff} are taken into consideration. Of course, this does not prevent us from suggesting that many other effects make their contribution in favour of or against the observed luminosity effect.

V TEMPERATURE SCALE

V. 1 EFFECTIVE TEMPERATURE

Model atmospheres have been developed in order to derive theoretical spectra which could be compared with real ones. Theoretical assumptions and mechanisms give spectral intensity distributions which should approach the real ones. If the agreement in detail between the theoretical spectrum and the stellar spectrum is good, one may conclude that themperature, pressure and structure of the model represent the stellar atmosphere well whereas the theory of spectrum formation and the abundances of the elements which have been adopted may describe the stellar atmosphere.

The problem is to bridge the theoretical and observational spectra and to arrive at a meaningful comparison between them. Assuming that a proper comparison has been done, the required basic information could be extracted either from a successful fit or from trying to understand the physical meaning of the misfit. Of course a perfect fit does not always ensure us that the parameters are exactly those of the model and that the whole process is completely clarified. Simplifications in the computation of models may produce the same models for a different set of temperature, gravity and chemical composition.

There are many methods of comparing the real spectra with the synthetic spectra using the continuum or the spectrum lines. The wide-band observations give information

on the energy distribution of the stars and the widest band that can be imagined includes all photons from $\lambda = 0$ to $\lambda = \infty$. Multicolour photometric scans and spectrophotometry give a more realistic picture of the spectrum of the star that can be considered with more confidence.

It has already been mentioned that during recent years the ultraviolet flux distributions on an absolute scale have been obtained for a considerable number of stars. This part of the spectrum is especially important for early type stars where they emit most of their flux. It is difficult to decide about the atmospheric parameters without knowing what the ultraviolet spectrum of a star looks like. On the other hand the theoretical work on computing model atmospheres has made tremendous progress. The theoretical stellar spectra are very elaborate and detailed and cover a wide range of temperatures and gravities.

A temperature scale for early type stars has been derived from the comparison of the observed stellar spectra with theoretical ones. The observed stars (Table 16) are O,B and early A stars. Data in the ultraviolet (1392 Å to 2740 Å) were provided by the Edinburgh TD1 team and are now published (Jamar et al. 1976). The fluxes in the bands 2500, 2460, 2260, 2190, 2060, 1920, 1860, 1660, 1490, 1460, 1392 Å were derived from consecutive spectral data. Each band is named according to its central wavelength and has a width of 100 Å. The fluxes obtained at these wavelengths were converted to magnitudes

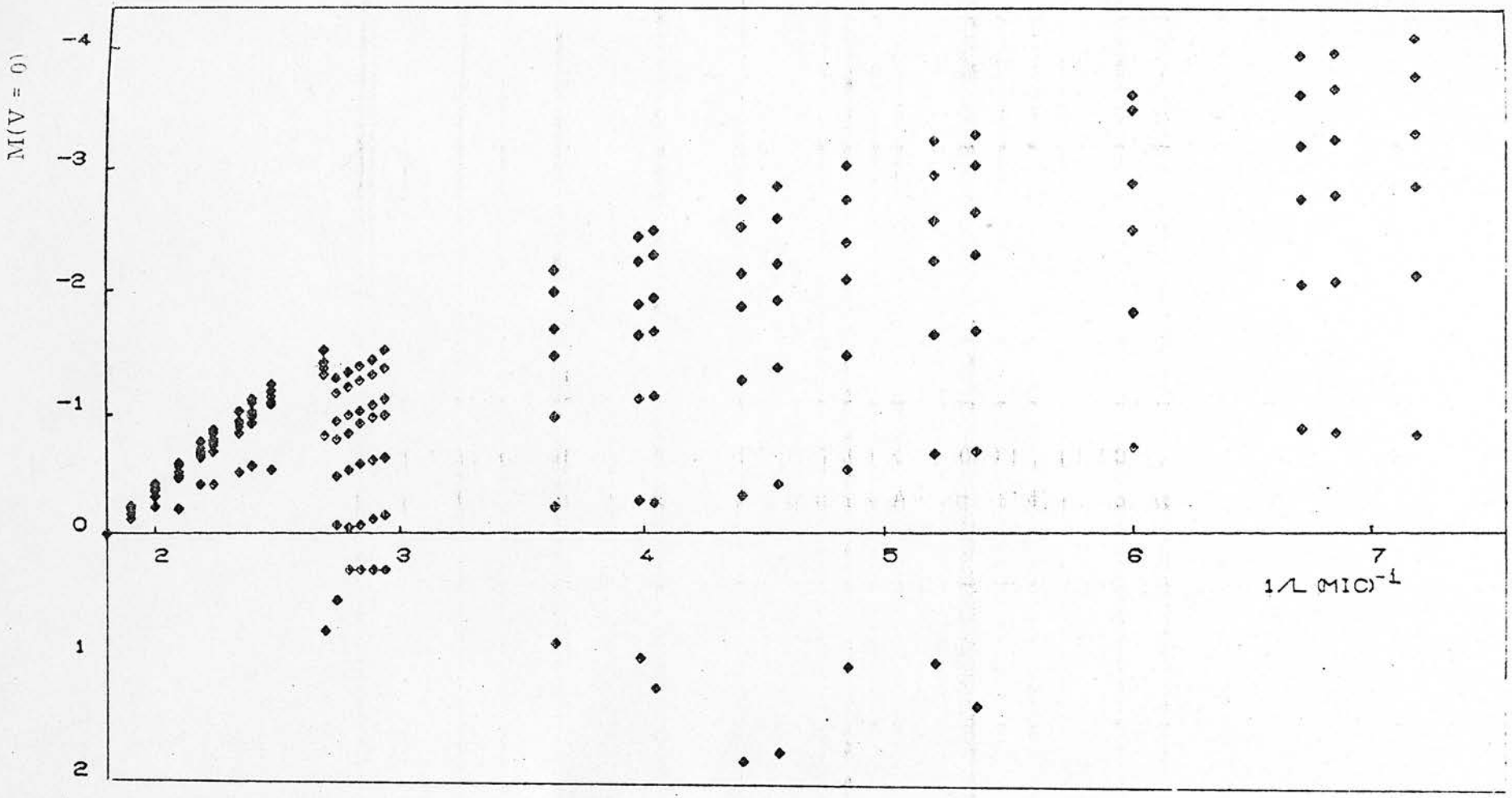

Fig. 28. Spectra distribution for log g = 4 and Teff 7500 K, 10000 K, 12500 K, 15000 K, 17500 K, 20000 K, 22500 K from Kurucz, Peytremann & Avrett(1974) model atmospheres.

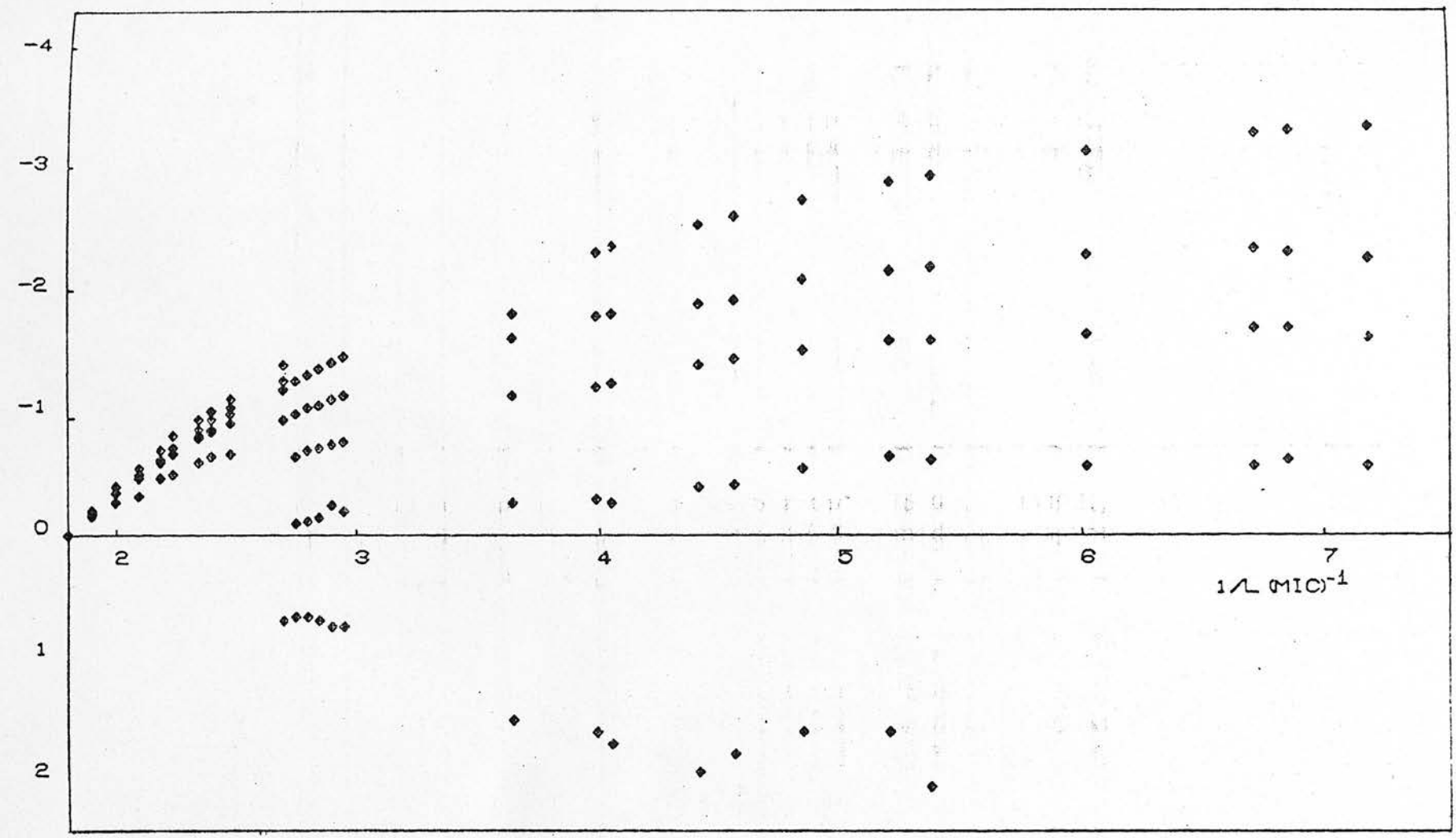

Fig. 29 Spectra distribution for log g = 2 and temperatures 7500 K, 10000 K, 12500 K, 15000 K, 20000 K from Kurucz, Peytremann & Avrett (1974) model atmospheres.

TABLE 16

Stars observed

	HD	Name	V	B-V	Sp.Tp
1	15318	ξ^2 Cet	4.27	-0.05	B9III
2	18326	-	7.28	+0.38	O8V
3	24398	ζ Per	2.83	+0.13	B1Ib
4	24431	-	6.72	+0.37	O9V
5	24760	ε Per	2.88	-0.17	BO.5V
6	30614	α Cam	4.38	+0.02	O9.5Ia
7	31327	-	6.06	+0.41	B2Ia
8	32249	ψ Eri	4.80	-0.20	B2V
9	33988	-	6.88	+0.25	B2V
10	34085	β Ori	0.08	-0.03	B8Ia
11	35468	γ Ori	1.63	-0.23	B2III
12	36371	χ Aur	4.75	+0.30	B5Ia
13	36512	ν Ori	4.60	-0.26	BOV
14	36879	-	7.58	+0.20	O6V
15	37128	ε Ori	1.70	-0.19	BOIa
16	38771	κ Ori	2.04	-0.18	BOIa
17	40589	-	6.05	+0.25	B9Ia
18	42087	3 Gem	5.76	+0.20	B2.5Ia
19	43384	9 Gem	6.28	+0.44	B3Ia
20	45910	-	6.77	+0.33	B2III
21	46149	-	7.58	+0.17	O8V
22	47240	-	6.15	+0.15	B1Ib
23	47839	15 Mon	4.66	-0.25	O7III
24	52382	-	6.48	+0.20	B2.5Ia
25	53367	-	6.97	+0.43	BOIV
26	54662	-	6.21	+0.03	O6V
27	58131	-	7.37	+0.34	B2V
28	58350	η CMa	2.47	-0.06	B5Ia
29	66811	ζ Pup	2.25	-0.28	O5V
30	77581	-	6.88	+0.56	BOIa
31	79186	-	5.00	+0.20	B3Ia
32	87734	η Leo	3.55	-0.02	AOIa
33	87901	α Leo	8.14	-0.11	B7V
34	91316	ρ Leo	3.85	-0.14	B1Ib
35	102647	β Leo	2.12	+0.09	A3V
36	149438	τ Sco	2.83	-0.24	BOV
37	152614	i Oph	4.37	-0.09	B8V
38	155763	ζ Dra	3.17	-0.11	B7III
39	160762	i Her	3.80	-0.17	B3IV
40	164353	67 Oph	3.97	+0.02	B5Ib
41	176437	γ Lyr	3.23	-0.04	B9III
42	182255	3 Vul	5.18	-0.12	B6III
43	188209	-	5.63	-0.07	O9.5I III
44	188260	13 Vul	4.57	-0.06	B9III
45	195810	ε Del	4.04	-0.12	B6III
46	197345	α Cyg	1.25	+0.09	A2Ia
47	214993	12 Lac	5.22	-0.12	B2III
48	218376	1 Cas	4.88	-0.02	BOIII
49	222173	i And	4.28	-0.10	B8V
50	224572	σ Cas	4.58	-0.06	B1V

m_λ, where $m_\lambda = -2.5 \log I_\lambda - 21.1$ (Oke et al. 1970) and I_λ is the mean flux at λ in erg s^{-1} $\AA^{-1}$ cm^{-2} (Nandy 1976c).

Data in the visible spectral range have been observed with a single or a two channel spectrum scanner (details are given in Chapter III) and they are listed in Appendix I, II.

The ATLAS computer programme (Kurucz 1970) has been used to provide the necessary theoretical spectra (Kurucz, Peytremann & Avrett 1974, and Kurucz 1976 private communication). The grid of model atmospheres used covers temperatures from 5500K to 50000K and gravities from $10^{0.5}$ to 10^5 cm s^{-2}. Fig. 28 and Fig. 29 illustrate the spectra distribution for some of their models with different gravities and temperatures.

For each star the observed and intrinsic flux distribution in the visible and ultraviolet has been plotted (Figs. 30 - 79). Corrections for interstellar extinction have been applied using the mean extinction law (Nandy et al. 1975c). Smooth curves have been drawn for each star through the data, one for λ 5556 $\AA$ up to the Balmer Jump and another curve through the shorter wavelengths. The curve that passes through visible (shortward of Balmer Jump) and ultraviolet values connects two sets of data obtained by different instruments, and any displacement needed for their combination is found to be within the limits of photometric accuracy.

The synthetic spectra from Kurucz, Peytremann & Avrett (1974) and private communication (1976) model

atmospheres have been superimposed on observed spectra and a temperature scale for early type stars has been derived assuming log g = 2 for supergiants, log g = 3 for giants and subgiants and log g = 4 for dwarfs (Table 17 column 7).

To illustrate this process, Fig. 80 shows the observed colour (m - V) for ζ Per (HD : 24398, B1Ib, E(B-V) = 0.35) by filled circles and that corrected for reddening $(m - V)_o$ by open circles. The solid line shows the fitted model.

In Table 17, T_{eff} is also given for some of these stars by previous workers using different techniques and models. $T_{eff}(2)$ Hanbury et al. (1967), $T_{eff}(3)$ Morton et al.(1968), $T_{eff}(4)$ Heintze (1969), $T_{eff}(5)$ Hyland (1969), $T_{eff}(6)$ Schild et al.(1971), $T_{eff}(7)$ and (8) Nandy et al.(1975b) and $T_{eff}(9)$ Code et al. (1976b).

The grid of models used is listed in Table 18. Assuming log g constant for T_{eff} = 8000K the step of 500K in temperature gives a difference in magnitude $\sim$0.3 mag for the visible part of the spectrum and $\sim$0.6 mag for the ultraviolet part of the spectrum. These differences for T_{eff} = 9000K have the values $\sim$0.2 mag and 0.4 mag respectively. For 10000K $< T_{eff} <$ 20000K the grid used has a step of 1000K in temperature and for T_{eff} = 12000K the step gives a difference $\sim$0.15 mag for the visible part and $\sim$0.3 mag for the ultraviolet part of the spectrum. For T_{eff} = 20000K the step is 2000K and the differences are

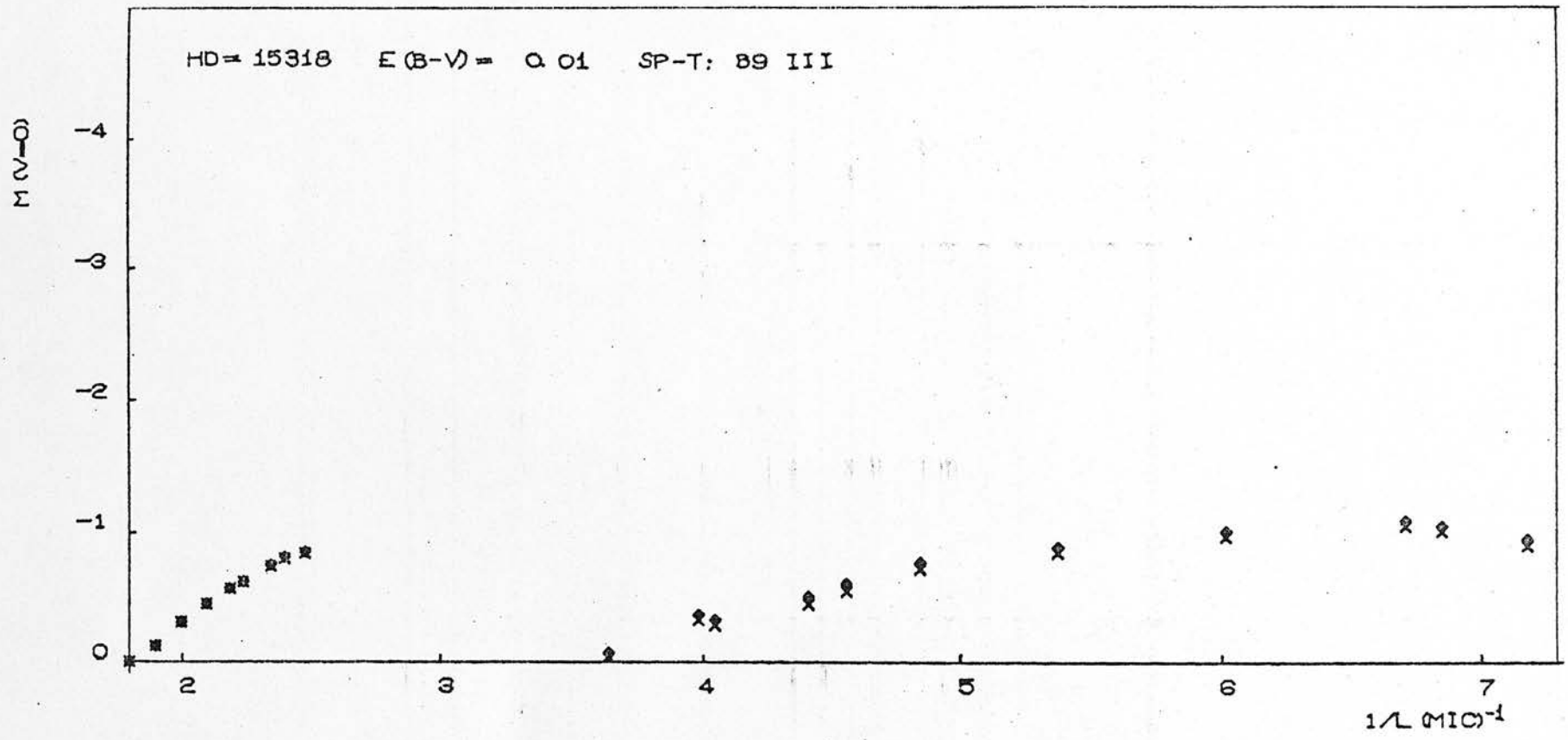

Fig. 30 × Observed magnitudes

◆ Magnitudes corrected for interstellar extinction

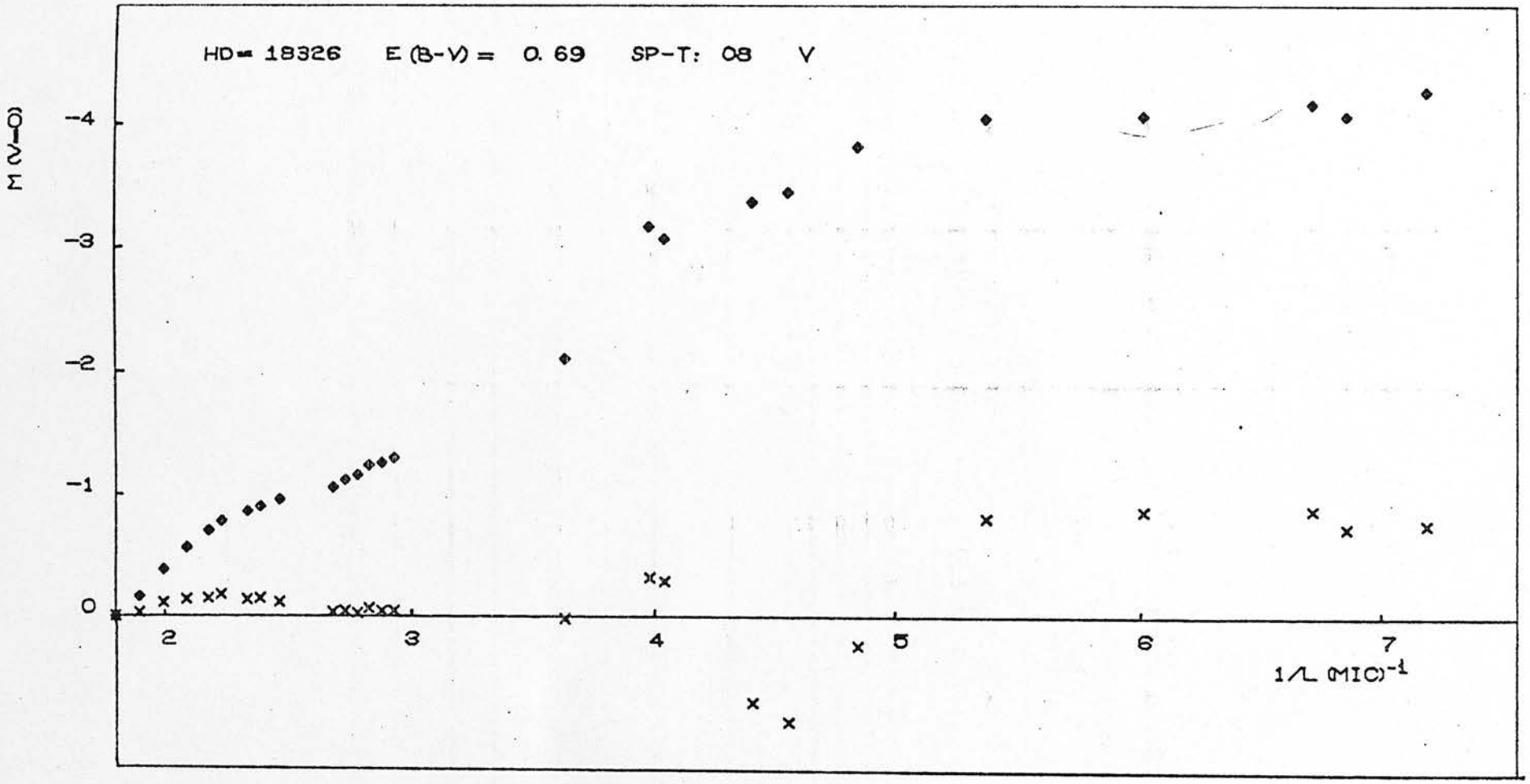

Fig. 31 × Observed magnitudes

◆ Magnitudes corrected for interstellar extinction

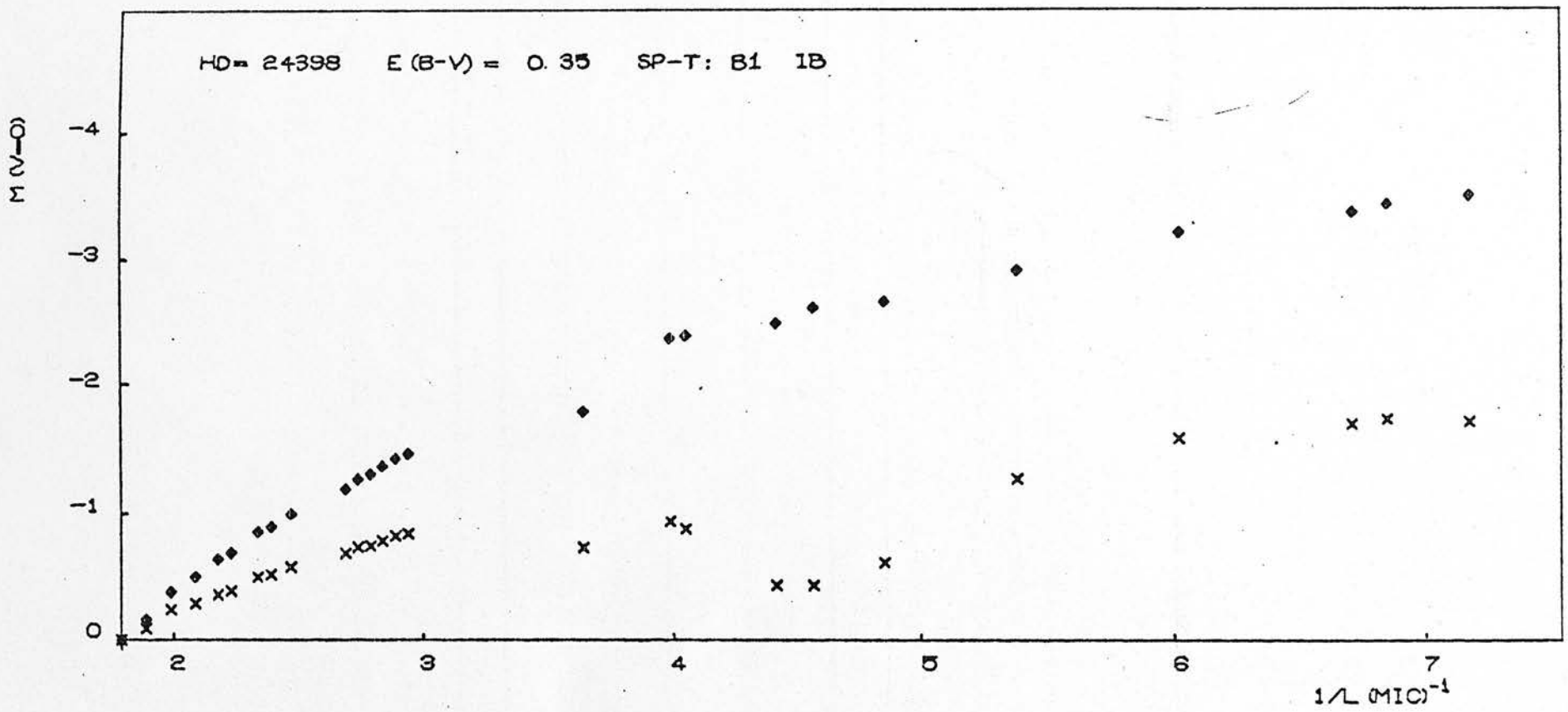

Fig. 32 × Observed magnitudes

◆ Magnitudes corrected for interstellar extinction

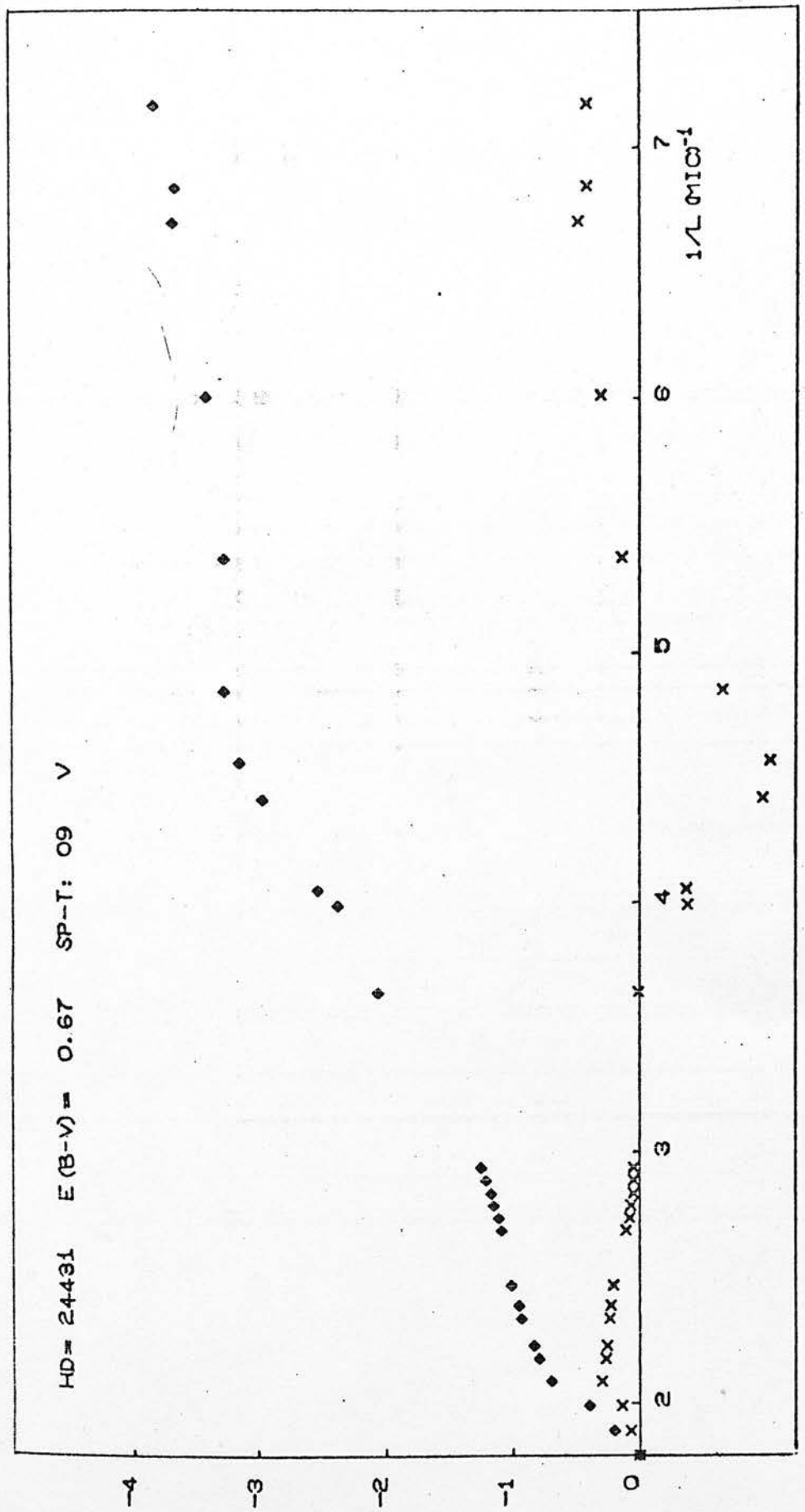

Fig. 33 × Observed magnitudes

◆ Magnitudes corrected for interstellar extinction

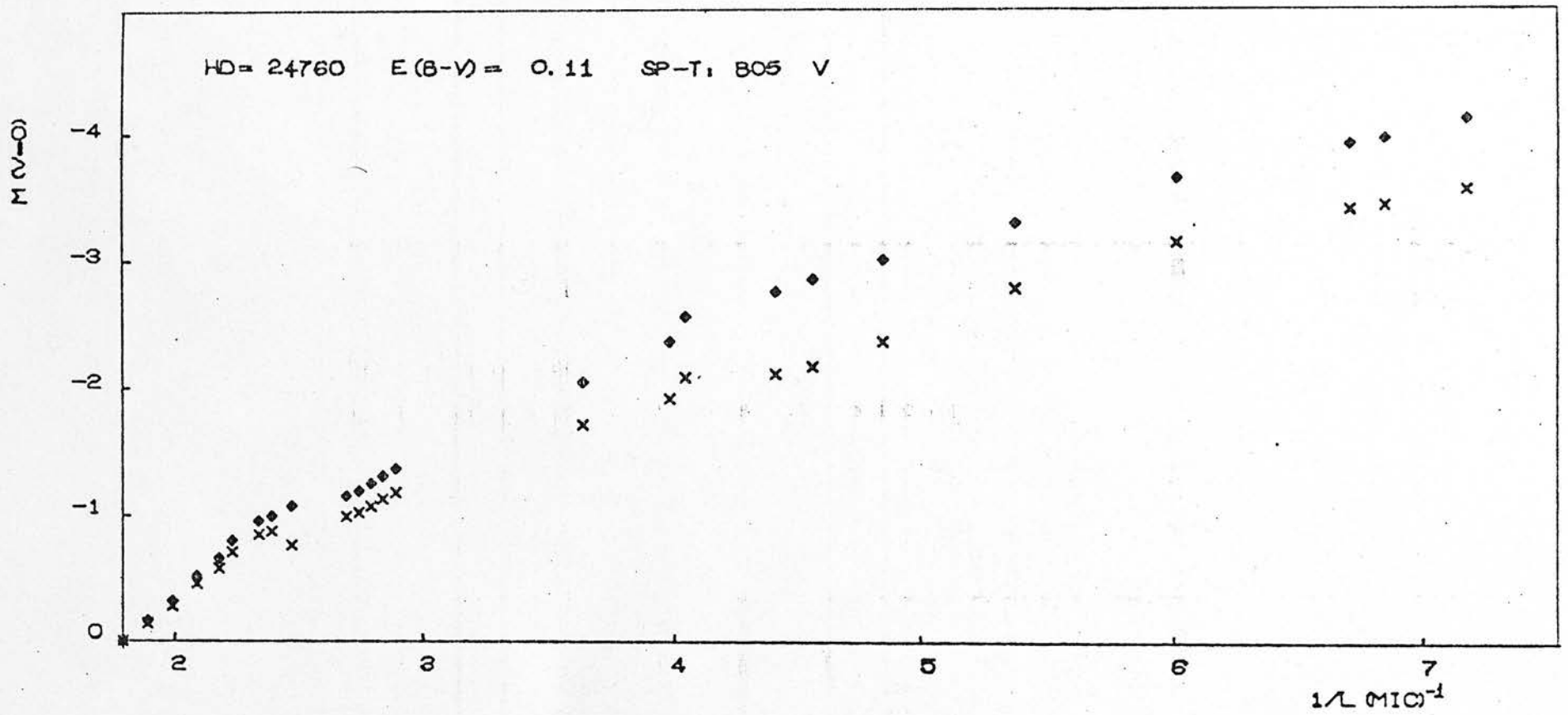

Fig. 34 × Observed magnitudes

◈ Magnitudes corrected for interstellar extinction

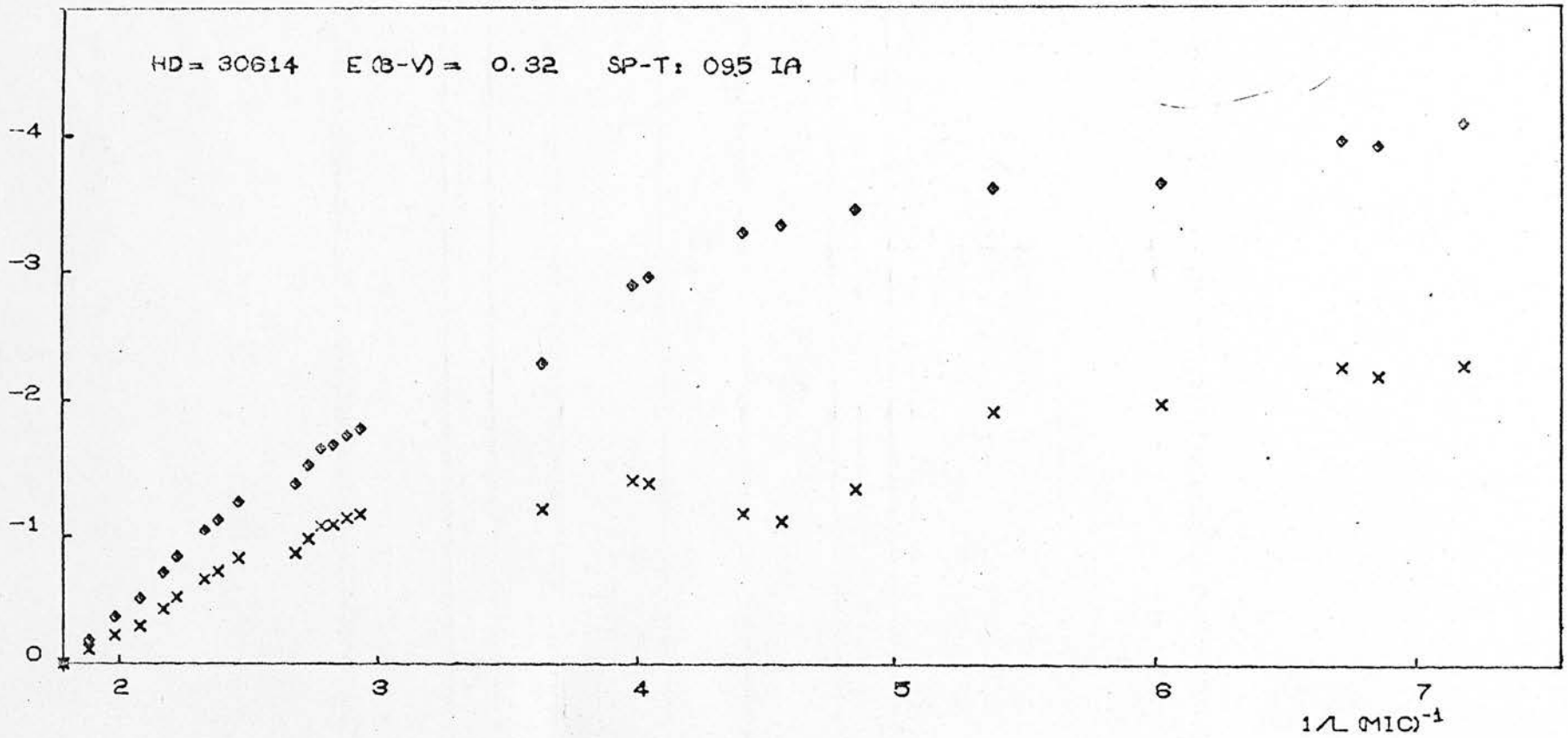

Fig. 35 × Observed magnitudes

◈ Magnitudes corrected for interstellar extinction

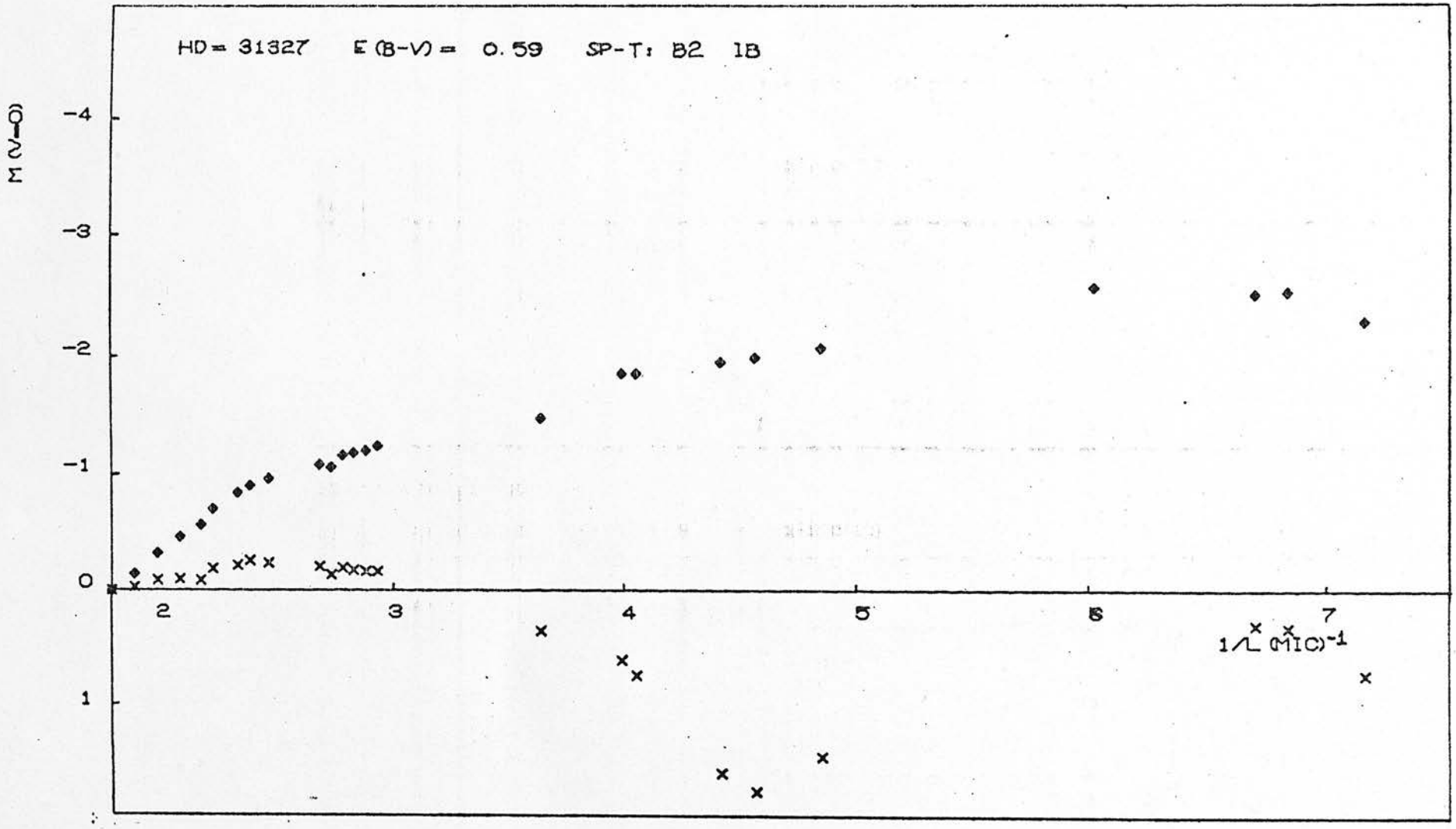

Fig. 36 × Observed magnitudes

◈ Magnitudes corrected for interstellar extinction

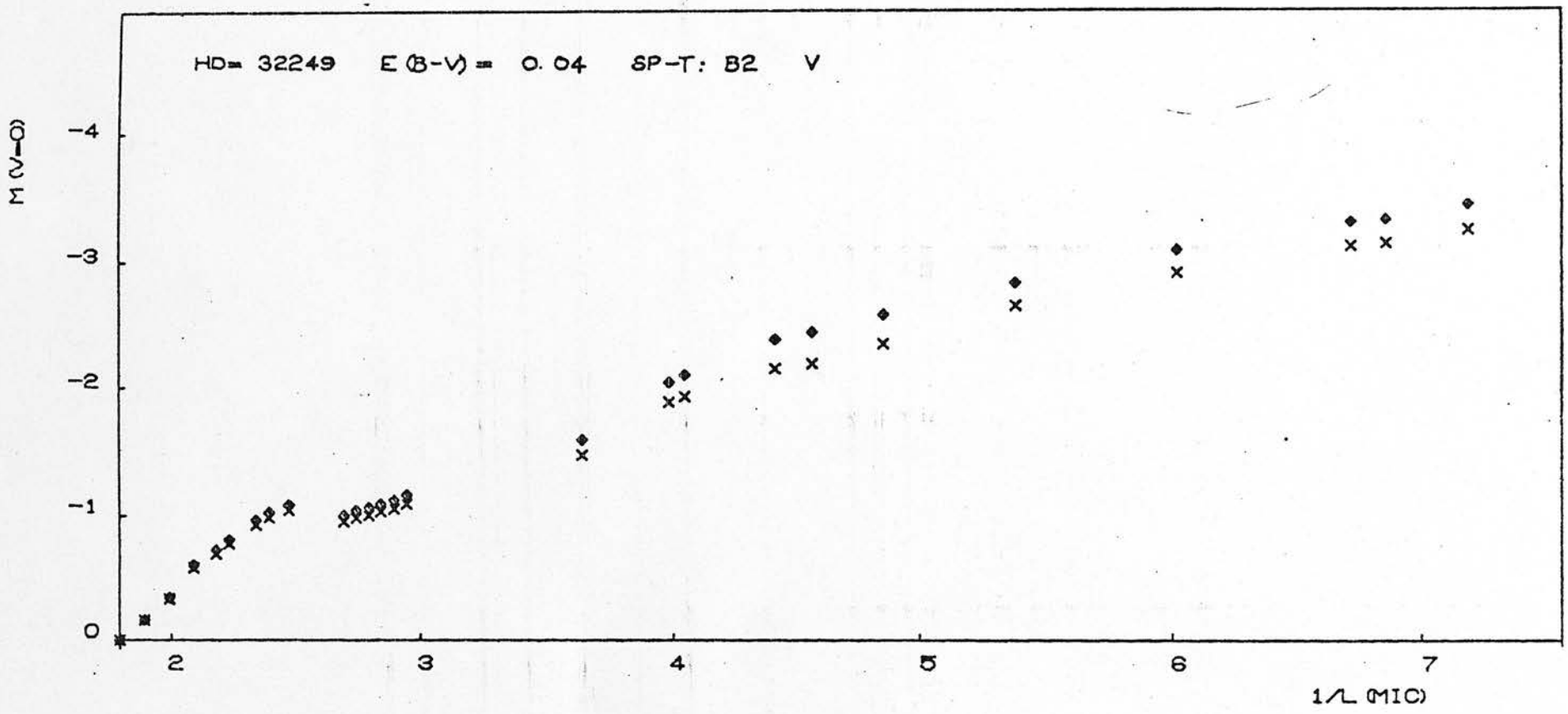

Fig. 37 × Observed magnitudes

◈ Magnitudes corrected for interstellar extinction

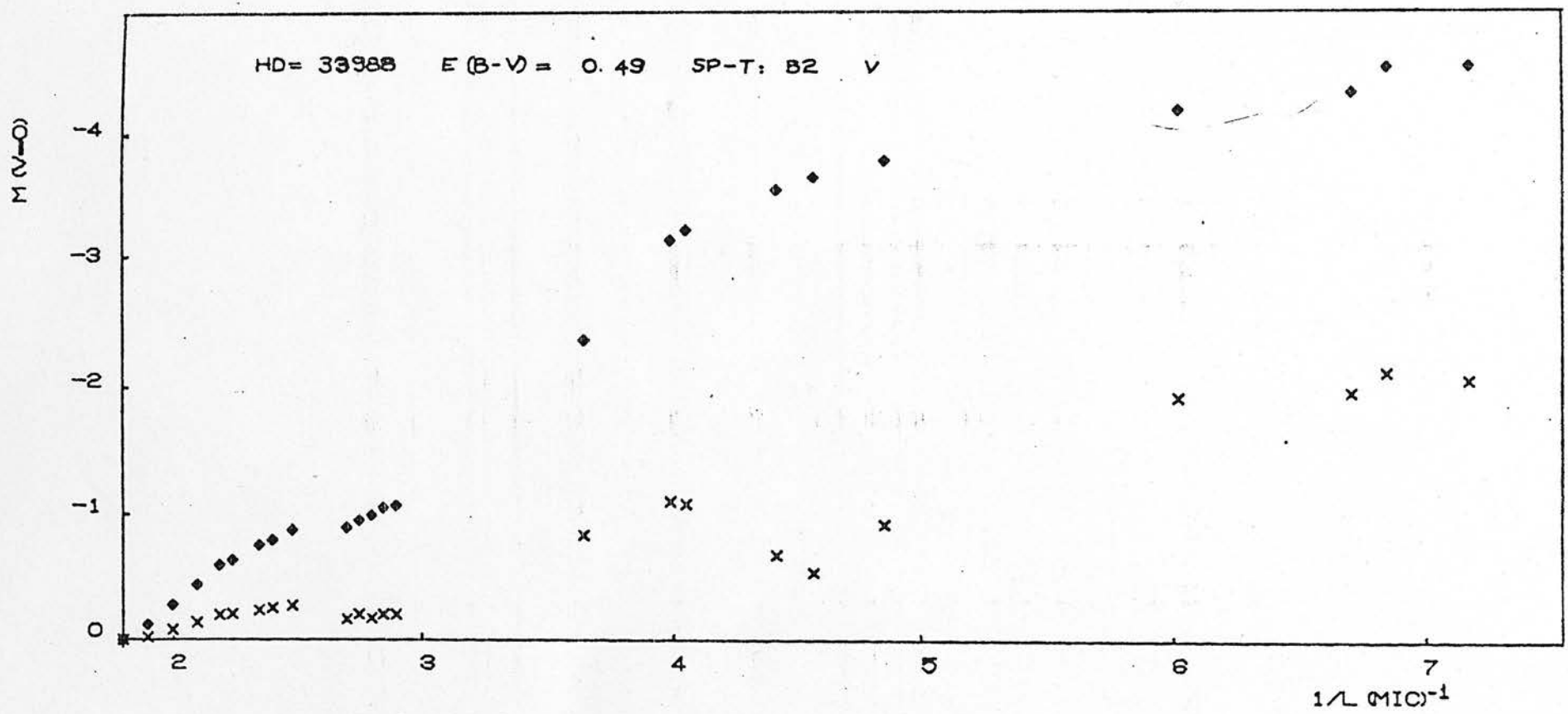

Fig. 38 × Observed magnitudes

◆ Magnitudes corrected for interstellar extinction

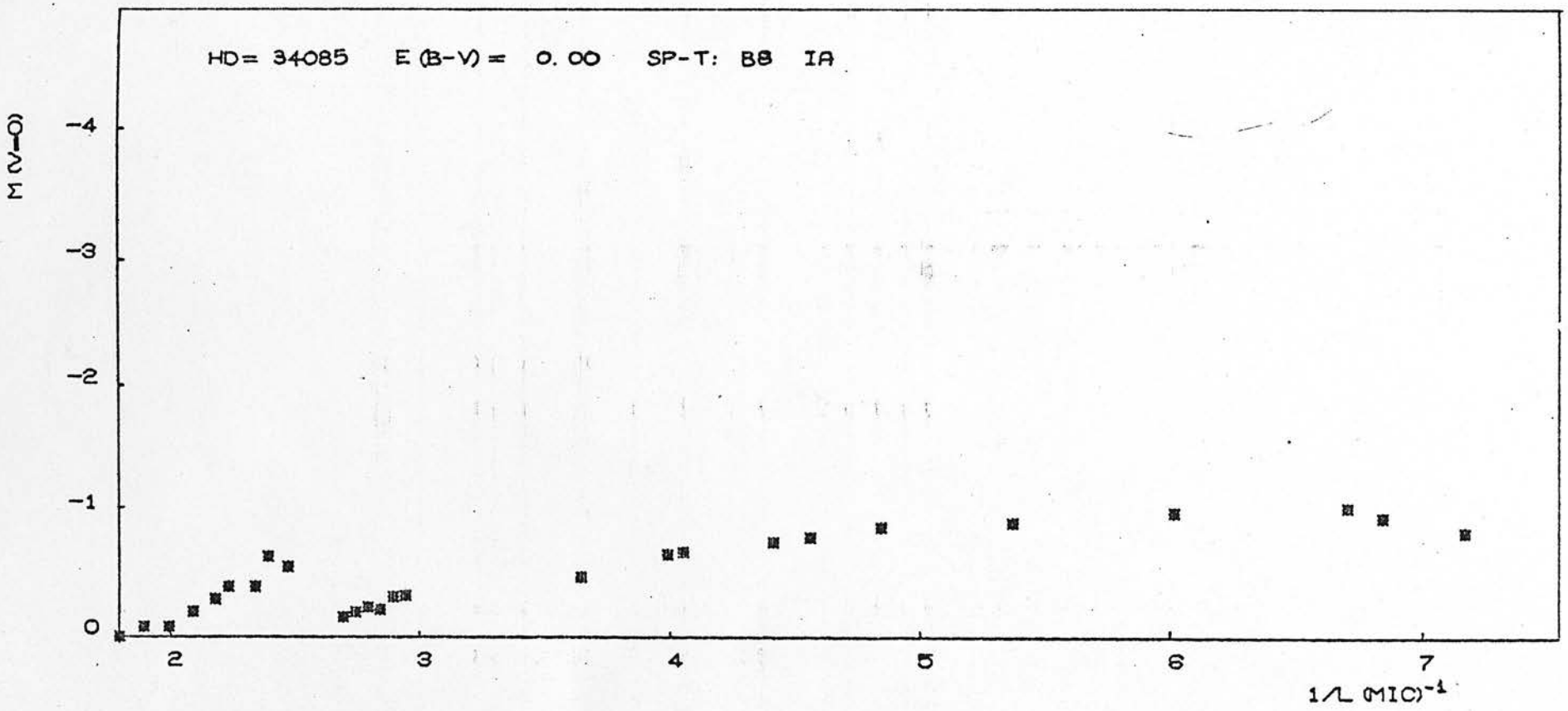

Fig. 39 × Observed magnitudes

◇ Magnitudes corrected for interstellar extinction

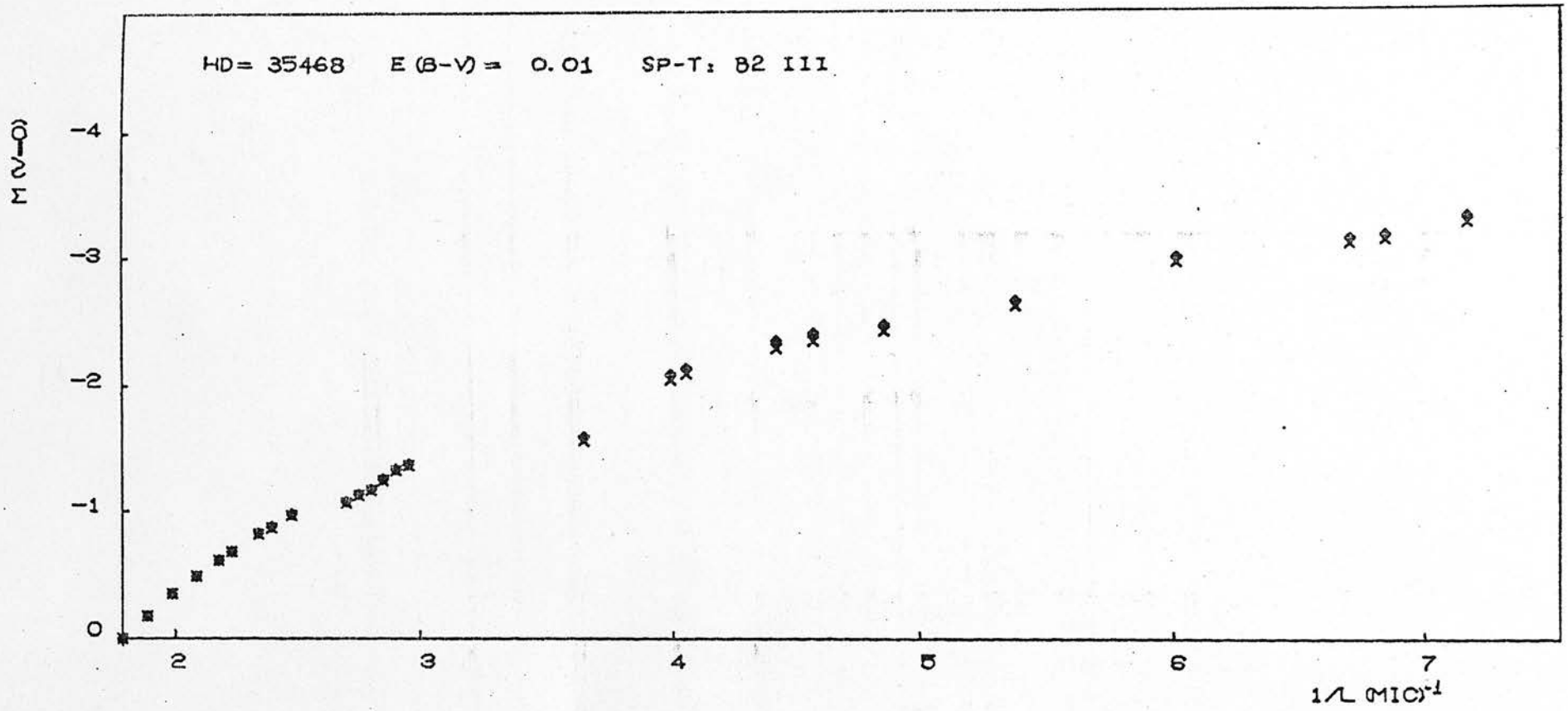

Fig. 40 × Observed magnitudes

◆ Magnitudes corrected for interstellar extinction

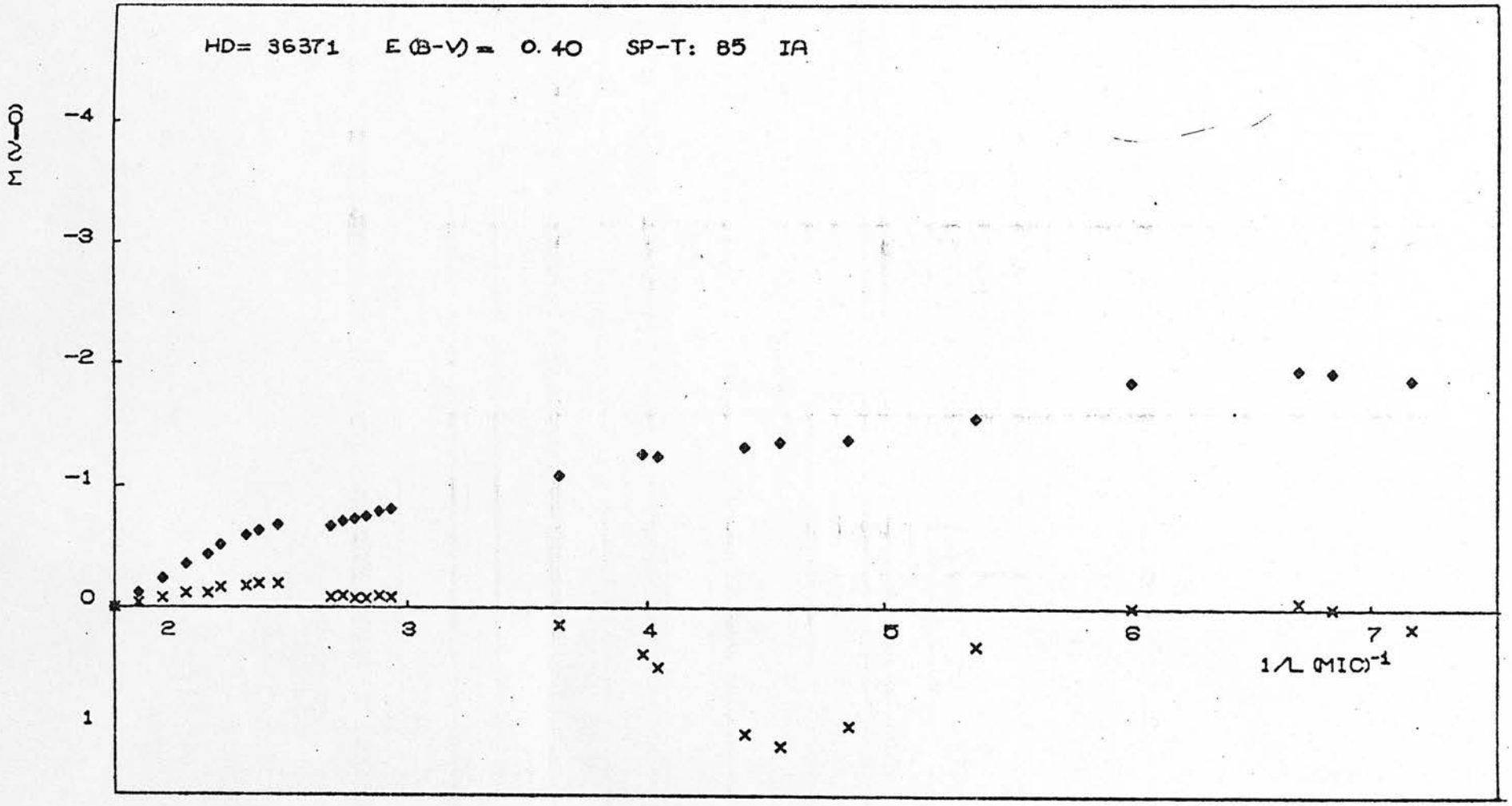

Fig. 41 × Observed magnitudes

◆ Magnitudes corrected for interstellar extinction

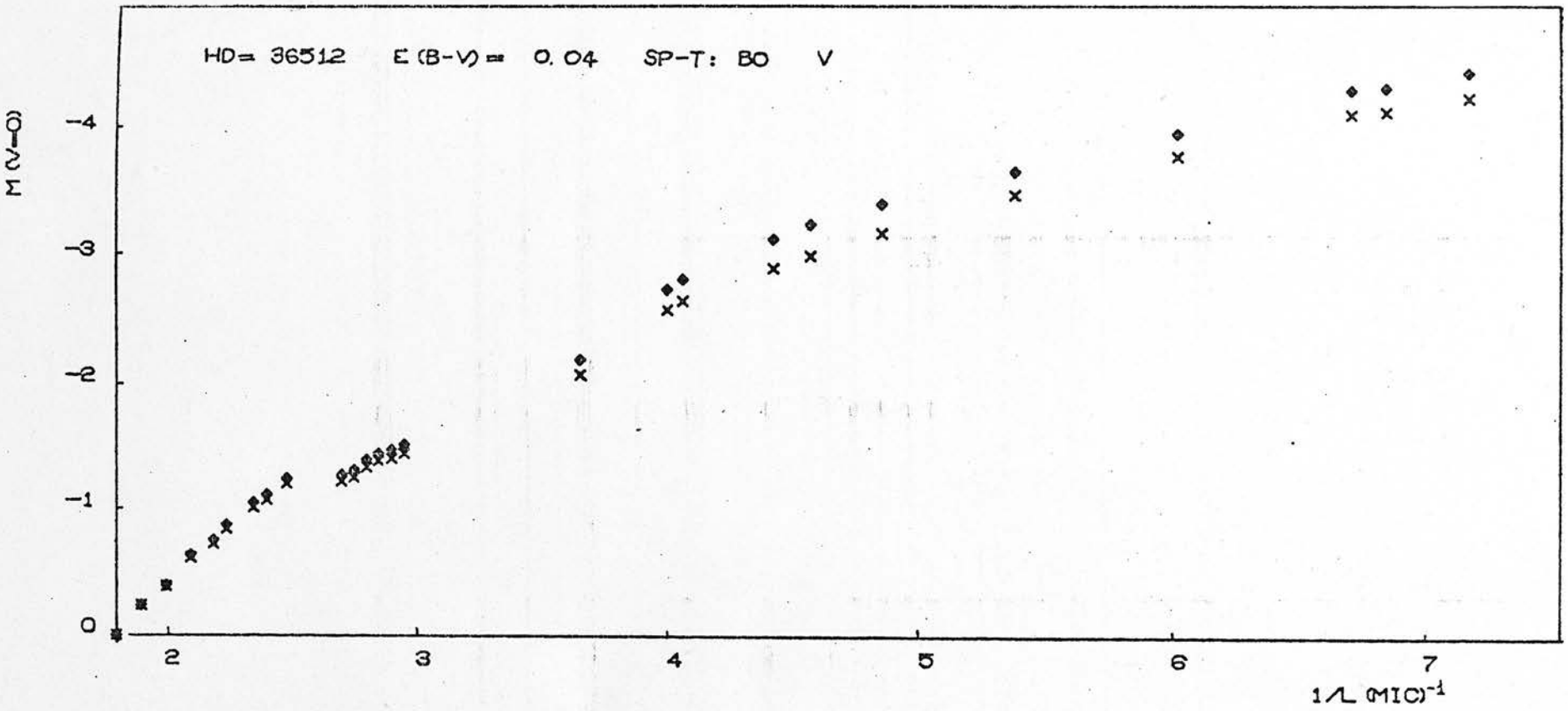

Fig. 42 × Observed magnitudes

◇ Magnitudes corrected for interstellar extinction

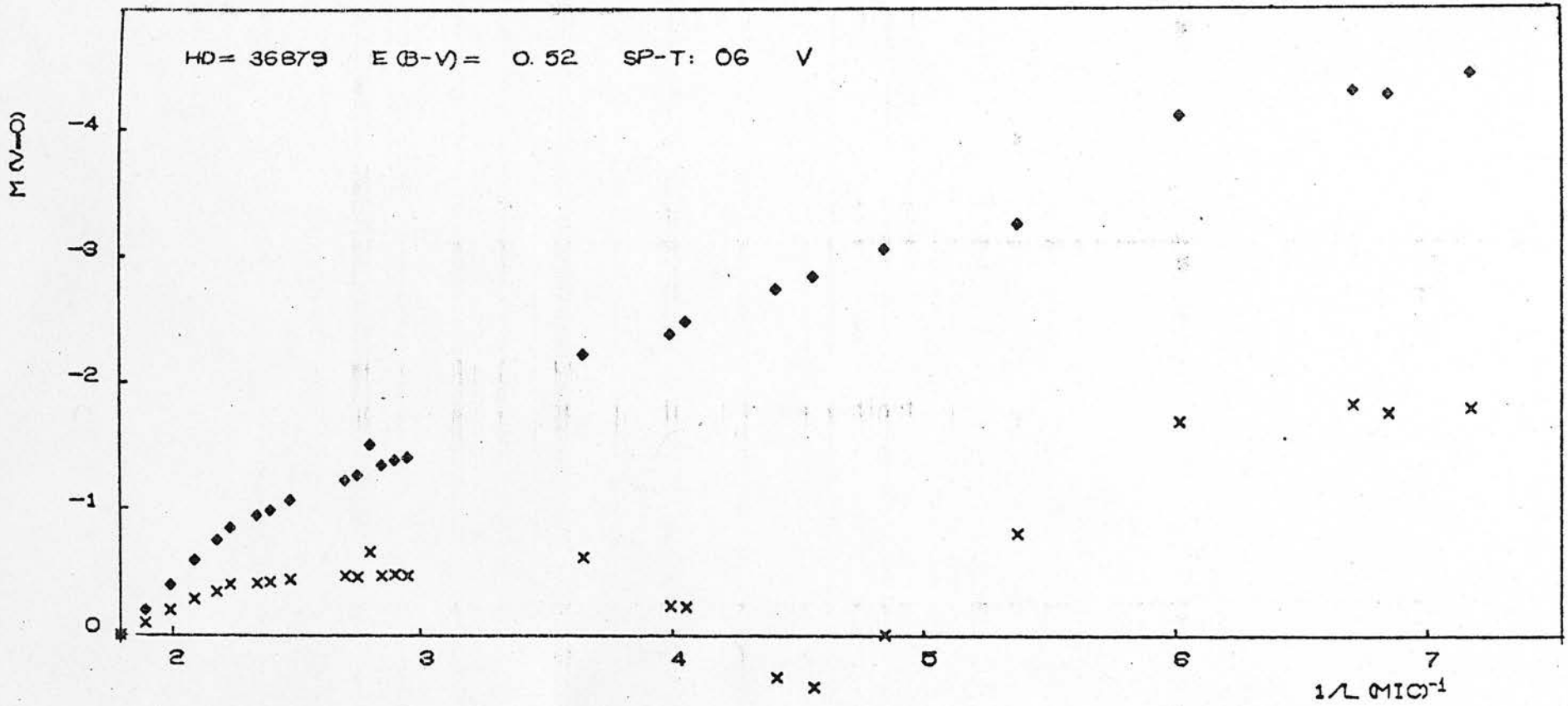

Fig. 43 × Observed magnitudes

◆ Magnitudes corrected for interstellar extinction

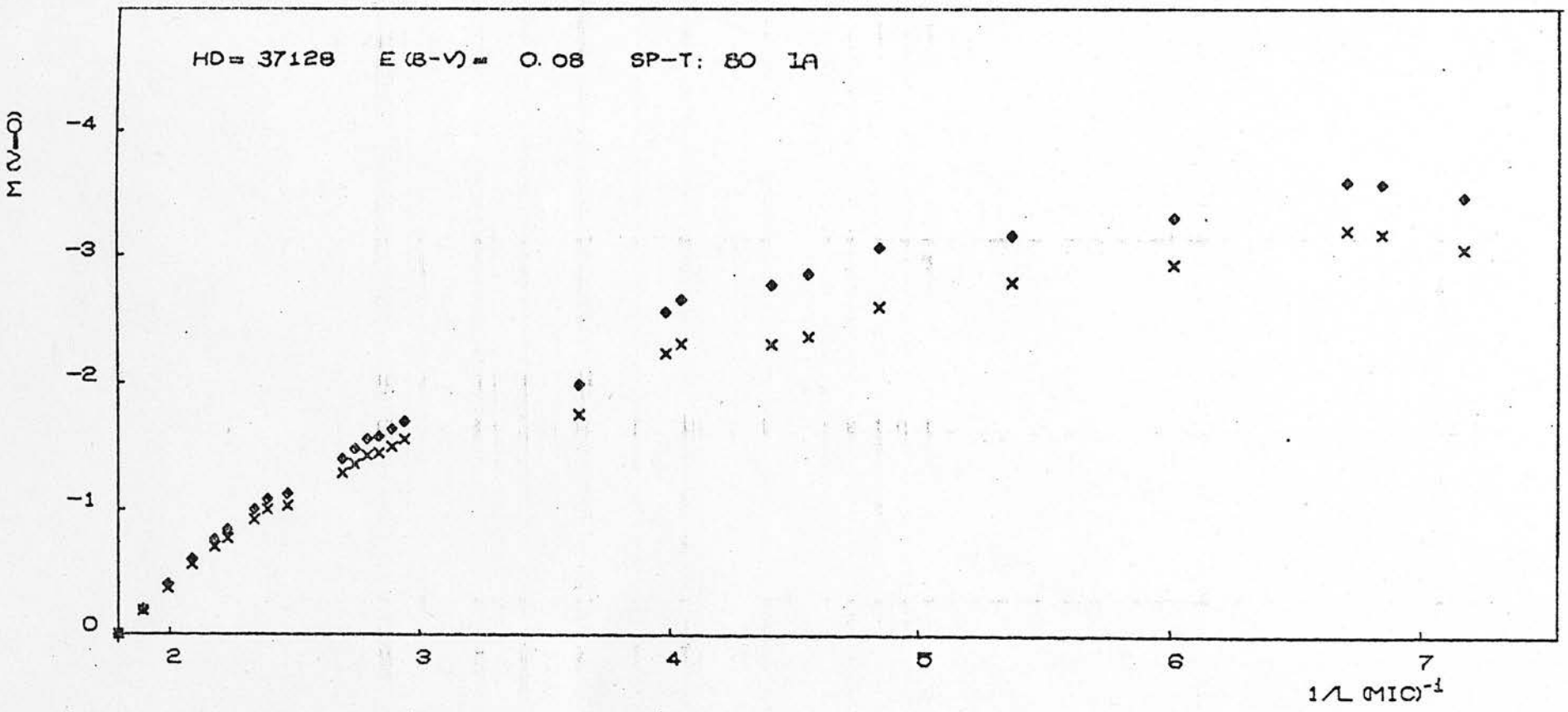

Fig. 44 × Observed magnitudes

◊ Magnitudes corrected for interstellar extinction

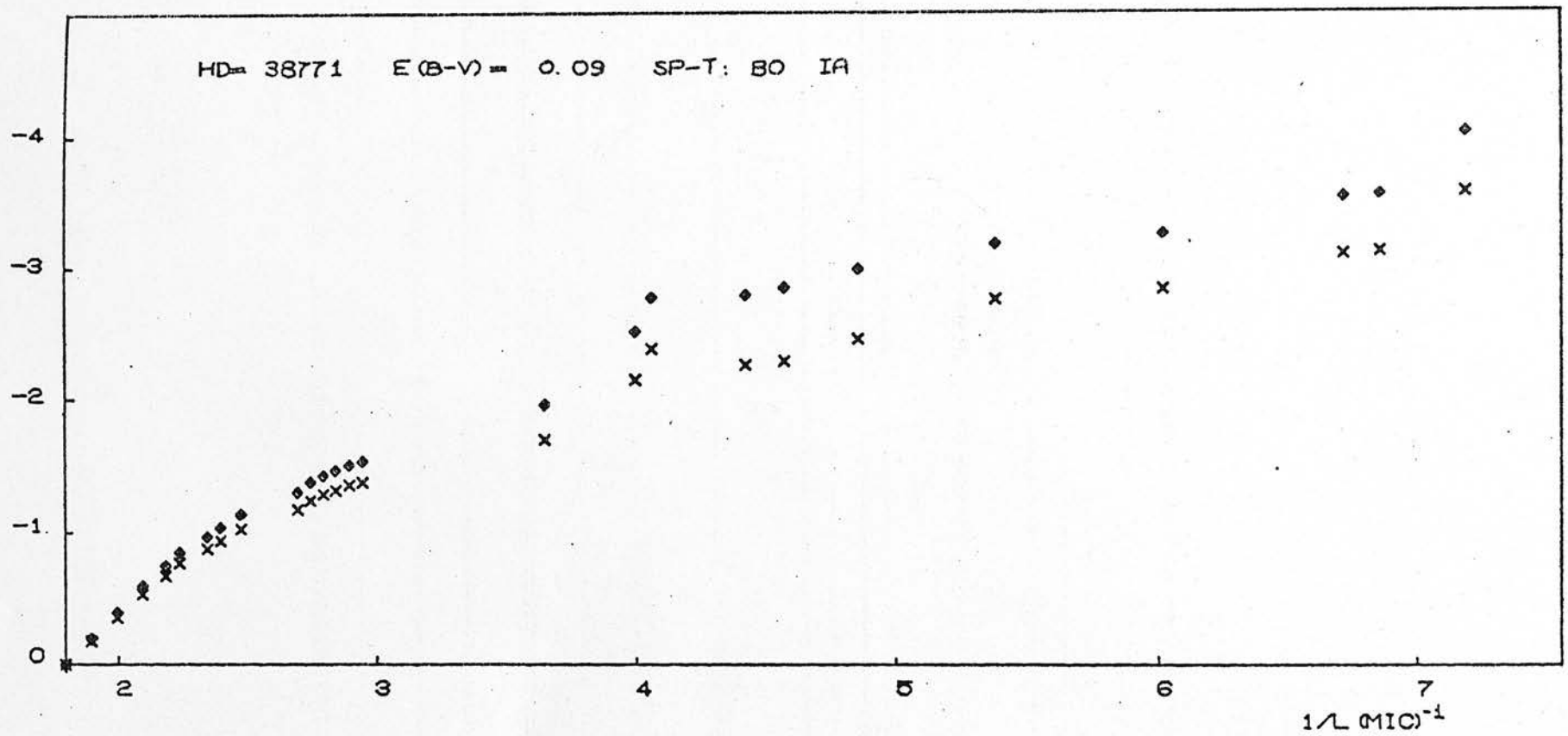

Fig. 45 × Observed magnitudes

♦ Magnitudes corrected for interstellar extinction

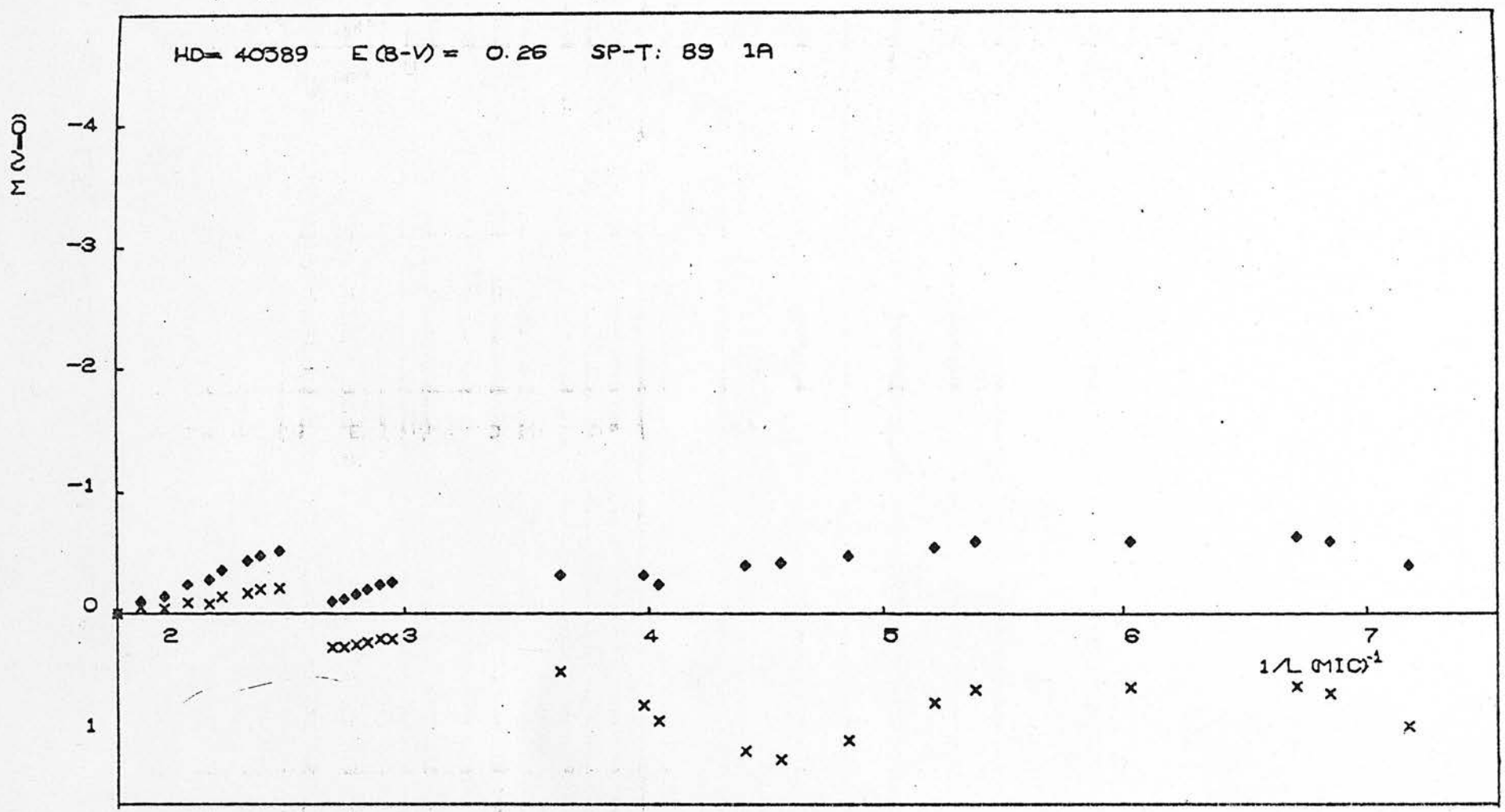

Fig. 46 × Observed magnitudes

◆ Magnitudes corrected for interstellar extinction

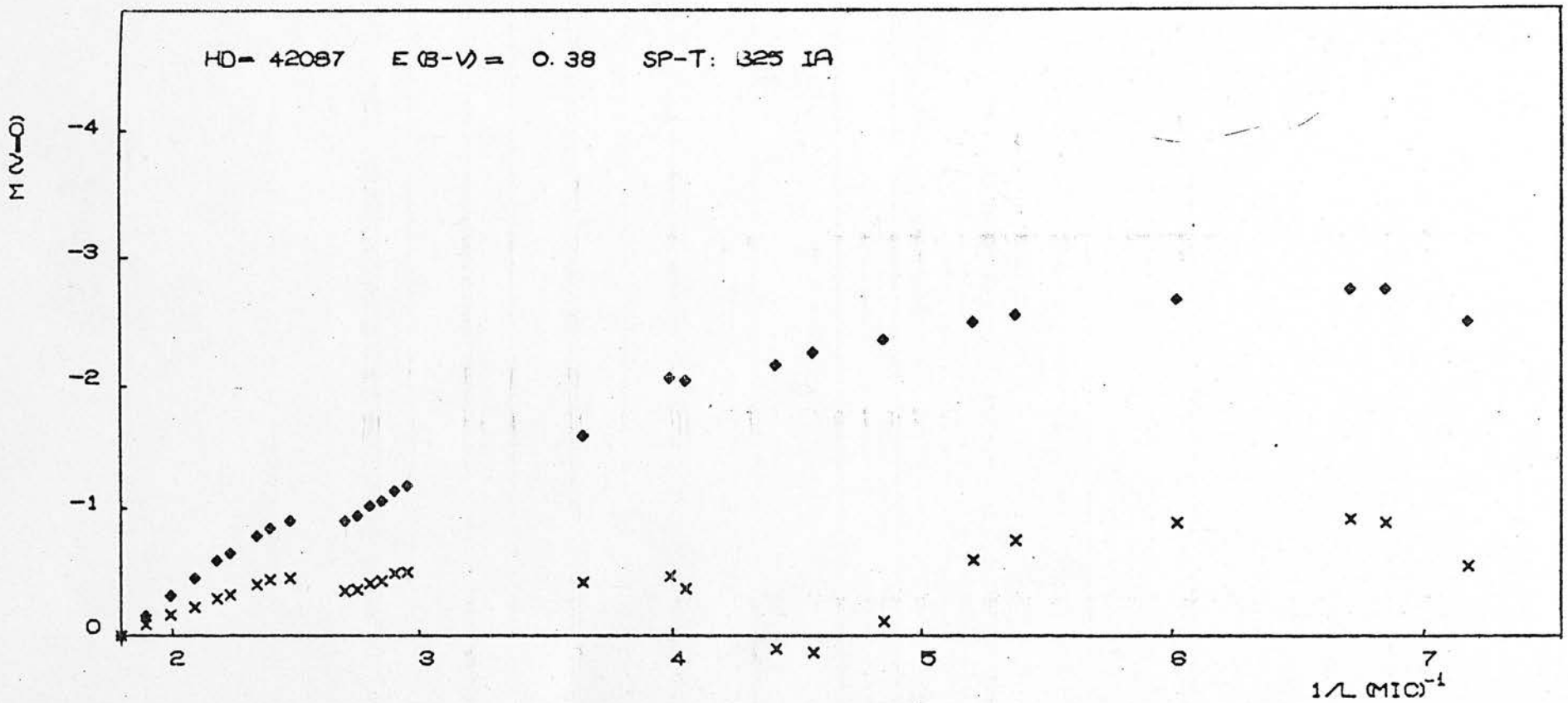

Fig. 47 × Observed magnitudes

◆ Magnitudes corrected for interstellar extinction

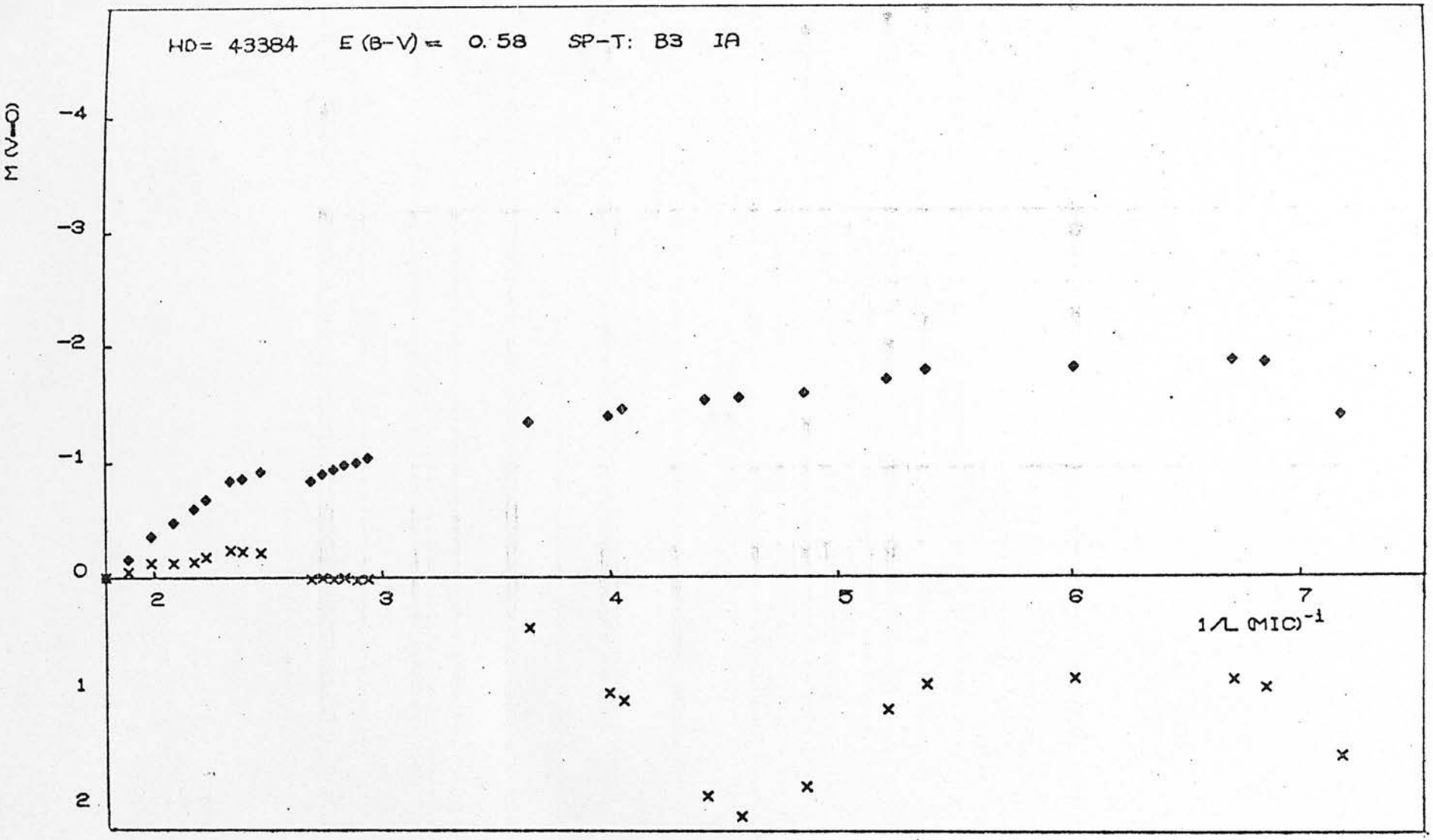

Fig. 48 × Observed magnitudes

♦ Magnitudes corrected for interstellar extinction

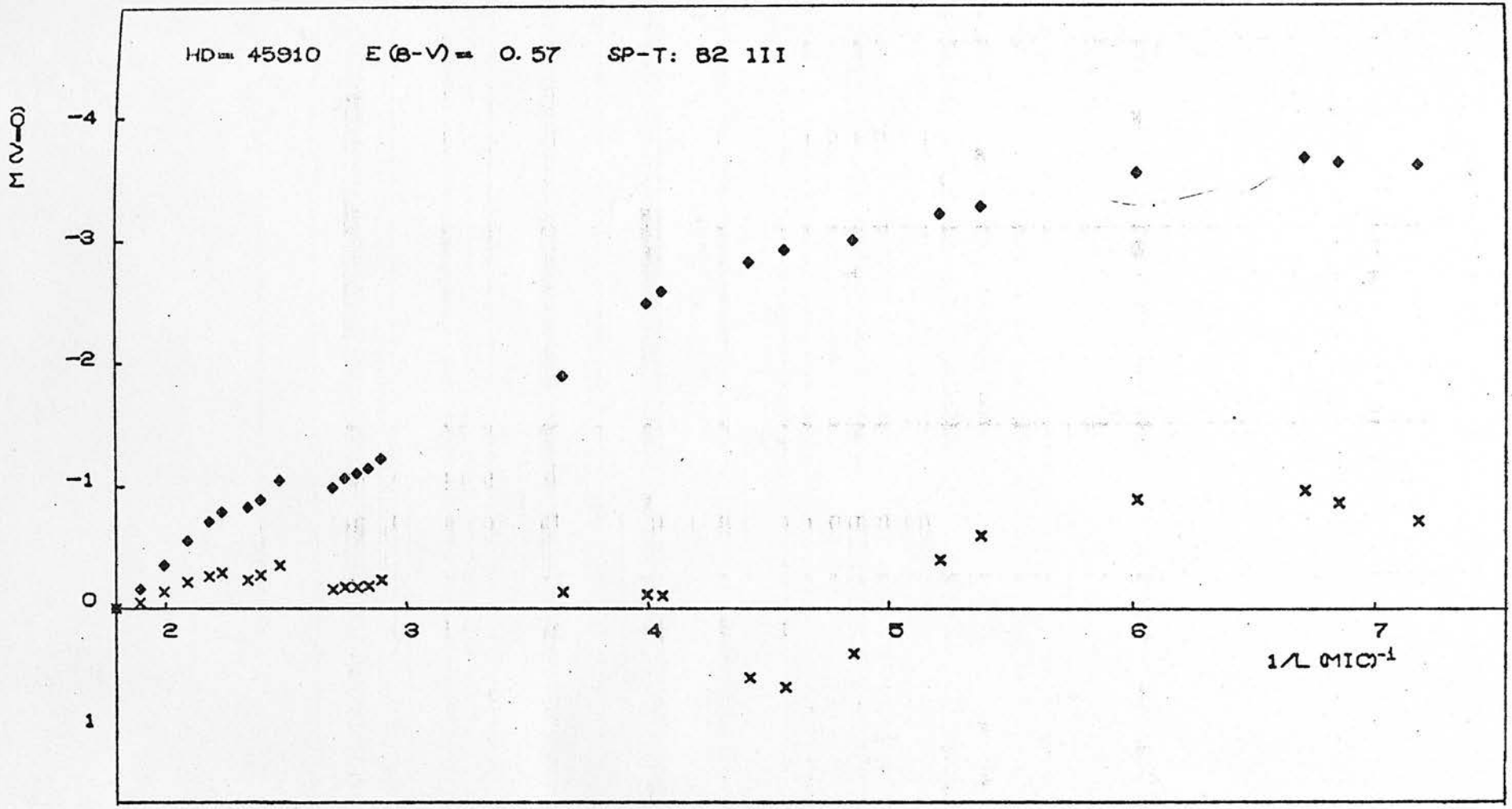

Fig. 49 × Observed magnitudes

◇ Magnitudes corrected for interstellar extinction

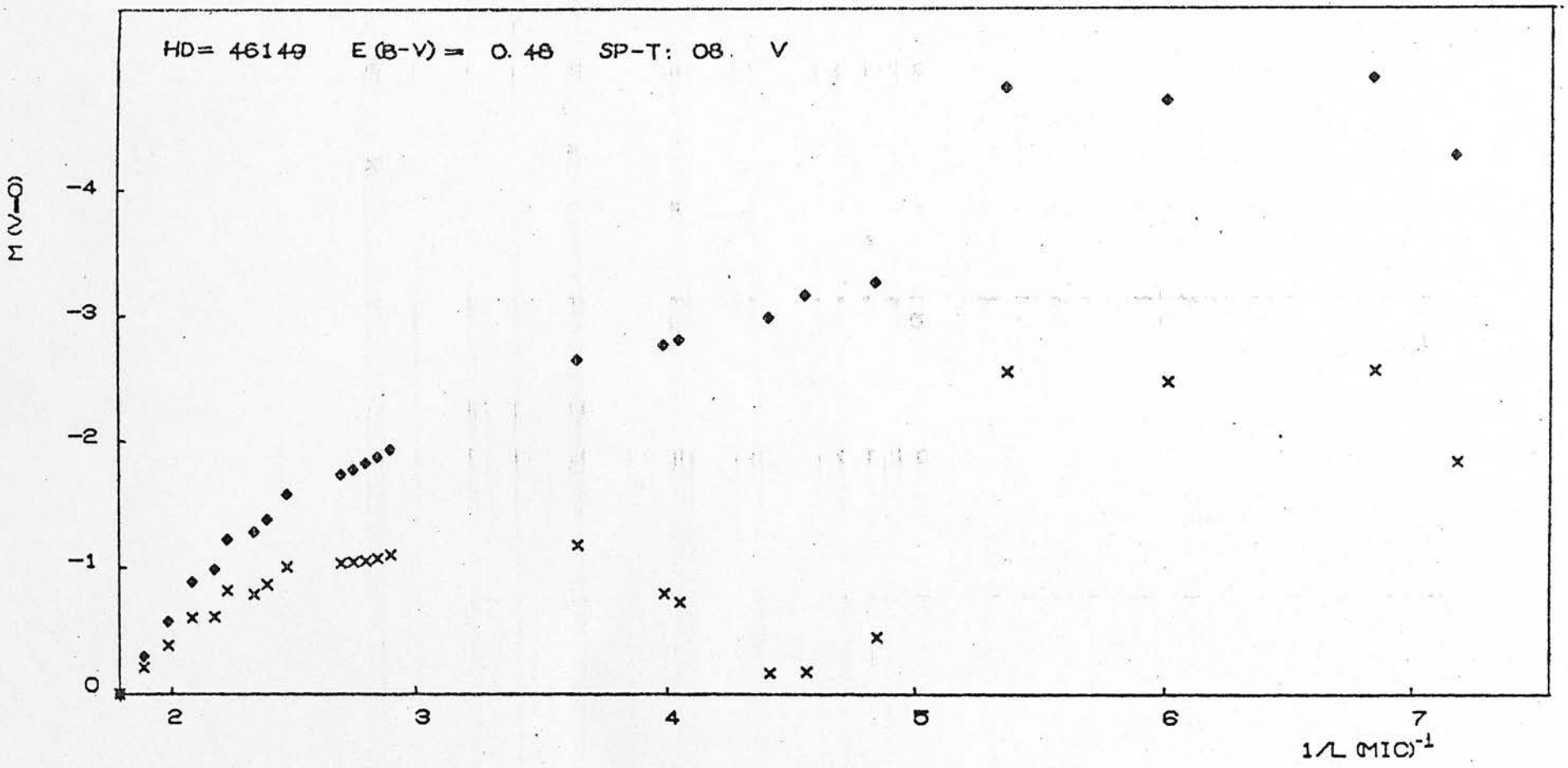

Fig. 50 × Observed magnitudes

◆ Magnitudes corrected for interstellar extinction

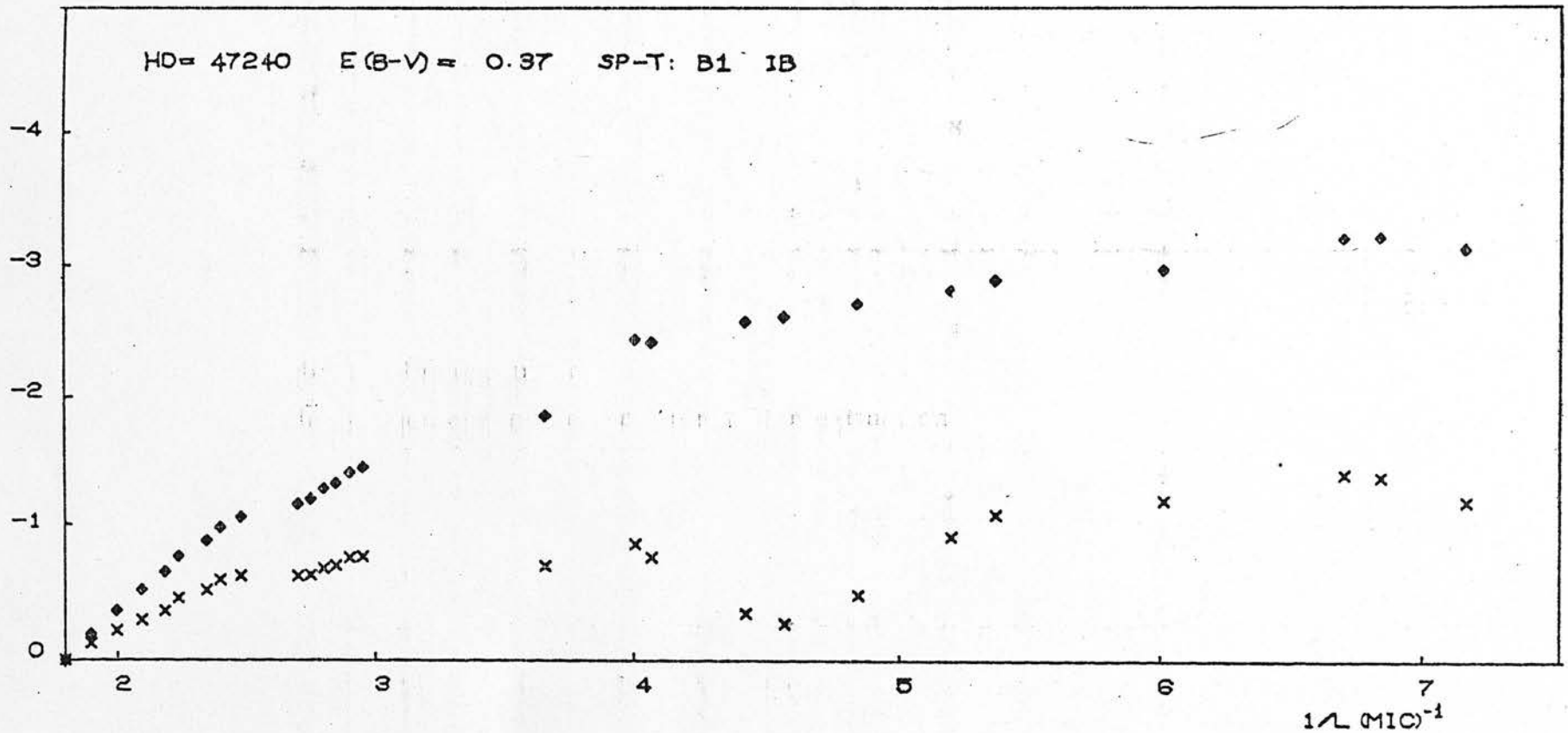

Fig. 51 × Observed magnitudes

◈ Magnitudes corrected for interstellar extinction

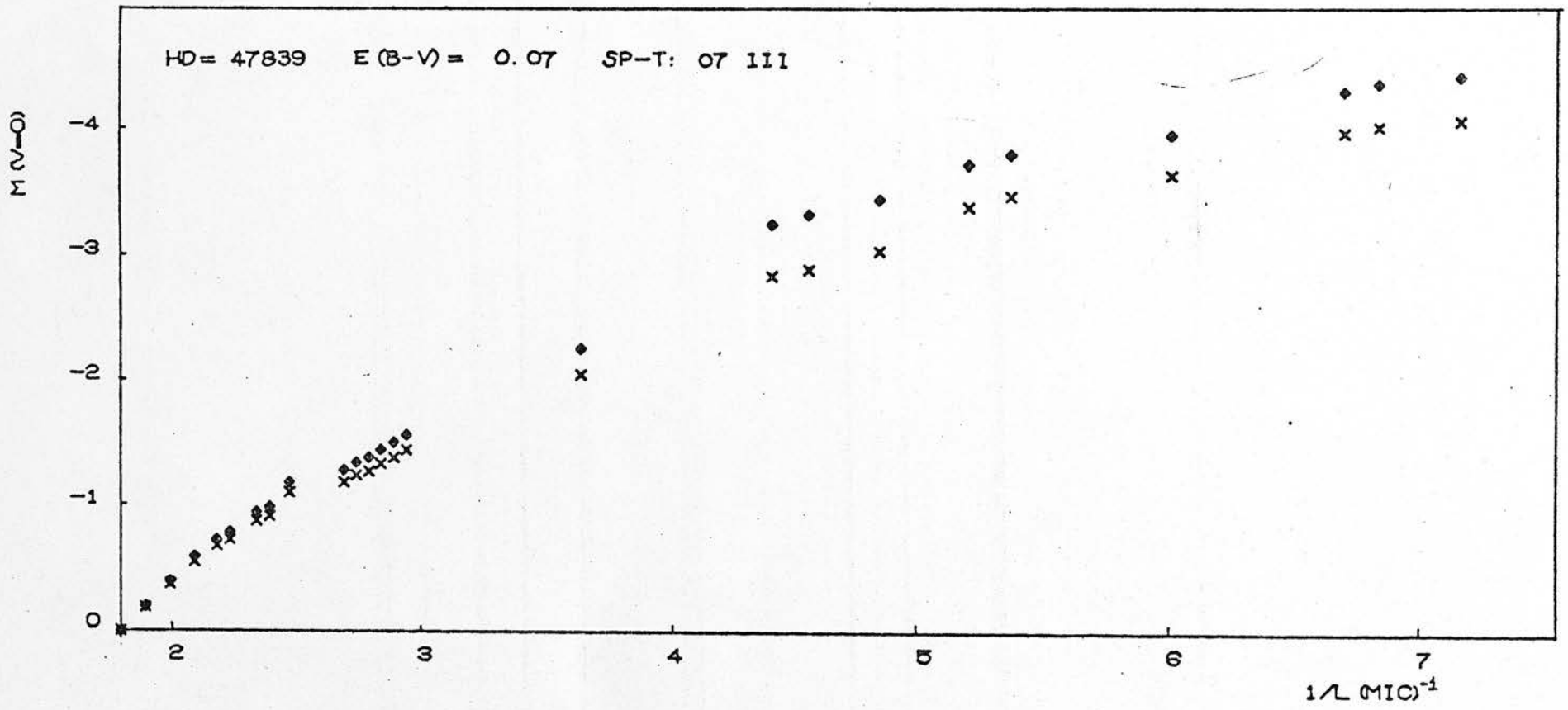

Fig. 52 × Observed magnitudes

◊ Magnitudes corrected for interstellar extinction

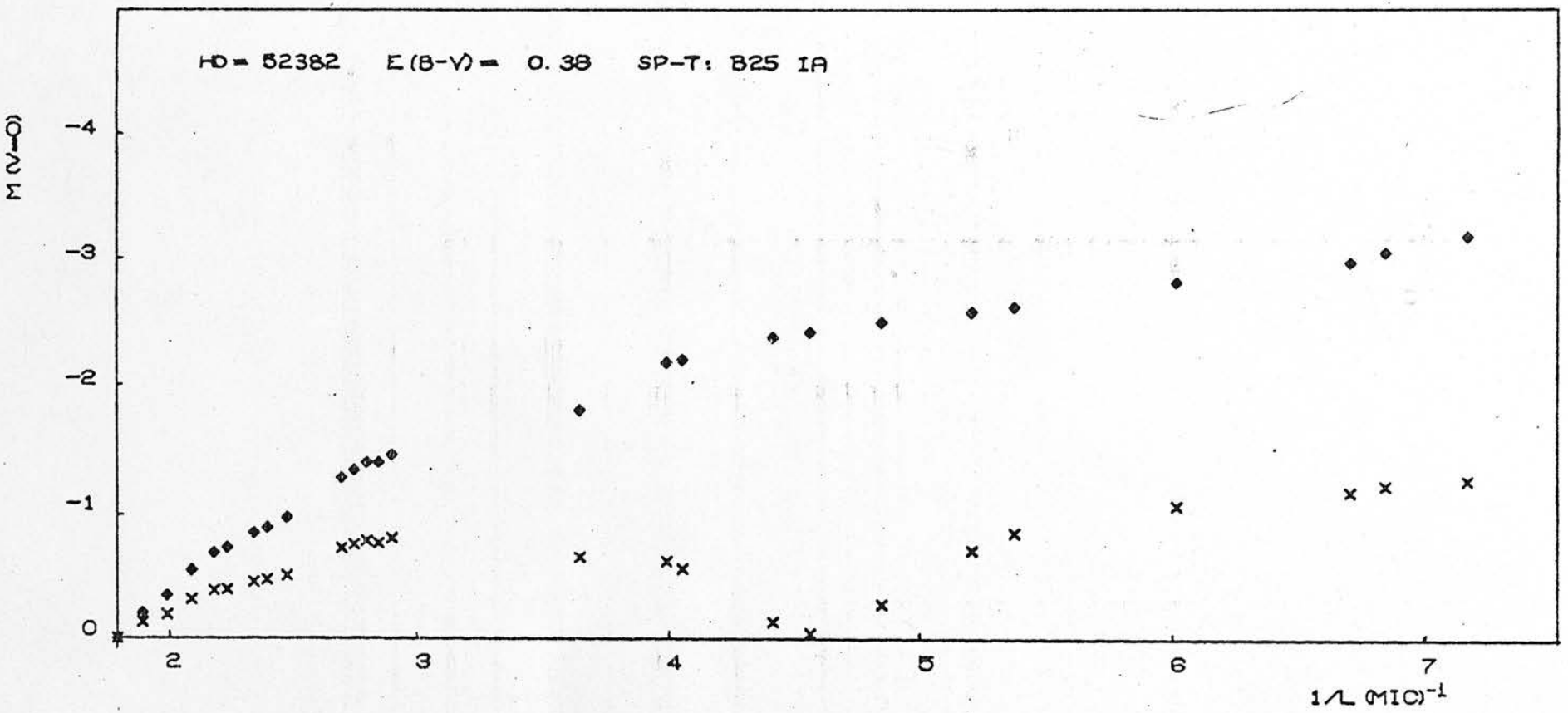

Fig. 53 × Observed magnitudes

◆ Magnitudes corrected for interstellar extinction

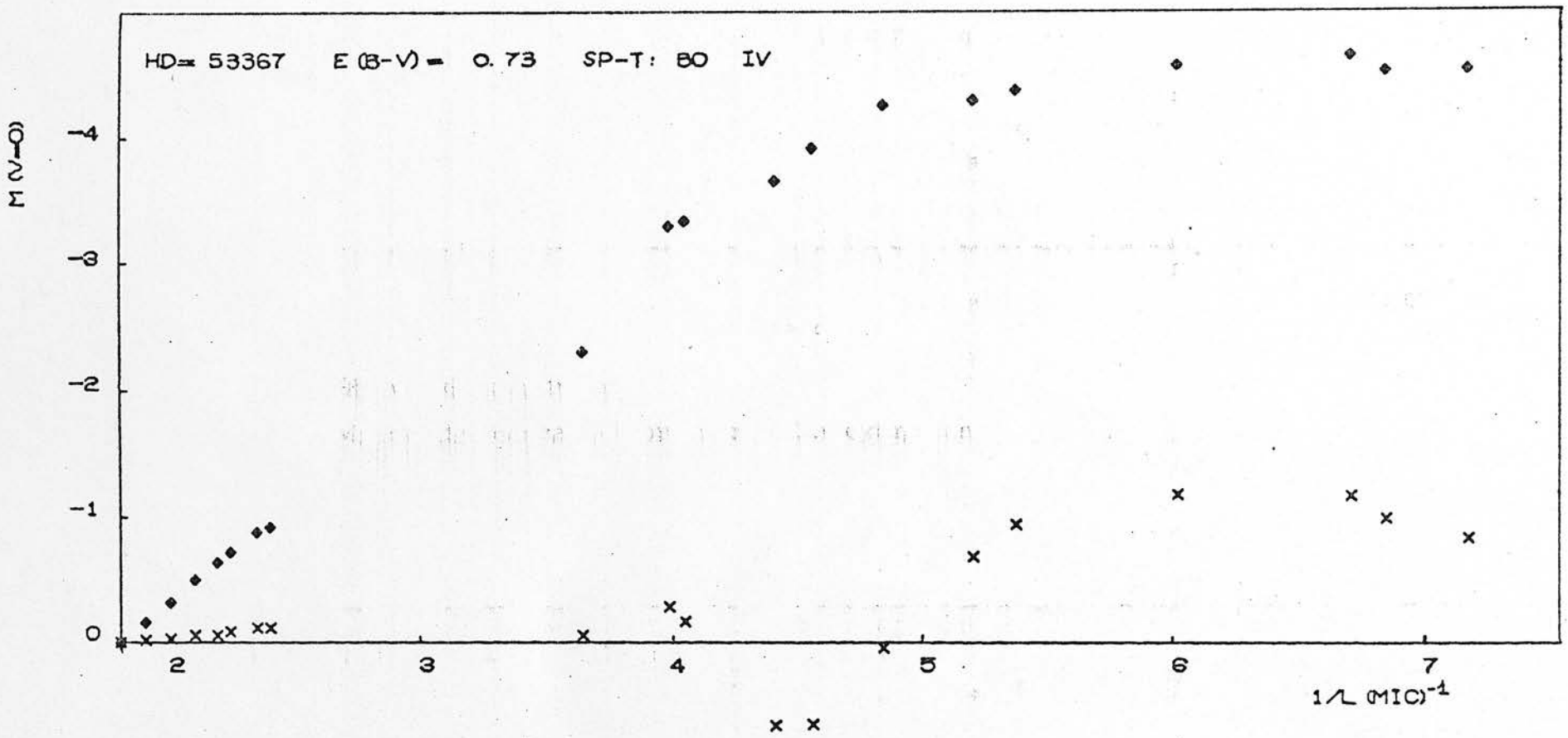

Fig. 54 × Observed magnitudes

◈ Magnitudes corrected for interstellar extinction

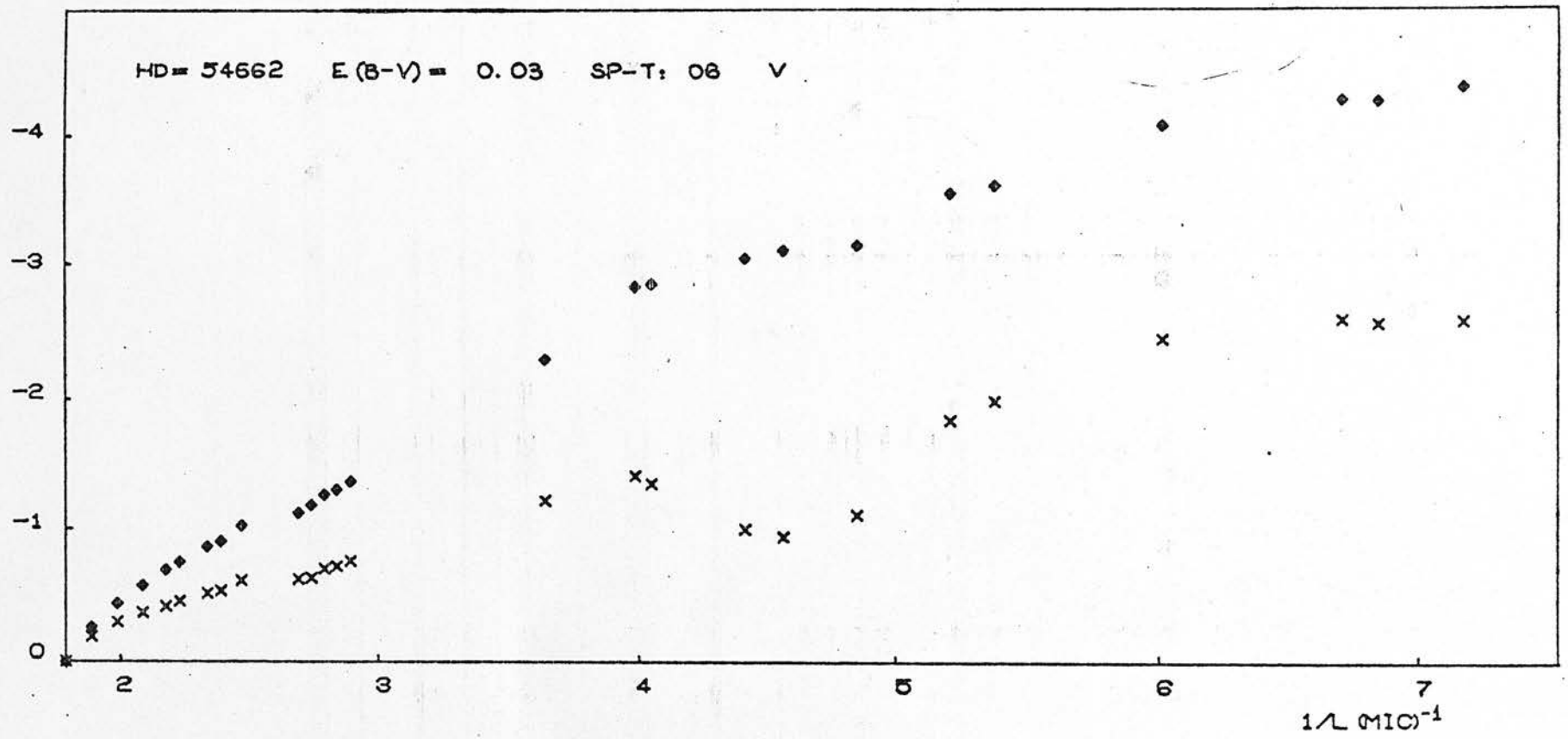

Fig. 55 × Observed magnitudes

◊ Magnitudes corrected for interstellar extinction

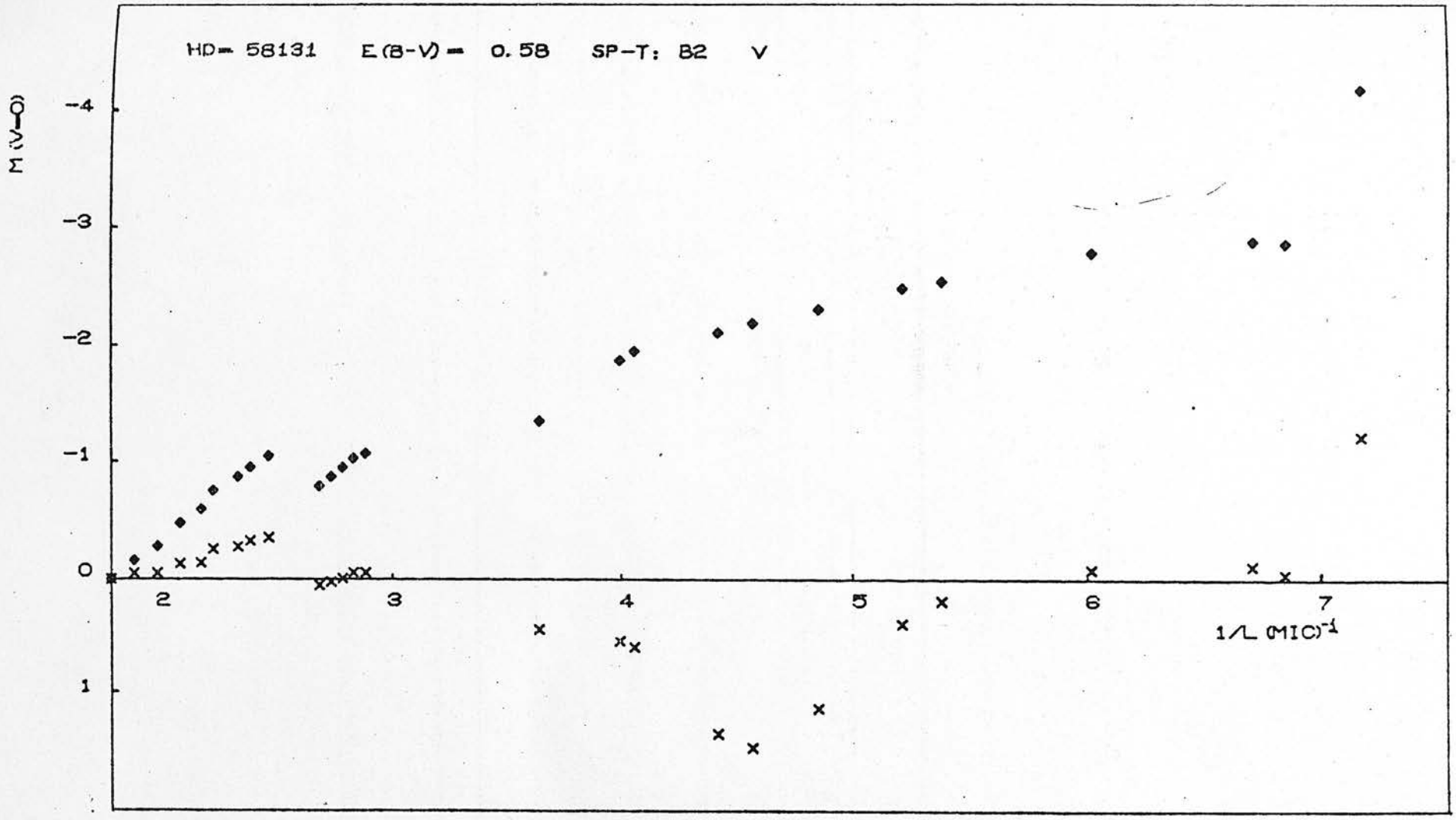

Fig. 56 × Observed magnitudes

◆ Magnitudes corrected for interstellar extinction

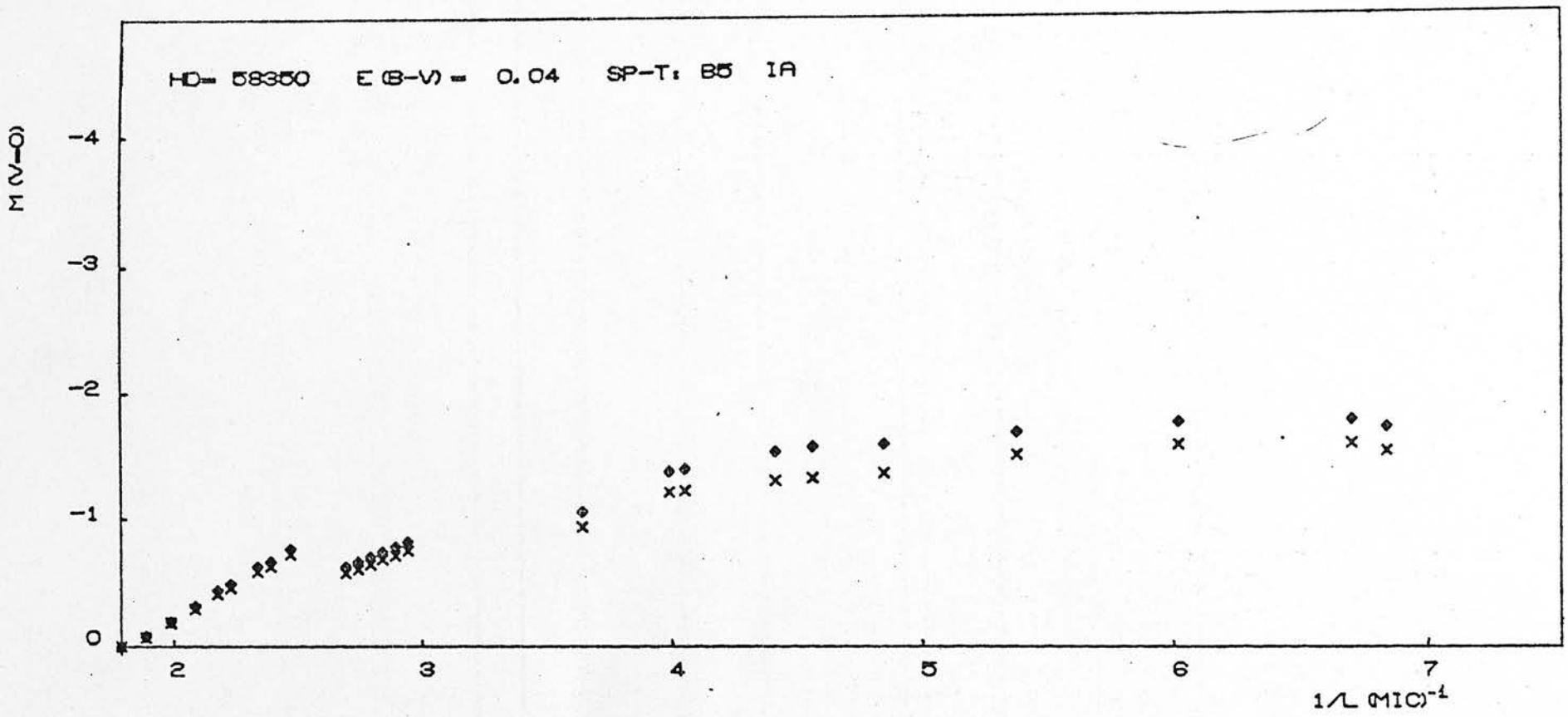

Fig. 57 × Observed magnitudes

◊ Magnitudes corrected for interstellar extinction

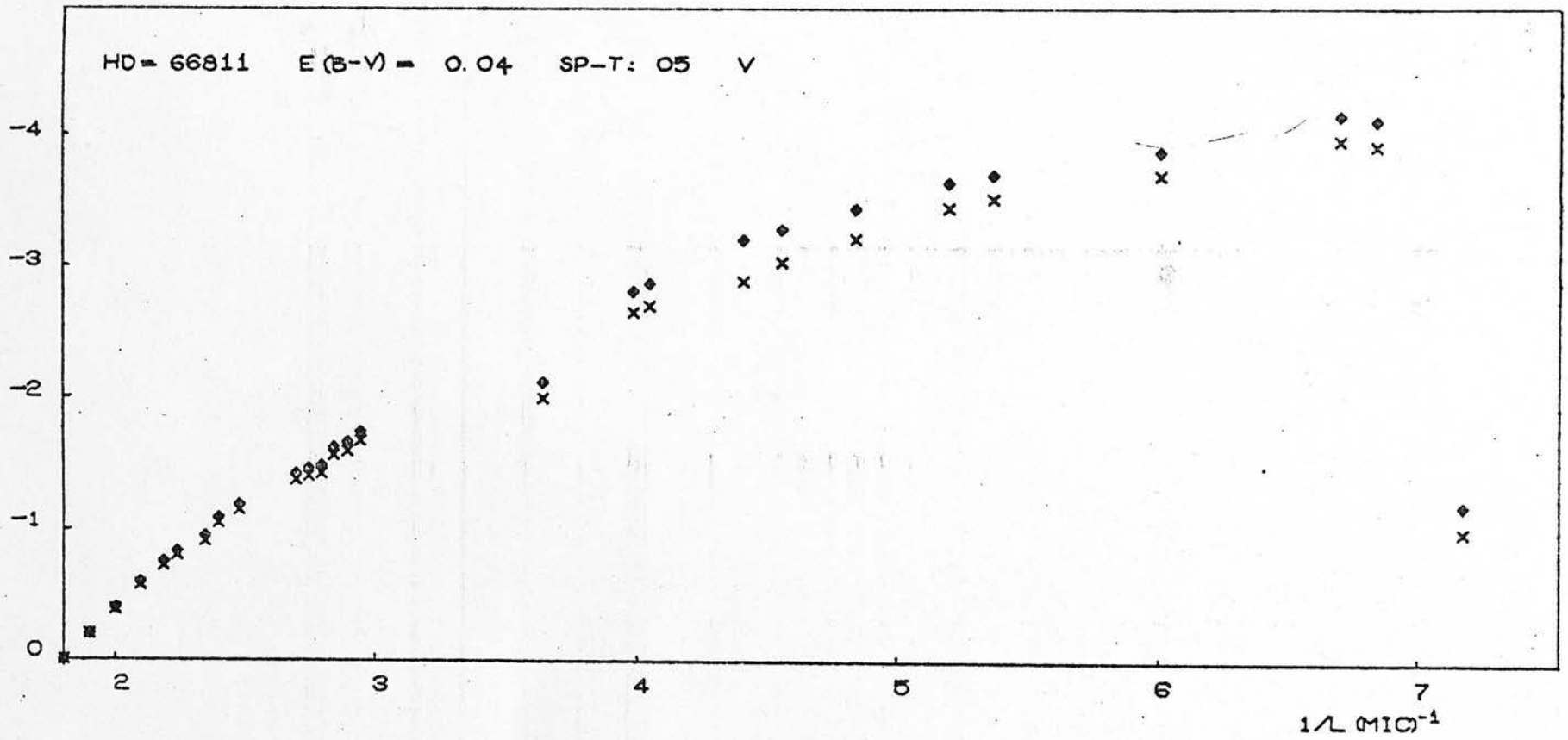

Fig. 58 × Observed magnitudes

◆ Magnitudes corrected for interstellar extinction

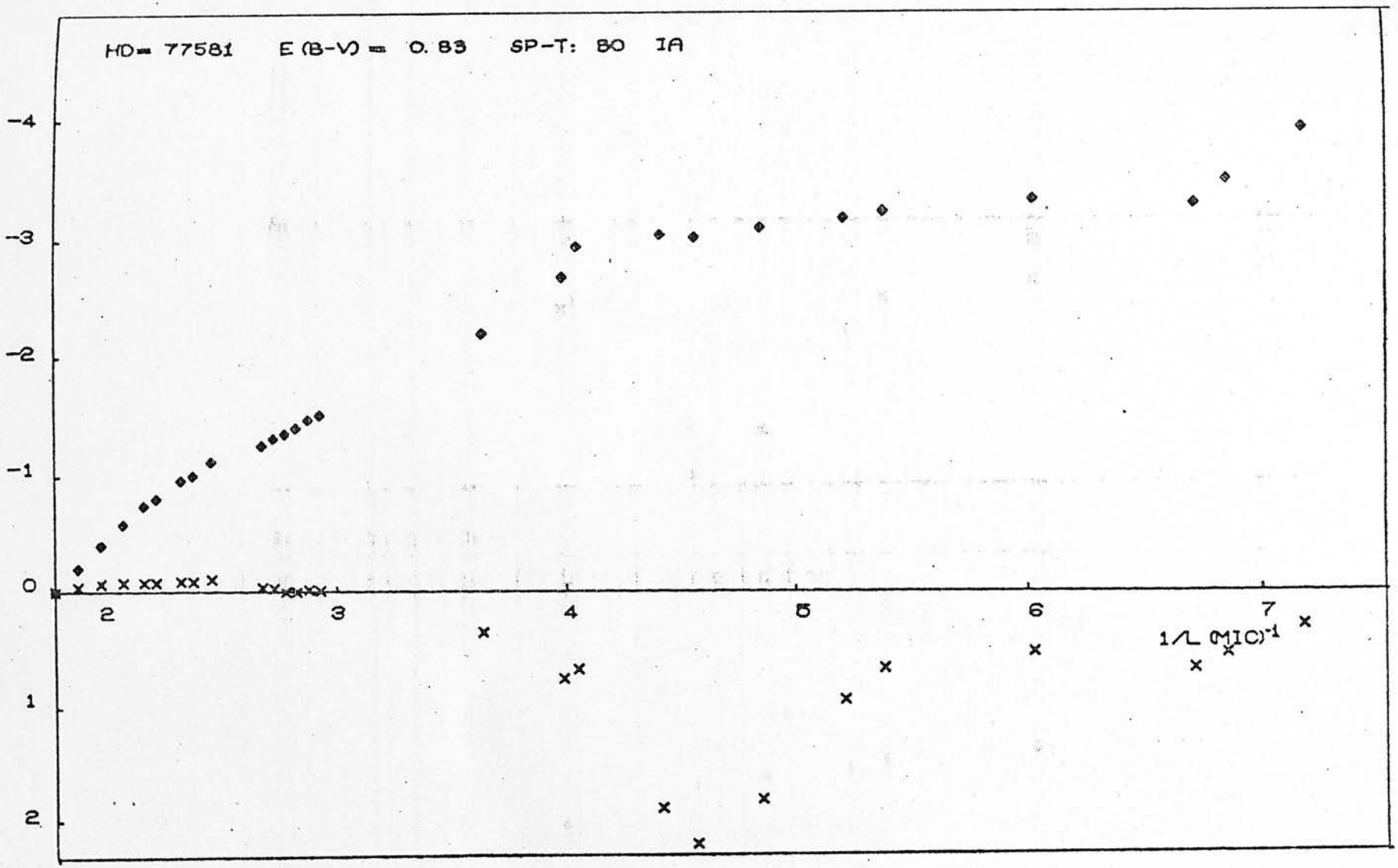

Fig. 59 × Observed magnitudes

◆ Magnitudes corrected for interstellar extinction

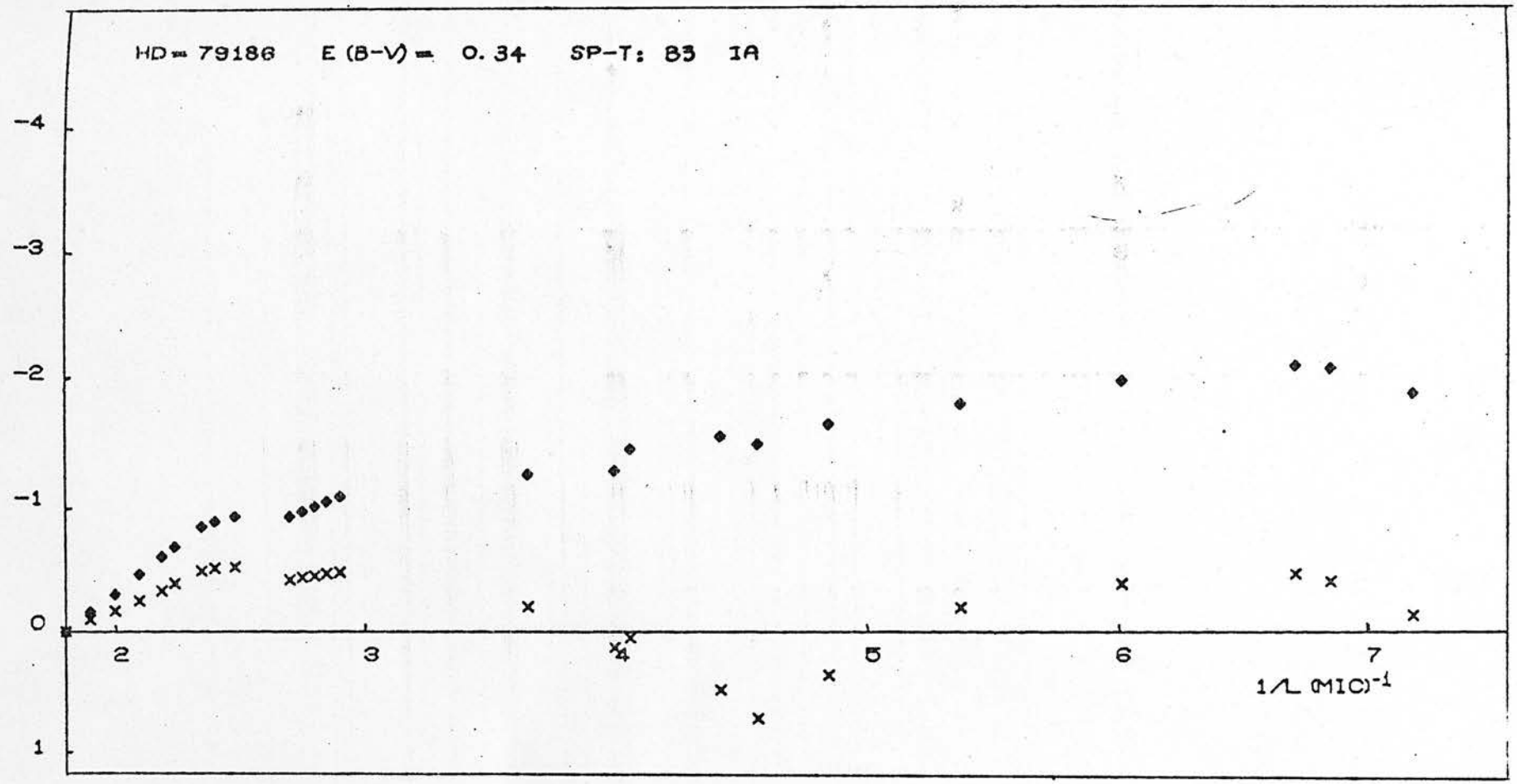

Fig. 60 × Observed magnitudes

◈ Magnitudes corrected for interstellar extinction

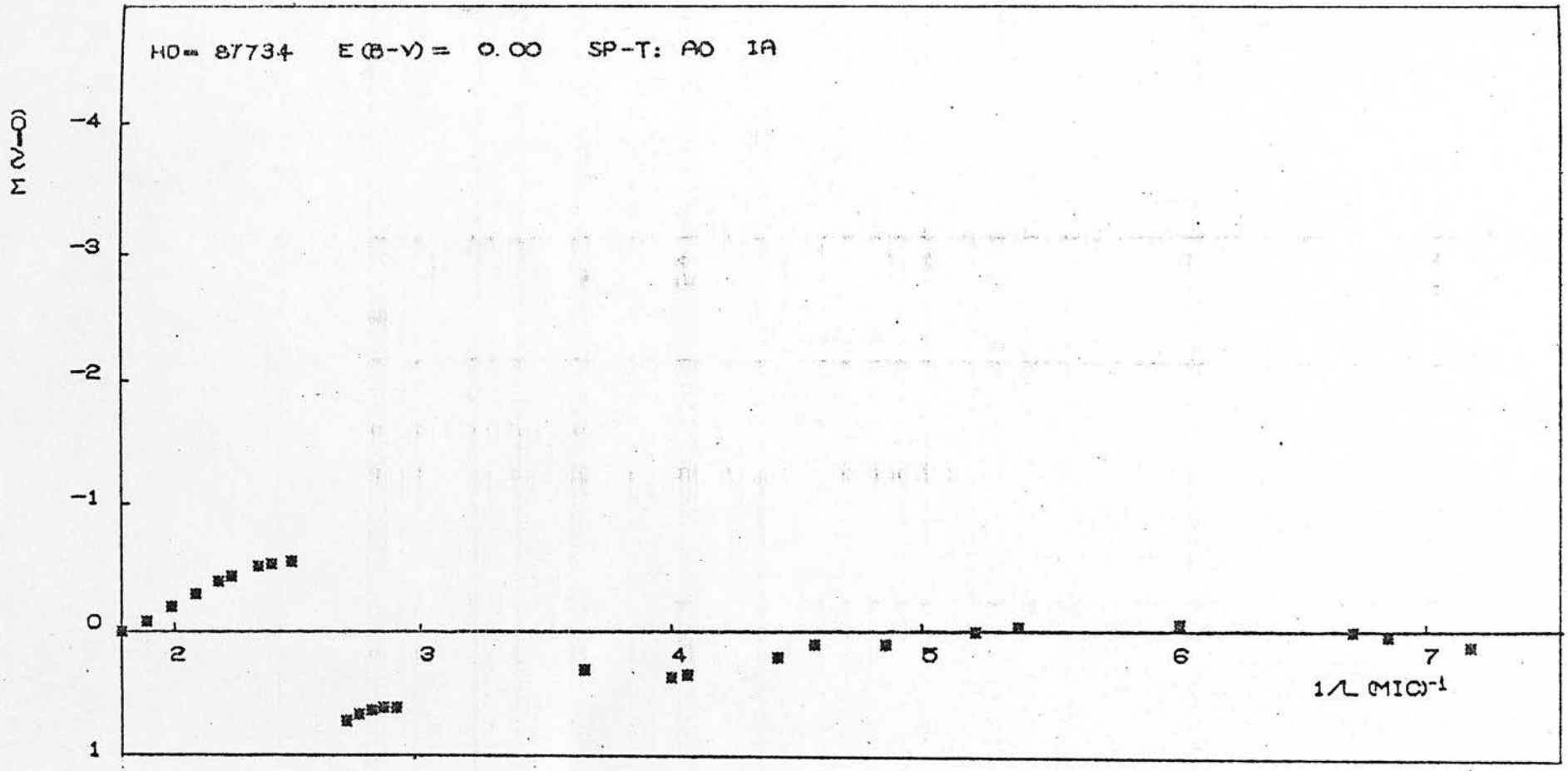

Fig. 61 × Observed magnitudes

◈ Magnitudes corrected for interstellar extinction

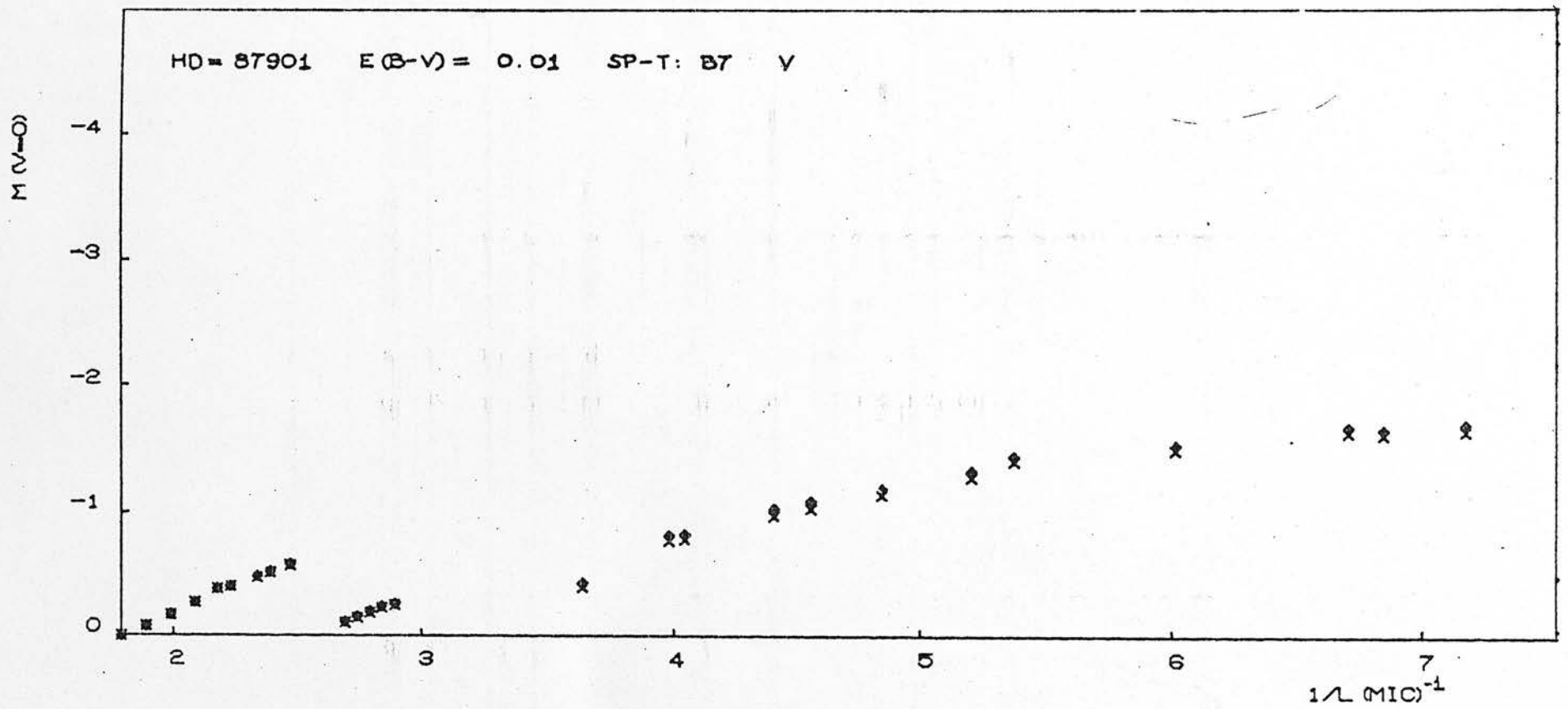

Fig. 62 × Observed magnitudes

♦ Magnitudes corrected for interstellar extinction

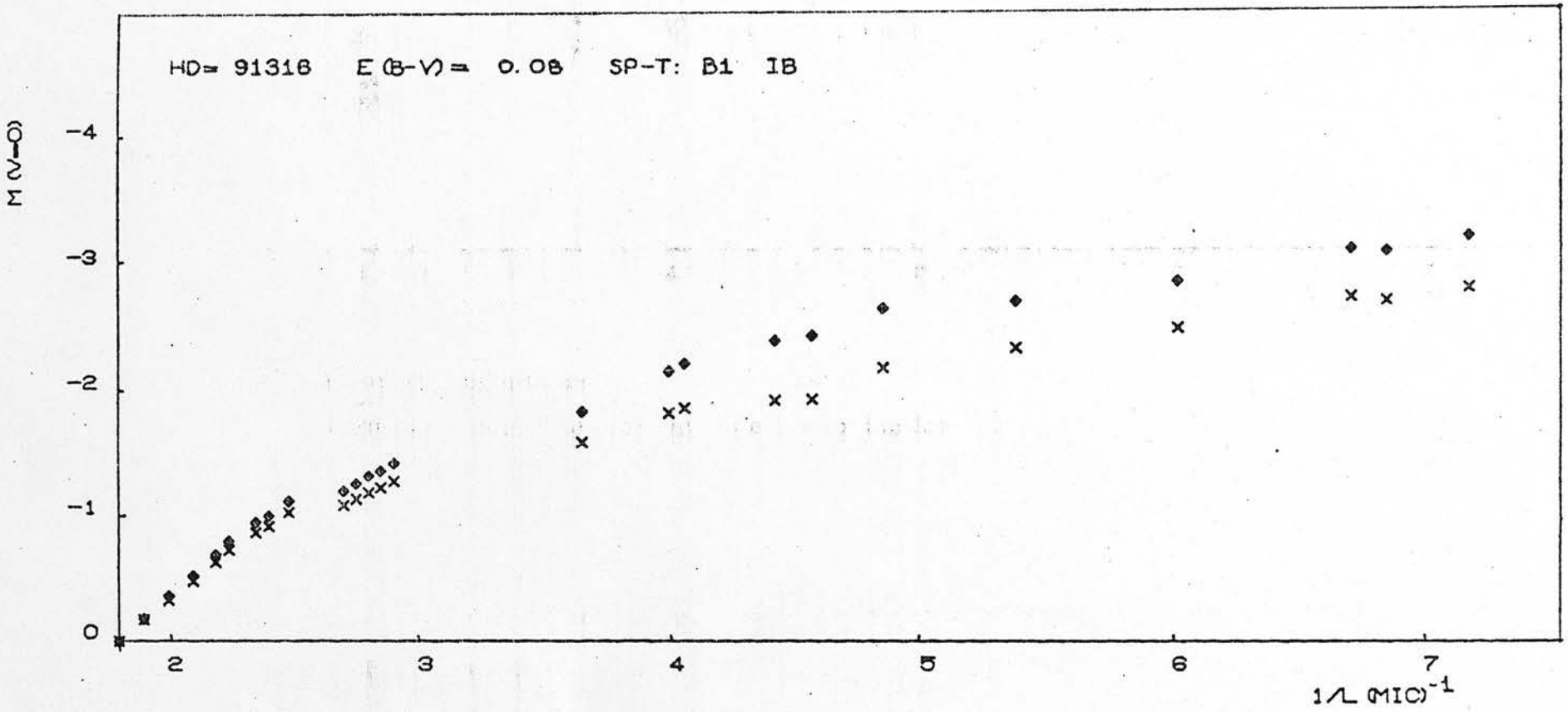

Fig. 63 × Observed magnitudes

◇ Magnitudes corrected for interstellar extinction

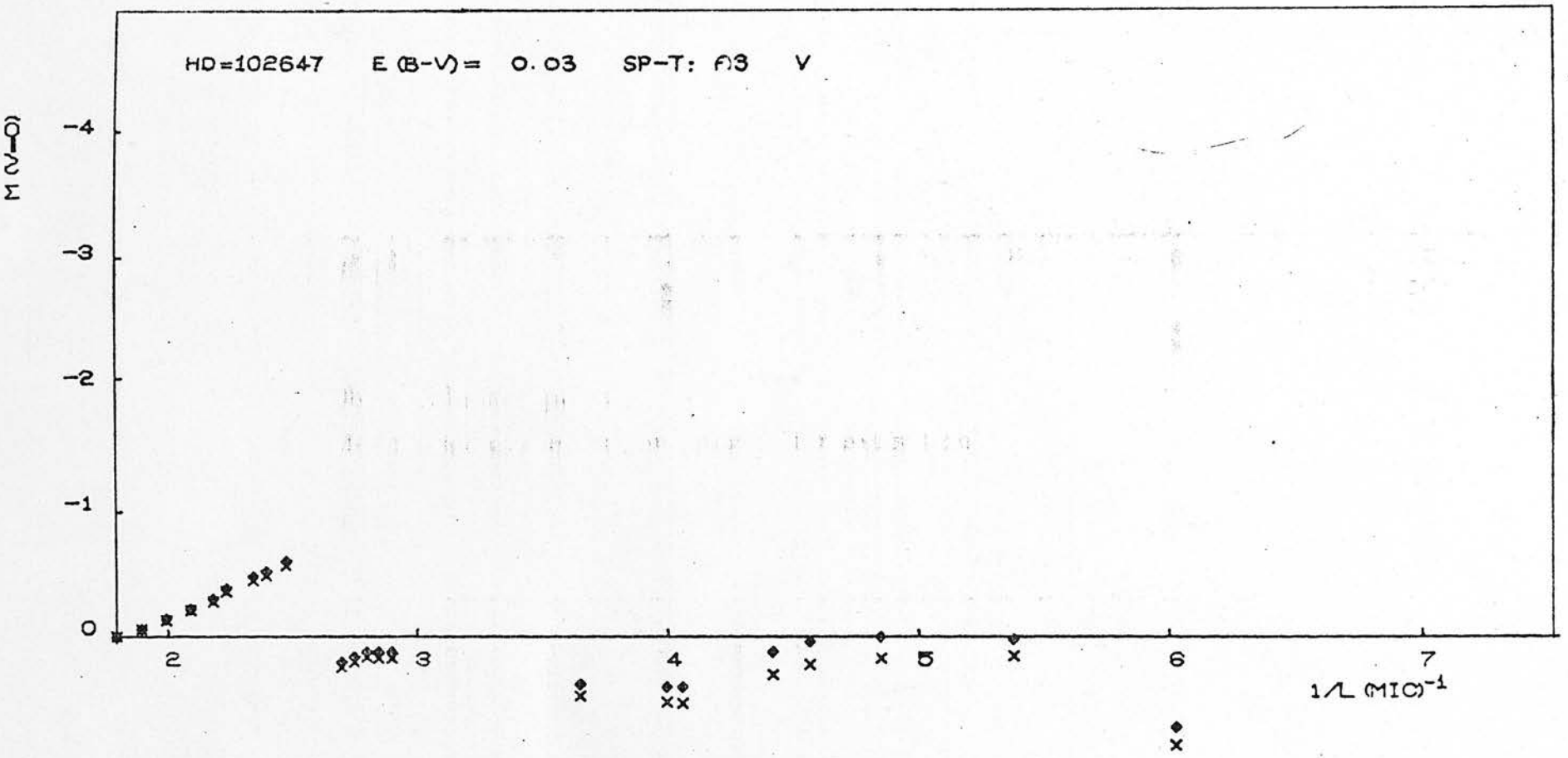

Fig. 64 × Observed magnitudes

◆ Magnitudes corrected for interstellar extinction

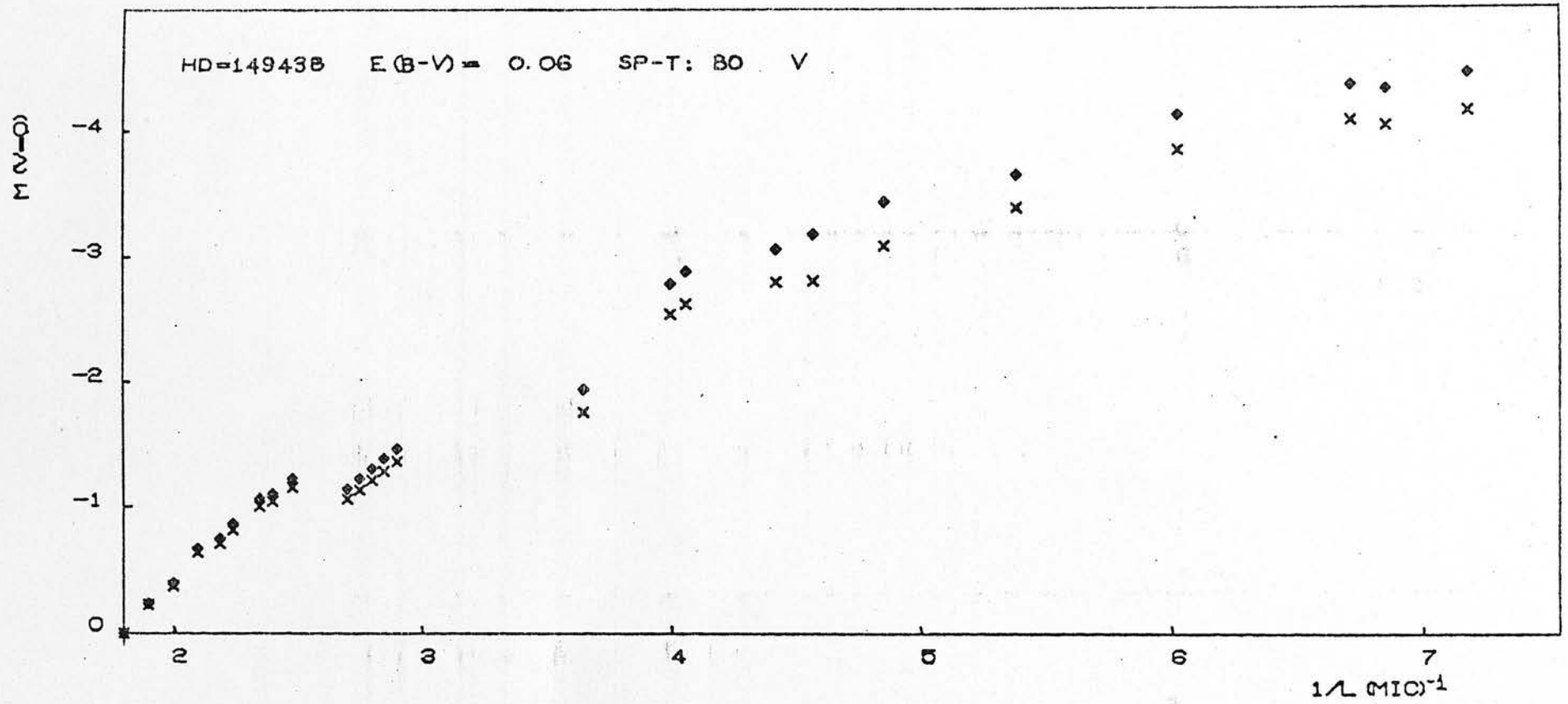

Fig. 65 × Observed magnitudes

◆ Magnitudes corrected for interstellar extinction

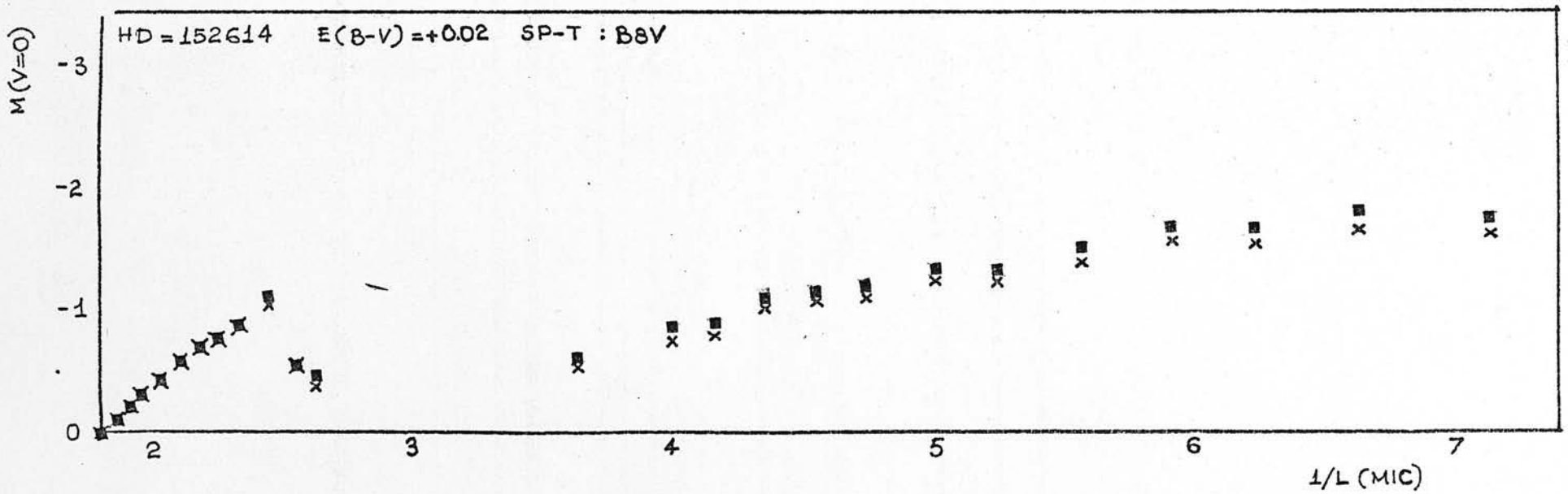

Fig.66

× Observed magnitudes

■ Magnitudes corrected for interstellar extinction

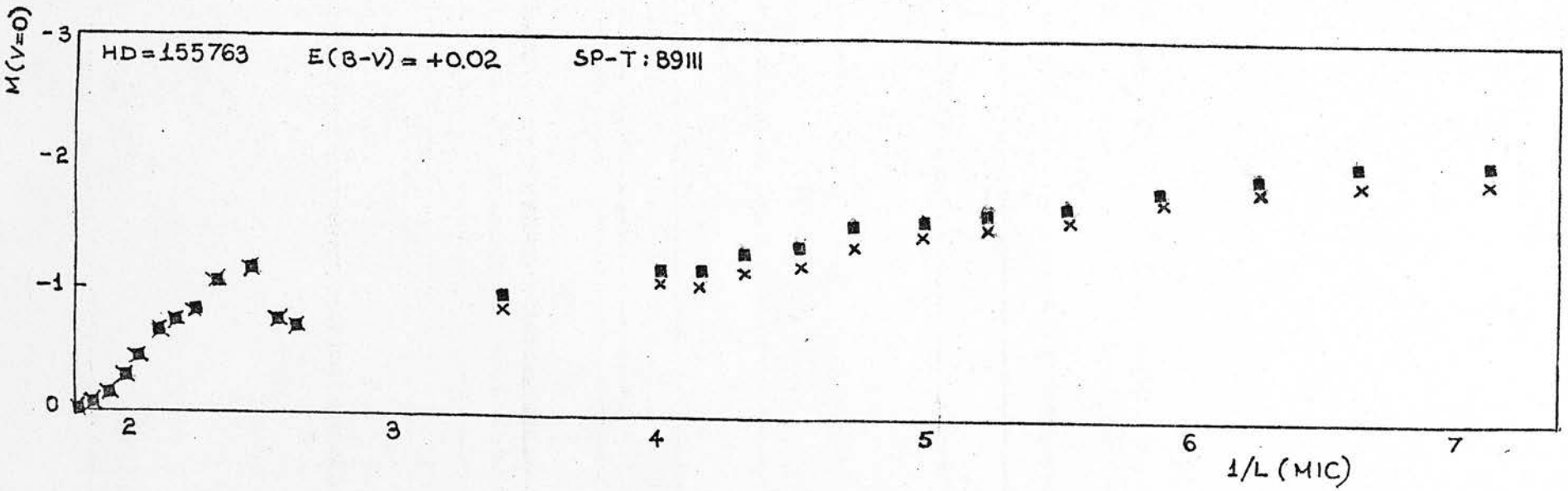

Fig. 67

× Observed magnitudes

■ Magnitudes corrected for interstellar extinction

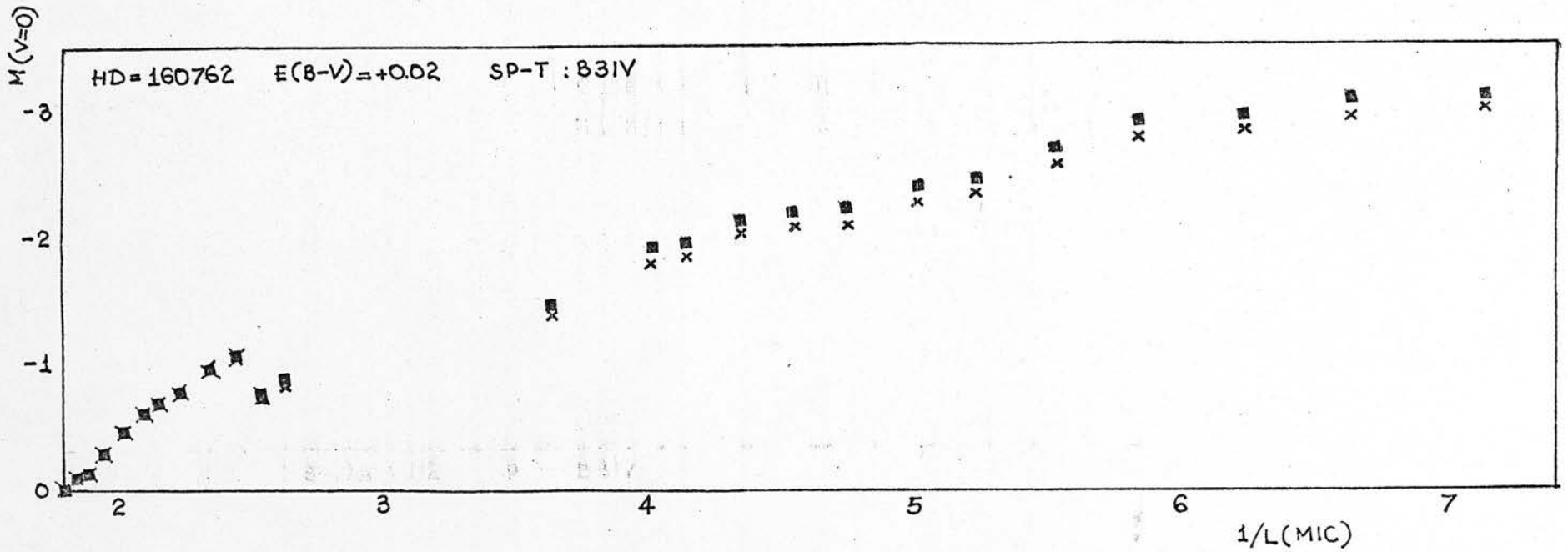

Fig. 68

× Observed magnitudes

■ Magnitudes corrected for intestellar extinction

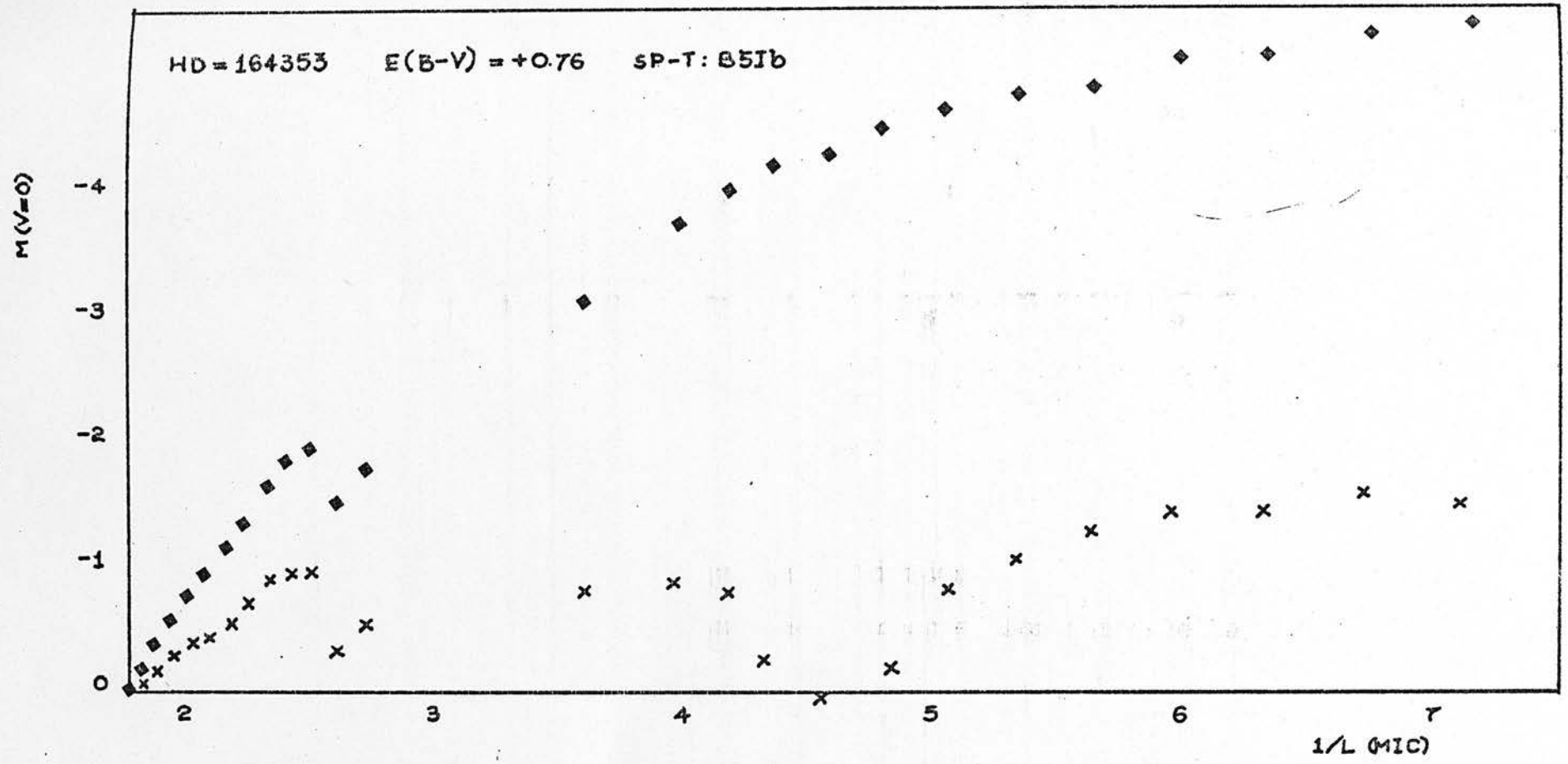

Fig. 69

× Observed magnitudes

◆ Magnitudes corrected for interstellar extinction

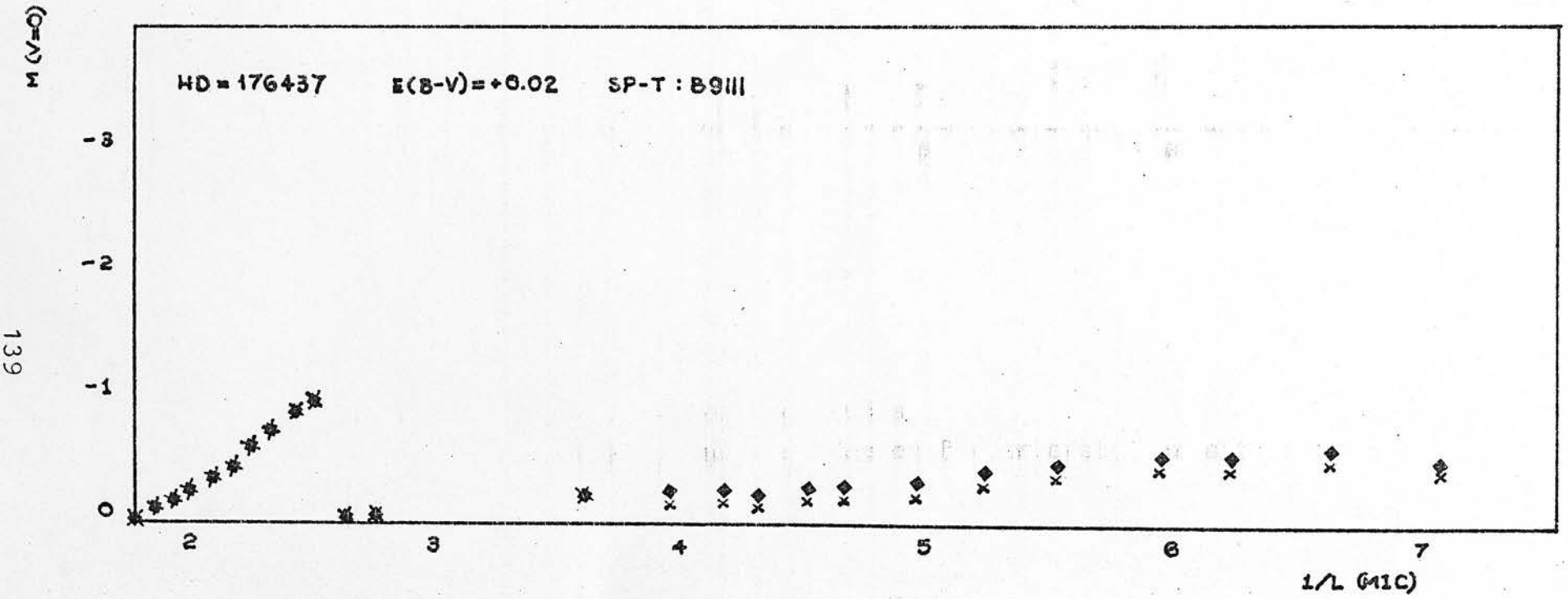

Fig. 70

× Observed magnitudes

◆ Magnitudes corrected for interstellar extinction

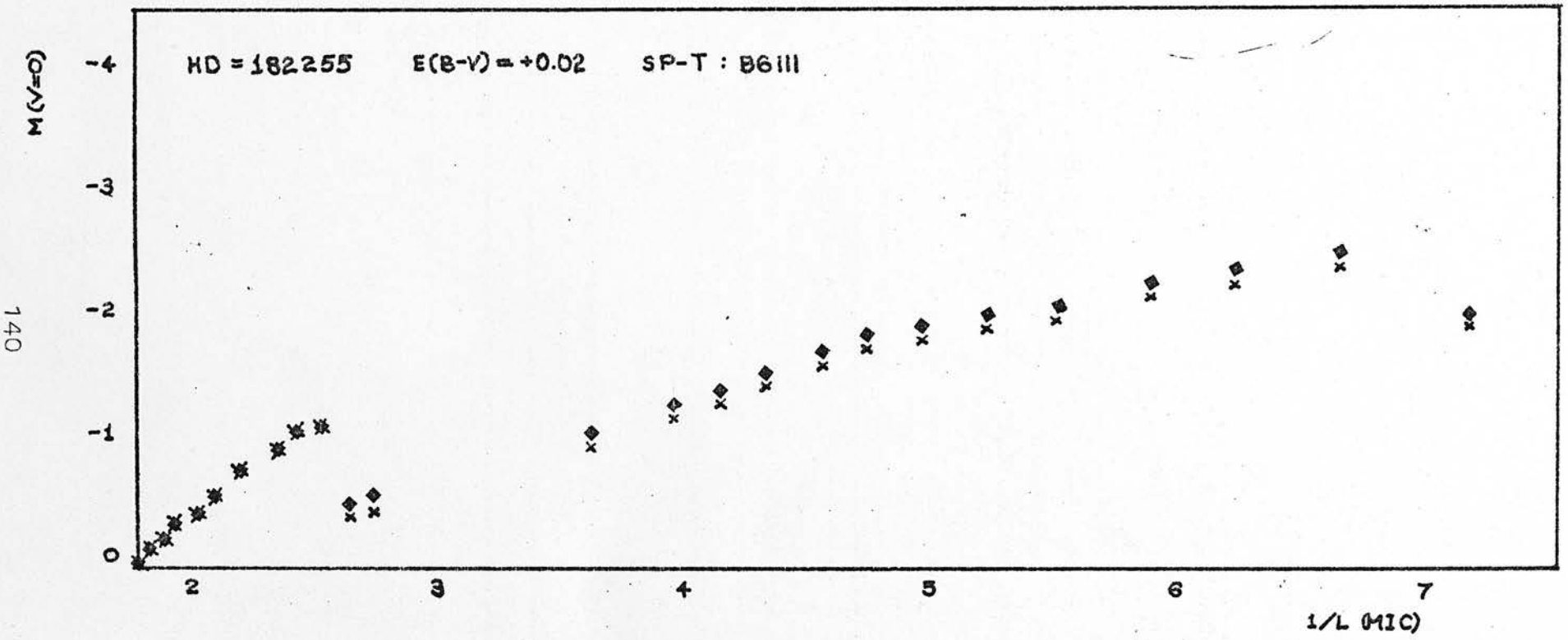

Fig. 71

× Observed magnitudes

◆ Magnitudes corrected for interstellar extinction

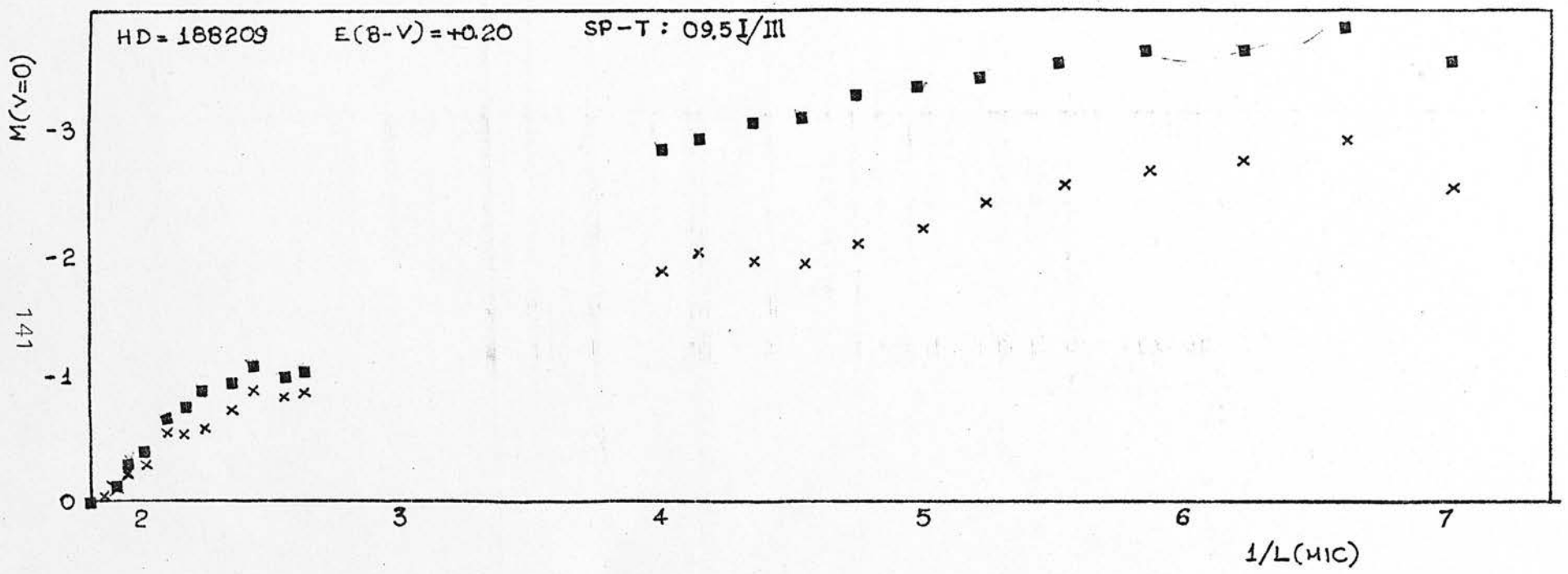

Fig. 72 × Observed magnitudes
■ Magnitudes corrected for interstellar extinction

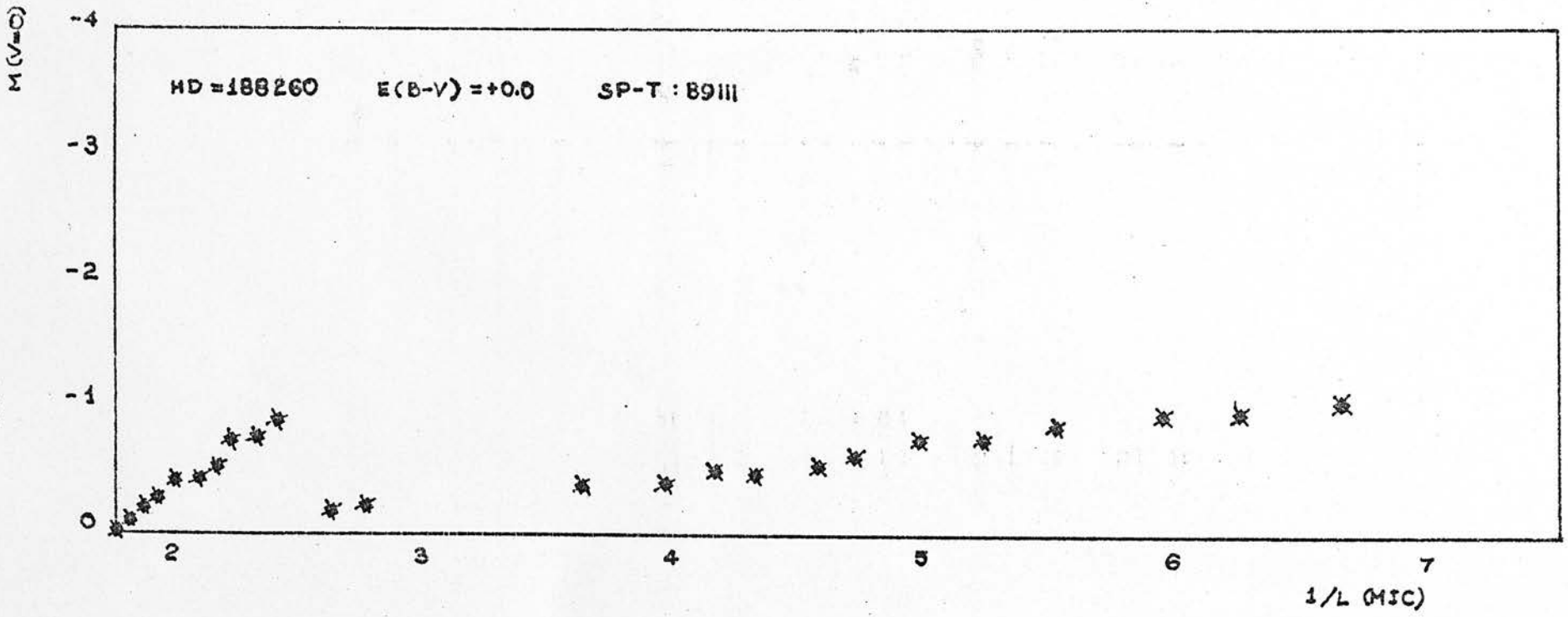

Fig. 73

× Observed magnitudes

◆ Magnitudes corrected for interstellar extinction

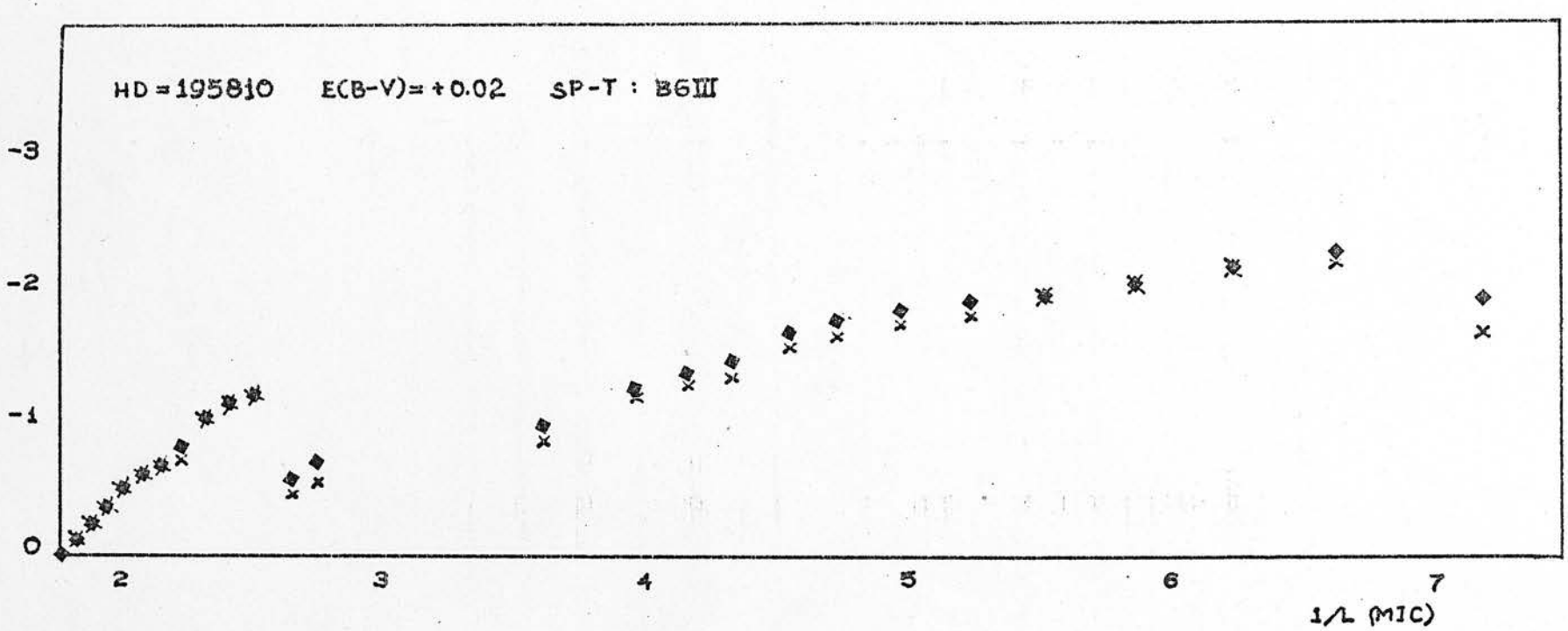

Fig. 74 × Observed magnitudes
◆ Magnitudes corrected for interstellar extinction

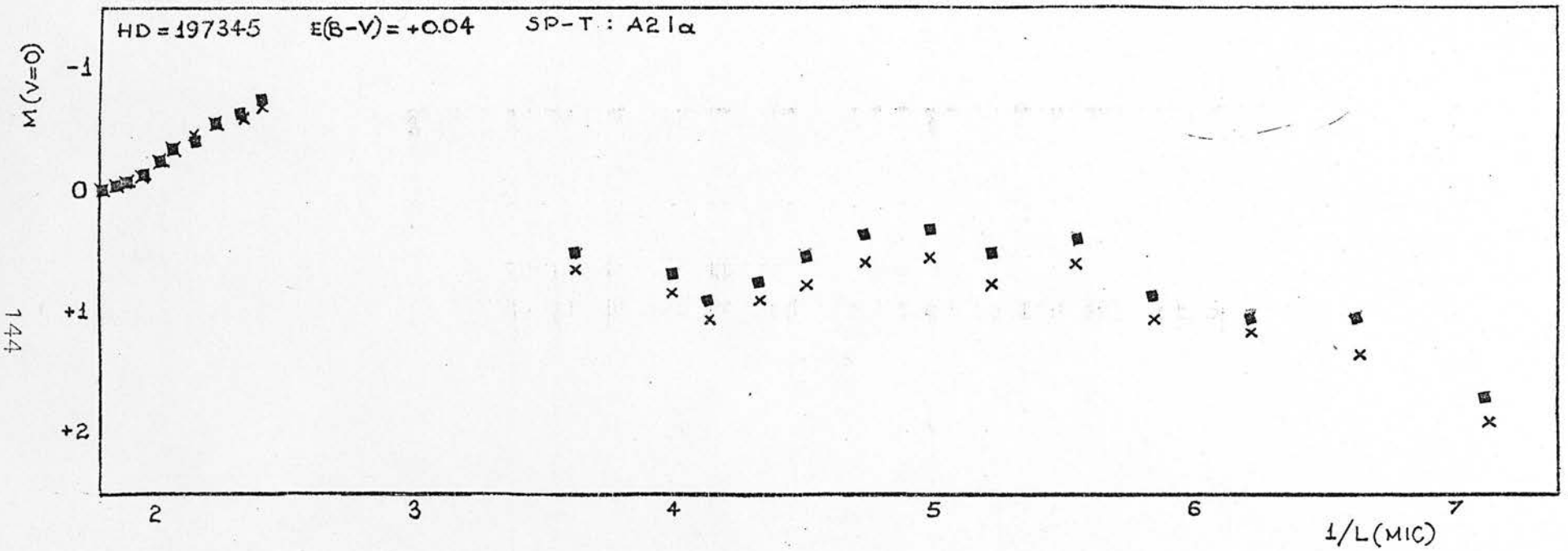

Fig. 75

× Observed magnitudes

■ Magnitudes corrected for interstellar extinction

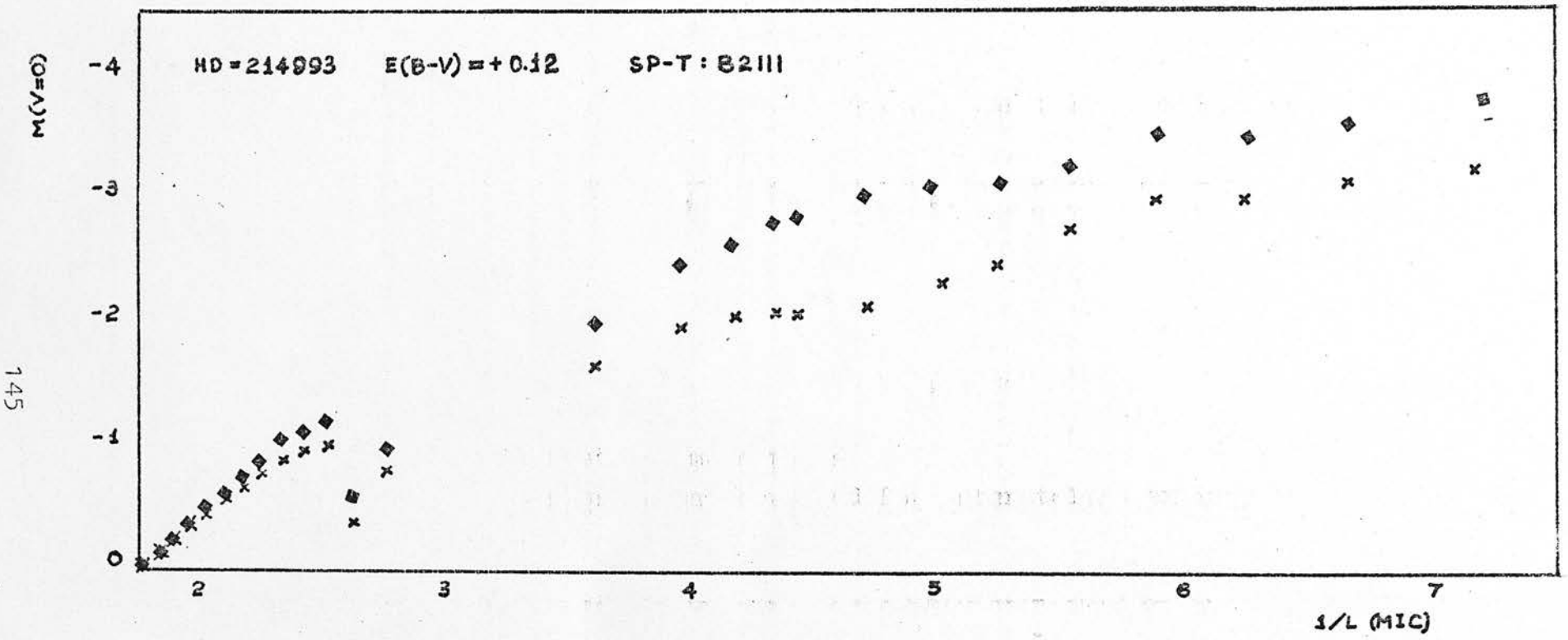

Fig. 76

× Observed magnitudes

◆ Magnitudes corrected for interstellar extinction

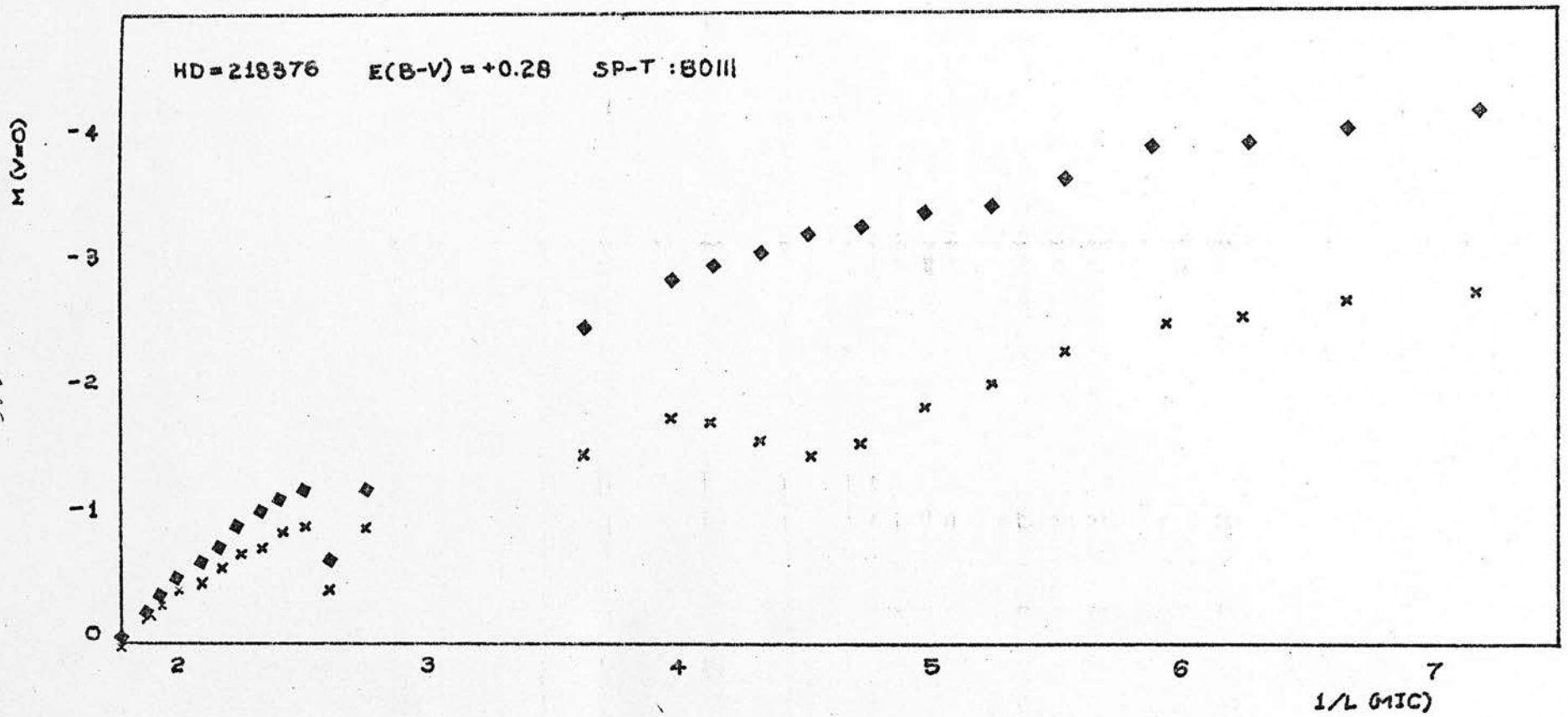

Fig. 77

× Observed magnitudes

◆ Magnitudes corrected for interstellar extinction

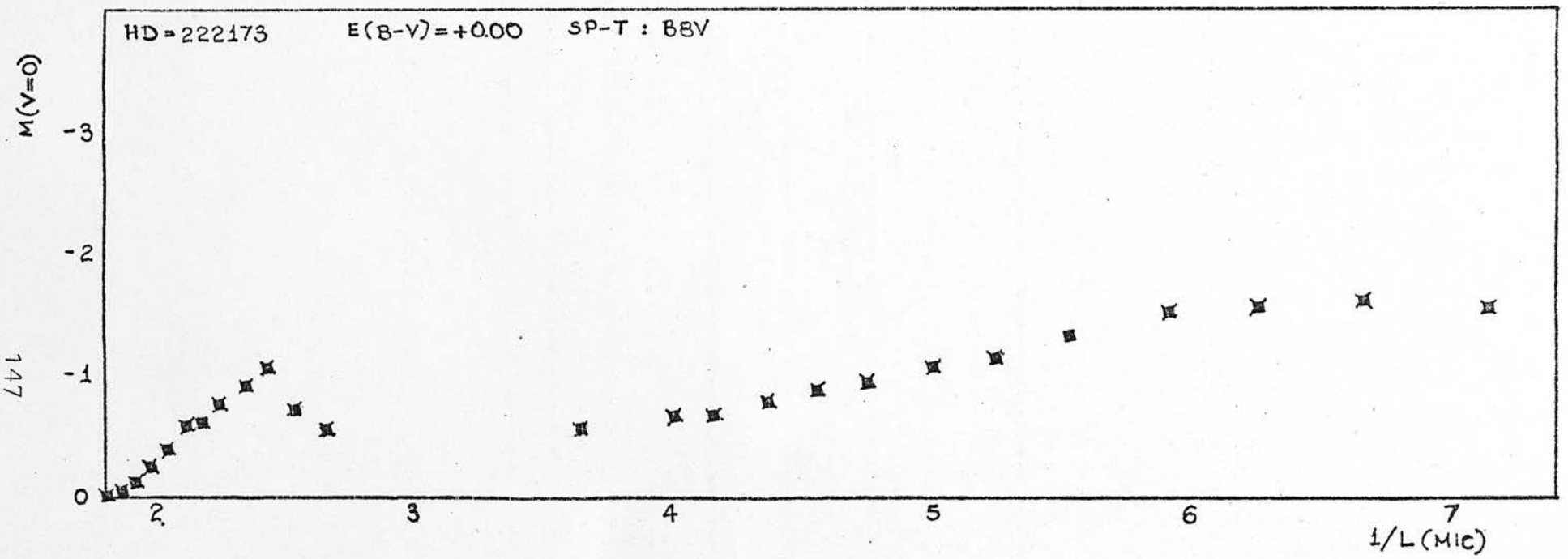

Fig. 78 × Observed magnitudes

■ Magnitudes corrected for interstellar extinction

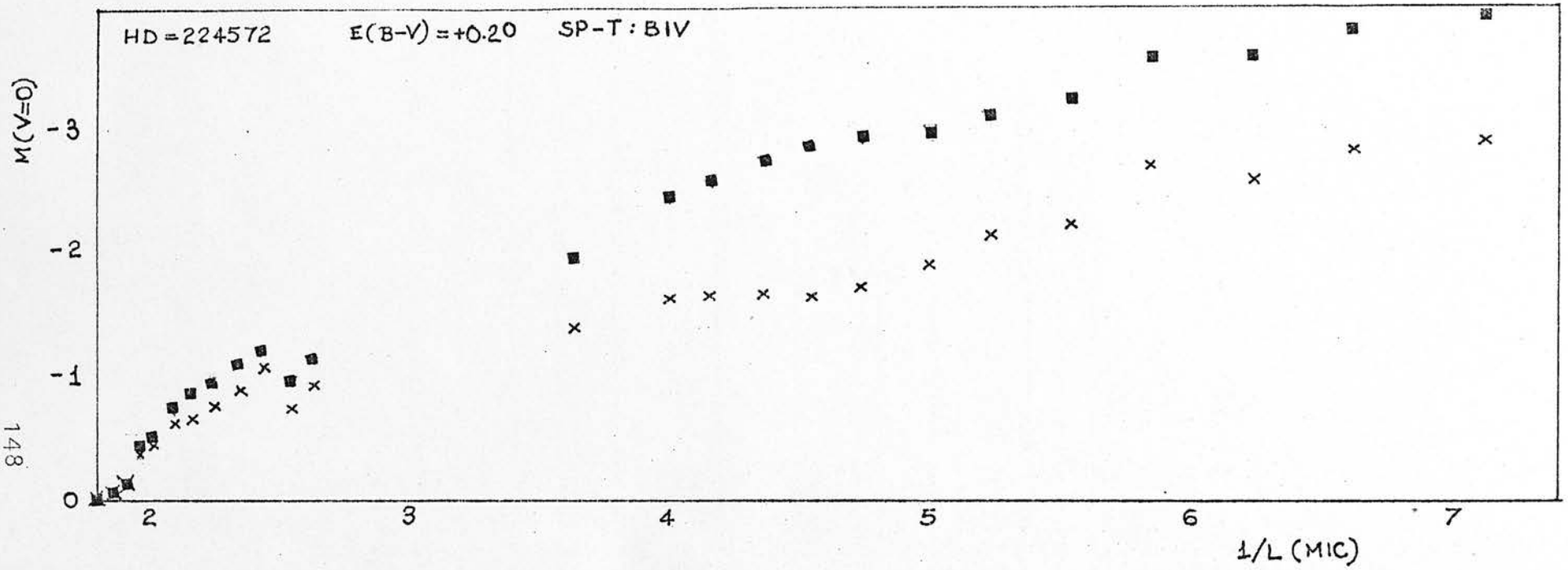

Fig. 79

× Observed magnitudes

■ Magnitudes corrected for interstellar extinction

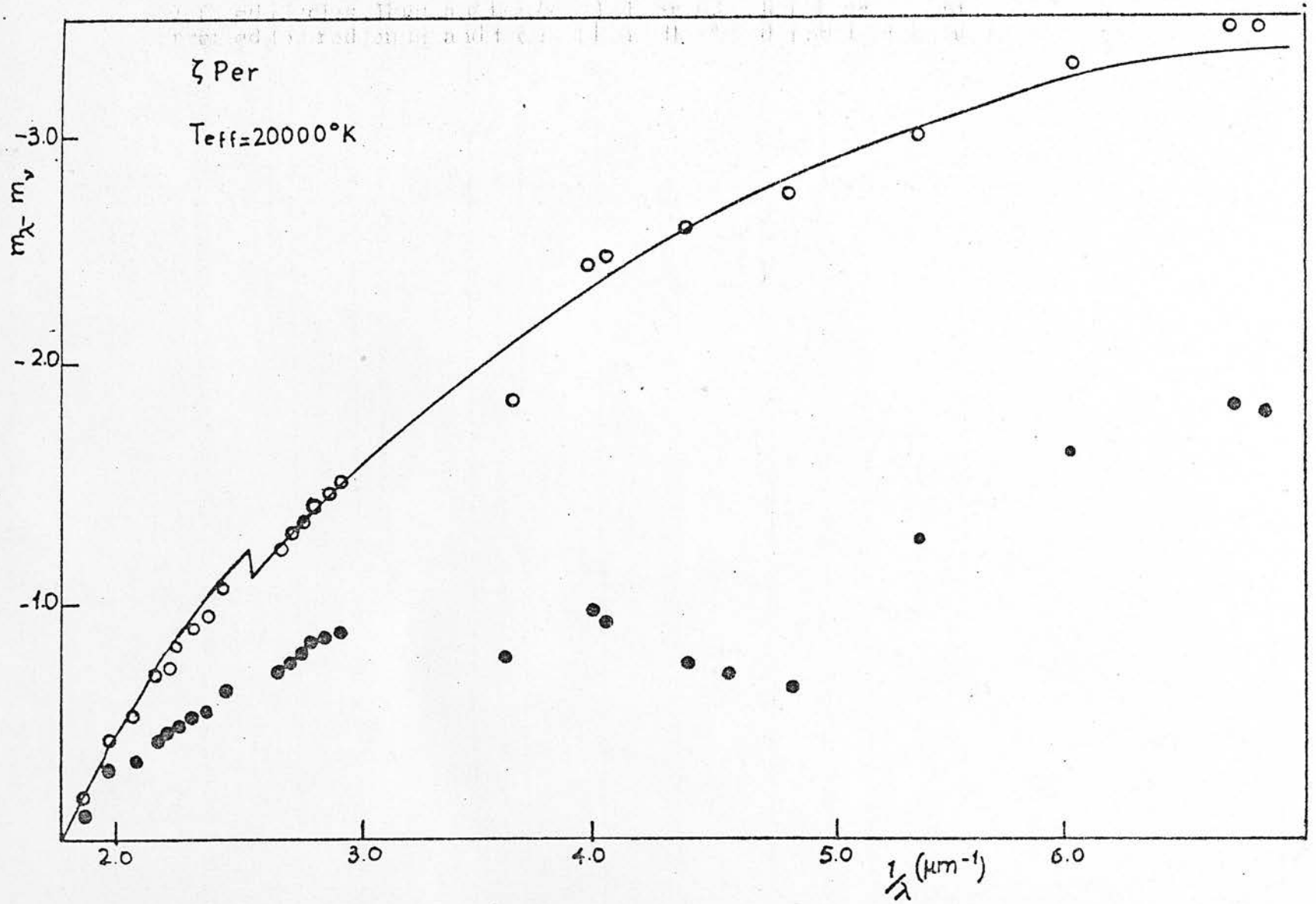

Fig. 80 The filled circles illustrate the (m-v) observed colours for ζ Per, the open circles $(m-v)_o$ corrected for reddening and the solid line the fitted model from Kurucz et al. (1974) model atmospheres

TABLE 17

Derived temperatures for the observed stars

HD	Sp	T_{eff}					
15318	B9III	10 100(1)	10 500(6)				
24398	B1Ib	20 100(1)					
24431	09V	26 000(1)	34 300(3)				
24760	B0.5V	24 000(1)	26 200(3)	25 400(4)	28 600(6)		
30614	09.5Ia	22 900(1)					
31327	B2Ia	17 000(1)					
32249	B2V	19 100(1)	20 500(3)				
33988	B2V	25 000(1)	20 500(3)				
34085	B8Ia	11 500(1)	11 200(2)	11 800(7)	11 700(8)	11 550(9)	
35468	B2III	18 500(1)	21 100(2)	21 450(5)	22 300(6)	21 580(9)	
36371	B5Ia	12 900(1)					
36512	B0V	24 500(1)	30 900(3)	29 100(4)	24 300(7)		
37128	B0Ia	22 000(1)	18 000(7)	21 300(8)	24 820(9)		
38771	B0Ia	22 000(1)	26 390(9)				
40589	B9Ia	10 100(1)					
42087	B2.5Ia	15 600(1)					
43384	B3Ia	14 400(1)					
45910	B2III	19 500(1)					
47240	B1Ia	20 000(1)					
52382	B2.5Ia	15 800(1)					
53367	B0IV	24 000(1)					
58131	B2V	18 900(1)	20 500(3)				
58350	B5Ia	12 900(1)	12 500(7)	13 100(8)	13 310(9)		
77581	B0Ia	22 100(1)					
79186	B3Ia	14 400(1)					
87734	A0Ia	9 200(1)					
87901	B7V	12 700(1)	13 600(3)	12 900(4)	12 650(5)	12 900(6)	12 900(9)
91316	B1Ib	19 000(1)					
102647	A3V	8 400(1)	8 840(3)	8 850(9)			
149438	B0V	24 400(1)	20 500(3)				
152614	B8V	11 550(1)	12 000(3)				
155763	B6III	13 500(1)	13 200(4)	13 400(6)			
160762	B3IV	16 500(1)	16 800(4)				
164353	B5Ib	28 000(1)	30 900(3)	25 500(4)			
176437	B9III	9 600(1)					
182255	B6III	14 000(1)					
188209	O9.5I/III	25 000(1)					
188260	B9III	9 800(1)					
195810	B6III	13 800(1)					
197345	A2Ia	8 950(1)	9 500(7)				
214993	B2III	19 000(1)					
218376	B0III	23 500(1)					
222173	B8V	11 600(1)	12 000(3)				
224572	B1V	22 800(1)	22 600(3)				

Reference (1) denotes the present work, and references (2) to (9) are given on p. 98.

TABLE 18

Grid of model atmospheres

Log g

T_{eff}(K)	0.5	1.0	1.5	2.0	2.5	3.0	3.5	4.0	4.5	5.0
5500	+	+	+	+	+	+	+	+	+	−
6000	+	+	+	+	+	+	+	+	+	−
6500	−	+	+	+	+	+	+	+	+	−
7000	−	+	+	+	+	+	+	+	+	−
7500	−	+	+	+	+	+	+	+	+	−
8000	−	+	+	+	+	+	+	+	+	−
8500	−	+	+	+	+	+	+	+	+	−
9000	−	−	+	+	+	+	+	+	+	−
9500	−	−	+	+	+	+	+	+	+	−
10000	−	−	+	+	+	+	+	+	+	−
11000	−	−	−	+	+	+	+	+	+	−
12000	−	−	−	+	+	+	+	+	+	−
13000	−	−	−	+	+	+	+	+	+	−
14000	−	−	−	+	+	+	+	+	+	−
15000	−	−	−	+	+	+	+	+	+	−
16000	−	−	−	+	+	+	+	+	+	−
17000	−	−	−	+	+	+	+	+	+	−
18000	−	−	−	−	+	+	+	+	+	−
20000	−	−	−	−	+	+	+	+	+	−
22500	−	−	−	−	−	+	+	+	+	−
25000	−	−	−	−	−	+	+	+	+	−
30000	−	−	−	−	−	−	+	+	+	−
35000	−	−	−	−	−	−	+	+	+	+
40000	−	−	−	−	−	−	−	+	+	+
45000	−	−	−	−	−	−	−	−	+	+
50000	−	−	−	−	−	−	−	−	+	+

0.2 mag for the visible part and 0.3 mag in the ultraviolet part.

Taking into account the various errors in the visible and ultraviolet due to photometry and introduced by the correction of interstellar extinction (discussed in Chapter III), these were found to be smaller than the step of the models used. So it has been suggested that the error in the estimation of T_{eff} for the observed stars is of the order of the temperature step of the grid of the models used providing that these models are almost realistic.

T_{eff} for the same stars has been derived computationally as well. Each spectrum is divided into three parts, first the visible part before the BJ, second the visible part after the BJ and third the ultraviolet part of the spectrum. Let us assume that X_i is the difference in magnitudes between an observed point of the first part of the spectrum and the corresponding point of the model for this wavelength (linear interpolation has been applied for the calculation of the theoretical fluxes at the observed wavelengths when they do not coincide). Following the same process we estimate Y_i and Z_i differences in magnitudes for the other two parts of the spectrum. If $T_{eff}(V)$ is the temperature of the visible part which corresponds to the model for which $\sigma_v^{(1)} = \Sigma X_i^2 + \Sigma Y_i^2$ is minimum, $T_{eff}(U)$ will be the temperature of the UV part of the spectrum where $\sigma_v^{(1)} = \Sigma Z_i^2$ is minimum. Assuming $T_{eff}(V)$ for the UV part and $T_{eff}(U)$ for the visible part two new values for σ can be estimated, $\sigma_U^{(2)}$ and $\sigma_V^{(2)}$ respectively.

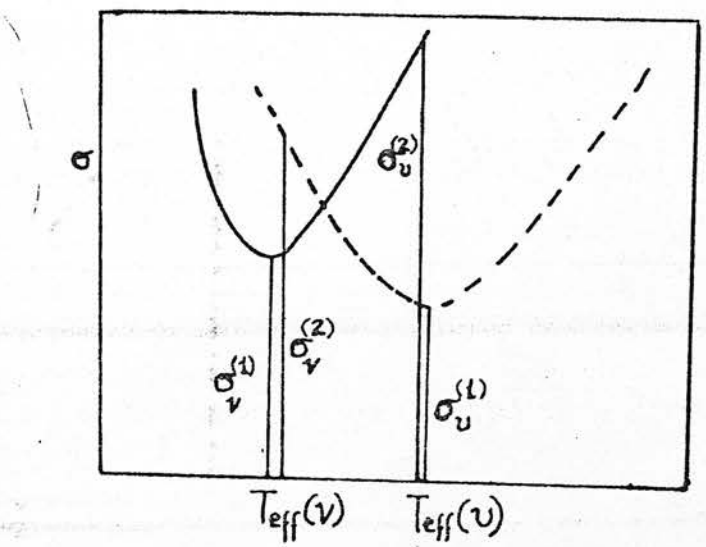

Fig. 81. An ideal plot of the described process.

Fig. 81 gives a picture of the process described in this paragraph. Knowing $T_{eff}(V)$, $T_{eff}(U)$, $\sigma_v^{(1)}$, $\sigma_v^{(2)}$, $\sigma_u^{(1)}$, $\sigma_u^{(2)}$, the weighted T_{eff} will be equal to

$$T_{eff}(W) = \frac{T_{eff}(V)\left(\sigma_v^{(1)} + \sigma_v^{(2)}\right) + T_{eff}(U)\left(\frac{1}{\sigma_u^{(1)}} + \frac{1}{\sigma_u^{(2)}}\right)}{\left(\sigma_v^{(1)} + \sigma_v^{(2)}\right) + \left(\frac{1}{\sigma_u^{(1)}} + \frac{1}{\sigma_u^{(2)}}\right)}$$

assuming $T_{eff}(V) < T_{eff}(U)$ and $\sigma_v^{(1)}, \sigma_v^{(2)}, \sigma_u^{(1)}, \sigma_u^{(2)} > 1$; but if $T_{eff}(V) > T_{eff}(U)$ then

$$T_{eff}(W) = \frac{T_{eff}(U)\left(\sigma_u^{(1)} + \sigma_u^{(2)}\right) + T_{eff}(V)\left(\frac{1}{\sigma_v^{(1)}} + \frac{1}{\sigma_v^{(2)}}\right)}{\left(\sigma_u^{(1)} + \sigma_u^{(2)}\right) + \left(\frac{1}{\sigma_v^{(1)}} + \frac{1}{\sigma_v^{(2)}}\right)}$$

and if $\sigma_j^{(i)} < 1$ it is replaced by its reciprocal, i = 1,2 and J = V,U.

This method has been applied and it has been found that the disagreement between T_{eff}(weighted) and T_{eff}(superimposed) is 500K for cool stars and up to 1200K for the hot stars.

V. 2 DISCUSSION ON THE USED MODELS

Models are realistic if they can predict the energy distribution for stars that can be well observed. There are three approaches to model-atmosphere construction: empirical, semi-empirical and theoretical.

In the empirical approach a temperature-pressure structure is hand-adjusted until it reproduces, as closely as possible, the observed flux intensity, making use of a model-atmosphere program containing the stellar opacity sources. The second model-atmosphere approach is semi-empirical. In this case an opacity function is constructed based on free parameters that are determined such that the model calculation agrees with observations. Then a mode or modes of energy transport are assumed and a model constructed that conserves energy. The third approach is theoretical, in that all opacities are computed theoretically and the temperature/pressure structure is determined by conservation of energy. This method is not very useful for later type stars, because the line opacity is difficult to calculate.

The models used to derive the effective temperatures of this project are theoretical, and the assumptions and approximations made by Kurucz, Peytremann & Avrett (1974), who ran the computational program, are the following:

i) The atmosphere is in a steady state.

ii) The flux of energy is constant with depth in the atmosphere since the energy source for a star lies far below the atmosphere and since no energy comes into the atmosphere from above.

iii) The atmosphere is homogeneous except in the normal direction.

iv) The atmosphere is thin relative to the radius of the star so we can consider plane layers instead of concentric shells.

v) There is no relative motion of the layers in the normal direction: there is no net acceleration of the atmosphere, so the pressure balances the gravitational attraction, i.e.

$$\rho \frac{d^2r}{dt^2} = -\rho g + \frac{dP}{dr} = 0$$

g is the gravitational acceleration which is approximately constant because the atmosphere is thin.

vi) The atomic abundances are specified and constant throughout the atmosphere.

Solar abundances and microturbulence velocity 2 $km.sec^{-1}$ have been chosen as the most representative values. Solar abundances compiled by Withbroe (1971) have been adopted and if abundances for the Sun are not known Allen's (1963) list is used. It has been assumed 0.9 hydrogen and 0.1 helium by number, and the following logarithmic abundances of the other elements relative

to the total are:

Li	-11.45	Be	-10.99	B	-9.25	C	-3.48	N	-3.99	O	-3.22	F	-7.49	Ne	-4.60	Na	-5.81	Mg	-4.51
Al	-5.65	Si	-4.50	P	-6.62	S	-4.84	Cl	-6.40	Ar	-5.40	K	-7.00	Ca	-5.72	Sc	-8.98	Ti	-7.31
V	-7.95	Cr	-6.35	Mn	-6.55	Fe	-4.65	Co	-7.55	Ni	-5.77	Cu	-7.60	Zn	-7.63	Ga	-9.21	Ge	-8.73
As	-9.70	Se	-9.40	Br	-9.40	Kr	-8.80	Rb	-9.42	Sr	-9.23	Y	-10.43	Zr	-9.63	Nb	-9.75	Mo	-10.15
Tc	-20.00	Ru	-10.45	Rh	-10.50	Pd	-10.48	Ag	-11.38	Cd	-10.08	In	-10.34	Sn	-10.34	Sb	-11.30	Te	-10.00
I	-10.60	Xe	-10.00	Cs	-10.26	Ba	-10.25	La	-10.24	Ce	-10.41	Pr	-10.42	Nd	-10.23	Pm	-20.00	Sm	-10.39
Eu	-11.56	Gd	-10.93	Tb	-11.60	Dy	-10.94	Ho	-11.50	Er	-11.29	Tm	-11.62	Yb	-11.24	Lu	-11.21	Hf	-11.40
Ta	-11.70	W	-9.45	Re	-11.40	Os	-11.30	Ir	-9.84	Pt	-10.40	Au	-11.73	Hg	-9.05	Tl	-11.85	Pb	-10.13
Bi	-11.25	Po	-20.00	At	-20.00	Rn	-20.00	Fr	-20.00	Ra	-20.00	Ac	-20.00	Th	-11.23	Pa	-20.00	U	-11.45
Np	-20.00	Pu	-20.00	Am	-20.00	Cm	-20.00	Bk	-20.00	Cf	-20.00	Es	-20.00						

In blanketing calculations, it is important to have as complete a line list as possible. The temperature structure in a heavily blanketed stellar atmosphere is determined more by the amount of space between the lines themselves. Thus if a large number of weak lines are included, they can fill in the spaces and produce a considerable difference in the flux that emerges.

The first attempt to include the effects of a large number of lines in a model atmosphere calculation was that of Strom & Kurucz (1966), in which 30 000 lines were used to construct crude distribution functions for a model (6500K). Peytremann (1970) has calculated a grid of blanketed models using approximately the same lines in a Monte Carlo treatment. Investigations have shown that the available line lists were seriously incomplete and do not predict observed blanketing.

The list of lines considered for the construction of the used models include as many as 1 760 000 lines and it is the richest used so far.

The spectrum has been divided into small wavelength intervals and the selected line data for each interval are slightly beyond both ends to pick up the wings of lines in neighbouring intervals. There are between 15 000 and 30 000 lines per interval above the Lyman limit with a falling of number in the Lyman continuum due to a shortage of spectral imformation on multiply ionised atoms.

The radiative damping constant is assumed equal to the classical

$$\Gamma_R = 2.223E13 / \lambda^2_{centre} \quad \text{(in sec}^{-1}\text{, } \lambda \text{ in nanometers)}$$

and the Van der Waals damping constant used is approximated by

$$\Gamma_W = \frac{\eta^2_{eff}}{Z_{eff}} 17 \left(\frac{8KT}{\pi M}\right)^{0.3} \left((161E-33)^{0.4} N_H + \left(\frac{1}{4}\right)^{0.3} (0.50E-33)^{0.4} N_{He} \right)$$

while the Stark damping is a fit by Peytremann:

$$\Gamma_S = 1E-8\, \eta^5_{eff} N_e (sec^{-1})$$

Convective flux was calculated but not included in the temperature correction except for T_{eff} = 8000K but even in these models convection plays only a minor role in comparison to the blanketing effect. The continuous opacities are HI, HII, HeI, HeII, HeIII, CI-IV, NII-V, OII-VI, NeI-VI, MgI, AlI, SiI, H_2^+, H^-, H Rayleigh scattering, and electron scattering.

Hydrogen lines are added separately to the total line absorption coefficient. After the total line absorption coefficient has been calculated for every wavelength point in the region, the fraction of the total number of points that fall below each one-tenth decade in opacity is determined.

It has been shown by Kurucz (1974c) that the program is capable of reproducing the solar spectrum reasonably well.

Comparison of the described published models has been made with selected published models to show the differences in the treatment of line blanketing and to non-LTE effects. Carbon & Gingerich (1969) have produced a grid of blanketed models for temperatures in the range 4000 to 10000K. The models included Balmer lines and a three-step distribution function. Blocking coefficients were not available in the far ultraviolet and so the used ultraviolet line opacity was from extrapolation, above 8500K only Balmer line blanketing was included.

A year later a new grid of blanketed models for B stars has appeared (Van Citters & Morton 1970) and 98 of the strongest lines in the ultraviolet have been included. A similar grid for O stars has been published by Bradley & Morton (1969) including 110 lines. Both models assumed ten times classical damping and a helium abundance 30% higher than Kurucz, Peytremann & Avrett (1974).

A grid of non-LTE atmospheres of B and O stars was

produced by Mihalas (1972) where there is a detailed treatment of hydrogen and helium statistical equilibrium but line blanketing opacity is not included. Fig. 82 shows the comparison of Mihalas (1972) non-LTE (solid line) and LTE (long dashed line) models with Kurucz, Peytremann & Avrett (1974) (short dashed line) model atmospheres.

Fowler (1972) used a list of 29 000 lines and for each line he assumed a Van der Waals damping constant approximately twice that of Kurucz, Peytremann & Avrett (1974) and a radiative damping constant which was thirty times larger than the classical one. Only a few lines were included in the far ultraviolet and carbon, magnesium, silicon continua were omitted.

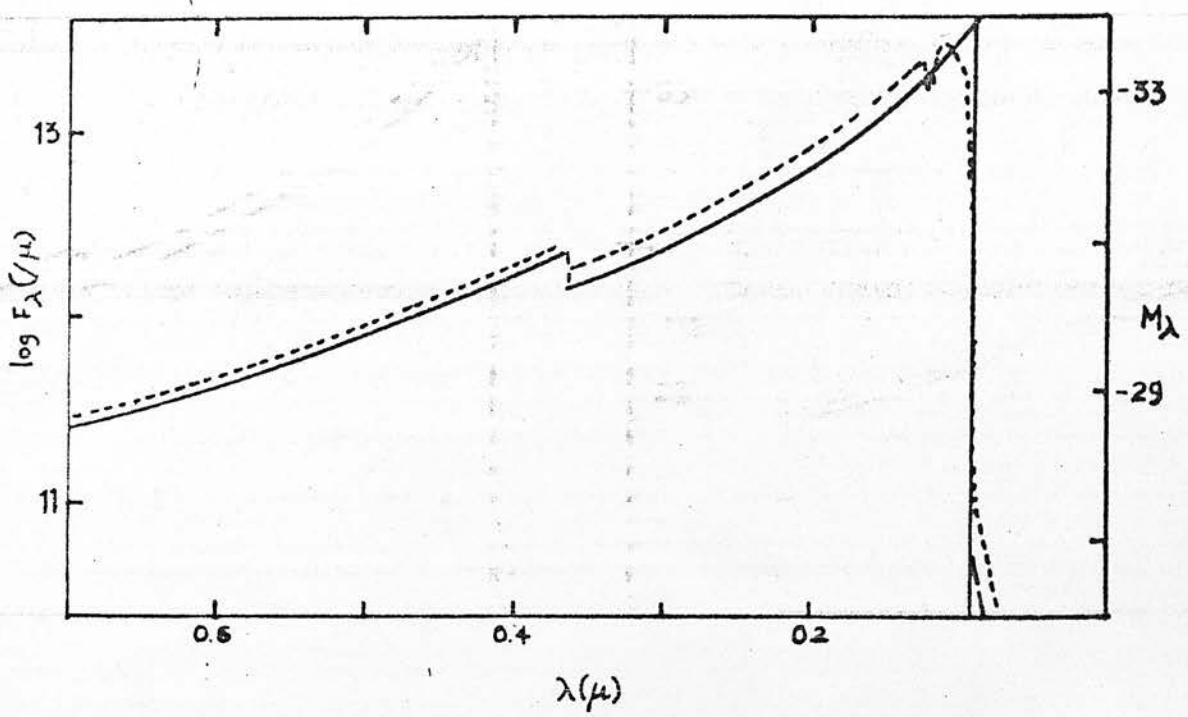

Fig. 82 Comparison of the Mihalas (20000, 4) non-LTE model (solid line) and LTE model (long dashed line) with Kurucz, Peytremann & Avrett (1974) model (short dashed line).

V. 3 DISCUSSION ON THE DERIVED TEMPERATURE SCALE

The temperature scale derived here is believed to be an improvement on previously published temperatures.

The observational data cover a wide range of wavelengths (1398 Å - 5556 Å) and the used models (Kurucz et al. 1974) are very elaborate and produced for a large number of temperatures and gravities. The line blanketing, which is very important for the spectral type and wavelength range studied here, has been computed for a very large number of lines for the first time.

The effect of gravity on the energy distribution is relatively small compared with the effect of temperature changes for different spectral types. For example a change in the gravity from log g = 4 to log g = 2 would be equivalent to a change in temperature of less than 500K at 10000K. Therefore in using the fluxes to determine the temperatures of B and early A stars, the gravity will not need to be known with great accuracy (Nandy & Schmidt 1975). The effect of gravity changes on the theoretical energy distribution is shown in Fig. 83.

A brief discussion on the derived temperatures by other workers (listed in Table 17, p. 150) is given below.

For T_{eff}(2) derived by Hanbury-Brown et al.(1967), the angular diameter has been used to find the absolute monochromatic flux at the surface of the star. It is known that the flux F_λ at the surface of a star is related

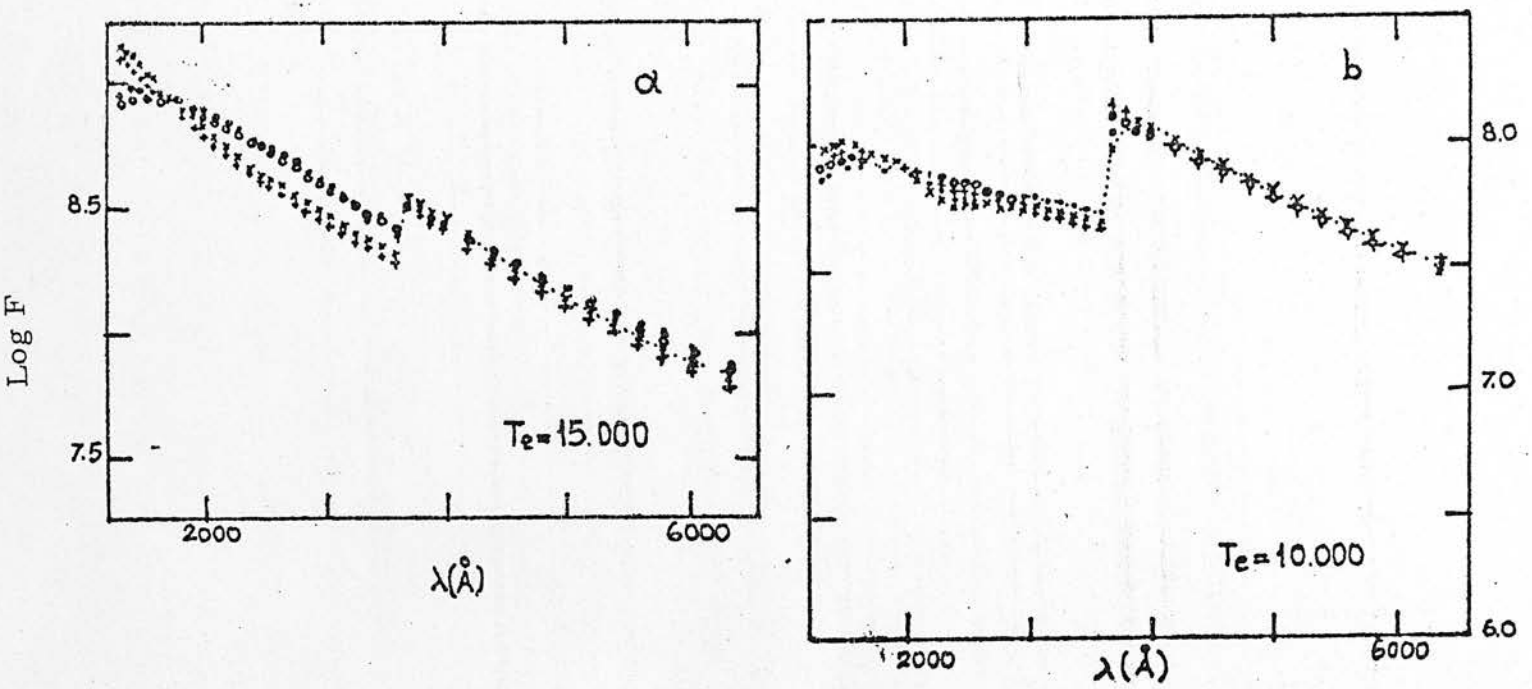

Fig. 83. The effect of line blanketing and variations in gravity on the model energy distribution for Teff 10000 K and 15000 K. The unit of flux is ergs cm^{-2} s^{-1} Sr^{-1} nm^{-1}. (Nandy & Schmidt, 1975). (logg = 2, • Blanketed, ○ Unblanketed) (logg = 4, × Blanketed, + Unblanketed)

to the absolute monochromatic flux received outside the Earth's atmosphere by:

$$F_\lambda = \frac{4 f_\lambda}{\theta_{UD}^2}$$

The values of f_λ have been taken from the fluxes published by Willstrop (1965) in the range 4000 Å to 6000 Å.

Grids of model atmospheres published by Mihalas et al. (1965), Strom et al. (1965), Mihalas et al. (1966) have been used to derive T_{eff}. These temperatures are based on energy distributions covering a small wavelength range. The interstellar extinction has not been taken into consideration and the used models do not include enough lines for the blanketing effect.

$T_{eff}(3)$ (Morton et al. 1968) were based on model atmospheres (Mihalas & Morton 1965, Mihalas 1966, Adams & Morton 1968, Hickok & Morton 1968). The temperatures were obtained by interpolating between the models using U-V as an independent variable for O and B types and B-V for cooler stars. Around AOV spectral types considerable weight was given to fit the H_γ profile and the absolute energy distribution in the visible with the new models. The models they used included absorption lines shortward of 1600 Å whereas early type stars have considerable blanketing in the 2000 - 3000 Å region (Underhill 1972). Flux from this region is redistributed to the visual, and if only the visual spectrum is compared with model atmospheres as did Morton & Adams, one would conclude too high temperatures.

$T_{eff}(4)$ have been derived by Heintze (1969). He determined the effective temperatures by comparing Balmer Jumps of stellar spectra with theoretical ones calculated by Mihalas (1965, 1966). There are many observational difficulties that are due to calibration of the Balmer Jump of the photometric standard and photometric uncertainties; and theoretical difficulties that are due to deviation from local thermodynamic equilibrium (LTE), blanketing effect, rotation and differences in metal content which can influence the predicted Balmer Jump. The deviations from LTE cause a decrease in the predicted Balmer Jump but blanketing increases it.

The temperatures $T_{eff}(5)$ (Hyland 1969) were found by fitting the model predictions to the observed energy distribution in the range 3300 - 5000 Å with greatest weight being given to the Paschen continuum. The models on which observations were fitted have been published by Morton et al. (1968), Hickok et al. (1968), Mihalas et al. (1965), Adams et al. (1968), Mihalas (1966). The facts that the used models include absorption lines shortward of 1600 Å only, and that the observations do not cover a wide wavelength range, introduce uncertainties in the derived temperatures.

For $T_{eff}(6)$ (Schild et al. 1976), the observed Balmer Jump and the Paschen continuum have been compared with models published by Mihalas et al. (1965), Adams et al. (1968), Van Citter et al. (1970). The temperatures have been determined by fitting the models to observed continuum

fluxes and extrapolated to the ultraviolet and infrared. Equal weight was given to Balmer discontinuity and to the Paschen continuum in estimating effective temperatures except for the reddened stars where the Balmer discontinuity was given most of the weight.

For $T_{eff}(7)$, Nandy & Schmidt (1975) have combined observational data in the ultraviolet and UBV values in the visible and compared with models (Kurucz 1970) that allow the inclusion of line opacity based on about 750 000 spectral lines. The derived temperatures were based on wide band photometry in the visible, so uncertainties were introduced in the estimation of the continuum.

$T_{eff}(8)$ have been found by Nandy & Schmidt (1975) as well by using a different process that described for $T_{eff}(7)$. The flux at several ultraviolet wavelengths and the angular diameters of some of the stars measured by Hanbury Brown et al. (1974) were used in order to derive these temperatures.

Only one discrepancy was found between $T_{eff}(7)$ and $T_{eff}(8)$ (for five stars) and this was the hottest star. So it has been suggested that this may be related to non-LTE effects (Nandy & Schmidt 1975).

Finally Code et al.(1976) have found empirical effective temperatures by using the angular diameters and absolute flux distribution. The observed fluxes from the infrared $\lambda >$ 8080 Å to the ultraviolet λ = 1100 Å have been integrated and the effective temperatures derived using the relation

$$T_{eff} = \left(\frac{F}{\sigma}\right)^{1/4}$$

where F is the integrated stellar flux at the surface of the star and σ is the Stefan-Boltzmann constant.

The ultraviolet fluxes were obtained by the OAO-2 satellite over the spectral ranges 1100 - 2000 Å and 2000 - 3500 Å with spectral resolutions of about 10 and 20 Å respectively. The fluxes in the visible were centred at 25 wavelengths (passband 50 Å) in the spectral range of 3300 - 8080 Å. An extension of fluxes in the infrared was attempted by using the broad band I,J,K,L,M,N magnitudes of Johnson.

The observed fluxes were corrected for interstellar extinction and then were integrated in five wavelength bands 1100 - 1300, 1300 - 1800, 1800 - 3300, 3300 - 8100, 8100 - ∞. The total absolute flux integrated over the entire spectrum has been used for the estimation of $T_{eff}(9)$.

Some of the stars (Code et al. 1976b) coincide with stars of the present project. The temperatures derived for the common stars have been used for the comparison of the two scales.

It can be seen from Table 17 that for the cooler stars there is a very good agreement between $T_{eff}(1)$ and $T_{eff}(9)$.

For the stars HD 34085, 58350, 87901 and 102 647 $\Delta T_{eff} = T_{eff}(1) - T_{eff}(9)$ has the values +250K, -400, +500, -450 respectively. All these differences are within the limits of the accuracy of $T_{eff}(1)$ scale.

For the hot stars HD 35468, 37128, and 3877, ΔT_{eff} is between 2000 - 4000K. These differences are too high to be within the limits of accuracy of both scales.

For these seven common stars the angular diameters known from Hanbury Brown et al. (1974) and their fluxes have been used for another estimation of T_{eff}.

The observed fluxes corrected for interstellar extinction were extrapolated towards the ultraviolet and to the infrared using the fluxes of the best fit model (Kurucz et al. 1974). The wide spectral range fluxes so derived were integrated and T_{eff}(ang. diam.) are listed in Table 19.

TABLE 19

T_{eff} for stars of known angular diameter

HD	T_{eff} (angular diameter)	T_{eff}(g) (Code et al.1976b)
34085	11700 K	11550 K
35468	20500 "	21580 "
37128	23500 "	24820 "
38771	24600 "	26300 "
58350	13200 "	13310 "
87901	12500 "	12210 "
102647	8600 "	8850 "

In this Table the effective temperatures $T_{eff}(9)$ found by Code et al. (1976b) are listed as well. From Tables 17 and 19 it can be seen that the agreement between T_{eff}(ang.diam.) and $T_{eff}(9)$ is better than $T_{eff}(1)$ and $T_{eff}(9)$ for the hot stars. The discrepancy between $T_{eff}(1)$ and T_{eff}(ang.diam.) may be related to non-LTE effects (Nandy & Schmidt 1975) as it happens for the hottest stars of the sample.

It has also to be emphasised that the $T_{eff}(1)$ scale was determined using ultraviolet fluxes no shorter than 1350 Å. But it has been found that the flux emitted by the very hot stars in shorter wavelengths becomes appreciably large. Code et al. (1976b) have calculated that for $T_{eff} \sim 12500$K the flux for $\lambda < 1100$ Å is less than 1% of the total flux whereas for $T_{eff} \sim 35000$K it is $\sim 35\%$ of the total flux.

The derived $T_{eff}(1)$ for stars with spectral types earlier than O9 are much lower than expected for their spectral type. Therefore the derived values were considered meaningless and are not listed in Table 17. Similarly cool effective temperatures are indicated by ultraviolet flux measurements of the essentially unreddened O stars 15 Mon (O7) and ζ Pup (O5) (Stecher 1970, Boksenberg et al. 1973) but these ultraviolet temperatures are unfortunately rather sensitive to any small amount of reddening that may be present.

The dereddened colour index $(1910 - V)_o$ has been chosen by Lesh (1976) as a temperature indicator. This

suggestion was made by A.D. Code because this colour index is not strongly affected by lines or continuum edges. Lesh (1975) has used T_{eff} for stars with $(1910 - V)_o < 0$ and spectral types earlier than A2 and the least square line fitting through the data points has the expression:

$$\theta_{eff} = 0.565 + 0.111(1910 - V)_o$$

where

$$\theta_{eff} = 5040/T_{eff}$$

Fig. 84 shows the dereddened colour index $(1920 - V)_o$ available from observations presented here and the derived expression is:

$$\theta_{eff} = 0.556 + 0.106(1920 - V)_o$$

Comparing the last two equations it is obvious that the two temperature scales are very competitive.

The derived T_{eff} for the observed stars against MK spectral type are shown in Fig. 85 and T_{eff} against the parameter Q where $Q = (U - B) - 0.72(B - V)$ are shown in Fig. 86. T_{eff} derived by Johnson (1966) and by Schild, Peterson & Oke (1971) are also plotted in these diagrams. It can be seen from these diagrams that supergiants are separated from the main sequence stars. The difference in temperature for stars having exactly the same spectral type can be explained as partially due to the differences in gravity or extinction since both are not known precisely. In some cases like the star (HD 33988, B2V) which shows a large value of T_{eff} this cannot be explained as a gravity or extinction effect. This can possibly be explained if

we assume that the photometric error is very high or it is a wrong identification or it is not a normal star or the spectral type B2V taken from Blanco et al. (1968) is wrong for that particular star. It rather agrees with a BO spectral type. It must be considered that Underhill (1977) pointed out "The Be and shell stars which appear to have UV spectra corresponding to earlier types, when examined at high resolution from the ground do have earlier types than the MK type. For instance, in 1952 I showed ζ Tau was about B1 rather than B4 as given by MK type".

θ_{eff} versus Q has been plotted in Fig. 87 and compared with the diagrams of Figs. 85, 86. This seems to be a better presentation for the different luminosity classes because it forms more distinctive curves. For supergiants with $Q < 0.3$, θ_{eff} can be identified with a straight line.

From the diagrams of Figs. 85, 86, 87 it is clear that giants are cooler than main sequence stars of the same spectral type. Such differences have been pointed out in Chapter IV where the observed luminosity effect is discussed.

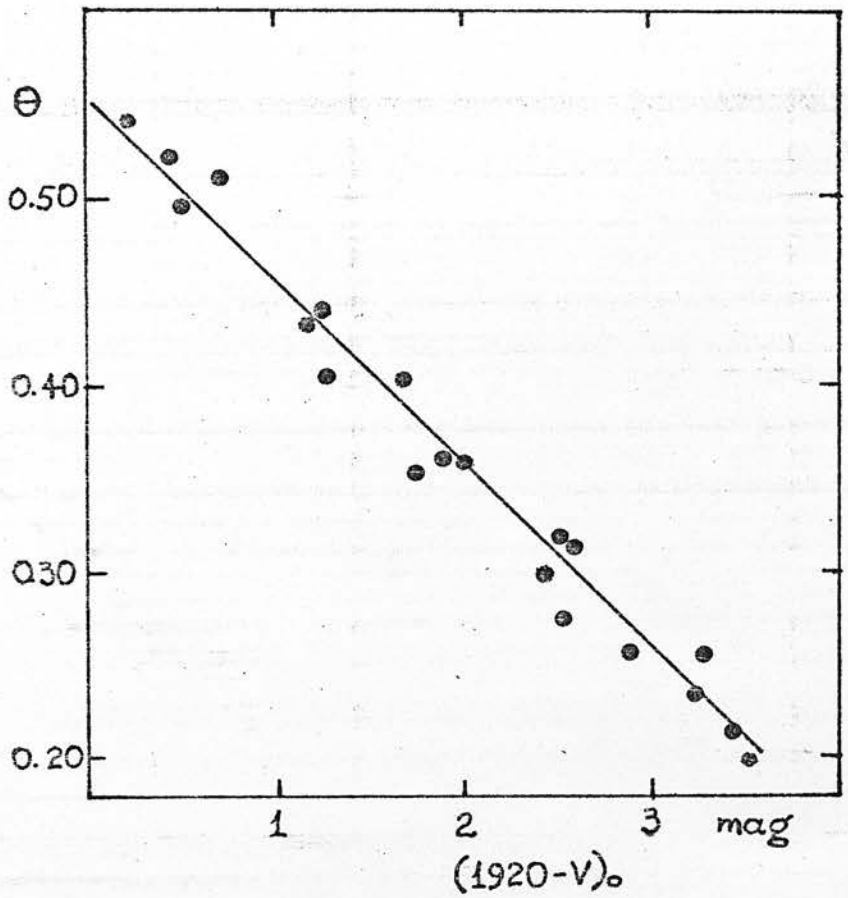

Fig. 84. Temperature distribution for the dereddened colour index $(m_{1920} - V)_o$

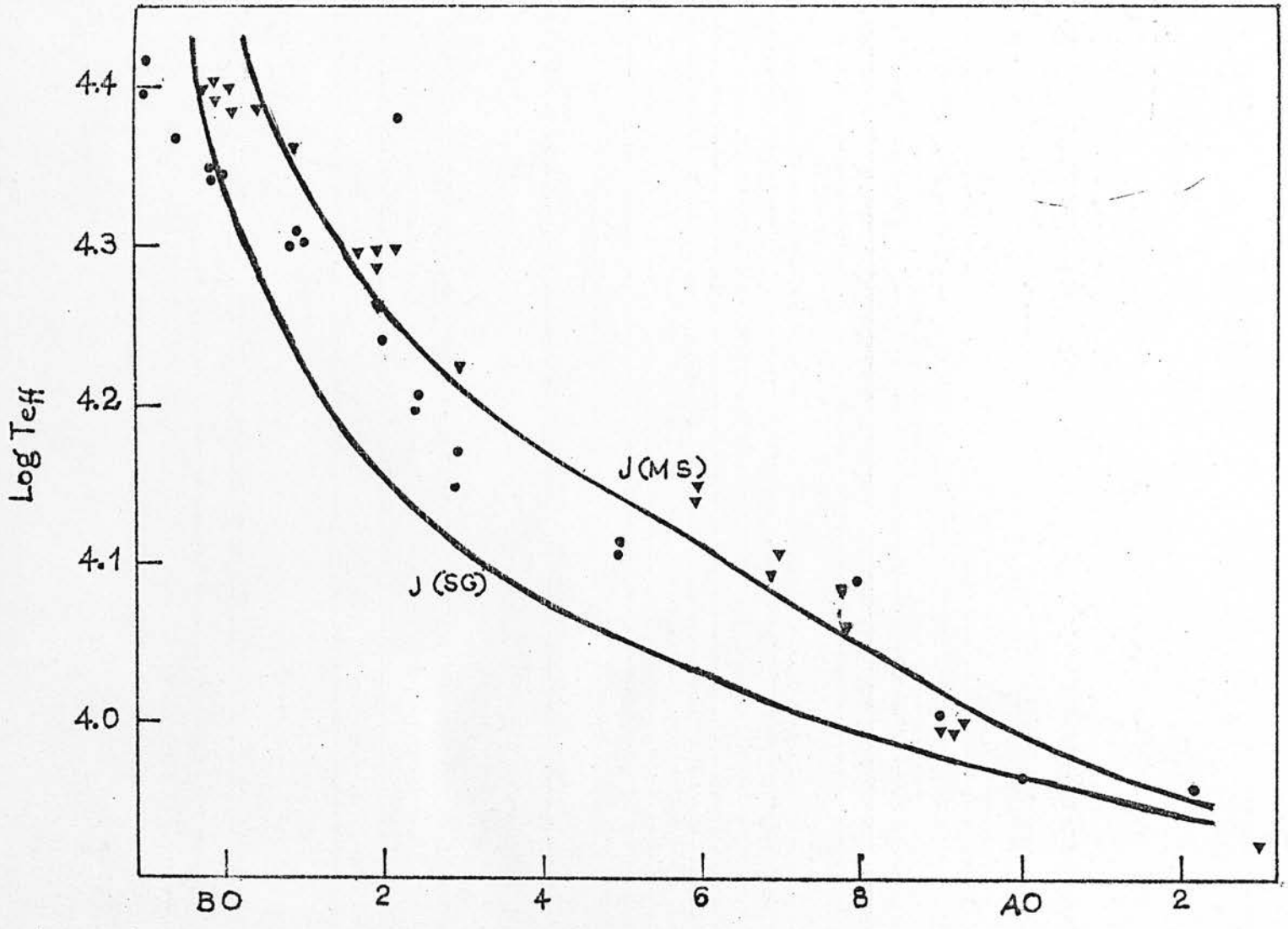

Fig. 85. Temperature distribution for hot stars. Filled circles for supergiants, triangles for main sequence, solid lines show temperature from Johnson (1966).

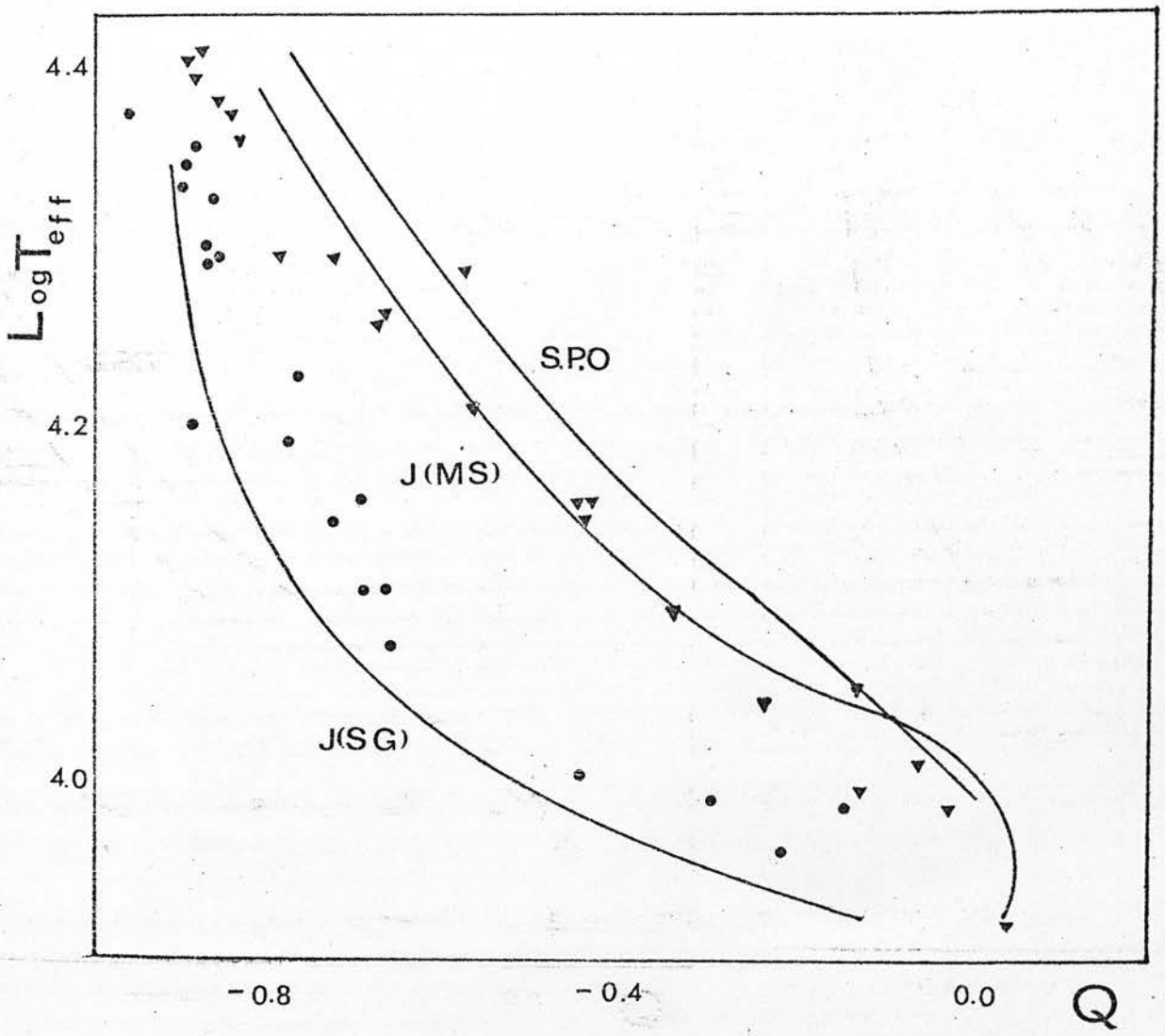

Fig. 86. Temperature distribution for hot stars. Filled circles for supergiants, triangles for main sequence stars, solid lines show temperature from Johnson (1966) and Schild, Peterson & Oke (1971)

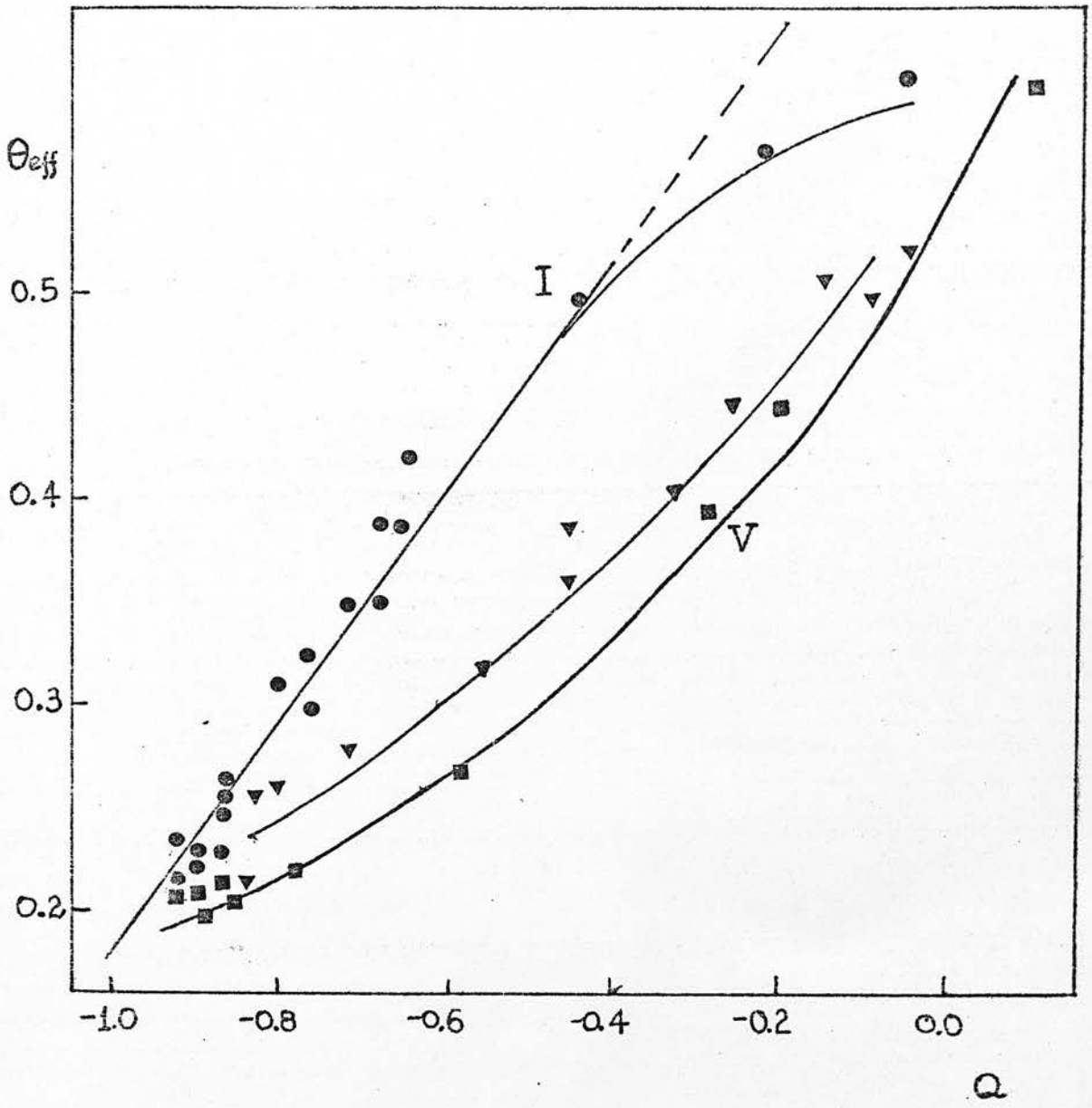

Fig. 87. Temperature distribution for hot stars. Filled circles for supergiants and giants, triangles for subgiants and squares for dwarfs.

VI CONCLUSIONS

VI 1. CONCLUDING REMARKS

a. The d.c. ratiometer (commercial by Brookdeal) used for the first time in astronomy has shown very good results in facing the major problems (the elimination of the stellar scintillation changes in atmospheric transparency, and guiding errors) of conventional photoelectric spectrum scanners. Spectra taken with it have proved its good performance.

b. The deficiency in the ultraviolet flux of early type giants and supergiants relative to that of the main sequence stars decreased going to later types and there is a crossover at B9. Intrinsic (B-V) values of the giants and supergiants are less negative than for the corresponding main sequence stars (Fig. 25) that gives small positive values of Δ m at the B photometric wavelength. This, together with the positive slope of the Δm vs $1/\lambda$ curve in the ultraviolet, gives the impression that the same effect is present for the whole spectral region observed and supports the interpretation that the luminous B stars are intrinsically cooler than the main sequence stars.

c. The lines at 1550 Å and 1400 Å, predominantly due to CIV and SiIV respectively, appear more strongly in giants and supergiants than in the corresponding main sequence stars for the spectral range B0 to A2 discussed so far.

d. The B-type giants and supergiants studied show stronger absorption near 1920 Å than the corresponding main sequence stars.

e. The 1720 Å feature [NIV (1719), CII (1720 - 1722), AlII (1719 - 1725)] first reported by Underhill *et al.* (1972) is present in the B-type giants and supergiants studied here; it is generally weaker than the 1920 Å feature and seems to be sensitive to luminosity. More than a year after these results have been established a paper appeared by Code & Meade (1976) coming to the same conclusions.

f. The structure in the Δm *vs* $1/\lambda$ curve near 1920 Å, 1720 Å, 1550 Å and 1400 Å appears to be superimposed upon an additional Δm component, which increases progressively towards shorter wavelength..

g. The continua of the observed spectra (1392 Å to 5556 Å) have been compared with synthetic spectra from Kurucz, Peytremann & Avrett (1974) blanketed model stellar atmospheres. Assuming log g = 2 for supergiants and giants, log g = 3 for subgiants and log g = 4 for main sequence stars a temperature scale has been derived for B and early A spectral type stars which agrees fairly well with previous determination by other workers.

The derived T_{eff} for stars of the same spectral type but different luminosity class have deviations up to 3000K for the very hot stars. These deviations become smaller as we go to cooler stars.

h. The dereddened colour index $(M_{1920} - V)_o$ is a good indicator of the temperature scale, for the studied spectral range, and it was found to be in very good agreement with that found by Lesh (1976):

$$\theta_{eff} = 0.556 + 0.102(M_{1920} - V)_o \qquad \text{(Kontizas 1977)}$$

$$\theta_{eff} = 0.565 + 0.111(M_{1910} - V)_o \qquad \text{(Lesh 1976)}$$

i. The differences in T_{eff} for stars having the same spectral type but different luminosity can be seen very well in the θ vs Q diagram. For the supergiants with $Q \leq -0.3$ the temperature can be presented as a straight line.

VI. 2 SUGGESTIONS FOR FUTURE WORK

The observations presented here extend previous photometric and spectrophotometric observations. The suggestions made for the luminosity effect are still based on a not very large selection of stars and do not cover all the possible spectral types and luminosities for the early type stars.

Observations with higher resolutions are worthwhile making for a better estimation of the surface gravity. Higher resolution spectra are also needed for the very hot stars (O spectral type) where the observed portion of the spectrum is very little affected by temperature changes. The fundamental atmosphere parameters T_{eff}, surface gravity and abundance have to be extracted from the line spectrum H, HeI and HeII available for the analysis.

It would be interesting to make a further investigation of the spectral lines in the ultraviolet (1410 Å, 1550 Å, 1620 Å, 1720 Å and 1900 Å) for a better study of their sensitivity to spectral type and luminosity.

More elaborate models are suggested where departures from LTE have been indicated. This is especially important for stars with high temperature and low gravity.

It is worthwhile making comparison of the observed spectra with stellar models where Carson's new radiative opacities are adopted.

APPENDIX I

In Table 20, data for the stars used in Fig. 21, 22, 23, 25 to show the luminosity effect are listed. Columns 1 and 2 give the HD numbers and the names of the stars. Columns 3, 4, 5 and 6 give the MK spectral type, the V magnitude, B-V colour index and E_{B-V} colour excess respectively. The energy distribution for these stars is given in Table 21.

TABLE 20

Observed Stars

HD	Star	MK Type	V	B-V	E_{B-V}
37128	ε Ori	B0Ia	1.70	-0.19	0.08
75821		B0III	5.10	-0.21	0.09
149438	τ Sco	B0V	2.83	-0.25	0.05
36512	υ Ori	B0V	4.60	-0.26	0.04
64760		B1Ib	4.23	-0.15	0.07
40111	139 Tau	B1Ib	4.82	-0.08	0.14
122451	β Cen	B1II	0.61	-0.22	0.02
37209		B1V	5.70	-0.23	0.03
52089	ε CMa	B2II	1.50	-0.22	0.00
175191	σ Sgr	B2V	2.10	-0.21	0.03
132200	ϰ Cen	B2V	3.12	-0.22	0.02
53138	o^2 CMa	B3Ia	3.05	-0.08	0.06
51283		B3II-III	5.28	-0.19	0.00
120315	η UMa	B3V	1.86	-0.20	0.00
58350	η CMa	B5Ia	2.40	-0.07	0.03
209952	α Gru	B5V	1.73	-0.13	0.03
34085	β Ori	B8Ia	0.17	-0.03	0.00
213998	η Aqr	B8V	4.02	-0.09	0.00
94367		A0Ia	5.28	+0.15	0.14
161868	γ Oph	A0V	3.76	+0.04	0.04
197345	α Cyg	A2Ia	1.26	+0.09	0.04
215789	ε Gru	A2V	3.48	+0.08	0.02
186882	δ Cyg	B9III	2.92	-0.03	0.03
205021	β Cep	B2III	3.18	-0.25	0.01
886	γ Peg	B2IV	2.83	-0.23	0.01
3360	ζ Cas	B2V	3.61	-0.20	0.04
218045	α Peg	B9V	2.49	-0.05	0.01

TABLE 21

Normalised Fluxes (Flux (V=0) = $D_\lambda * 10^{-12}$ erg $cm^{-2} sec^{-1}$ Å $^{-1}$

	HD = 37128	HD = 75821	HD = 149438	HD = 36512
$\frac{1}{\lambda}$ (μm^{-1})	D_λ	D_λ	D_λ	D_λ
7.246	89854.1	142498.6	189351.3	208979.8
7.143	70453.0	124759.3	168452.3	198018.6
7.042	80131.6	121147.6	163827.1	188807.8
6.944	80920.2	126533.5	171846.7	187219.9
6.849	77812.7	123675.2	170617.5	184937.3
6.757	76945.6	119253.8	164595.8	181540.3
6.667	75180.5	116479.6	157670.1	174611.5
6.579	67071.7	104412.0	149749.6	165235.2
6.494	52741.5	81097.9	135471.8	141113.0
6.410	52738.3	78859.6	123745.0	130870.7
6.329	60155.2	89930.7	130687.9	137286.0
6.250	56443.2	80394.8	128713.4	130037.6
6.173	52657.1	74979.4	122574.1	123898.5
6.098	56944.2	85247.0	124841.7	128849.1
6.024	63069.8	89733.2	131048.1	133320.7
5.952	66751.7	92943.8	133792.7	—
5.882	64304.0	87350.5	131688.9	132915.8
5.814	61907.0	83774.2	125322.3	130555.2
5.747	59128.5	78028.8	112109.2	121148.2
5.618	58385.2	79432.2	100619.8	109518.1
5.556	56940.3	75382.5	97968.3	104657.2
5.495	55729.9	72939.3	95269.8	102555.4
5.435	54707.0	71934.6	92009.7	99935.7
5.376	52320.9	67018.2	87037.3	97696.7
5.319	50564.2	64009.5	85249.6	93755.2
5.263	48782.1	61686.6	81390.7	90498.8
5.208	47682.4	58259.2	77258.6	84682.2
5.155	47345.5	60778.1	74719.7	82396.6
5.102	46730.1	58652.0	73998.6	82775.4

TABLE 21 (Contd.)

Normalised Fluxes

$\frac{1}{\lambda}$ (μm^{-1})	HD = 37128 D_λ	HD = 75821 D_λ	HD = 149438 D_λ	HD = 36512 D_λ
5.051	46549.6	60594.2	72583.2	78333.2
5.000	46063.1	60743.9	70892.6	77160.3
4.950	46014.2	57862.2	68376.7	76138.2
4.902	45160.8	55104.0	66334.2	72572.5
4.854	43415.2	56354.1	63941.0	69570.9
4.808	42193.7	51855.9	61768.2	67977.3
4.762	41941.7	50774.0	60236.2	65544.0
4.717	42135.6	52669.8	58769.8	65983.7
4.673	41724.5	54939.2	57690.7	66860.3
4.587	40212.1	47683.2	53401.3	60075.0
4.545	40115.1	49775.0	52998.7	58676.8
4.505	40317.5	45876.9	53175.7	57546.4
4.464	38779.4	47281.3	51028.6	55634.9
4.425	38170.2	47480.9	50093.8	55696.9
4.386	37177.3	44395.0	48932.8	54883.5
4.348	35791.5	42246.3	46759.2	51796.4
4.310	35538.5	41999.9	46088.6	49996.3
4.274	35685.1	41917.4	46090.4	48870.9
4.237	35150.3	41564.0	44982.5	48475.0
4.202	34069.1	38774.1	43612.8	47304.6
4.167	33287.6	37941.2	42304.5	45082.6
4.132	32711.0	37907.2	41373.0	43880.7
4.098	32273.4	37867.1	40845.9	41926.2
4.065	31909.3	36764.5	40452.9	41867.4
4.032	31133.3	35462.6	38710.7	42137.2
4.000	30313.0	33294.3	37008.8	39407.9
3.968	29408.6	32291.4	35914.3	39208.3
3.937	28157.0	33202.6	34409.9	38525.8
3.650	19272.2	29804.6	22741.9	25504.8

TABLE 21 (Contd.)

Normalised Fluxes

	HD = 64760	HD = 40111	HD = 122451	HD = 37209
$\frac{1}{\lambda}$ (μm^{-1})	D_λ	D_λ	D_λ	D_λ
7.246	63144.3	53200.2	70327.0	140225.0
7.143	74317.0	48716.3	65830.6	119884.3
7.042	75132.4	49248.7	64824.8	115250.9
6.944	79730.2	51448.8	68565.3	124636.3
6.849	80366.8	52734.8	70302.0	126122.6
6.757	78231.2	51256.3	69962.0	117527.4
6.667	73361.6	48368.3	68417.2	111089.7
6.579	61976.4	41818.4	90741.5	99692.3
6.494	49066.7	37367.0	101069.7	86433.6
6.410	50213.3	35257.5	79599.9	85701.9
6.329	54853.5	38650.0	79422.1	90081.7
6.250	53538.2	37065.0	76110.7	85198.5
6.173	49872.0	34289.7	72689.1	85718.0
6.098	55718.9	38189.5	77426.8	91014.8
6.024	60016.1	41558.1	83416.7	98241.7
5.952	64059.6	44036.6	84752.7	98465.3
5.882	58301.9	38269.1	78176.4	88770.7
5.814	53573.2	37147.7	72483.6	87151.4
5.747	55998.7	39335.0	72327.5	77974.5
5.618	54250.3	36080.2	56042.7	72226.3
5.556	53326.0	35035.6	55631.5	69840.8
5.495	51269.9	33474.0	54821.7	67782.2
5.435	49797.2	31997.8	52417.3	68640.9
5.376	46027.8	30634.4	49005.2	62083.9
5.319	42913.3	28757.7	46721.4	59763.4
5.263	40687.0	26631.4	44084.9	60704.2
5.208	39811.8	24427.6	42079.0	55800.4
5.155	39257.7	23047.0	41508.9	52777.2
5.102	39501.6	22719.1	41714.7	50728.6

TABLE 21 (Contd.)

Normalised Fluxes

$\frac{1}{\lambda}$ (μm^{-1})	HD = 64760 D_λ	HD = 40111 D_λ	HD = 122451 D_λ	HD = 37209 D_λ
5.051	40285.7	23356.6	41930.7	50884.9
5.000	39991.6	22884.6	41391.1	49775.7
4.950	41198.4	21888.0	41964.2	49362.0
4.902	39160.2	20878.9	41275.4	47196.0
4.854	36918.9	19321.6	39753.2	48640.8
4.808	37414.1	19763.1	38866.9	47079.6
4.762	37179.5	18129.7	38728.6	45100.1
4.717	38817.7	19541.2	39333.3	45191.8
4.673	36781.3	18671.4	39359.9	44232.5
4.587	36557.2	17894.7	38317.3	43851.6
4.545	37490.1	19498.6	38440.2	43557.6
4.505	36917.3	19437.8	38177.9	44247.7
4.464	35798.8	18430.7	37377.6	39782.7
4.425	36410.5	18685.6	36634.9	39211.9
4.386	34955.8	19126.5	36048.2	38695.4
4.348	33570.5	18223.5	35074.2	37511.7
4.310	33809.9	17561.9	34057.4	37379.8
4.274	33932.6	20462.8	33560.6	35981.4
4.237	32950.3	18956.1	33213.7	35745.9
4.202	32339.4	19467.2	32440.6	32752.0
4.167	32193.0	19927.8	31720.0	31784.8
4.132	31579.2	18933.9	30937.0	31922.0
4.098	30500.6	20895.2	30247.2	32479.7
4.065	31315.4	19859.8	29936.2	31322.6
4.032	29912.6	20283.4	29330.7	28783.2
4.000	28651.6	19949.9	28249.9	28557.3
3.968	26551.6	19307.4	27651.0	29511.1
3.937	26649.9	18792.9	26328.4	27601.0
3.650	19190.0	14623.1	11173.0	19533.7

TABLE 21 (Contd.)

Normalised Fluxes

$\frac{1}{\lambda}$ (μm^{-1})	HD = 52089 D_λ	HD = 175191 D_λ	HD = 132200 D_λ	HD = 53138 D_λ
7.246	76823.2	75987.2	87485.5	23093.3
7.143	63670.9	74482.0	80131.4	20454.1
7.042	63803.2	72495.1	78207.0	22354.5
6.944	71024.1	74136.2	81318.9	24632.9
6.849	70075.1	75326.5	81160.0	25920.4
6.757	65494.3	72552.2	77493.9	24498.7
6.667	61098.3	69001.2	73100.6	22259.6
6.579	54239.1	64590.2	66932.2	19898.5
6.494	47823.5	62014.8	62437.8	18289.8
6.410	47828.2	61795.2	62288.4	19342.2
6.329	51399.9	62696.4	62804.3	20583.7
6.250	51349.1	59734.9	60926.8	20125.9
6.173	52741.4	57571.4	61179.5	20639.8
6.098	58047.5	60136.0	63485.1	22239.0
6.024	61814.7	64395.7	67049.0	23424.4
5.952	61670.3	64542.3	66425.4	23679.4
5.882	56954.8	62780.2	63361.2	21905.9
5.814	53435.5	60084.2	60773.5	19596.8
5.747	52771.0	57448.1	57571.2	18987.9
5.618	48161.9	46011.5	52275.4	18144.2
5.556	48159.2	47407.8	51386.4	19381.9
5.495	47730.1	46909.3	50323.8	19782.3
5.435	43980.4	45403.4	47876.3	17903.5
5.376	40126.0	42165.1	44469.7	15079.3
5.319	37751.1	41159.5	43197.4	14461.1
5.263	34840.9	39721.9	41206.1	13446.9
5.208	32811.1	38040.8	39437.2	12355.7
5.155	32813.6	36701.6	38386.0	12334.8
5.102	33901.5	37366.6	39102.0	13298.0

TABLE 21 (Contd.)

Normalised Fluxes

$\frac{1}{\lambda}$ (μm^{-1})	HD = 52089 D_λ	HD = 175191 D_λ	HD = 132900 D_λ	HD = 53138 D_λ
5.051	34366.4	36795.2	38647.7	14298.8
5.000	34681.6	36157.0	38144.3	14700.8
4.950	36067.8	36007.2	37222.9	15472.8
4.902	34809.0	34659.1	37132.1	15374.2
4.854	34530.4	34051.0	35070.5	15061.8
4.808	33715.1	32846.3	34023.1	14541.0
4.762	33787.5	32358.2	33032.6	14667.9
4.717	35551.9	32358.2	33106.0	15932.3
4.673	35818.9	33259.4	33710.4	16446.9
4.587	35403.3	30020.9	31602.0	16813.6
4.545	35925.1	30252.0	32104.6	17211.5
4.505	35572.1	29653.7	30903.5	10807.4
4.464	34654.1	29297.8	30312.5	5949.0
4.425	34354.0	28733.0	29809.8	16433.9
4.386	34471.5	28382.6	29300.4	16770.7
4.348	33467.1	27614.2	28692.5	16789.0
4.310	32504.6	26861.7	28217.6	16314.8
4.274	31986.3	25573.4	26926.8	15620.0
4.237	31516.0	24966.2	25880.9	14842.4
4.202	30924.2	24533.5	24948.7	14508.6
4.167	30260.6	23989.4	25159.0	14793.9
4.132	29506.8	23032.3	25192.5	15001.2
4.098	29094.7	22870.3	24244.3	15293.3
4.065	28685.6	22070.4	23685.4	15014.3
4.032	27681.4	21609.5	23294.8	14487.9
4.000	26787.0	20953.5	22211.8	14082.2
3.968	25999.2	20243.7	21187.3	13410.3
3.937	24944.1	20568.4	28722.8	12677.6
3.650	17666.3	13610.0	14810.4	10886.9

TABLE 21 (Contd.)

Normalised Fluxes

$\frac{1}{\lambda}$ (μm^{-1})	HD = 51283 D_λ	HD = 120315 D_λ	HD = 58350 D_λ	HD = 209952 D_λ
7.246	50656.6	55164.7	13971.2	29204.5
7.143	46920.3	56300.3	14127.3	28534.7
7.042	47008.0	55661.3	16007.5	28418.9
6.944	50430.9	57169.0	17966.3	29313.3
6.849	51736.9	57651.2	18525.6	30044.1
6.757	49896.0	55582.3	17385.7	28958.1
6.667	44646.4	52493.0	16275.3	27794.9
6.579	40039.8	50017.8	14931.4	27076.7
6.494	37052.1	48387.4	13602.2	26320.3
6.410	35327.5	48383.5	14136.5	26338.4
6.329	38961.5	48908.6	15325.2	25997.9
6.250	37777.5	46276.1	14683.6	25037.0
6.173	38153.0	44800.5	14760.2	24600.0
6.098	42870.9	47025.3	16293.5	25048.6
6.024	43698.1	48630.6	17219.7	25507.1
5.952	43666.1	48333.9	17045.7	25822.8
5.882	38949.6	46925.6	15528.7	25126.5
5.814	26822.8	44814.6	14231.2	23656.7
5.747	-3667.5	42575.3	13431.0	22992.3
5.618	29575.7	36326.8	13971.0	20819.2
5.556	30407.0	37733.2	15149.6	20876.9
5.495	35305.6	37353.0	15432.1	21071.5
5.435	26407.1	35537.6	13940.2	20345.1
5.376	29934.4	33824.4	11953.0	19184.9
5.319	32410.2	33051.6	12067.9	18945.6
5.263	29414.3	32094.4	11525.5	18691.4
5.208	17774.4	31290.1	10817.8	18316.1
5.155	32640.8	30142.0	11039.3	18137.7
5.102	40472.8	30444.7	11656.9	18154.5

TABLE 21 (Contd.)

Normalised Fluxes

$\frac{1}{\lambda}$ (μm^{-1})	HD = 51283 D_λ	HD = 120315 D_λ	HD = 58350 D_λ	HD = 209952 D_λ
5.051	23265.6	29888.9	12396.3	18038.7
5.000	17425.9	29150.9	12005.0	17335.2
4.950	23335.2	29021.3	12811.3	16991.1
4.902	31651.1	28275.5	12726.7	16792.0
4.854	19421.1	27289.1	12408.5	16181.8
4.808	20179.0	26621.8	12755.0	15985.2
4.762	20016.5	26336.0	13032.8	15631.1
4.717	22836.2	26138.8	13592.4	15552.9
4.673	19713.3	26775.0	14368.2	15418.3
4.587	16969.2	24440.0	13685.7	14682.6
4.545	27134.6	24818.8	13923.1	14672.2
4.505	23648.8	24297.3	14053.1	14278.4
4.464	22832.9	23735.1	13058.2	13863.6
4.425	24968.0	23344.3	13332.1	13532.8
4.386	32654.4	22919.9	13775.4	13477.8
4.348	21643.1	22755.9	13744.2	13300.7
4.310	17108.0	21753.2	13476.9	12734.3
4.274	22447.5	21090.4	12556.7	12022.9
4.237	17689.9	20424.4	12045.5	11519.4
4.202	20790.6	19910.3	11823.3	11198.4
4.167	16557.5	19308.2	11840.0	10957.2
4.132	17170.6	18986.1	11929.7	10972.8
4.098	19824.9	18717.0	11999.4	10906.5
4.065	19267.9	18169.1	11909.1	10695.3
4.032	23503.2	18081.3	11535.4	10725.0
4.000	23123.1	17521.3	11418.4	10576.8
3.968	10635.4	17144.0	10912.6	10006.5
3.937	13078.2	17105.4	10506.7	9814.3
3.650	14665.5	11416.7	-	-

TABLE 21 (Contd.)

Normalised Fluxes

$\frac{1}{\lambda}$ (μm^{-1})	HD = 34085 D_λ	HD = 213998 D_λ	HD = 94367 D_λ	HD = 161868 D_λ
7.246	8643.1	13557.2	1638.4	2109.4
7.143	8800.3	13616.8	1881.6	2009.9
7.042	9427.2	13427.1	2035.2	2526.1
6.944	10294.7	13531.7	2141.8	3025.8
6.849	11186.1	14251.3	2688.4	3401.5
6.757	11030.3	14434.7	2410.6	3395.8
6.667	10516.6	14186.4	2427.2	3753.3
6.579	10390.0	13300.9	2532.4	3591.0
6.494	10116.2	12804.4	2447.3	3841.7
6.410	10108.5	12513.8	1995.0	3723.9
6.329	10417.3	12313.7	2153.7	3546.6
6.250	10528.8	12294.7	2295.8	4062.5
6.173	10182.1	12226.4	1748.1	4402.0
6.098	10363.4	12347.6	1569.7	4474.9
6.024	11158.4	14930.0	2594.6	4405.6
5.952	11609.7	13408.6	2554.6	4545.3
5.882	11122.5	11930.5	2587.1	4890.4
5.814	10398.2	11336.5	2103.7	4482.1
5.747	9686.9	10942.2	1360.1	3938.3
5.618	9690.2	10965.0	3968.8	4823.7
5.556	10368.1	11013.6	5032.6	4780.5
5.495	10597.3	11528.8	3543.8	4391.3
5.435	9845.0	11239.4	2817.9	4484.7
5.376	9006.8	10803.1	2382.5	4373.7
5.319	8874.5	10948.3	3790.2	4134.5
5.263	8743.1	11255.0	3982.4	4216.1
5.208	8546.8	10295.3	2702.9	4209.9
5.155	8657.2	10133.5	3110.3	4264.6
5.102	9010.7	10692.6	2787.7	4132.2

TABLE 21 (Contd.)

Normalised Fluxes

$\frac{1}{\lambda}$ (μm^{-1})	HD = 34085 D_λ	HD = 213998 D_λ	HD = 94367 D_λ	HD = 161868 D_λ
5.051	9319.5	10382.6	2239.6	4331.8
5.000	9115.5	9981.6	2079.6	4148.3
4.950	9190.1	10063.9	2749.0	3958.3
4.902	9274.6	9625.7	3094.4	3817.1
4.854	9028.7	9758.6	2753.2	4006.1
4.808	9027.2	9089.9	2516.2	4158.0
4.762	9117.2	9632.5	2180.0	4169.2
4.717	9233.6	8955.7	3020.9	3998.6
4.673	9282.9	9005.0	2191.0	3712.7
4.587	9173.6	8311.4	2555.2	3620.5
4.545	9158.3	8472.1	2157.5	3762.7
4.505	9000.8	8330.2	2050.5	3837.8
4.464	8639.6	8258.8	2598.3	3644.2
4.425	8614.6	8214.8	2444.8	3845.3
4.386	8724.7	7973.0	2764.6	3667.9
4.348	8801.6	7701.4	2980.9	3641.8
4.310	8375.9	7402.0	1965.9	3446.6
4.274	7769.4	6788.8	2157.6	3337.3
4.237	7427.2	6209.8	2578.9	3363.5
4.202	7272.4	6118.7	2216.0	3114.4
4.167	7232.5	6288.1	2117.1	3036.1
4.132	7343.7	6612.0	2219.5	3036.6
4.098	7503.8	6433.0	2218.9	3038.4
4.065	7504.5	6540.8	3200.5	3068.4
4.032	7453.8	6271.6	2649.9	2967.0
4.000	7411.4	6076.7	2828.6	3036.3
3.968	6970.8	5758.6	2741.2	2842.1
3.937	6689.3	5795.7	2761.0	2778.8
3.650	-	-	3303.5	2824.0

TABLE 21 (Contd.)

Normalised Fluxes

	HD = 197345	HD = 215789
$\frac{1}{\lambda}$ (μm^{-1})	D_λ	D_λ
7.246	506.9	184.9
7.143	582.3	276.7
7.042	618.3	232.7
6.944	704.8	377.1
6.849	847.3	345.2
6.757	924.7	286.3
6.667	1062.4	372.2
6.579	1121.7	370.0
6.494	1081.9	483.5
6.410	1034.8	634.4
6.329	1120.9	785.1
6.250	1175.5	876.6
6.173	1112.3	1035.4
6.098	1054.3	1121.5
6.024	1141.6	1169.8
5.952	1281.1	1224.2
5.882	1194.3	1213.9
5.814	1294.6	1439.4
5.747	1437.1	1382.0
5.618	1673.8	2376.5
5.556	1929.6	2514.2
5.495	1971.7	2674.1
5.435	1712.6	2368.7
5.376	1583.4	2453.0
5.319	1757.7	2567.6
5.263	1857.3	2458.2
5.208	1952.5	2177.8
5.155	2087.2	2477.9
5.102	2242.5	2598.5

TABLE 21 (Contd.)

Normalised Fluxes

$\frac{1}{\lambda}$ (μm^{-1})	HD = 197345 D_λ	HD = 215789 D_λ
5.051	2228.1	2417.9
5.000	2061.6	2503.8
4.950	1926.3	2561.9
4.902	1912.5	2332.3
4.854	1949.5	2144.6
4.808	2009.5	2055.2
4.762	2076.3	1920.8
4.717	1856.9	2057.9
4.673	1777.3	2143.6
4.587	1771.1	1608.7
4.545	1820.4	1499.9
4.505	1748.7	1685.3
4.464	1535.7	1300.1
4.425	1471.0	1399.5
4.386	1591.6	1660.7
4.348	1676.7	1361.9
4.310	1568.1	1269.2
4.274	1396.9	1113.1
4.237	1288.0	1017.5
4.202	1226.8	1082.3
4.167	1238.8	1060.7
4.132	1381.9	933.6
4.098	1473.1	1225.7
4.065	1447.9	1359.5
4.032	1504.5	1047.6
4.000	1578.6	1017.9
3.968	1430.4	1362.5
3.937	1442.2	1336.8
3.650	-	-

TABLE 21 (Contd.)

Wavelength $\frac{1}{\lambda}$ (μm^{-1})	HD = 186882		HD = 205021	
	Observed m_λ (V=0)	Corrected m_λ (V=0)	Observed m_λ (V=0)	Corrected m_λ (V=0)
1.54	0.53	0.54	0.52	0.52
1.58	0.49	0.50	0.44	0.44
1.61	0.41	0.41	0.38	0.38
1.63	0.39	0.39	0.36	0.36
1.67	0.32	0.32	0.26	0.26
1.70	0.29	0.29	0.19	0.19
1.72	0.22	0.22	0.14	0.14
1.75	0.11	0.11	0.10	0.10
1.77	0.07	0.07	0.03	0.03
1.80	0.00	0.00	0.00	0.00
1.83	-0.04	-0.04	-0.07	-0.07
1.85	-0.10	-0.10	-0.13	-0.13
1.88	-0.15	-0.15	-0.18	-0.18
1.91	-0.22	-0.22	-0.24	-0.24
1.94	-0.26	-0.26	-0.29	-0.29
1.98	-0.30	-0.30	-0.33	-0.33
2.01	-0.37	-0.37	-0.38	-0.38
2.04	-0.41	-0.41	-0.44	-0.44
2.08	-0.44	-0.45	-0.50	-0.50
2.11	-0.47	-0.48	-0.56	-0.56
2.15	-0.54	-0.55	-0.63	-0.63
2.19	-0.58	-0.59	-0.71	-0.71
2.23	-0.62	-0.63	-0.77	-0.77
2.27	-0.65	-0.66	-0.83	-0.83
2.32	-0.68	-0.70	-0.89	-0.89
2.36	-0.74	-0.76	-0.96	-0.96
2.41	-0.81	-0.83	-1.11	-1.11

TABLE 21 (Contd.)

Wavelength	HD = 886		HD = 3360		HD = 218045	
$\frac{1}{\lambda}$ (μm^{-1})	Observed m_λ (V=0)	Corrected m_λ (V=0)	Observed m_λ (V=0)	Corrected m_λ (V=0)	Observed m_λ (V=0)	Corrected m_λ (V=0)
1.54	0.50	0.51	0.46	0.51	0.40	0.40
1.58	0.43	0.44	0.39	0.43	0.35	0.35
1.61	0.36	0.36	0.32	0.35	0.32	0.32
1.63	0.35	0.35	0.29	0.32	0.26	0.26
1.67	0.26	0.26	0.23	0.25	0.21	0.21
1.70	0.18	0.18	0.18	0.20	0.17	0.17
1.72	0.12	0.12	0.16	0.17	0.12	0.12
1.75	0.06	0.06	0.08	0.09	0.09	0.09
1.77	0.04	0.04	0.02	0.02	0.04	0.04
1.80	0.00	0.00	0.00	0.00	0.00	0.00
1.83	-0.06	-0.06	-0.09	-0.09	-0.01	-0.01
1.85	-0.11	-0.11	-0.15	-0.15	-0.12	-0.12
1.88	-0.17	-0.17	-0.21	-0.22	-0.17	-0.17
1.91	-0.24	-0.24	-0.25	-0.26	-0.20	-0.20
1.94	-0.27	-0.27	-0.32	-0.34	-0.25	-0.25
1.98	-0.32	-0.32	-0.35	-0.37	-0.29	-0.29
2.01	-0.38	-0.38	-0.40	-0.43	-0.34	-0.34
2.04	-0.44	-0.44	-0.44	-0.47	-0.39	-0.39
2.08	-0.48	-0.49	-0.48	-0.52	-0.45	-0.45
2.11	-0.54	-0.55	-0.55	-0.59	-0.49	-0.49
2.15	-0.60	-0.61	-0.61	-0.66	-0.53	-0.53
2.19	-0.66	-0.67	-0.67	-0.73	-0.56	-0.56
2.23	-0.75	-0.76	-0.73	-0.79	-0.62	-0.62
2.27	-0.81	-0.82	-0.83	-0.90	-0.68	-0.68
2.32	-0.85	-0.87	-0.86	-0.94	-0.72	-0.73
2.36	-0.92	-0.94	-0.94	-1.02	-0.76	-0.77
2.41	-1.00	-1.02	-0.99	-1.07	-0.80	-0.81

APPENDIX II

In Table 22 the observed stars used for the derived temperature scale are given. Columns 1 and 2 give the HD number and the names of the stars while the V magnitudes, B-V colour indices and spectral types are listed in Columns 3, 4 and 5 respectively.

Table 22 gives the magnitudes, observed and corrected for interstellar extinction, normalised to V = 0.

TABLE 22

Stars observed

	HD	Name	V	B-V	Sp.Tp
1	15318	ξ^2 Cet	4.27	-0.05	B9III
2	18326	-	7.28	+0.38	O8V
3	24398	ζ Per	2.83	+0.13	B1Ib
4	24431	-	6.72	+0.37	O9V
5	24760	ε Per	2.88	-0.17	BO.5V
6	30614	α Cam	4.38	+0.02	O9.5Ia
7	31327	-	6.06	+0.41	B2Ia
8	32249	ψ Eri	4.80	-0.20	B2V
9	33988	-	6.88	+0.25	B2V
10	34085	β Ori	0.08	-0.03	B8Ia
11	35468	γ Ori	1.63	-0.23	B2III
12	36371	χ Aur	4.75	+0.30	B5Ia
13	36512	ν Ori	4.60	-0.26	BOV
14	36879	-	7.58	+0.20	O6V
15	37128	ε Ori	1.70	-0.19	BOIa
16	38771	κ Ori	2.04	-0.18	BOIa
17	40589	-	6.05	+0.25	B9Ia
18	42087	3 Gem	5.76	+0.20	B2.5Ia
19	43384	9 Gem	6.28	+0.44	B3Ia
20	45910	-	6.77	+0.33	B2III
21	46149	-	7.58	+0.17	O8V
22	47240	-	6.15	+0.15	B1Ib
23	47839	15 Mon	4.66	-0.25	O7III
24	52382	-	6.48	+0.20	B2.5Ia
25	53367	-	6.97	+0.43	BOIV
26	54662	-	6.21	+0.03	O6V
27	58131	-	7.37	+0.34	B2V
28	58350	η CMa	2.47	-0.06	B5Ia
29	66811	ζ Pup	2.25	-0.28	O5V
30	77581	-	6.88	+0.56	BOIa
31	79186	-	5.00	+0.20	B3Ia
32	87734	η Leo	3.55	-0.02	AOIa
33	87901	α Leo	8.14	-0.11	B7V
34	91316	ρ Leo	3.85	-0.14	B1Ib
35	102647	β Leo	2.12	+0.09	A3V
36	149438	τ Sco	2.83	-0.24	BOV
37	152614	i Oph	4.37	-0.09	B8V
38	155763	ζ Dra	3.17	-0.11	B7III
39	160762	i Her	3.80	-0.17	B3IV
40	164353	67 Oph	3.97	+0.02	B5Ib
41	176437	γ Lyr	3.23	-0.04	B9III
42	182255	3 Vel	5.18	-0.12	B6III
43	188209	-	5.63	-0.07	O9.5I III
44	188260	13 Vel	4.57	-0.06	B9III
45	195810	ε Del	4.04	-0.12	B6III
46	197345	α Cyg	1.25	+0.09	A2Ia
47	214993	12 Lac	5.22	-0.12	B2III
48	218376	1 Cas	4.88	-0.02	BOIII
49	222173	i And	4.28	-0.10	B8V
50	224572	σ Cas	4.58	-0.06	B1V

TABLE 23

Observed and corrected for interstellar extinction, magnitudes

Wavelength	HD = 15318		HD = 18326		HD = 24398	
$\frac{1}{\lambda}$ (μm^{-1})	Observed m_λ (V=0)	Corrected m_λ (V=0)	Observed m_λ (V=0)	Corrected m_λ (V=0)	Observed m_λ (V=0)	Corrected m_λ (V=0)
1.80	0.000	0.000	0.000	0.000	0.000	0.000
1.90	-0.118	-0.120	-0.022	-0.160	-0.090	-0.160
2.00	-0.296	-0.300	-0.104	-0.380	-0.240	-0.380
2.10	-0.434	-0.440	-0.139	-0.560	-0.287	-0.500
2.19	-0.552	-0.560	-0.148	-0.700	-0.360	-0.640
2.24	-0.601	-0.610	-0.180	-0.780	-0.390	-0.690
2.35	-0.730	-0.740	-0.136	-0.860	-0.493	-0.860
2.40	-0.789	-0.800	-0.141	-0.900	-0.515	-0.900
2.48	-0.828	-0.840	-0.118	-0.960	-0.573	-1.000
2.70	-	-	-0.039	-1.060	-0.682	-1.200
2.75	-	-	-0.044	-1.120	-0.734	-1.280
2.80	-	-	-0.028	-1.160	-0.746	-1.320
2.85	-	-	-0.067	-1.240	-0.785	-1.380
2.90	-	-	-0.046	-1.260	-0.624	-1.440
2.95	-	-	-0.044	-1.300	-0.843	-1.480
3.65	-0.039	-0.070	0.019	-2.120	-0.735	-1.820
4.00	-0.318	-0.360	-0.330	-3.200	-0.944	-2.400
4.06	-0.276	-0.320	-0.300	-3.100	-0.887	-2.420
4.42	-0.440	-0.500	0.705	-3.400	-0.438	-2.520
4.57	-0.537	-0.600	0.867	-3.480	-0.435	-2.640
4.85	-0.701	-0.760	0.235	-3.850	-0.618	-2.690
5.21	-5.503	-	-	-	-	-
5.38	-0.833	-0.880	-0.816	-4.080	-1.285	-2.940
6.02	-0.953	-1.000	-0.871	-4.100	-1.604	-3.240
6.71	-1.032	-1.080	-0.888	-4.200	-1.720	-3.400
6.85	-0.991	-1.040	-0.733	-4.100	-1.752	-3.460
7.18	-0.889	-0.940	-0.767	-4.300	-1.738	-3.530

TABLE 23 (Contd.)

Wavelength $\frac{1}{\lambda}$ (μm^{-1})	HD = 24431		HD = 24760		HD = 30614	
	Observed m_λ (V=0)	Corrected m_λ (V=0)	Observed m_λ (V=0)	Corrected m_λ (V=0)	Observed m_λ (V=0)	Corrected m_λ (V=0)
1.80	0.000	0.000	0.000	0.000	0.000	0.000
1.90	-0.066	-0.200	-0.138	-0.160	-0.108	-0.180
2.00	-0.132	-0.400	-0.276	-0.320	-0.216	-0.360
2.10	-0.292	-0.700	-0.453	-0.520	-0.281	-0.500
2.19	-0.264	-0.800	-0.572	-0.660	-0.412	-0.700
2.24	-0.257	-0.840	-0.710	-0.800	-0.507	-0.820
2.35	-0.237	-0.940	-0.845	-0.960	-0.642	-1.020
2.40	-0.223	-0.960	-0.879	-1.000	-0.704	-1.100
2.48	-0.203	-1.020	-0.766	-1.080	-0.801	-1.240
2.70	-0.108	-1.100	-0.997	-1.160	-0.847	-1.380
2.75	-0.075	-1.120	-1.028	-1.200	-0.958	-1.520
2.80	-0.061	-1.160	-1.080	-1.260	-1.060	-1.650
2.85	-0.041	-1.180	-1.133	-1.320	-1.068	-1.680
2.90	-0.041	-1.220	-1.186	-1.380	-1.116	-1.750
2.95	-0.041	-1.260	-	-	-1.145	-1.800
3.65	-0.003	-2.080	-1.740	-2.080	-1.184	-2.300
4.00	0.387	-2.400	-1.943	-2.400	-1.403	-2.900
4.06	0.375	-2.560	-2.118	-2.600	-1.383	-2.960
4.42	0.986	-3.000	-2.146	-2.800	-1.158	-3.300
4.57	1.041	-3.180	-2.207	-2.900	-1.092	-3.360
4.85	0.666	-3.300	-2.409	-3.060	-1.349	-3.480
5.21	-	-	-	-	-	-
5.38	-0.131	-3.300	-2.840	-3.360	-1.937	-3.640
6.02	-0.304	-3.440	-3.205	-3.720	-1.995	-3.680
6.71	-0.490	-3.700	-3.472	-4.000	-2.272	-4.000
6.85	-0.411	-3.680	-3.503	-4.040	-2.203	-3.960
7.81	-0.420	-3.850	-3.637	-4.200	-2.287	-4.130

TABLE 23 (Contd.)

Wavelength $\frac{1}{\lambda}$ (μm^{-1})	HD = 31327		HD = 32249		HD = 33988	
	Observed m_λ (V=0)	Corrected m_λ (V=0)	Observed m_λ (V=0)	Corrected m_λ (V=0)	Observed m_λ (V=0)	Corrected m_λ (V=0)
1.80	0.000	0.000	0.000	0.000	0.000	0.000
1.90	-0.022	-0.140	-0.152	-0.160	-0.020	-0.120
2.00	-0.084	-0.320	-0.324	-0.340	-0.080	-0.280
2.10	-0.100	-0.460	-0.576	-0.600	-0.140	-0.440
2.19	-0.088	-0.560	-0.688	-0.720	-0.200	-0.600
2.24	-0.187	-0.700	-0.765	-0.800	-0.210	-0.640
2.35	-0.220	-0.840	-0.918	-0.960	-0.240	-0.760
2.40	-0.251	-0.900	-0.976	-1.020	-0.260	-0.800
2.48	-0.240	-0.960	-1.031	-1.080	-0.280	-0.880
2.70	-0.207	-1.080	-0.941	-1.000	-0.170	-0.900
2.75	-0.140	-1.060	-0.978	-1.040	-0.207	-0.960
2.80	-0.192	-1.160	-0.994	-1.060	-0.180	-1.000
2.85	-0.177	-1.180	-1.022	-1.090	-0.210	-1.060
2.90	-0.162	-1.200	-1.050	-1.120	-0.210	-1.080
2.95	-0.166	-1.240	-1.087	-1.160	-4.645	-
3.65	0.349	-1.480	-1.476	-1.600	-0.850	-2.400
4.00	0.594	-1.860	-1.894	-2.060	-1.120	-3.200
4.06	0.724	-1.860	-1.945	-2.120	-1.100	-3.280
4.42	1.550	-1.960	-2.162	-2.400	-0.685	-3.600
4.57	1.713	-2.000	-2.208	-2.460	-0.550	-3.700
4.85	1.413	-2.080	-2.363	-2.600	-0.940	-3.840
5.21	-2.617	-	-	-	-	-
5.38	-2.764	-	-2.671	-2.860	-	-
6.02	0.161	-2.600	-2.933	-3.120	-1.957	-4.250
6.71	0.292	-2.540	-3.148	-3.340	-2.000	-4.400
6.85	0.319	-2.560	-3.165	-3.360	-2.160	-4.600
7.18	0.711	-2.310	-3.275	-3.480	-2.100	-4.610

TABLE 23 (Contd.)

Wavelength $\frac{1}{\lambda}$ (μm^{-1})	HD = 34085		HD = 35468		HD = 36371	
	Observed m_λ (V=0)	Corrected m_λ (V=0)	Observed m_λ (V=0)	Corrected m_λ (V=0)	Observed m_λ (V=0)	Corrected m_λ (V=0)
1.80	0.000	0.000	0.000	0.000	0.000	0.000
1.90	-0.080	-0.080	-0.178	-0.180	-0.040	-0.120
2.00	-0.080	-0.080	-0.356	-0.360	-0.080	-0.240
2.10	-0.200	-0.200	-0.494	-0.500	-0.120	-0.360
2.19	-0.300	-0.300	-0.622	-0.630	-0.120	-0.440
2.24	-0.400	-0.400	-0.691	-0.700	-0.170	-0.520
2.35	-0.400	-0.400	-0.840	-0.850	-0.180	-0.600
2.40	-0.640	-0.640	-0.889	-0.900	-0.200	-0.640
2.48	-0.560	-0.560	-0.988	-1.000	-0.200	-0.690
2.70	-0.160	-0.160	-1.085	-1.100	-0.090	-0.680
2.75	-0.200	-0.200	-1.144	-1.160	-0.100	-0.720
2.80	-0.240	-0.240	-1.184	-1.200	-0.080	-0.740
2.85	-0.220	-0.220	-1.263	-1.280	-0.080	-0.760
2.90	-0.320	-0.320	-1.342	-1.360	-0.100	-0.800
2.95	-0.330	-0.330	-1.382	-1.400	-0.090	-0.820
3.65	-0.480	-0.480	-1.589	-1.620	0.140	-1.100
4.00	-0.660	-0.660	-2.078	-2.120	0.380	-1.280
4.06	-0.680	-0.680	-2.125	-2.170	0.490	-1.260
4.42	-0.760	-0.760	-2.330	-2.390	1.040	-1.340
4.57	-0.800	-0.800	-2.387	-2.450	1.140	-1.380
4.85	-0.880	-0.880	-2.461	-2.520	0.970	-1.400
5.21	-	-	-	-	-	-
5.38	-0.920	-0.920	-2.677	-2.720	0.310	-1.580
6.02	-1.000	-1.000	-3.023	-3.070	-0.010	-1.800
6.71	-1.040	-1.040	-3.172	-3.220	-0.060	-1.980
6.85	-0.960	-0.960	-3.201	-3.250	-0.010	-1.960
7.18	-0.840	-0.840	-3.349	-3.400	0.150	-1.900

TABLE 23 (Contd.)

Wavelength $\frac{1}{\lambda}$ (μm^{-1})	HD = 36512		HD = 36879		HD = 37128	
	Observed m_λ (V=0)	Corrected m_λ (V=0)	Observed m_λ (V=0)	Corrected m_λ (V=0)	Observed m_λ (V=0)	Corrected m_λ (V=0)
1.80	0.000	0.000	0.000	0.000	0.000	0.000
1.90	-0.232	-0.240	-0.096	-0.200	-0.184	-0.200
2.00	-0.384	-0.400	-0.192	-0.400	-0.368	-0.400
2.10	-0.616	-0.640	-0.283	-0.600	-0.551	-0.600
2.19	-0.728	-0.760	-0.344	-0.760	-0.696	-0.760
2.24	-0.845	-0.880	-0.408	-0.860	-0.770	-0.840
2.35	-1.018	-1.060	-0.414	-0.960	-0.916	-1.000
2.40	-1.076	-1.120	-0.428	-1.000	-0.992	-1.080
2.48	-1.201	-1.250	-0.446	-1.080	-1.022	-1.120
2.70	-1.221	-1.280	-0.471	-1.240	-1.282	-1.400
2.75	-1.258	-1.320	-0.469	-1.280	-1.355	-1.480
2.80	-1.334	-1.400	-0.667	-1.520	-1.429	-1.560
2.85	-1.382	-1.450	-0.476	-1.360	-1.444	-1.580
2.90	-1.410	-1.480	-0.485	-1.400	-1.499	-1.640
2.95	-1.447	-1.520	-0.474	-1.420	-1.554	-1.700
3.65	-2.076	-2.200	-0.634	-2.246	-1.752	-2.000
4.00	-2.594	-2.760	-0.237	-2.400	-2.247	-2.580
4.06	-2.665	-2.840	-0.222	-2.500	-2.330	-2.680
4.42	-2.922	-3.160	0.334	-2.760	-2.324	-2.800
4.57	-3.028	-3.280	0.416	-2.860	-2.386	-2.890
4.85	-3.203	-3.440	-0.002	-3.080	-2.626	-3.100
5.21	-	-	-2.966	-	-5.157	-
5.38	-3.511	-3.700	-0.820	-3.280	-2.822	-3.200
6.02	-3.813	-4.000	-1.707	-4.140	-2.966	-3.340
6.71	-4.148	-4.340	-1.844	-4.340	-3.236	-3.620
6.85	-4.165	-4.360	-1.772	-4.310	-3.210	-3.600
7.18	-4.275	-4.480	-1.818	-4.480	-3.090	-3.500

TABLE 23 (Contd.)

Wavelength $\frac{1}{\lambda}$ (μm^{-1})	HD = 38771		HD = 40589		HD = 42087	
	Observed m_λ (V=0)	Corrected m_λ (V=0)	Observed m_λ (V=0)	Corrected m_λ (V=0)	Observed m_λ (V=0)	Corrected m_λ (V=0)
1.80	0.000	0.000	0.000	0.000	0.000	0.000
1.90	-0.180	-0.200	-0.048	-0.100	-0.084	-0.160
2.00	-0.360	-0.400	-0.036	-0.140	-0.168	-0.320
2.10	-0.540	-0.600	-0.081	-0.240	-0.228	-0.460
2.19	-0.680	-0.760	-0.072	-0.280	-0.296	-0.600
2.24	-0.777	-0.860	-0.134	-0.360	-0.329	-0.660
2.35	-0.885	-0.980	-0.167	-0.440	-0.401	-0.800
2.40	-0.950	-1.050	-0.194	-0.480	-0.442	-0.860
2.48	-1.040	-1.150	-0.263	-0.520	-0.456	-0.920
2.70	-1.187	-1.320	0.285	-0.100	-0.358	-0.920
2.75	-1.260	-1.400	0.286	-0.120	-0.368	-0.960
2.80	-1.302	-1.450	0.266	-0.160	-0.417	-1.040
2.85	-1.337	-1.490	0.242	-0.200	-0.434	-1.080
2.90	-1.372	-1.530	0.218	-0.240	-0.491	-1.160
2.95	-1.396	-1.560	0.213	-0.260	-0.508	-1.200
3.65	-1.721	-2.000	0.486	-0.320	-0.422	-1.600
4.00	-2.186	-2.560	0.762	-0.320	-0.479	-2.060
4.06	-2.426	-2.820	0.898	-0.240	-0.376	-2.040
4.42	-2.305	-2.840	1.147	-0.400	0.101	-2.160
4.57	-2.333	-2.900	1.218	-0.420	0.134	-2.260
4.85	-2.507	-3.040	1.059	-0.480	-0.111	-2.360
5.21	-5.107	-	0.745	-0.550	-0.608	-2.500
5.38	-2.814	-3.240	0.630	-0.600	-0.763	-2.560
6.02	-2.899	-3.320	0.617	-0.600	-0.902	-2.680
6.71	-3.168	-3.600	0.608	-0.640	-0.936	-2.760
6.85	-3.181	-3.620	0.669	-0.600	-0.906	-2.760
7.18	-3.639	-4.100	0.931	-0.400	-0.554	-2.500

TABLE 23 (Contd.)

Wavelength	HD = 43384		HD = 45910		HD = 46149	
$\frac{1}{\lambda}$ (μm^{-1})	Observed m_λ (V=0)	Corrected m_λ (V=0)	Observed m_λ (V=0)	Corrected m_λ (V=0)	Observed m_λ (V=0)	Corrected m_λ (V=0)
1.80	0.000	0.000	0.000	0.000	0.000	0.000
1.90	-0.044	-0.160	-0.050	-0.160	-0.204	-0.300
2.00	-0.128	-0.360	-0.135	-0.360	-0.388	-0.580
2.10	-0.126	-0.480	-0.215	-0.560	-0.607	-0.900
2.19	-0.136	-0.600	-0.262	-0.720	-0.616	-1.000
2.24	-0.172	-0.680	-0.300	-0.800	-0.822	-1.240
2.35	-0.231	-0.840	-0.240	-0.840	-0.796	-1.300
2.40	-0.222	-0.860	-0.275	-0.900	-0.872	-1.400
2.48	-0.212	-0.920	-0.350	-1.060	-1.014	-1.600
2.70	0.018	-0.840	-0.155	-1.000	-1.050	-1.760
2.75	0.005	-0.900	-0.180	-1.080	-1.051	-1.800
2.80	0.011	-0.940	-0.180	-1.120	-1.063	-1.850
2.85	0.006	-0.980	-0.190	-1.160	-1.084	-1.900
2.90	0.021	-1.000	-0.240	-1.240	-1.115	-1.960
2.95	0.015	-1.040	-	-	-	-
3.65	0.448	-1.350	-0.140	-1.920	-1.192	-2.680
4.00	1.013	-1.400	-0.120	-2.520	-0.803	-2.800
4.06	1.080	-1.460	-0.110	-2.620	-0.738	-2.840
4.42	1.911	-1.540	0.575	-2.860	-0.164	-3.020
4.57	2.094	-1.560	0.650	-2.960	-0.176	-3.200
4.85	1.833	-1.600	0.370	-3.040	-0.452	-3.300
5.21	1.168	-1.720	-0.410	-3.260	-	-
5.38	0.943	-1.800	-0.610	-3.320	-2.590	-4.860
6.02	0.894	-1.820	-0.905	-3.600	-2.510	-4.760
6.71	0.904	-1.880	-0.980	-3.720	-3.250	-
6.85	0.970	-1.860	-0.880	-3.680	-2.598	-4.940
7.18	1.570	-1.400	-0.730	-3.660	-1.862	-4.320

TABLE 23 (Contd.)

Wavelength $\frac{1}{\lambda}$ (μm^{-1})	HD = 47240		HD = 47839		HD = 52382	
	Observed m_λ (V=0)	Corrected m_λ (V=0)	Observed m_λ (V=0)	Corrected m_λ (V=0)	Observed m_λ (V=0)	Corrected m_λ (V=0)
1.80	0.000	0.000	0.000	0.000	0.000	0.000
1.90	-0.126	-0.200	-0.186	-0.200	-0.124	-0.200
2.00	-0.230	-0.380	-0.375	-0.400	-0.188	-0.340
2.10	-0.310	-0.540	-0.557	-0.600	-0.308	-0.540
2.19	-0.380	-0.680	-0.684	-0.740	-0.376	-0.680
2.24	-0.479	-0.800	-0.739	-0.800	-0.389	-0.720
2.35	-0.531	-0.920	-0.887	-0.960	-0.441	-0.840
2.40	-0.620	-1.020	-0.923	-1.000	-0.462	-0.880
2.48	-0.646	-1.100	-1.115	-1.200	-0.496	-0.960
2.70	-0.650	-1.200	-1.196	-1.300	-0.718	-1.280
2.75	-0.660	-1.240	-1.251	-1.360	-0.748	-1.340
2.80	-0.710	-1.320	-1.285	-1.400	-0.777	-1.400
2.85	-0.730	-1.360	-1.341	-1.460	-0.754	-1.400
2.90	-0.790	-1.440	-1.397	-1.520	-0.791	-1.460
2.95	-0.800	-1.480	-1.453	-1.580	-	-
3.65	-0.722	-1.880	-2.063	-2.280	-0.642	-1.820
4.00	-0.899	-2.460	-	-	-0.619	-2.200
4.06	-0.800	-2.440	-5.248	-	-0.556	-2.220
4.42	-0.369	-2.600	-2.864	-3.280	-0.139	-2.400
4.57	-0.290	-2.640	-2.919	-3.360	-0.046	-2.440
4.85	-0.510	-2.740	-3.066	-3.480	-0.271	-2.520
5.21	-0.960	-2.840	-3.411	-3.760	-0.708	-2.600
5.38	-1.130	-2.920	-3.509	-3.840	-0.843	-2.640
6.02	-1.232	-3.000	-3.672	-4.000	-1.062	-2.840
6.71	-1.440	-3.240	-4.014	-4.350	-1.176	-3.000
6.85	-1.420	-3.250	-4.068	-4.410	-1.226	-3.080
7.18	-1.230	-3.160	-4.112	-4.470	-1.264	-3.210

TABLE 23 (Contd.)

Wavelength	HD = 53367		HD = 54662		HD = 58131	
$\frac{1}{\lambda}$ (μm^{-1})	Observed m_λ (V=0)	Corrected m_λ (V=0)	Observed m_λ (V=0)	Corrected m_λ (V=0)	Observed m_λ (V=0)	Corrected m_λ (V=0)
1.80	0.000	0.000	0.000	0.000	0.000	0.000
1.90	-0.014	-0.160	-0.190	-0.260	-0.044	-0.160
2.00	-0.028	-0.320	-0.300	-0.440	-0.048	-0.280
2.10	-0.055	-0.500	-0.367	-0.580	-0.126	-0.480
2.19	-0.056	-0.640	-0.420	-0.700	-0.136	-0.600
2.24	-0.085	-0.720	-0.460	-0.760	-0.255	-0.760
2.35	-0.114	-0.880	-0.513	-0.880	-0.271	-0.880
2.40	-0.117	-0.920	-0.535	-0.920	-0.322	-0.960
2.48	-	-	-0.613	-1.040	-0.352	-1.060
2.70	-	-	-0.622	-1.140	0.058	-0.800
2.75	-	-	-0.640	-1.200	0.025	-0.880
2.80	-	-	-0.706	-1.280	-0.009	-0.960
2.85	-	-	-0.725	-1.320	-0.054	-1.040
2.90	-	-	-0.764	-1.380	-0.059	-1.080
2.95	-	-	-	-	-	-
3.65	-0.057	-2.320	-1.235	-2.320	0.438	-1.360
4.00	-0.283	-3.320	-1.424	-2.880	0.533	-1.880
4.06	-0.163	-3.360	-1.367	-2.900	0.580	-1.960
4.42	0.663	-3.680	-1.018	-3.100	1.331	-2.120
4.57	0.659	-3.940	-0.955	-3.160	1.454	-2.200
4.85	0.042	-4.280	-1.128	-3.200	1.113	-2.320
5.21	-0.685	-4.320	-1.857	-3.600	0.380	-2.508
5.38	-0.947	-4.400	-2.005	-3.660	0.183	-2.560
6.02	-1.184	-4.600	-2.484	-4.120	-0.086	-2.800
6.71	-1.176	-4.680	-2.640	-4.320	-0.116	-2.900
6.85	-0.998	-4.560	-2.602	-4.310	-0.050	-2.880
7.18	-0.832	-4.570	-2.628	-4.420	-1.230	-4.200

TABLE 23 (Contd.)

Wavelength $\frac{1}{\lambda}$ (μm^{-1})	HD = 58350		HD = 66811		HD = 77581	
	Observed m_λ (V=0)	Corrected m_λ (V=0)	Observed m_λ (V=0)	Corrected m_λ (V=0)	Observed m_λ (V=0)	Corrected m_λ (V=0)
1.80	0.000	0.000	0.000	0.000	0.000	0.000
1.90	-0.070	-0.080	-0.192	-0.200	-0.034	-0.200
2.00	-0.184	-0.200	-0.384	-0.400	-0.068	-0.400
2.10	-0.296	-0,320	-0.576	-0.600	-0.074	-0.580
2.19	-0.418	-0.450	-0.728	-0.760	-0.076	-0.740
2.24	-0.465	-0.500	-0.805	-0.840	-0.078	-0.800
2.35	-0.598	-0.640	-0.918	-0.960	-0.089	-0.960
2.40	-0.636	-0.680	-1.056	-1.100	-0.087	-1.000
2.48	-0.731	-0.780	-1.151	-1.200	-0.107	-1.120
2.70	-0.581	-0.640	-1.381	-1.440	-0.032	-1.260
2.75	-0.618	-0.680	-1.418	-1.480	-0.025	-1.320
2.80	-0.654	-0.720	-1.434	-1.500	0.001	-1.360
2.85	-0.692	-0.760	-1.572	-1.640	0.001	-1.410
2.90	-0.730	-0.800	-1.610	-1.680	-0.019	-1.480
2.95	-0.767	-0.840	-1.687	-1.760	-0.009	-1.520
3.65	-0.956	-1.080	-2.016	-2.140	0.353	-2.220
4.00	-1.234	-1.400	-2.674	-2.840	0.753	-2.700
4.06	-1.245	-1.420	-2.725	-2.900	0.675	-2.960
4.42	-1.322	-1.560	-2.912	-3.240	1.878	-3.060
4.57	-1.348	-1.600	-3.068	-3.320	2.189	-3.040
4.85	-1.383	-1.620	-3.243	-3.480	1.794	-3.120
5.21	-	-	-3.481	-3.680	0.933	-3.200
5.38	-1.531	-1.720	-3.551	-3.740	0.666	-3.260
6.02	-1.613	-1.800	-3.733	-3.920	0.524	-3.360
6.71	-1.628	-1.820	-4.008	-4.200	0.664	-3.320
6.85	-1.565	-1.760	-3.965	-4.160	0.530	-3.520
7.18	-	-	-1.005	-1.210	0.290	-3.960

TABLE 23 (Contd.)

Wavelength	HD = 79186		HD = 87734		HD = 87901	
	Observed	Corrected	Observed	Corrected	Observed	Corrected
$\frac{1}{\lambda}$ (μm^{-1})	m_λ (V=0)	m_λ (V=0)	m_λ (V=0)	m_λ (V=0)	m_λ (V=0)	m_λ (V=0)
1.80	0.000	0.000	0.000	0.000	0.000	0.000
1.90	-0.095	-0.160	-0.080	-0.080	-0.078	-0.080
2.00	-0.165	-0.300	-0.200	-0.200	-0.166	-0.170
2.10	-0.250	-0.460	-0.300	-0.300	-0.264	-0.270
2.19	-0.330	-0.600	-0.400	-0.400	-0.372	-0.380
2.24	-0.390	-0.680	-0.440	-0.440	-0.391	-0.400
2.35	-0.483	-0.840	-0.520	-0.520	-0.470	-0.480
2.40	-0.505	-0.880	-0.540	-0.540	-0.509	-0.520
2.48	-0.520	-0.920	-0.560	-0.560	-0.568	-0.580
2.70	-0.420	-0.920	0.700	0.700	-0.105	-0.120
2.75	-0.435	-0.960	0.650	0.650	-0.144	-0.160
2.80	-0.445	-1.000	0.620	0.620	-0.184	-0.200
2.85	-0.470	-1.040	0.600	0.600	-0.223	-0.240
2.90	-0.480	-1.080	0.600	0.600	-0.242	-0.260
2.95	-	-	-	-	-	-
3.65	-0.205	-1.260	0.300	0.300	-0.399	-0.430
4.00	0.126	-1.290	0.360	0.360	-0.768	-0.810
4.06	0.040	-1.460	0.340	0.340	-0.776	-0.820
4.42	0.462	-1.560	0.200	0.200	-0.970	-1.030
4.57	0.690	-1.500	0.100	0.100	-1.027	-1.090
4.85	0.340	-1.660	0.100	0.100	-1.131	-1.190
5.21	-	-	0.000	0.000	-1.278	-1.330
5.38	-0.200	-1.820	-0.040	-0.040	-1.403	-1.450
6.02	-0.385	-2.000	-0.060	-0.060	-1.493	-1.540
6.71	-0.470	-2.120	0.000	0.000	-1.632	-1.680
6.85	-0.410	-2.100	0.040	0.040	-1.611	-1.660
7.18	-0.140	-1.900	0.120	0.120	-1.649	-1.700

TABLE 23 (Contd.)

Wavelength $\frac{1}{\lambda}$ (μm^{-1})	HD = 91316		HD = 102647		HD = 149438	
	Observed m_λ (V=0)	Corrected m_λ (V=0)	Observed m_λ (V=0)	Corrected m_λ (V=0)	Observed m_λ (V=0)	Corrected m_λ (V=0)
1.80	0.000	0.000	0.000	0.000	0.000	0.000
1.90	-0.164	-0.180	-0.054	-0.060	-0.228	-0.240
2.00	-0.328	-0.360	-0.128	-0.140	-0.376	-0.400
2.10	-0.471	-0.520	-0.202	-0.220	-0.644	-0.680
2.19	-0.626	-0.690	-0.276	-0.300	-0.712	-0.760
2.24	-0.730	-0.800	-0.354	-0.380	-0.828	-0.880
2.35	-0.866	-0.950	-0.448	-0.480	-1.016	-1.080
2.40	-0.912	-1.000	-0.487	-0.520	-1.054	-1.120
2.48	-1.022	-1.120	-0.563	-0.600	-1.166	-1.240
2.70	-1.082	-1.200	0.244	0.200	-1.072	-1.160
2.75	-1.135	-1.260	0.207	0.160	-1.146	-1.240
2.80	-1.189	-1.320	0.169	0.120	-1.222	-1.320
2.85	-1.224	-1.360	0.171	0.120	-1.298	-1.400
2.90	-1.279	-1.420	0.173	0.120	-1.374	-1.480
2.95	-	-	-	-	-	-
3.65	-1.592	-1.840	0.471	0.380	-1.778	-1.960
4.00	-1.827	-2.160	0.528	0.400	-2.552	-2.800
4.06	-1.870	-2.220	0.532	0.400	-2.636	-2.900
4.42	-1.924	-2.400	0.300	0.120	-2.820	-3.080
4.57	-1.936	-2.440	0.229	0.040	-2.822	-3.200
4.85	-2.182	-2.660	0.178	0.000	-3.104	-3.460
5.21	-	-	-	-	-	-
5.38	-2.342	-2.720	0.152	0.020	-3.416	-3.680
6.02	-2.506	-2.880	0.860	0.720	-3.880	-4.160
6.71	-2.756	-3.140	2.144	2.000	-4.112	-4.400
6.85	-2.730	-3.120	-5.409	-	-4.078	-4.370
7.18	-2.830	-3.240	-	-	-4.192	-4.500

TABLE 23 (Contd)

Wavelength	HD = 164353		HD = 176437		HD = 182255	
	Observed	Corrected	Observed	Corrected	Observed	Corrected
$1/\lambda$ (μm^{-1})	m_λ (V=0)	m_λ (V=0)	m_λ (V=0)	m_λ (V=0)	m_λ (V=0)	m_λ (V=0)
1.80	0.00	0.00	0.00	0.00	0.00	0.00
1.84	-0.08	-0.14	-0.06	-0.06	-0.10	-0.10
1.90	-0.23	-0.38	-0.13	-0.13	-0.19	-0.19
1.96	-0.28	-0.52	-0.15	-0.16	-0.28	-0.29
2.03	-0.45	-0.80	-0.29	-0.30	-0.37	-0.38
2.10	-0.45	-0.91	-0.35	-0.36	-0.53	-0.54
2.18	-0.54	-1.12	-0.45	-0.46	-0.64	-0.65
2.26	-0.70	-1.38	-0.61	-0.63	-0.77	-0.79
2.35	-0.85	-1.65	-0.75	-0.77	-0.86	-0.88
2.44	-0.94	-1.82	-0.87	-0.89	-1.04	-1.06
2.55	-0.92	-1.91	-0.88	-0.91	-1.05	-1.08
2.65	-0.35	-1.44	-0.03	-0.06	-0.46	-0.49
2.78	-0.53	-1.75	-0.01	-0.04	-0.47	-0.53
3.65	-0.72	-3.08	-0.20	-0.26	-1.00	-1.06
4.00	-0.79	-3.95	-0.14	-0.22	-1.26	-1.34
4.17	-0.75	-4.32	-0.14	-0.23	-1.35	-1.44
4.35	-0.21	-4.50	-0.02	-0.13	-1.51	-1.62
4.55	+0.01	-4.75	-0.07	-0.19	-1.62	-1.74
4.76	-0.23	-4.80	-0.15	-0.27	-1.73	-1.85
5.00	-0.83	-4.92	-0.25	-0.36	-1.83	-1.94
5.26	-1.01	-4.70	-0.31	-0.41	-1.91	-2.01
5.55	-1.33	-4.81	-0.37	-0.46	-2.04	-2.13
5.88	-1.49	-5.08	-0.44	-0.53	-2.21	-2.30
6.25	-1.48	-5.07	-0.44	-0.54	-2.29	-2.39
6.66	-1.60	-5.25	-0.46	-0.56	-2.42	-2.52
7.14	-1.48	-5.39	-0.42	-0.52	-1.91	-2.01

Table 23 (Contd)

	HD = 188260		HD =195810	
	Observed	Corrected	Observed	Corrected
$1/\lambda(mm^{-1})$	$m_\lambda(V=0)$	$m_\lambda(V=0)$	$m_\lambda(V=0)$	$m_\lambda(V=0)$
1.80	0.00	0.00	0.00	0.00
1.84	-0.05	-0.05	-0.10	-0.10
1.90	-0.18	-0.18	-0.24	-0.24
1.96	-0.24	-0.24	-0.34	-0.35
2.03	-0.45	-0.45	-0.53	-0.54
2.10	-0.48	-0.48	-0.55	-0.56
2.18	-0.50	-0.50	-0.65	-0.66
2.26	-0.60	-0.60	-0.84	-0.86
2.35	-0.72	-0.72	-1.01	-1.03
2.44	-0.84	-0.84	-1.14	-1.16
2.55	-0.75	-0.75	-1.12	-1.15
2.66	-0.14	-0.14	-0.52	-0.55
2.78	-0.19	-0.19	-0.64	-0.67
3.65	-0.10	-0.10	-0.87	-0.99
4.00	-0.25	-0.25	-1.16	-1.24
4.17	-0.27	-0.27	-1.23	-1.32
4.35	-0.43	-0.43	-1.37	-1.48
4.55	-0.55	-0.55	-1.50	-1.62
4.76	-0.62	-0.62	-1.58	-1.70
5.00	-0.73	-0.73	-1.70	-1.81
5.26	-0.78	-0.78	-1.78	-1.88
5.55	-0.84	-0.84	-1.89	-1.98
5.88	-0.92	-0.92	-2.04	-2.13
6.25	-0.94	-0.94	-2.11	-2.21
6.66	-1.03	-1.03	-2.22	-2.32
7.14	-0.17	-0.17	-1.77	-1.87

HD =214953

Observed Calculated

π_λ(V=0)	π_λ(V=
0.00	0.00
-0.07	-0.08
-0.21	-0.23
-0.28	-0.32
-0.50	-0.55
-0.47	-0.54
-0.54	-0.63
-0.72	-0.83
-0.87	-1.00
-0.97	-1.11
-0.99	-1.15
-0.38	-0.55
-0.80	-0.99
-1.61	-1.98
-1.94	-2.44
-2.01	-2.57
-2.02	-2.70
-2.02	-2.77
-2.13	-2.85
-2.29	-3.04
-2.45	-3.03
-2.71	-3.26
-2.91	-3.46
-2.85	-3.42
-3.04	-3.62
-3.15	-3.77

Table 23 (Condt)

wavelength $1/\lambda$ (μm^{-1})	HD = 224572 Observed m_λ(V=0)	HD = 224572 Corrected m_λ(V=0)	HD= 218376 Observed m_λ(V=0)	HD= 218376 Corrected m_λ(V=0)
1.80	0	0	0	0
1.84	-0.01	-0.03	-0.02	-0.11
1.90	-0.16	-0.20	-0.06	-0.26
1.96	-0.31	-0.37	-0.09	-0.33
2.03	-0.40	-0.49	-0.13	-0.53
2.10	-0.61	-0.73	-0.17	-0.52
2.18	-0.63	-0.78	-0.21	-0.64
2.26	-0.71	-0.89	-0.25	-0.87
2.35	-0.83	-1.01	-0.29	-1.00
2.44	-1.03	-1.26	-0.32	-1.09
2.55	-0.71	-0.97	-0.36	-1.11
2.66	-0.87	-1.16	-0.40	-0.56
2.78	--	--	-0.45	-1.25
3.65	-1.35	-1.95	-0.87	-2.26
4.00	-1.66	-2.49	-1.16	-2.84
4.17	-1.66	-2.60	-1.32	-3.00
4.35	-1.61	-2.73	-1.58	-3.15
4.55	-1.61	-2.87	-1.75	-3.25
4.76	-1.69	-2.89	-1.68	-3.28
5.00	-1.89	-2.97	-1.51	-3.37
5.26	--	--	-1.36	-3.42
5.55	-2.20	-3.12	-1.28	-3.70
5.88	-2.68	-3.63	-1.32	-3.92
6.25	-2.58	-3.53	-1.33	-3.83
6.66	-2.77	-3.73	-1.35	-4.07
7.14	-2.82	-3.83	-1.44	-4.22

Table 23 (Condt)

Wavelength	HD = 160762		HD = 188209		HD = 197345	
$1/\lambda$ (μm^{-1})	Observed m_λ (V=0)	Corrected m_λ (V=0)	Observed m_λ (V=0)	Corrected m_λ (V=0)	Observed m_λ (V=0)	Corrected m_λ (V=0)
1.80	0	0	0	0	0	
1.84	-0.04	-0.04	-0.02	-0.04	-0.01	-0.01
1.90	-0.16	-0.16	-0.17	-0.21	-0.10	-0.11
1.96	-0.36	-0.37	-0.34	-0.40	-0.20	-0.21
2.03	-0.48	-0.49	-0.36	-0.45	-0.35	-0.37
2.10	-0.62	-0.63	-0.55	-0.67	-0.46	-0.48
2.18	-0.64	-0.65	-0.51	-0.75	-0.45	-0.48
2.26	-0.71	-0.73	-0.63	-0.91	-0.54	-0.58
2.35	-0.87	-0.89	-0.78	-0.91	-0.60	-0.64
2.44	-1.04	-1.06	-0.89	-1.12	-0.72	-0.76
2.55	-0.69	-0.71	-0.71	-0.97	--	--
2.66	-0.71	-0.74	-0.81	-1.10	--	--
2.78	--	--	--	--	--	--
3.65	-1.37	-1.43	--	--	+0.68	+0.56
4.00	-1.75	-1.85	-1.97	-2.80	+0.91	+0.75
4.17	-1.83	-1.92	-2.01	-2.95	+1.18	+0.90
4.35	-2.00	-2.11	-1.98	-3.10	+0.97	+0.75
4.55	-2.07	-2.19	-1.98	-3.24	+0.75	+0.51
4.76	-2.14	-2.26	-2.11	-3.31	+0.62	+0.38
5.00	-2.30	-2.41	-2.29	-3.37	+0.62	+0.40
5.26	-2.39	-2.49	-2.45	-3.43	+0.75	+0.55
5.55	-2.60	-2.69	-2.59	-3.51	+0.67	+0.42
5.88	-2.80	-2.89	-2.69	-3.64	+1.16	+0.98
6.25	-2.78	-2.87	-2.75	-3.70	+1.23	+1.05
6.66	-2.96	-3.15	-2.86	-3.82	+1.36	+1.18
7.14	-3.00	-3.10	-2.54	-3.55	+1.97	+1.75

Table 23 (Condt)

	HD = 152614		HD = 155763		HD = 222173	
wavelength $1/\lambda(\mu m^{-1})$	Observed m_λ (V=0)	Corrected m_λ (V=0)	Observed m_λ (V=0)	Corrected m_λ (V=0)	Observed m_λ (V=0)	Corrected m_λ (V=0)
1.80	0	0	0	0	0	0
1.84	-0.04	-0.04	-0.03	-0.03	-0.04	-0.04
1.90	-0.18	-0.19	-0.19	-0.19	-0.18	-0.18
1.96	-0.34	-0.35	-0.38	-0.39	-0.31	-0.31
2.03	-0.47	-0.48	-0.51	-0.52	-0.46	-0.46
2.10	-0.60	-0.61	-0.70	-0.71	-0.61	-0.61
2.18	-0.64	-0.66	-0.73	-0.74	-0.66	-0.66
2.26	-0.72	-0.74	-0.86	-0.88	-0.76	-0.76
2.35	-0.83	-0.85	-1.03	-1.05	-0.90	-0.90
2.44	-1.02	-1.04	-1.21	-1.23	-1.09	-1.09
2.55	-0.49	-0.51	-0.78	-0.80	-0.68	-0.68
2.66	-0.37	-0.40	-0.72	-0.75	-0.50	-0.50
2.78	--	--	--	--	--	--
3.65	-0.52	-0.58	-0.90	-0.96	-0.52	-0.52
4.00	-0.77	-0.85	-1.08	-1.16	-0.68	-0.68
4.17	-0.77	-0.86	-1.05	-1.14	-0.66	-0.66
4.35	-1.02	-1.13	-1.26	-1.37	-0.80	-0.80
4.55	-1.08	-1.20	-1.36	-1.48	-0.85	-0.85
4.76	-1.17	-1.29	-1.46	-1.58	-0.98	-0.98
5.00	-1.27	-1.38	-1.55	-1.66	-1.08	-1.08
5.26	-1.27	-1.37	-1.60	-1.70	-1.18	-1.18
5.55	-1.40	-1.49	-1.64	-1.73	-1.27	-1.27
5.88	-1.55	-1.64	-1.77	-1.86	-1.50	-1.50
6.25	-1.56	-1.65	-1.79	-1.88	-1.62	-1.62
6.66	-1.67	-1.76	-1.91	-2.00	-1.63	-1.63
7.14	-1.63	-1.73	-1.91	-2.01	-1.58	-1.58

APPENDIX III

A1: ULTRAVIOLET ENERGY DISTRIBUTIONS OF LUMINOUS EARLY-TYPE STARS FROM TD1 SATELLITE OBSERVATIONS: Humphries, C. M., Nandy, K., Kontizas, E., 1975. Astrophys. J., 195, 111.

A2: THE EFFECTIVE TEMPERATURE OF EARLY-TYPE STARS: Nandy, K., Kontizas, E., 1976. Stars and galaxies from observational points of view, Proc IIIrd European Astronomical Meeting Tbilisi, 1975, pp. 82.

A3: Meeting of the Royal Astronomical Society 1975 Friday October 12. The Observatory, 96, 80.

A4: SPECTROGRAPHIC DETERMINATION OF THE CHROMATIC CURVE OF A REFRACTING TELESCOPE: Papathanasoglou, D., Deligiannis, J., Kontizas, E., 1976. The Observatory, 96, 158.

A5: ABSOLUTE SPECTROPHOTOMETRY OF NOVA CYGNI 1975: Kontizas, E., Kontizas, M., Smyth, M.J., 1976. Mon. Not. R. ast. Soc., 176, 79P.

THE ASTROPHYSICAL JOURNAL, 195:111–119, 1975 January 1

ULTRAVIOLET ENERGY DISTRIBUTIONS OF LUMINOUS EARLY-TYPE STARS FROM TD1 SATELLITE OBSERVATIONS

C. M. HUMPHRIES, K. NANDY, AND E. KONTIZAS
Royal Observatory, Edinburgh, Scotland
Received 1974 June 6; revised 1974 August 1

ABSTRACT

Ultraviolet spectra are presented for supergiants, giants, and main-sequence stars in the spectral type range from B0 to A2. The observations were obtained in the spectral range 2750–1350 Å with the S2/68 Ultraviolet Sky Survey Telescope in the TD1 satellite. The effect of luminosity has been studied by comparing the ultraviolet energy distributions of luminous and main-sequence stars of the same spectral type. The flux deficiencies which are observed in the energy distributions of luminous stars are interpreted as the result of lower effective temperatures for luminous stars than for corresponding main-sequence stars, and an estimate is given of the effective temperature scale for B-type supergiants.

Subject headings: early-type stars — spectra, ultraviolet — spectrophotometry

I. INTRODUCTION

Differences between the ultraviolet energy distributions of early-type supergiants and dwarfs of the same spectral type have been noted in earlier work (Carruthers 1969; Weber, Henry, and Carruthers 1971; Bless and Savage 1972; Laget 1972). That the normalized ultraviolet fluxes are observed to be systematically lower for supergiants than for dwarfs has been interpreted by Mihalas (1970), from model atmosphere calculations, as the result of differences in surface gravity and effective temperature. Ultraviolet absorption features which occur in the spectra of luminous stars and which are absent or present only weakly in main-sequence stars have also been reported by Underhill, Leckrone, and West (1972) and by Thompson, Humphries, and Nandy (1974). The broad absorption feature at 1720 Å has been considered as originating in the extended envelopes of supergiant and shell stars (Underhill *et al.* 1972; Tarafdar and Vardya 1973), whereas the absorption centered at 1920 Å has been interpreted as a photospheric line blocking effect. The ultraviolet spectrophotometric observations reported so far have been limited to a fairly small number of luminous stars, however, and there is a clear need for further observational data.

II. OBSERVATIONS AND DATA REDUCTION

In the present paper we have used observations obtained with the S2/68 Ultraviolet Sky Survey telescope in the European satellite TD1 to study the effect of luminosity in the ultraviolet by comparing the energy distribution of giants and supergiants with those of main-sequence stars of similar spectral type. The spectrometer covers the spectral region 2550–1350 Å, sampling at 20 Å intervals with a spectral resolution of 35 Å, and a photometer channel gives a broad-band measurement centered at 2750 Å. Details of the instrumentation and performance of the S2/68 experiment have been described by Boksenberg *et al.* (1973). The spectral efficiency of the instrument was measured on an absolute basis as a function of wavelength. Separate calibrations were performed independently by teams from Britain and Belgium, the results of which agreed within the estimated experimental errors of ±20 percent over the entire wavelength range. The separate results have been combined to obtain a mean calibration of the instrumental spectral response (Humphries *et al.* 1974), and this has been used to derive the fluxes presented here.

The luminous stars which have been considered are listed in table 1 together with the main-sequence stars used for comparison. Each of the stars included was selected on the basis of small interstellar reddening. The MK spectral types and photometric data have been taken from Blanco *et al.* (1968), and the intrinsic colors of Johnson (1966) were used to derive values of E_{B-V}. The observed ultraviolet flux distributions of these stars normalized to $V = 0$ are shown in figure 1. From these, magnitude differences defined as $\Delta m_\lambda = (m_\lambda - V)_{\text{luminous}} - (m_\lambda - V)_{\text{dwarf}}$ have been derived for pairs of luminous and dwarf stars of similar spectral type. Corrections for interstellar reddening were applied using a mean extinction law derived from the available ultraviolet observations from OAO-2 (Bless and Savage 1972) and TD1 (Boksenberg *et al.* 1973). Since E_{B-V} for the stars in table 1 is in most cases less than 0.05 mag, the error in the corrected Δm_λ arising from uncertainties in the extinction law is exceedingly small. The corrected Δm_λ values are plotted as a function of $1/\lambda$ in figures 2*a*–2*j*. Also shown in this diagram are the corresponding magnitude differences at the wavelengths of the photometric *U* and *B* bands. The spectral coverage is incomplete for two of the stars in table 1 (HD 122451 [B1 II] and HD 51283 [B3 II–III]), and these have not been included in figure 2; the observations which are available for these stars, however, give good agreement with the general trends which are described below.

Values of Δm_λ in the visible wavelength range of figure 2 indicate that the stars considered here have the normal *UBV* photometric properties characteristic

TABLE 1

OBSERVED STARS

Star	HD	MK Type	V	$B-V$	E_{B-V}
ϵ Ori.....	37128	B0 Ia	1.70	−0.19	0.08
... .	75821	B0 III	5.10	−0.21	0.09
τ Sco.....	149438	B0 V	2.83	−0.25	0.05
υ Ori.....	36512	B0 V	4.60	−0.26	0.04
... .	64760	B1 Ib	4.23	−0.15	0.07
139 Tau.....	40111	B1 Ib	4.82	−0.08	0.14
β Cen.....	122451	B1 II	0.61	−0.22	0.02
... .	37209	B1 V	5.70	−0.23	0.03
ϵ CMa.....	52089	B2 II	1.50	−0.22	0.00
σ Sgr.....	175191	B2 V	2.10	−0.21	0.03
κ Cen.....	132200	B2 V	3.12	−0.22	0.02
o^2 CMa.....	53138	B3 Ia	3.05	−0.08	0.06
... .	51283	B3 II–III	5.28	−0.19	0.00
η UMa.....	120315	B3 V	1.86	−0.20	0.00
η CMa.....	58350	B5 Ia	2.40	−0.07	0.03
α Gru.....	209952	B5 V	1.73	−0.13	0.03
β Ori.....	34085	B8 Ia	0.17	−0.03	0.00
η Aqr.....	213998	B8 V	4.02	−0.09	0.00
... .	94367	A0 Ia	5.28	+0.15	0.14
γ Oph.....	161868	A0 V	3.76	+0.04	0.04
α Cyg.....	197345	A2 Ia	1.26	+0.09	0.04
ϵ Gru.....	215789	A2 V	3.48	+0.08	0.02

of early-type stars. At $1/\lambda = 2.30\,\mu^{-1}$, ΔB values either are zero or take small positive values ($\sim$0.1 mag), since, in the spectral type range considered, $(B-V)$ is not strongly dependent on luminosity. The ΔU values (at $1/\lambda = 2.78\,\mu^{-1}$) are approximately zero for spectral types near B0 but become progressively more negative toward later spectral types. These values are consistent with measurements of the Balmer discontinuities in early-type stars by Barbier (1952) and Chalonge (1956); the magnitude of the Balmer jump is larger for main-sequence stars than for luminous stars, and the difference in Balmer jump between main-sequence and luminous stars systematically increases from early B to A2 stars.

Figure 2 shows that shortward of the Balmer jump Δm_λ increases with $1/\lambda$, indicating that the normalized fluxes of luminous stars become fainter with decreasing wavelength as compared with the fluxes of the corresponding main sequence stars (cf. fig. 1). This applies both to supergiants and to giants, and for all spectral types from B0 to B8. In this spectral type range the slopes of the curves in figures 2*a*–2*h* are remarkably similar. For the pairs which contain a supergiant, Δm increases typically by 0.7 mag from $1/\lambda = 4.0\,\mu^{-1}$ (2500 Å) to $1/\lambda = 7.15\,\mu^{-1}$ (1400 Å); for the pairs which contain a giant the corresponding increase in Δm is 0.4 mag. Figure 2*a* includes the pair consisting of ϵ Ori (HD 37128, B0 Ia) and υ Ori (HD 36512, B0 V) which have also been observed photometrically at 1115 Å by Carruthers (1969). Carruthers's measurements (photometer A values in table 2 of his paper) give a normalized flux ratio for υ Ori/ϵ Ori of 2.4, i.e., a Δm value of nearly 1.0 mag at this wavelength. This fits well with the present observations if the data in figure 2*a* are extrapolated to $1/\lambda = 9.0\,\mu^{-1}$.

For the A-type stars in figures 2*i*–2*j*, Δm increases with $1/\lambda$ up to $1/\lambda \approx 5.5\,\mu^{-1}$ (1800 Å) in a manner similar to that already described. Beyond this value of $1/\lambda$, however, the slope of the curve changes sign and the ultraviolet flux deficiency between the A-type supergiants and their main-sequence counterparts start decreasing. For the A0 pair shown here, the normalized flux of the supergiant becomes comparable to that of the dwarf at 1400 Å. For the A2 stars shortward of 1600 Å the normalized flux of the supergiant becomes larger than that of the dwarf.

Other noteworthy aspects of figure 2 are: (1) The lines at 1550 Å ($1/\lambda = 6.45\,\mu^{-1}$) and 1400 Å ($1/\lambda = 7.14\,\mu^{-1}$), predominantly due to C IV and Si IV, respectively, appear more strongly in giants and supergiants than the corresponding main-sequence stars in the spectral type range observed; a comparison of the measured equivalent widths of these lines in supergiant and main-sequence stars has been given previously by Code and Bless (1970). (2) The B-type giants and supergiants studied here all show stronger absorption near 1920 Å ($1/\lambda = 5.2\,\mu^{-1}$) than the corresponding main-sequence stars. The presence of this feature in the spectra of luminous stars was reported earlier by Thompson *et al.* (1974). It appears from our data that the 1920 Å absorption is somewhat weaker for luminous B0–B1 stars than for luminous stars in the range B2–B8. In the latter range, however, the relative strength seems to remain fairly constant. (3) The 1720 Å ($1/\lambda = 5.81\,\mu^{-1}$) feature first reported by Underhill *et al.* (1972) is present in the B-type giants and supergiants studied here, and is generally weaker than the 1920 Å feature. The ratio of the strength of this band to that of the 1920 Å band appears to vary; for example, in η CMa the strengths of the two features are comparable whereas for β Ori the 1720 Å feature is considerably weaker than that at 1920 Å. It should be noted, however, that in our data 1720 Å lies in the overlap region at the extremities of the short- and

medium-wavelength spectrometer channels where vignetting of the primary image occurs. Although corrections are applied in the data reduction to compensate for this, the measured absorption strengths here may still be affected slightly by the instrumental effect. (4) Δm_λ is observed to be nonzero in the regions between the known strong bands and lines. Thus, structure in the Δm_λ versus $1/\lambda$ curve near 1920, 1720, 1550, and 1400 Å appears to be superposed upon an additional Δm component, which increases progressively toward shorter wavelengths.

III. DISCUSSION

The observations presented here extend previous photometric and spectrophotometric observations and confirm that the early-type giants and supergiants are deficient in their ultraviolet fluxes with respect to main-sequence stars. Such deficiencies could be caused by one or a combination of the following: (*a*) The difference in surface gravities between main-sequence and luminous stars may be important, as suggested by Carruthers (1969) and by Mihalas (1970). Included here are gravity-dependent changes both of the continuum flux and of the line opacities. (*b*) There may be an intrinsic temperature difference between main-sequence and luminous stars as suggested also by Mihalas (1970), with the luminous star having an effective temperature cooler than the main-sequence star of similar spectral type. (*c*) Many B stars are known to be multiple systems, and the observed spectra may be affected by fainter companions of different spectral type. Although this could give rise to an effect similar to that observed here the curves plotted in figures 2*a*–2*h* for eight B-type pairs all show strong similarities and cannot reasonably be explained by having in each case an additional unidentified component of the required spectral type and magnitude. We therefore discount this explanation as being extremely improbable and proceed to examine in further detail possibilities (*a*) and (*b*).

We first note qualitatively that whereas a temperature difference would produce a systematic effect over the whole of the observed spectral range, differences between luminous and main-sequence stars in the extent of line blocking are expected to produce significant effects only in the ultraviolet region. In this context the values of $(B - V)$ are of particular interest. Intrinsic $(B - V)$ values of the giants and supergiants are less negative than for the corresponding main-sequence stars, giving rise to small positive values of Δm at the B photometric wavelength in figure 2. This, together with the positive slope of the Δm_λ versus $1/\lambda$ curve in the ultraviolet, suggests that the same effect is present across the entire spectral region observed and hence supports the interpretation that the luminous B stars are intrinsically cooler than the main-sequence stars.

To obtain a typical value for the size of the effect which we seek to explain, we consider the early B-type stars since these are least affected by the differences in Balmer jump. For pairs containing supergiants, Δm in the 1420 Å region is observed (fig. 2) to be ~0.6 mag, corresponding to a value of 1.7 for the ratio R of the normalized flux at this wavelength of the main-sequence star to that of the supergiant. Recent line-blanketed model atmosphere calculations by Kurucz, Peytremann, and Avrett (1973) suggest that surface-gravity differences alone are not sufficient to account for values of R as large as this. Some results of the Kurucz *et al.* calculations which permit comparison with the present observations are given in table 2. Computed values of F_{1422}/F_{5000} at $\log g = 4.0$ and $\log g = 3.0$ or $\log g = 2.0$ are shown for effective temperatures of 20,000° and 15,000° K. The final column in table 2 gives the ratio of the normalized flux at the higher surface gravity to that at the lower surface gravity. Comparison of the computed values of R with the observed value of ~1.7 indicates that, for a given effective temperature, gravity-dependent effects make only a small contribution (less than 20%) to the observed ultraviolet flux deficiencies of supergiants; and that the major contribution arises from an intrinsic temperature difference between main-sequence and luminous stars of the same spectral type. Although the Kurucz *et al.* models assume conditions of local thermodynamic equilibrium (LTE), the computed values of R given above are not expected to be changed significantly by inclusion of non-LTE effects for the temperature range considered here.

TABLE 2

COMPUTED VALUES OF F_{1422}/F_{5000} FOR DIFFERENT EFFECTIVE TEMPERATURES AND SURFACE GRAVITIES*

	log g			
T_e (° K)	4.0	3.0	2.0	R
20,000.....	21.3	20.2	...	1.05
15,000.....	9.5	...	8.4	1.13

* From line blanketed model atmosphere calculations by Kurucz, Peytremann, and Avrett (1973).

Figure 3 shows the Δm_λ versus $1/\lambda$ curves for pairs of main-sequence stars and for pairs of supergiants: figure 3*a* compares B3 V, B5 V, and B8 V stars with a B1 V star while figure 3*b* compares B3 Ia, B5 Ia, and B8 Ia stars with a B1 Ia star. The slope of the line is proportional to the temperature difference for the pair of stars compared. It is seen that the slopes of the lines for the main-sequence pairs are approximately the same as for the corresponding supergiant pairs. In other words, the decrements in effective temperature in passing from B1 through B3 and B5 to B8 are similar for main-sequence and supergiant stars.

In order to obtain an approximate measure of the difference in effective temperature between supergiant and dwarf stars of the same spectral type, we have first adopted the effective temperature scale for main-sequence stars given by Schild, Peterson, and Oke (1971). Using this for the temperature of the main-sequence star, we have then determined in each case the supergiant temperature, assuming blackbody energy distributions, required to match the observed

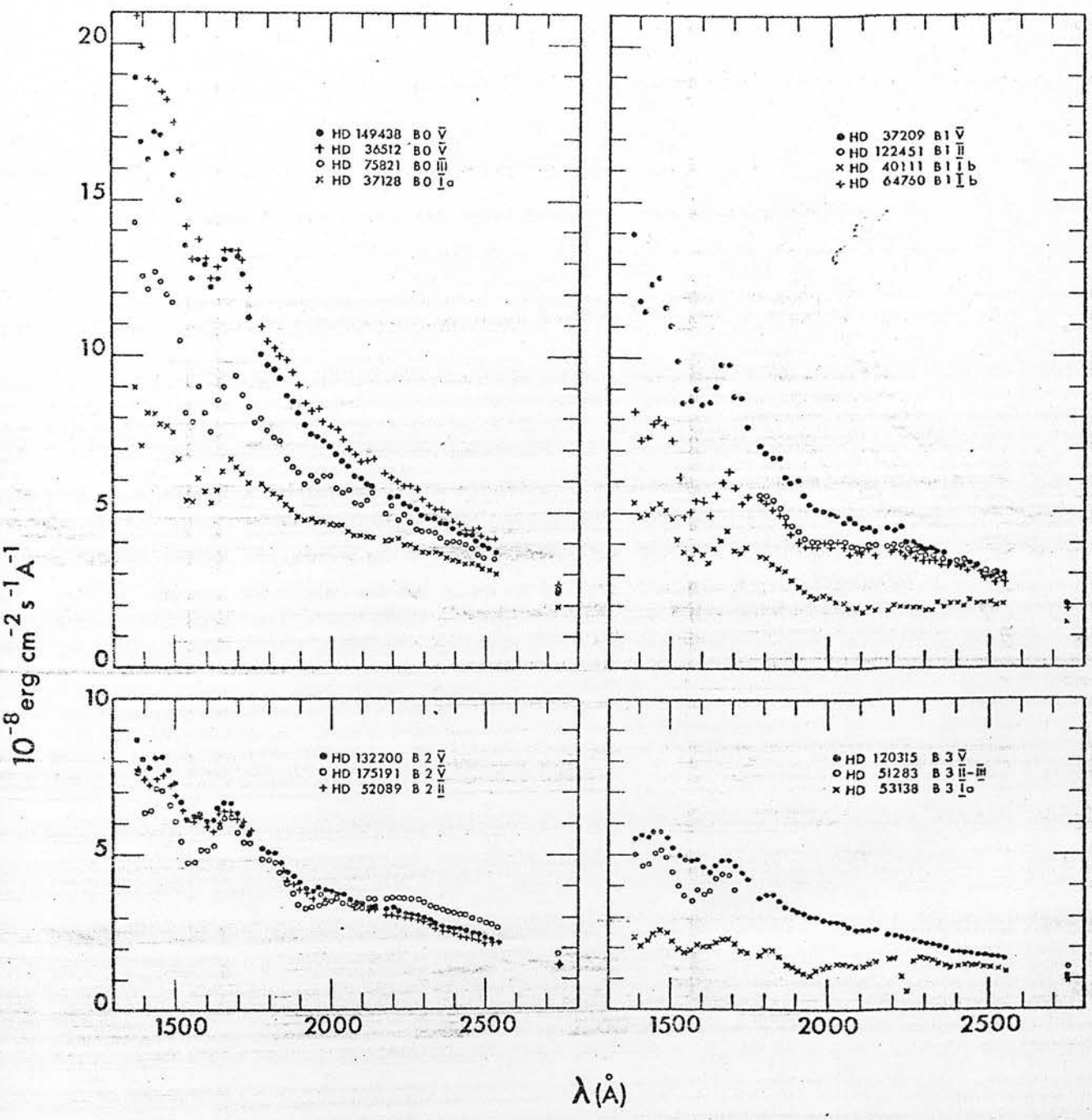

FIG. 1a

FIG. 1.—Ultraviolet flux distributions normalized to $V = 0$ for luminous and main-sequence stars

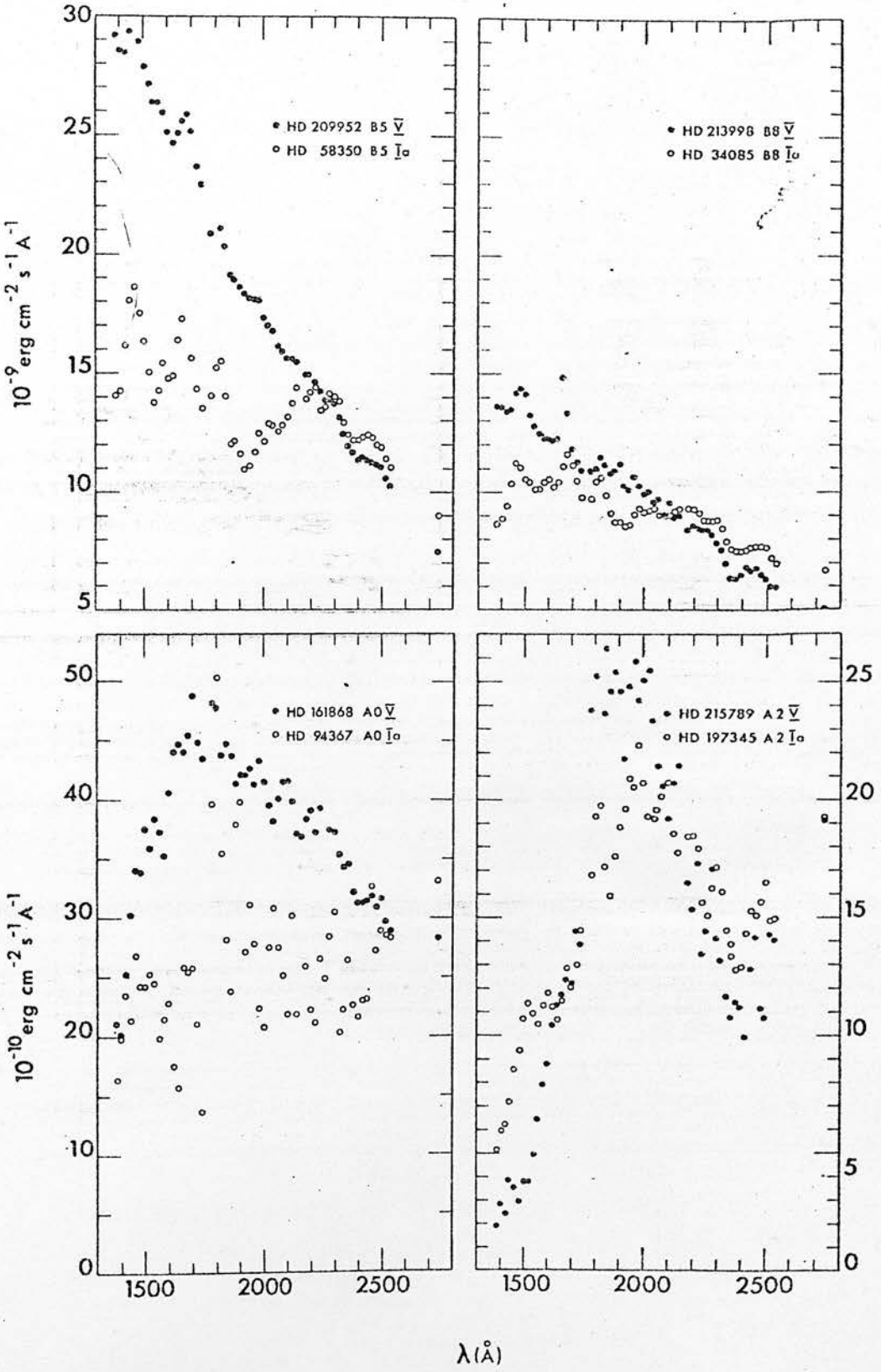
HD 209952 B5 V
HD 58350 B5 Ia
HD 213998 B8 V
HD 34085 B8 Ia
HD 161868 A0 V
HD 94367 A0 Ia
HD 215789 A2 V
HD 197345 A2 Ia
10^-9 erg cm^-2 s^-1 A^-1
10^-10 erg cm^-2 s^-1 A^-1
λ(Å)

FIG. 1b

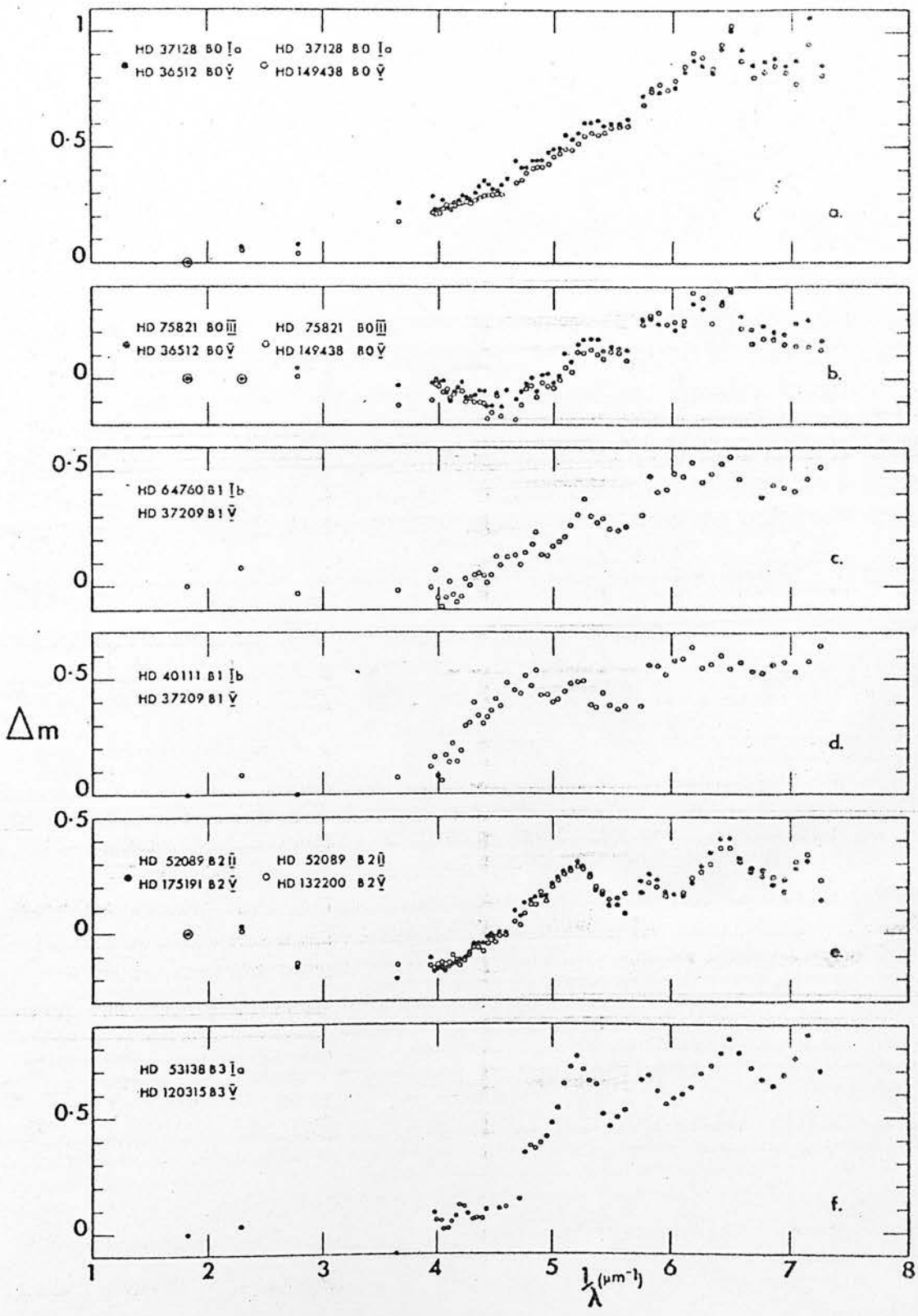

FIG. 2a

FIG. 2.—Magnitude differences Δm_λ shown as a function of $1/\lambda$ for pairs of luminous and dwarf stars of similar spectral type. For each pair, Δm is zero at the photometric V wavelength ($1/\lambda = 1.82\ \mu^{-1}$).

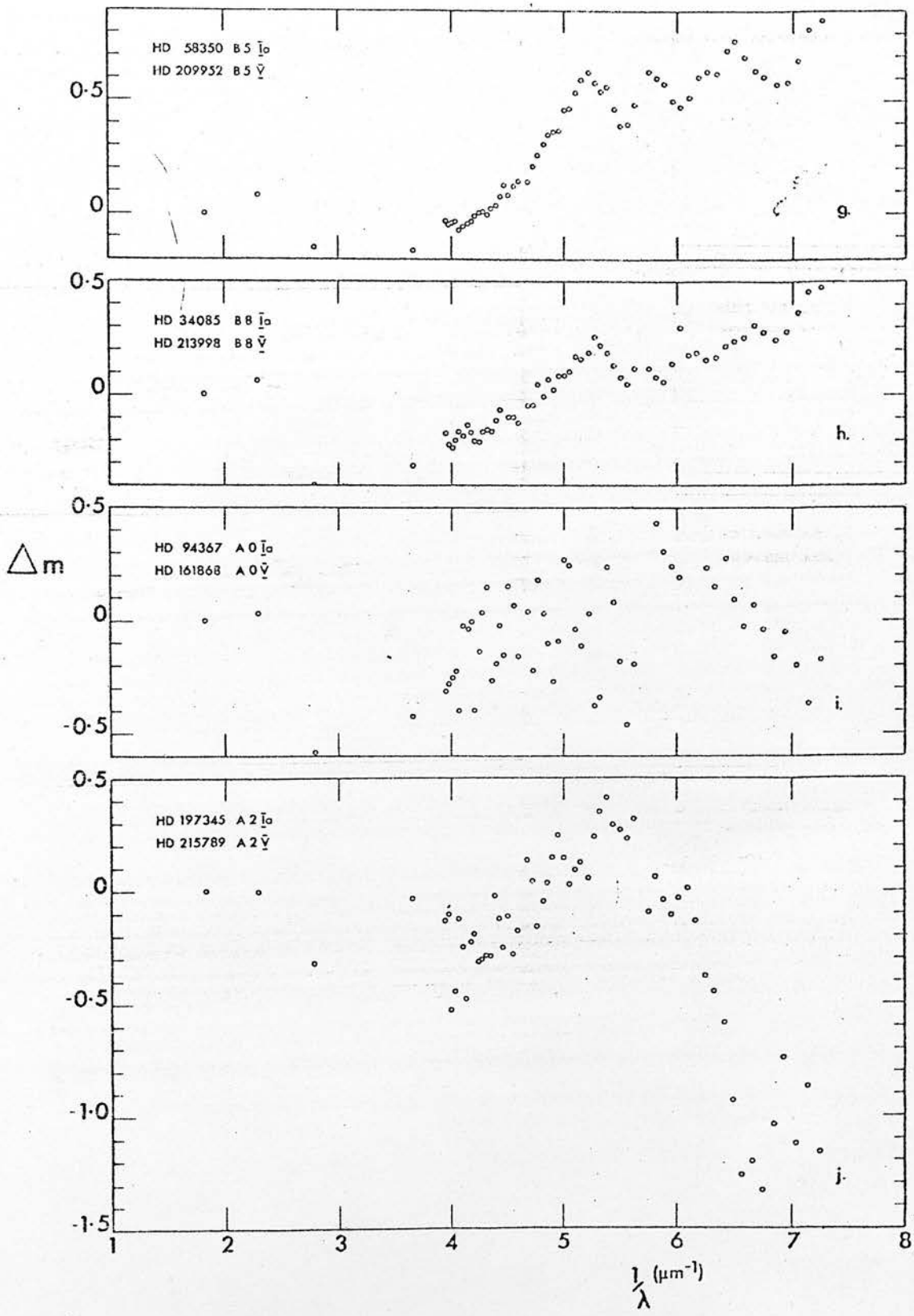
HD 58350 B 5 Ia
HD 209952 B 5 V
g.
HD 34085 B 8 Ia
HD 213998 B 8 V
h.
HD 94367 A 0 Ia
HD 161868 A 0 V
i.
HD 197345 A 2 Ia
HD 215789 A 2 V
j.
Δm
0·5
0
-0·5
-1·0
-1·5
1
2
3
4
5
6
7
8
1/λ (μm⁻¹)

FIG. 2b

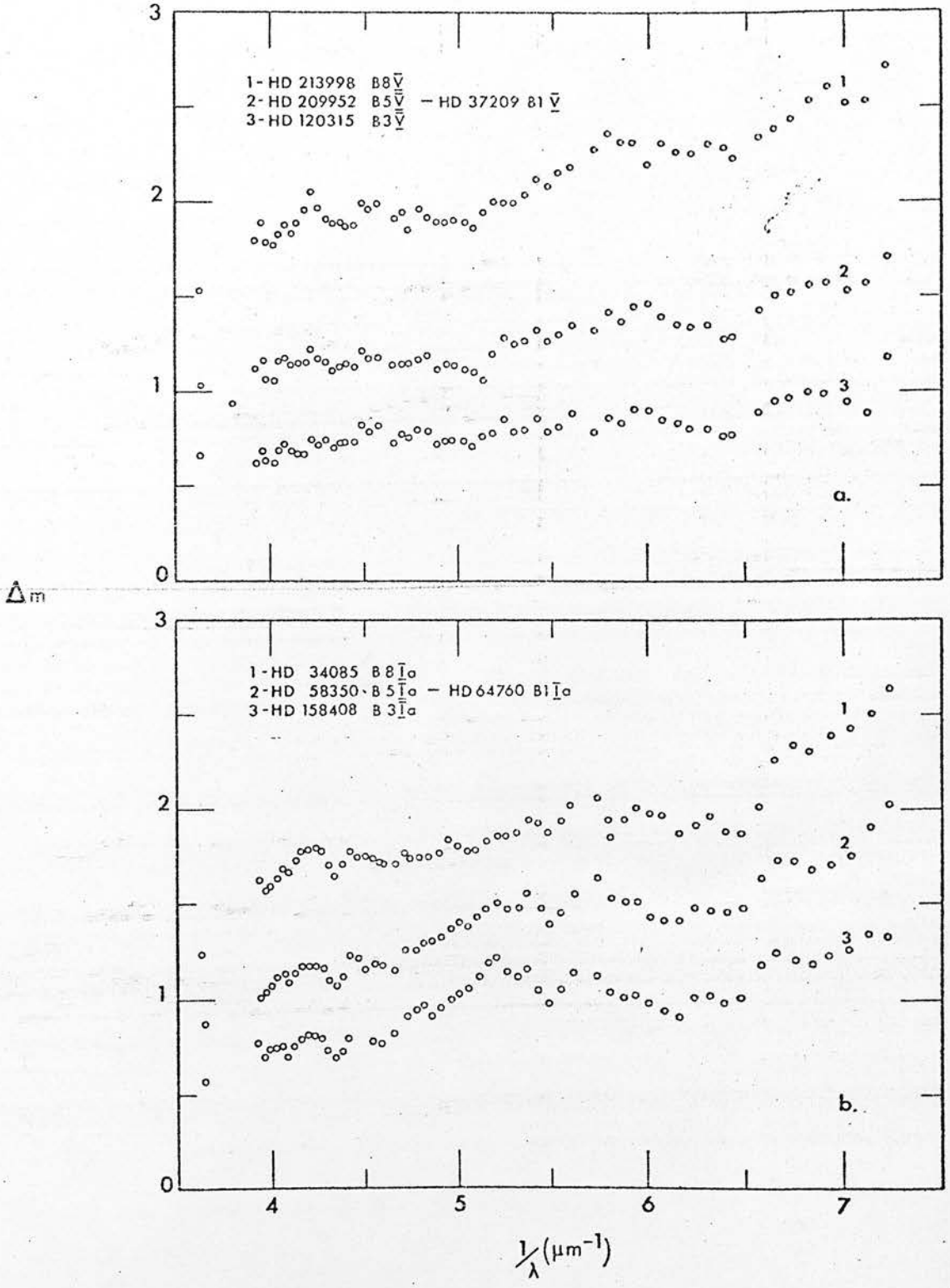

FIG. 3.—Magnitude differences Δm_λ obtained by comparing ultraviolet flux distributions of (*a*) main-sequence stars with HD 37209 (B1 V), (*b*) supergiants with HD 64760 (B1 Ia).

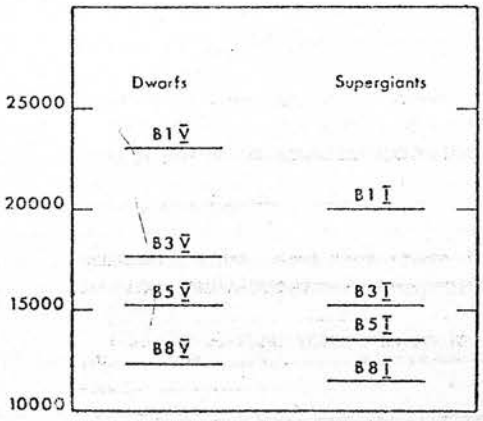

FIG. 4.—Effective temperature scale for supergiants and dwarfs.

Δm curves of figure 2. The results for spectral types B1, B3, B5, and B8 are illustrated in figure 4. Thus, by assuming that the difference in color temperature is the same as the difference in effective temperature between a supergiant and a dwarf, the effective temperature of a B1 supergiant is found to be approximately 3000° K cooler than that of a B1 main-sequence star; for type B5, the effective temperature of the supergiant is found to be approximately 1700° K cooler than that of the main-sequence star. As a further test, a comparison of the normalized energy distributions of o^2 CMa (B3 Ia) and α Gru (B5 V) shows that the slope of the Δm_λ versus $1/\lambda$ curve is close to zero, indicating that these stars have similar effective temperatures.

The interpretation that luminous stars have lower effective temperatures than main-sequence stars is highly plausible in terms of a simple physical picture and is not new. For example, Stalio (1971) reached the same conclusion by considering the experimentally determined Balmer jumps for supergiants and comparing these with model atmosphere data. The temperature scale derived by Stalio for B-type supergiants fits closely with that given here.

Although the present sample contains only a few B-type giants, it appears from their normalized ultraviolet flux distributions (cf. fig. 1) that they have effective temperatures which are intermediate between those of the corresponding supergiants and main-sequence stars, and that these lie somewhat closer to the main-sequence temperatures than to the supergiant temperatures.

For the A-type stars shown in figures 1 and 2 the observed fluxes longward of 1800 Å are consistent with the interpretation given above. At shorter wavelengths this trend reverses, and the luminous stars apparently become brighter relative to the main-sequence stars. However, since our observations here are limited to the spectra of only two A-type luminous and main-sequence pairs, it is not yet possible to decide whether the observed effect is a general one. It is not clear, for example, whether the short-wavelength changes in slope of figures 2*i* and 2*j* are caused by the supergiants or by the dwarfs. Underhill (1973) has pointed out that substantial variations are observed between the fluxes of A-type dwarfs shortward of 1800 Å. This has also been noted by Humphries, Nandy, and Thompson (1973) from photometric measurements at 1490 Å.

It is emphasized that the suggestions made here are still based on only a small selection of stars. The sample size could have been increased readily by including stars with significant reddening, and this will be done when the interstellar extinction laws for different galactic regions have been determined accurately. Further observations are particularly required for A-type stars and for B-type giants.

We wish to thank Dr. E. Peytremann of the University of Mons for communicating the results of model atmosphere calculations in advance of publication.

REFERENCES

Barbier, D. 1952, *Ann. d'Ap.*, **15**, 113.
Blanco, V. M., Demers, S., Douglass, G. G., and FitzGerald, M. P. 1968, *Pub. U.S. Naval Obs.*, Vol. 21.
Bless, R. C., and Savage, B. D. 1972, *Ap. J.*, **171**, 293.
Boksenberg, A., Evans, R. G., Fowler, R. G., Gardner, I. S. K., Houziaux, L., Humphries, C. M., Jamar, C., Macau, D., Macau, J. P., Malaise, D., Monfils, A., Nandy, K., Thompson, G. I., Wilson, R., and Wroe, H. 1973, *M.N.R.A.S.*, **163**, 291.
Carruthers, G. R. 1969, *Ap. and Space Sci.*, **5**, 387.
Chalonge, D. 1956, *Ann. d'Ap.*, **19**, 258.
Code, A. D., and Bless, R. C. 1970, *IAU Symposium No. 36*, ed. L. Houziaux and H. E. Butler (Dordrecht: Reidel), p. 173.
Humphries, C. M., Jamar, C., Malaise, D., and Wroe, H. 1974, submitted to *Astr. and Ap.*
Humphries, C. M., Nandy, K., and Thompson, G. I. 1973, *M.N.R.A.S.*, **163**, 1.
Johnson, H. L. 1966, *Ann. Rev. Astr. and Ap.*, 4, 193.
Kurucz, R. L., Peytremann, E., and Avrett, E. H. 1973, *Blanketed Model Atmospheres for Early Type Stars* (Washington: Smithsonian Institution Press).
Laget, M. 1972, *The Scientific Results from the Orbiting Astronomical Observatory* (OAO-2), ed. A. D. Code (NASA SP-310), p. 283.
Mihalas, D. 1970, *Ap. and Space Sci.*, **8**, 50.
Schild, R., Peterson, D. M., and Oke, J. B. 1971, *Ap. J.*, **166**, 95.
Stalio, R. 1971, *Proc. Third Colloquium on Astrophysics*, ed. M. Hack (Trieste), p. 28.
Tarafdar, S. P., and Vardya, M. S. 1973, *M.N.R.A.S.*, **163**, 35P.
Thompson, G. I., Humphries, C. M., and Nandy, K. 1974, *Ap. J. (Letters)*, **187**, L81.
Underhill, A. B. 1973, *IAU Colloquium on Stellar Chromospheres*, ed. S. D. Jordan and E. H. Avrett (NASA SP-317), p. 128.
Underhill, A. B., Leckrone, D. S., and West, D. K. 1972, *Ap. J.*, **171**, 63.
Weber, S. V., Henry, R. C., and Carruthers, G. R. 1971, *Ap. J.*, **166**, 543.

C. M. HUMPHRIES and K. NANDY: Royal Observatory, Edinburgh EH9 3HJ, Scotland

E. KONTIZAS: National Observatory of Athens, Thission, Athens 306, Greece

THE EFFECTIVE TEMPERATURE OF EARLY TYPE STARS

K. Nandy and E. Kontizas

Royal Observatory, Edinburgh, U.K.

Presented by K. Nandy

ЭФФЕКТИВНАЯ ТЕМПЕРАТУРА ЗВЕЗД РАННИХ ТИПОВ

Introduction. In an earlier paper (Nandy and Schmidt, 1975) it has been shown that by the combination of models and the observed spectral distributions from the visible to the far ultraviolet, a temperature scale of B and early A type stars can be derived. During recent years the ultraviolet flux distributions on an absolute scale have been obtained for a considerable number of stars with the sky survey telescope (S2/68) on board the ESRO satellite TD1. The experiment gives spectra at a resolution of 30Å over the wavelength range from 1350Å to 2500Å, and a broad band measurement centred at 2740Å (Boksenberg et al. 1973). We have also started a program of obtaining spectrophotometric observations in the visible wavelength range of a selected number of stars for which ultraviolet data are available. This would give the wavelength coverage of the spectral data from the visible to the far ultraviolet. In this note we shall present the results for 34 stars in the spectral range from B0 to A2.

Observations and reductions. Spectrophotometric observations in the visible wavelength range (6000Å - 3400Å) were obtained with a photoelectric scanner at the Cassegrain focus of the 100-cm reflector of Kavalur Observatory, Indian Institute of Astrophysics, India. The observations were made between 3400Å and 5000Å in the second order and between 6000Å and 4500Å in the first order. The spectra were scanned with a slit of 50Å width. Ultraviolet data are taken from the spectra obtained with the sky survey telescope in the TD1 satellite. In order to achieve greater photometric accuracy the magnitudes at several wavelengths (2500Å, 2460Å, 2260Å, 2190Å, 2050Å, 1860Å, 1660Å, 1490Å and 1390Å) are derived from consecutive spectral data points. These magnitudes have an effective passband of 100Å. The mean photometric error of the ultraviolet magnitudes obtained in this way is ±0.04 for stars brighter than V = 5.0 rising to ±0.12 for fainter stars.

The sample of stars studied here contains reddened and unreddened dwarfs and supergiants. The spectral distributions of the reddened stars have been corrected for interstellar reddening, using the mean extinction law derived from the TD1 data. The mean value of total extinction per unit visual colour excess, $A(\lambda)\ E_{B-V}$ has been derived by combining all the available ground based and ultraviolet data (Nandy et al. 1975). To illustrate, we have shown in Figure 1 the observed colour $(m_\lambda - V)$ for Per (HD 24398, B1I_b, $E_{B-V} = 0.35$) by filled circles and the $(m_\lambda - V)_o$ corrected for reddening by open circles.

Results. For the comparison of the observed spectral distributions of the stars (corrected for reddening) with those from model atmosphere,

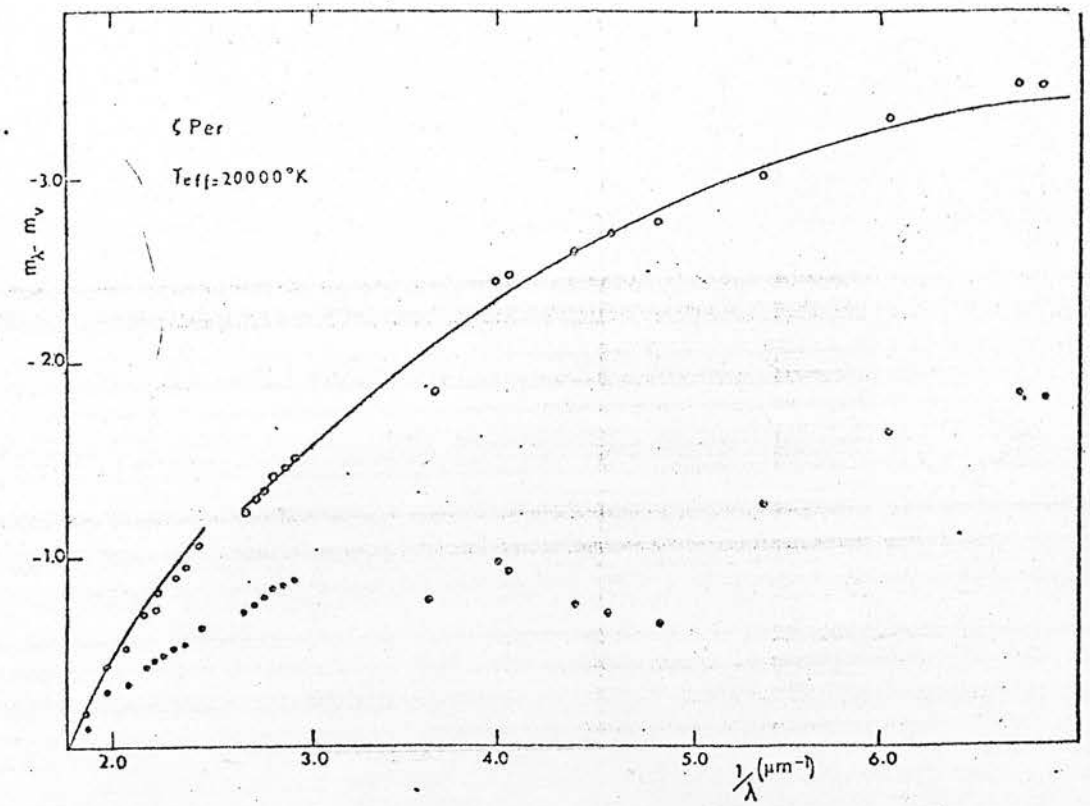

Fig. 1. The observed $(m_\lambda - V)$ plotted against $\frac{1}{\lambda}(\mu m^{-1})$ for Per (UD 24398) is shown by filled circles; the corrected $(m_\lambda - V)$ is denoted by open circles. The model computations are indicated by solid line.

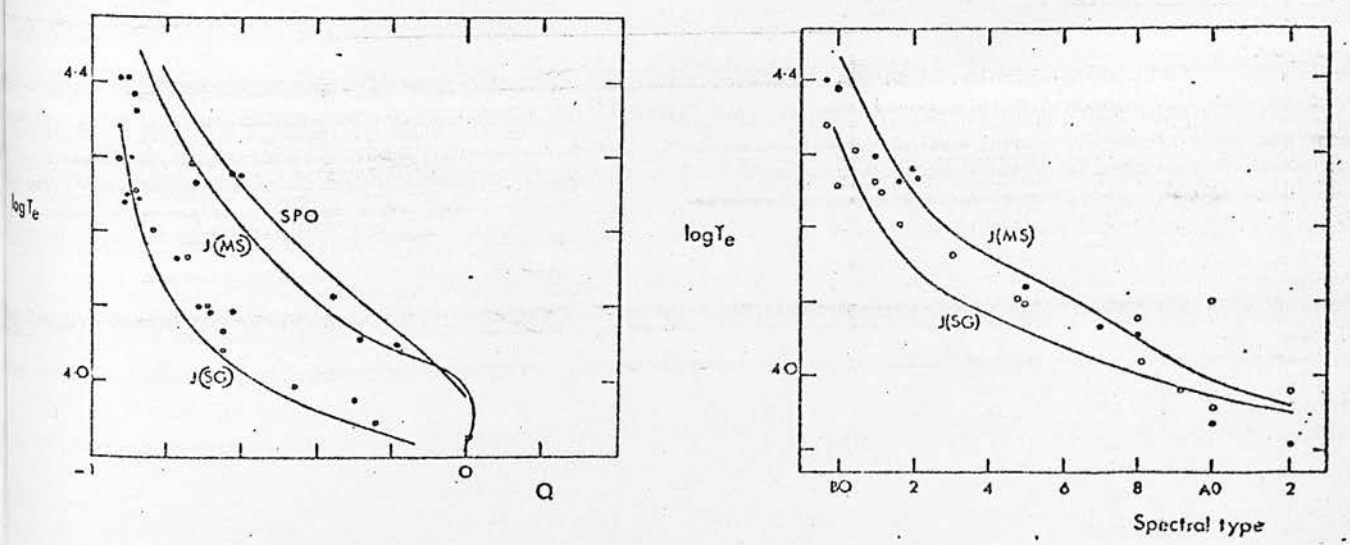

Fig. 2.

a) log Te vs Q
b) log Te vs MK spectral type

Open circle are supergiants and filled circles are main sequence stars.

we have constructed a series of model atmospheres, using the model atmosphere program ATLAS (Kurucz 1970, 1973). The version used allows the inclusion of line opacity through the use of distribution functions based on about 750 000 spectral lines (Kurucz, Paytremann and Avrett, 1972). The effect of line blanketing and the effects of variations in the gravity have been discussed by Nandy and Schmidt (1975). For hotter models the chief effect of line blanketing appears in the form of an increase in the continuum flux from about 5 per cent at 6000Å to about 15 per cent in the ultraviolet around 1500Å. The effect of gravity on the flux distributions is relatively small compared with the effect of temperature changes. Therefore, for B- and early A-type stars the value of log g need not be known with great accuracy. For supergiants we used log g = 2, and 4 for main sequence stars. The temperature is established by fitting the computed $(m_\lambda - V)$ from the models with the observed spectral distributions (as shown in Figure 1 by the solid curve). In Figure 2 we have plotted the effective temperature of the stars studied here, as determined by this method, against MK spectral type and against the parameter Q $(U - B) - 0.72\,(B - V)$. The temperature scales derived by Johnson (1966) and by Schild, Peterson and Oke (1971) are also shown in Figure 2. It can be seen that the supergiants are separated from the main sequence stars in the log Te vs Q plot. For early B stars the supergiants are cooler than the main sequence stars of the same spectral type but become hotter near B8.

Details of these results will be presented elsewhere.

Acknowledgement. We should like to thank Prof. M.K.V. Bappu for granting us time on the tèlescope of Kavalur Observatory, and Mr. Rajmohon and Parth Sarathi for their assistance.

References

Boksenberg, A., Evans, R.G., Fowler, R.G., Gardener, I.S.K., Houziaux, L., Humphries, C., Jamar, C., Macau, D., Malaise, D., Monfils, A., Nandy, K., Thompson, G.I., Wilson, R., Wroe, H., 1973, Mon. Not. R. astr. Soc. 163, 291.

Johnson, H.L., 1066, Ann. Rev. Ast. and Astrophys., 4, 193.

Kurucz, R.L., 1970, Smithsonian Astrophys. Obs. Special Report 309
1973a, Centre for Astrophysics Preprint No. 15
1973b, Centre for Astrophysics Preprint No. 29.

Kurucz, R.L., Paytremann, E., Avrett, E.H., 1972, Blanketed Model Atmospheres for Early Type Stars (Washington D.C., Smithsonian Inst. Press)

Nandy, K. and Schmidt, E.G., 1975, Astrophys. J., 198, 119.

Nandy, K., Thompson, G.I., Jamar, C., Monfils, A., Wilson, R., 1975, in press in Astronomy and Astrophysics.

Schild, R., Peterson, D.M., Oke, J.B., 1971, Astrophys. J., 166, 95.

THE OBSERVATORY

A REVIEW OF ASTRONOMY

EDITED BY

R. F. GRIFFIN S. J. BURNELL

D. H. P. JONES P. J. ANDREWS

Vol. 96 No. 1012

1976 JUNE

Price £1

premaximum spectra and to analyze the relative strengths of the various emission features in different spectral lines.

The President. Thank you, Dr. Andrews. I'll ask Dr. Smyth of ROE also to talk on the optical spectrum of the nova, and then we'll have a few questions on this aspect.

Dr. M. J. Smyth. These are spectrophotometric measurements of Nova Cygni made by Mr. and Mrs. Kontizas of the Observatory of Athens, who are now research students in the Department of Astronomy at Edinburgh. We have developed at Edinburgh a simple photoelectric spectrum scanner which they were using this summer on the 25-inch Newall refractor (formerly of Cambridge Observatories) at the Penteli station near Athens. The nova was "discovered", as far as Athens was concerned, by Professor Plakidis, a Fellow of this Society, who at the age of 84 may well claim to be its most senior discoverer. The spectral scans between 4000 and 7000 ångströms were made with the low resolution of fifty ångströms that was being used at the time for studies of reddened early-type stars; with hindsight, a higher resolution could have been used. An unusual feature of the spectrum scanner is the use of a small fraction of the undispersed starlight to provide a reference beam for compensating changes in atmospheric transparency and seeing during a long scan. Equal-altitude ratio spectra, that is the ratio of the main, spectrum-scanning, beam to the reference beam, of α Lyrae were obtained on the same nights as the nova. Since the reference beam measures practically the *B* flux of the star, at each wavelength the ratio spectrum gives the ratio of monochromatic flux to *B* flux; hence by using the known *B* magnitude difference between star and nova we can obtain the ratio spectrum of nova to α Lyrae continuum. Such nova/α Lyrae spectra show a rather featureless spectrum at maximum, with weak P Cygni profiles for $H\alpha$ and $H\beta$, and then strongly developed broad emission lines on successive nights. Rapid spectral variations on a time-scale of hours, as reported elsewhere, were noticed. Using the known absolute spectral distribution for α Lyrae we can finally derive absolute fluxes of Nova Cygni over the range 4000 to 7000 ångströms.

The President. We must congratulate the optical astronomers on these fine spectra. We have time for one or two questions.

Professor Seaton. Is it a recurrent nova?

Dr. Andrews. No, certainly not. It has been hypothesized that this is a virgin nova. One could argue that all novae are recurrent novae, but this is the first known outburst of this one.

Professor Seaton. I notice that the forbidden *Fe* X line is observed. This implies the presence of hot (about 10^6 degrees) gas. For recurrent novae hot gas may be produced by interaction between ejected gas and ambient gas from a previous outburst.

The President. We must continue with the papers so as to leave a little time at the end for discussion. The next paper is by Patricia Whitelock on infrared observations of the nova.

Dr. P. A. Whitelock. The observations I am going to describe are primarily the results of broad-band photometry between the visual and twelve microns. The nova light curves show that the 2·2 micron peak lags about half a day behind the optical peak; also obvious is the very much slower intensity decline at longer wavelengths. In fifteen days the optical intensity decreases by five magnitudes, while that at ten microns drops only three magnitudes.

THE OBSERVATORY

A REVIEW OF ASTRONOMY

EDITED BY

R. F. GRIFFIN S. J. BURNELL

D. H. P. JONES P. J. ANDREWS

Vol. 96 No. 1013

1976 AUGUST

Price £1

orientations of the orbit were equally likely, the probability of eclipses would be just 12/124, *i.e.* about 10 per cent; but the above argument which suggests that $\sin i \sim 1$ implies that the probability of eclipses is substantially greater than that. It would accordingly be worth while for photometric observers to watch for eclipses at the proper times, as well as to measure the ultraviolet colour of the system in an effort to refine the estimates of the spectral types of the components. Eclipses, if they occur, should last up to $3\frac{1}{2}$ days; primary eclipses should have depths of about $0^{m}{\cdot}2$ in V, $0^{m}{\cdot}5$ in B and $0^{m}{\cdot}9$ in U. Our orbital elements allow the times of possible eclipses to be predicted with an error which is little more than one day at the end of this century.

Since the expected radius of the Ko III star is nearly a tenth of the orbital separation of the components, there might well be some interaction between the two stars. HD 200428/9 may prove to be a rewarding object, therefore, for spectroscopic as well as photometric observers.

References

(1) A. J. Cannon & W. H. Pickering, *Ann. H. C. O.*, 98, 245, 1923.
(2) A. Beer, R. O. Redman & G. G. Yates, *Mem. R.A.S.*, 67, 1, 1954.
(3) R. F. Griffin, *M.N.*, 155, 1, 1971.
(4) C. W. Allen, *Astrophysical Quantities*, third edition (Athlone, London), 1973, p. 206.
(5) D. J. Stickland, *M.N.*, 175, 473, 1976.
(6) C. W. Allen, *Astrophysical Quantities*, first edition (Athlone, London), 1955, pp. 177 and 183.
(7) L. B. Lucy & M. A. Sweeney, *A.J.*, 76, 544, 1971.
(8) G. A. Radford & R. F. Griffin, *The Observatory*, 95, 187 and 289, 1975; 96, 98, 1976.
(9) C. W. Allen[4], p. 209.
(10) O. C. Wilson, in *Modern Astrophysics, A Memorial to Otto Struve*, (ed. M. Hack) (Gauthier-Villars, Paris), 1967, p. 241.
(11) R. Mäckle, H. Holweger, R. Griffin & R. Griffin, *A. & A.*, 38, 239, 1975.

NOTES FROM OBSERVATORIES

Spectrographic Determination of the Chromatic Curve of a Refracting Telescope

By D. Papathanasoglou and J. Deligiannis
Department of Astronomy, University of Athens
and
E. Kontizas
Department of Astronomy, University of Edinburgh

This paper describes a method of determining the chromatic curve of a refracting telescope. It has the advantage that it can be applied easily with simple equipment to cover a wide range of the spectrum. The principle of the process is the following:

In front of the objective is placed a diaphragm, having a hole at a distance l from the optical axis (Fig. 1). The telescope is pointed at an extended source with a sharp edge (*e.g.* the Sun or the Moon). The image is arranged to fall on part of the length of a spectrograph slit, the limb crossing the slit perpendicularly near the mid-point.

The side of the spectrum which corresponds to the limb is curved (Fig. 2).

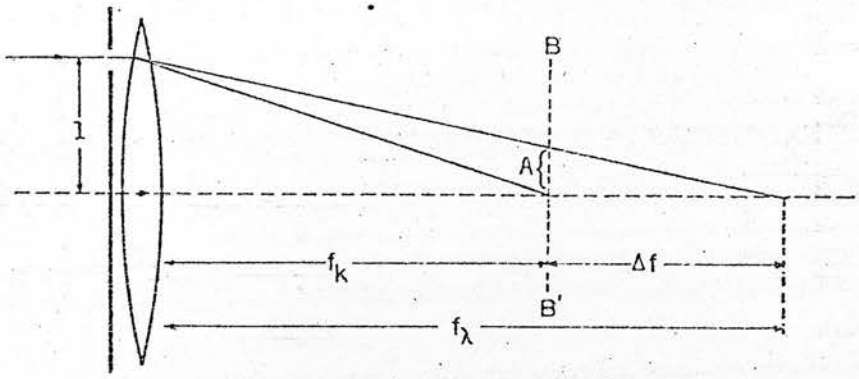

FIG. 1
Idealized Telescope

From this curve, which is hardly affected by the seeing, we can derive the chromatic curve as follows:

If f_k is the known focal length for a certain wavelength ($\lambda = k$) and $\Delta f = f_k - f_\lambda$, where f_λ is the focal length at wavelength λ, then:

$$\Delta f = af_k/(l-a)$$

where $a = A/M$, M is the magnification of the spectrograph perpendicular to the dispersion and A the measured value on the photographic plate as shown in Fig. 2.

An analogous method has been applied by Hartmann[1], who used extrafocal star spectra.

The above process has been applied to the Newall telescope ($D = 63$ cm, $F = 885$ cm), which was installed at Pentele Observatory, near Athens, in 1957, having been presented by Cambridge University. The diaphragm had a 7 cm diameter hole and $l = 21{\cdot}5$ cm. Two different spectrographs have been used and have given identical results, the first one with a grating[2] (modified) and the other with a direct-vision prism.

We also applied the same method using a correcting lens for this objective[3]. Both chromatic curves are presented in Fig. 3.

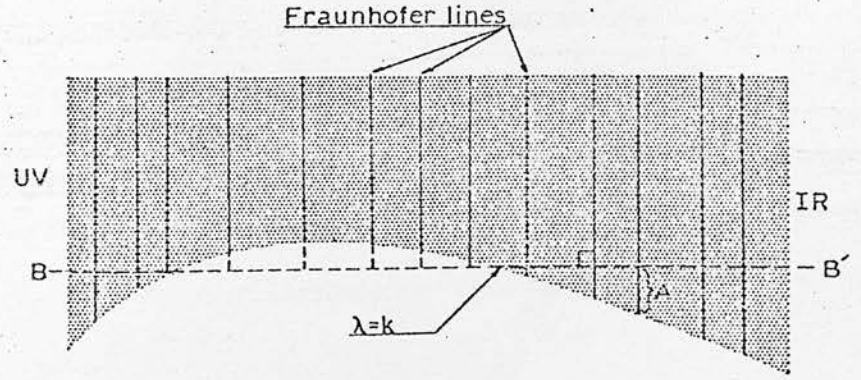

FIG. 2
The Spectrum

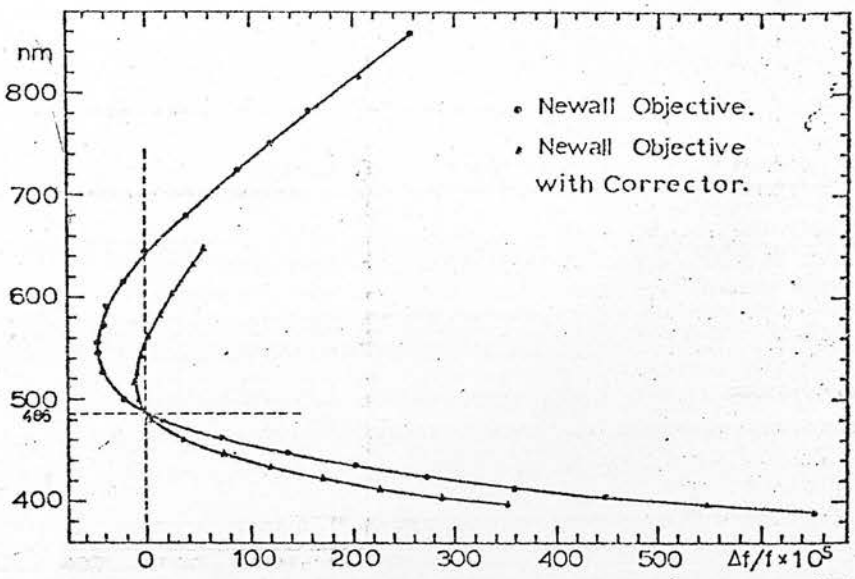

FIG. 3
Colour curves

References

(1) J. Hartmann, *Publ. Astrophys. Obs. Potsdam*, 15 (2), 1908.
(2) E. Kontizas and M. J. Smyth, to be published.
(3) H. F. Newall, *M.N.*, 56, 98, 1896.

HZ 43 AS A VISUAL BINARY

By Karl W. Kamper
David Dunlap Observatory

The white dwarf HZ 43, located at $13^h\ 14^m\ 0^s{\cdot}8$, $+29°\ 21'\ 50''$ (equator and epoch 1950·0), has been suggested as the optical counterpart to the X-ray source MX 1313+29, first observed with SAS-3[1]. A trigonometric parallax for this star was measured by the present author while at the Allegheny Observatory[2]. The value obtained, when corrected to absolute, is $+0''{\cdot}024 \pm 0''{\cdot}016$ (s.e.), which is only sufficiently precise to indicate that the star is no fainter than expected for a hot white dwarf. HZ 43 does, however, have a nearby red companion, which might be used to provide another distance estimate. That this companion is definitely physical is shown by our previously unpublished measures given in the Table, since the joint proper motion of the pair is $-0''{\cdot}14$/yr in α and $-0''{\cdot}10$/yr in δ. Orbital motion, as indicated by these measures, is very slow, as would be expected with a projected separation of 100 A.U. Nevertheless, if the discovery position angle, given by Luyten[3] as 280°, is accurate, there has been a slow decrease in angle.

Mon. Not. R. astr. Soc. (1976) 176, *Short Communication*, 79P–83P.

ABSOLUTE SPECTROPHOTOMETRY OF NOVA CYGNI 1975

E. Kontizas, M. Kontizas and M. J. Smyth

University of Edinburgh, Department of Astronomy, Royal Observatory, Edinburgh EH9 3HJ

(Received 1976 March 23)

SUMMARY

Ratiometric photoelectric spectrophotometry of Nova Cygni 1975 was carried out on 1975 August 31, September 2, 3. α Lyr was used as reference star and its abolute spectral energy distribution was used to reduce the spectrophotometry of the nova to absolute units. Emission strengths of Hα, Hβ, Hγ (in W cm^{-2}) were derived. The Balmer decrement Hα:Hβ:Hγ was compared with theory, and found to deviate less than had been reported for an earlier nova.

1. INTRODUCTION

Among the many independent discoverers of Nova Cygni 1975, and perhaps the most senior, was Professor S. Plakidis of the Athens Observatory. A photoelectric spectrum scanner, developed at Edinburgh and then in use on the 0·64-m Newall refractor (Newall 1896) at the Penteli station near Athens, was immediately used to observe the nova very close to maximum, and on two subsequent nights. Low spectral resolution, approximately 50 Å, was being used for continuum studies of reddened early-type stars, and was not changed for observations of the nova.

2. SPECTRAL SCANS

A feature of the spectrum scanner is the use of a small fraction of the undispersed starlight, abstracted behind the entrance aperture, to provide a reference beam for compensating changes in atmospheric transparency and seeing, and guiding errors. The ratio of the main (spectrum-scanning) beam to the reference beam is obtained by a commercial dc ratiometer*. The main and reference photomultipliers are respectively EMI 9558 (S 20 response) and EMI 9781 (S 5 response). A typical scanning speed is 250 Å min^{-1}. The ratiometer arrangement has proved its value (Smyth & Kontizas 1976, in preparation) on nights of doubtful transparency and on a telescope with poor guiding facilities. It does not compensate for errors due to atmospheric dispersion, but such errors are insignificant at the low resolution and small zenith distances involved. It has the added advantage that, since the spectral scan for any star is ratioed to a non-dispersed measure that is in effect a broadband magnitude for that star, the ratio of the spectra of two stars may be obtained provided only that their broadband magnitudes are known. Thus, if the spectral energy distribution of one star is known in absolute units, that of the second is immediately obtained.

For comparison with the nova, spectra of α Lyr were obtained within a time interval of half an hour and a similar small zenith distance (~10°), so that

* Ortec Brookdeal 9547.

differential atmospheric effects should be unimportant. Rapid variations of the nova spectrum, on a time-scale of an hour, were noted; similar spectral variability has been reported by several observers (e.g. *IAU Circ.* 2839), and Marcocci *et al.* (1976) have published *UBVRI* photometry showing variability about three weeks after maximum.

If F_λ refers to monochromatic flux and F_r refers to flux in the undispersed reference channel, then our observations yield immediately F_λ (nova)/F_r (nova) and F_λ (α Lyr)/F_r (α Lyr) over the wavelength range 4170 Å $< \lambda <$ 6754 Å. Measurement of shorter wavelengths was excluded by the use of a refractor with high ultraviolet absorption and a steep focal curve (Papathanasoglou, Deligiannis & Kontizas 1976). F_r (nova) and F_r (α Lyr) are obtained from published broadband photometry; the colour equation (Ref.) = $B-0{\cdot}3$ $(B-V)$ has been applied to allow for the unfiltered S 5 response of the reference photomultiplier. The Balmer lines in the spectrum of α Lyr, the only lines seen at low resolution, have been removed by hand interpolation. Thus we obtain the ratio spectra F_λ (nova)/F_λ (α Lyr). These are shown in Fig. 1, for the three nights 1975 August 30.95, September 1.90, and September 3.00.

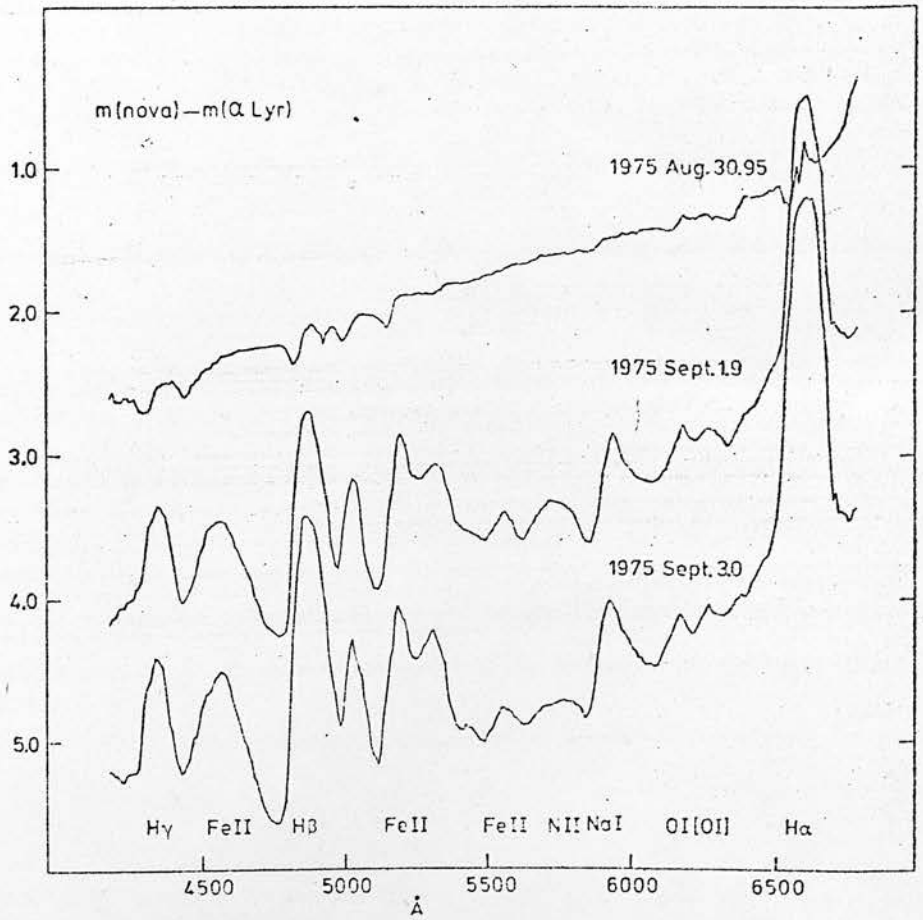

FIG. 1. *Spectra of Nova Cygni* 1975, *relative to the smoothed continuum of* α *Lyr, on three nights.*

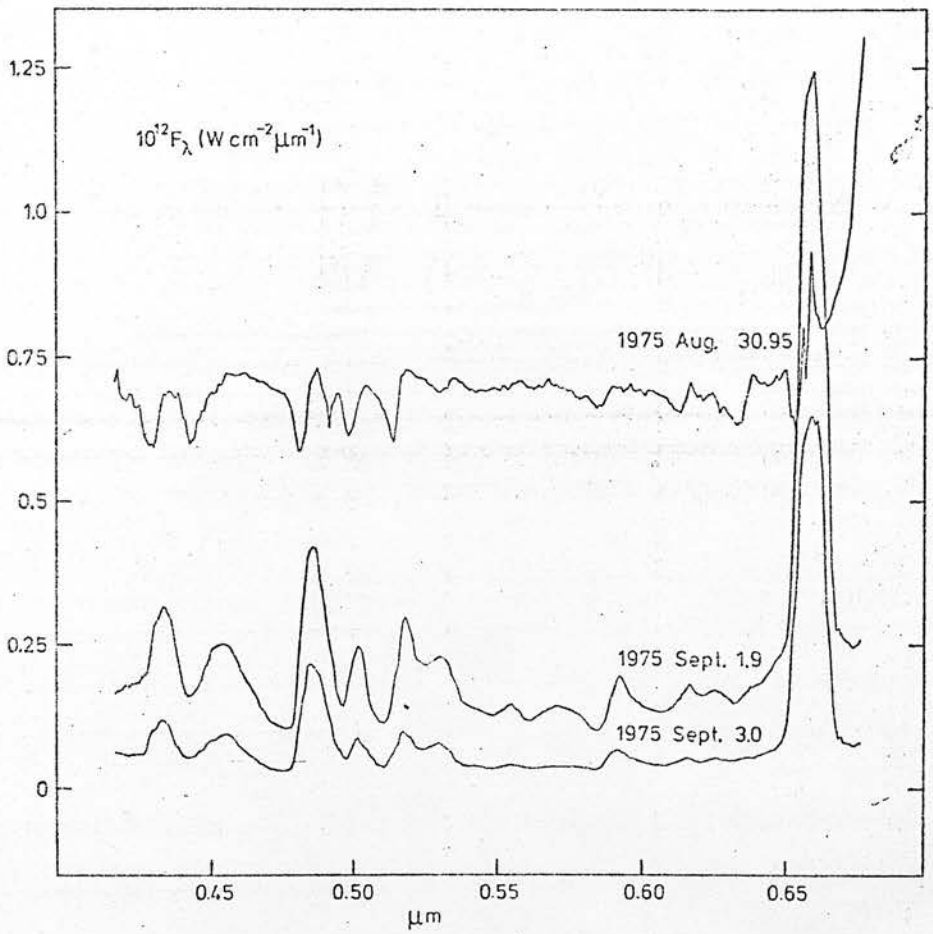

FIG. 2. *Spectral energy distribution of Nova Cygni* 1975 *on three nights.*

On the first night, close to maximum light, the spectrum is relatively featureless, showing broad, weak Balmer lines in emission with violet-shifted absorption components, the characteristic P Cygni profiles. On the two later nights the continuum is progressively weaker, but Hα, Hβ, Hγ, and the NaI D-lines show strong P Cygni profiles, and broad blended lines of Fe II and [O I] appear.

In order to obtain the spectral energy distribution in absolute units, we used the smoothed absolute calibration of α Lyr by Oke & Schild (1970), with polynomial interpolation to fit the plotted wavelengths. The resulting energy distributions in W cm^{-2} μm^{-1} for the nova on the three nights are shown in Fig. 2.

3. BALMER LINE STRENGTHS

The emission strengths (W cm^{-2}) of Hα, Hβ, and Hγ on the second and third nights were measured from Fig. 2 and are given in Table I. The principal uncertainty is in drawing the continuum from which the strengths are measured, and may amount to 10 per cent, or 0·04 in the logarithm. In drawing the continuum we have attempted to allow for the blending effect of nearby Fe II lines.

TABLE I

Observed emission strengths

	(W cm^{-2}) log F(Hα)	log F(Hβ)	log F(Hγ)
September 1.9	−13·97	−14·54	−14·89
September 3.0	−14·20	−14·74	−15·30

TABLE II

Hydrogen line ratios

		Theory	Observed	De-reddened $A_V = 1$	$A_V = 1{\cdot}5$	$A_V = 2$
log (Hα/Hβ)	Sept. 1.9	0·46	0·57	0·46	0·40	0·34
	Sept. 3.0	0·46	0·55	0·43	0·37	0·32
log (Hβ/Hγ)	Sept. 1.9	0·33	0·34	0·29	0·26	0·24
	Sept. 3.0	0·33	0·56	0·50	0·47	0·45

From these strengths the 'observed' ratios given in Table II are obtained. Values of the Balmer decrement are sensitive to interstellar reddening, and Table II contains also values of the ratios corrected for interstellar absorption $A_V = 1$, 1·5, and 2, assuming a wavelength dependence λ^{-1}. de Vaucouleurs has suggested in *IAU Circ.* 2839 an extinction of $A_V = 1{\cdot}45 \pm 0{\cdot}3$. The column headed 'theory' is a mean of values, derived from Brocklehurst (1971), which vary by no more than 0·04 in the logarithm over a wide range of temperatures and pressures. The de-reddened values for Hα/Hβ are in close accord with theory, but the value of Hβ/Hγ on the third night appears anomalously high. Brocklehurst finds good agreement between his theory and photoelectric observations for planetary nebulae, but Bahng (1972) finds a much smaller Balmer decrement, e.g. values of log (Hα/Hβ) between 0·23 and 0·20, for Nova Cephei 1971 about a month after maximum.

4. CONCLUSION

The use of a ratiometric spectrum scanner and of a reference star with a well-determined spectral energy distribution has enabled us to display the spectrum of Nova Cygni 1975, on three nights at and shortly after maximum, on an absolute energy scale. After allowance for interstellar reddening the Balmer emission line ratios are, with one exception, in good agreement with theory. Published scanner observations of novae include those for Nova Aquilae 1970 (Grenfell 1971), which show continuum points only; and those for Nova Serpentis 1970 (Wagner *et al.* 1971), which are given in relative energy units and do not include line strength measurements. Thus the only comparable measurements of the Balmer emission line ratios are those of Nova Cephei 1971 about a month after maximum, when Bahng (1972) found strong departure from theory; and of Nova Persei 1974, when Weiler & Bahng (1976) found Hα/Hβ near the theoretical value but a very low value of Hβ/Hγ.

After this paper had been submitted, photoelectric spectral scans by Tomkin, Woodman & Lambert (1976) appeared; their higher resolution should assist in the elimination of the effect of blending, but the spectra are not on an absolute scale and the Balmer line ratios cannot be directly determined.

ACKNOWLEDGMENTS

We are grateful to Professor S. Plakidis for notifying us of the new object and thus enabling us to obtain spectra near maximum. We thank Professor G. Contopoulos, Director of the National Observatory of Athens, for use of the Newall refractor, and Professor R. H. Stoy for help in the interpretation of the nova spectra.

REFERENCES

Bahng, J. D. R., 1972. *Mon. Not. R. astr. Soc.*, 158, 151.
Brocklehurst, M., 1971. *Mon. Not. R. astr. Soc.*, 153, 471.
Grenfell, T. C., 1971. *Publ. astr. Soc. Pacific*, 83, 66.
Marcocci, M., Messi, R., Natali, G. & Rossi, L., 1976. *Nature*, 259, 186.
Newall, H. F., 1896. *Mon. Not. R. astr. Soc.*, 56, 98.
Oke, J. B. & Schild, R. E., 1970. *Astrophys. J.*, 161, 1015.
Papathanasoglou, D., Deligiannis, J. & Kontizas, E., 1976. In press.
Tomkin, J., Woodman, J. & Lambert, D. L., 1976. *Astr. Astrophys.*, 48, 319.
Wagner, R. L., Tull, R. G., Byrd, G. G. & Loren, R. B., 1971. *Astrophys. J.*, 165, 431.
Weiler, E. J. & Bahng, J. D., 1976. *Mon. Not. R. astr. Soc.*, 174, 563.

ACKNOWLEDGEMENTS

I owe the credit for this thesis to both of my supervisors Dr. K. Nandy and Dr. M. Smyth whose inspiration and encouragement have guided me over the past three years. I am deeply grateful to Professor V.C. Reddish for helping and providing the necessary facilities for the completion of my project. I wish to thank also Professor H. Bruck for accepting me at Edinburgh University as a research student and for his help during the first two years of my studies. I would like to thank Dr. C. Humphries with whom I had useful discussions concerning the subject matter presented here and Dr. D. Morgan for the interest he has shown in my work. Dr. Nandy and I would like to thank Professor M.K.V. Bappu for granting time on the telescope of Kavalur Observatory. My thanks are also due to the workshop of the Royal Observatory of Edinburgh for doing the necessary mechanical work for the constructed spectrum scanner. I am indebted to the staff of the Royal Observatory of Edinburgh and Department of Astronomy for being so kind and helpful during my stay at Edinburgh.

Last, but by no means least, I wish to thank the Greeks, Professor D. Kotsakis, Professor G. Contopoulos, Professor M. Moutsoulas, Professor G. Banos and Dr. C. Banos whose encouragement and help have influenced my progress.

REFERENCES

Adams, T.F. & Morton, D.C., 1968. Astrophys. J., 152, 195.

Abt, H.M. & Hunter, J.H., 1962. Astrophys. J., 136, 381.

Alexander, D.R., 1975. Astrophys. J. Suppl. 29, 363.

Allen, C.W., 1963. "Astrophysical quantities", 2nd edn., Athlone Press, London.

Aller, L.H., 1963. The Atmospheres of the Sun and Stars: Ronald Press Co., New York.

Avrett, E.H. & Krook, M., 1963. Astrophys. J., 137, 874.

Auer, L.H. & Mihalas, D., 1968a. Astrophys. J., 151, 311.

" " " " " 1968b. " " 156, 157.

" " " " " 1968c. " " 156, 687.

" " " " " 1969. " " 158, 641.

" " " " " 1970. " " 196, 233.

" " " " " 1972. " " Suppl.24, 193.

Bahng, J.D.R., 1971. Publ. astr. Soc. Pacific,83, 327.

Barbier, D., 1952. Ann. Astrophys. No. 2, 15, 113.

Bascheck, B., 1975. Problems in Stellar Atmospheres and Envelopes, Ed. B. Bascheck, W.H. Kegel, G. Traving, Springer-Verlag, Berlin - Heidelberg - New York, p. 21.

Bates, B. 1975. Irish Astron. J., 12, 49.

Becker, W., 1966. Z. Astrophys., 64, 77.

Beeckmans, F., 1975. Astr. Astrophys., 45, 177.

Blanco, V.M., Demers, S., Douglass, G.G. & Fitzgerald, M.P., 1968. Publ. U.S. Naval Obs., 21.

Bless, R.C., Code, A.D. & Houk, T.E., 1968. Astrophys. J., 153, 561.

Bless, R.C. & Savage, B.D., 1972. Astrophys. J., 171, 293.

Bohlin, R.C. & Strongylis, J.G., 1976. Preprint presented at the XVI General Assembly of the I.A.U., Grenoble, France.

Bohm-Vitense, E., 1964. Smithsonian Astrophys. Obs. Sp. Rep., 167, 99.

Bohm-Vitense, E., 1975. Problems in Stellar Atmospheres and Envelopes, Ed. B. Bascheck, W.H. Kegel & G. Traving, Springer-Verlag, Berlin - Heidelberg - New York, p. 21.

Boggess, A. & Borgman, J., 1964. Astrophys. J., 140, 1636.

Boileau, A.R. & Miller, F.D., 1967. Applied Opt., 6, 1179.

Boksenberg, A., Evans, R.G., Fowler, R.G., Gardener, I.S.K., Houziaux, L., Humphries, C.M., Jamar, C., Macau, D., Malaise, D., Monfils, A., Nandy, K., Thompson, G.I., Wilson, R. & Wroe, H., 1973. Mon. Not. R. astr. Soc., 163, 291.

Bradley, P.T. & Morton, D.C., 1969. Astrophys. J., 156, 687.

Breger, M., 1976. Astrophys. J. Suppl. 32, 1.

Carbor, D.F. & Gingerich, O., 1969. Theory and Observation of Normal Stellar Atmospheres, Ed. Owen Gingerich, M.I.T. Press, p. 377.

Carruthers, G.R., 1969. Astrophys. Space Sci., 5, 387.

Carruthers, G.R., 1971. Astrophys. Space Sci., 14, 333.

Cayrel, R., 1969. Theory and Observations of Normal Stellar Atmospheres, Ed. Owen Gingerich, M.I.T. Press, p. 237.

Chalonge, D. & Divan, L., 1952. Ann. Astrophys., 15, 201.

Chalonge, D., 1956. Ann. Astrophys., 19, 258.

Code, A.D. & Liller, W.C., 1962. Stars and Stellar Systems, Vol. II, 281.

Code, A.D., Houck, T.E., McNall, J.F., Bless, R.C. & Lillie, C.F., 1970a. Astrophys. J., 161, 377.

Code, A.D. & Bless, R.C., 1970b. Ultraviolet Stellar Spectra and related ground based observations, I.A.U. Symposium

No. 36, Ed. Houziaux, L. & Butler, H.E., Dordrecht Reidel Holland, p. 173.

Code, A.D., 1974. Wisconsin Astrophys. No. 6.

Code, A.D. & Meade, M.R., 1976a. Wisconsin Astrophys. No. 30.

Code, A.D., Davis, J., Bless, R.C. & Brown, R.H., 1976b. Astrophys. J., 203, 417.

Collins, G.W. & Harrington, J.D., 1966. Astrophys. J., 146, 152.

Contopoulos, G. & Banos, C., 1976. Sky Telesc., 51, p. 153.

Cowley, C.R., 1970. The Theory of Stellar Spectra: Gordon & Breach Science Publishers, Paris, London, New York.

Cox, A.N., 1965. Stellar Structure, Ed. Aller, L.H. & MacLaughlin, D.B., University of Chicago Press, p. 195.

Davis, J. & Webb, R.J., 1974. Mon. Not. R. astr. Soc. 168, 163.

Dobronravin, P.P. & Nikonov, V.B., 1955. Izvest. Krymsk. Astrophys. Obs. 13, 32.

Dorschner, J., 1974. Astron. Nachr. 295, 147.

van Duinen, R. & Wesselius, P., 1976. Transactions of the I.A.U. Vol. XVIA part 3, p. 214.

EMI Photomultiplier tubes, Brochure ref. P001/fP70.

Flower, D.R., 1968. Planetary Nebulae, I.A.U. Symposium No. 34. Ed. Osterbrock, D. & O'Dell, C., Publ. D. Reidel, Dordrecht, Holland, p. 205.

Friedemann, C., 1973. Astron. Nachr., 294, 257.

Garrison, R.E., 1970. Astron. J., 75, 101.

Gaustad, J.E. & Spitzer, L. Jr., 1961. Astrophys. J., 134, 771.

Geake, J.E. & Wilcock, W.L., 1966. Mon. Not. R. astr. Soc., 116, 561.

Gebbie, H.A. & Twiss, R.Q., 1976. Reports on Progress in Physics, Vol. 29, 729.

Geltman, S., 1962. Astrophys. J., 136, 935.

Golay, M., 1974. Introduction to Astronomical Photometry, Astrophys. & Space Science Library, Vol. 41, Dordrecht Reidel Holland.

Grainger, J.F. & Ring, J., 1963. Mon. Not. R. astr. Soc., 125, 93.

Greeme, H.R., 1967. Astrophys. J., 147, 1092.

Greeme, A.R. & Wing, R.F., 1975. Astrophys. J., 200, 688.

Griem, H.R., 1960. Astrophys. J., 32, 883.

Guerin, P., 1959. Ann. Astrophys., 22, 611.

Gurzadyan, G.A., 1976. Transactions of the I.A.U., Vol. XVIA, part 3, p. 217.

Hanbury Brown, R., Davis, J., Allen, L.R. & Rome, J.M., 1967. Mon. Not. R. astr. Soc., 137, 393.

Hanbury Brown, R., Davis, J., Lake, R.J.W. & Thompson, R.J., 1974. Mon. Not. R. astr. Soc., 167, 475.

Hardie, R.H., 1962. Astronomical Techniques, Ed. Hiltner, W.A., The University of Chicago Press, Chicago-London, p. 178.

Hardorp, J. & Strittmatter, P., 1968. Astrophys. J., 151, 1057.

Haupt, W., Desjardins, R., Martzen, H.M., Rudolph, R., Schlosser, W., Schmidt-Kaler, Th. & Tug, H., 1976. Astron. & Astrophys., 50, 85.

Heintze, J.R.W., 1969. Theory and Observations of Normal Stellar Atmospheres, Ed. Owen Gingerich, M.I.T. Press, p. 265.

Heintze, J.R.W., 1973. Problems of Calibration of Absolute Magnitudes and Temperatures of Stars, Ed. Hauck, B. & Westerlund, B., Dordrecht Reidel Holland.

Henry, R.J.W., 1970. Astrophys. J., 161, 1153.

Henry, R.C., Western, A., Fedman, P.D., Fastie, W.G. & Moos, H.W., 1975. Astrophys. J., 201, 613.

Hickok, F.R. & Morton, D.C., 1968. Astrophys. J., 152, 203.

Higginbotham, N.A., 1974. Publ. astr. Soc. Pacific, 86, 272.

Hidalgo, M.B., 1968. Astrophys. J., 153, 981.

Hill, P.W., Kilkenny, D. & van Breda, I.G., 1974. Mon. Not. R. astr. Soc., 168, 451.

Hobbs, R.W., Harris, G.D. & Epstein, G., 1972. Publ. astr. Soc. Pacific, 84, 74.

Honeycutt, R.K., 1971. Applied Optics, 10, 1125.

Houziaux, L. & Butler, H.E. (Ed.), 1970. Ultraviolet Stellar Spectra and Related Ground Based Observations, I.A.U. Symposium No. 36, Dordrecht Reidel, Holland.

Humphries, C.M., Nandy, K. & Thompson, G.I., 1973. Mon. Not. R. astr. Soc., 163, 1.

Humphries, C.M., Nandy, K. & Kontizas, E., 1975. Astrophys. J., 195, 111.

Humphries, C.M., Jamar, C., Malaise, D. & Wroe, H., 1976. Astron. Astrophys., 49, 389.

Hyland, A.R., 1969. Theory and Observations of Normal Stellar Atmospheres, Owen Gingerich, M.I.T. Press, p. 271.

Jamar, C., Macau-Hercot, D., Monfils, A., Thompson, G.I., Houziaux, L. & Wilson, R., 1976. Ultraviolet Bright Star Photometric Catalogue.

James, J.F. & Sternberg, R.S., 1968. The Design of Optical Spectrometers, Chapman & Hall Ltd., London.

Jenkins, E.B. & Savage, B.D., 1974. Astrophys. J., 187, 243.

John, T.L., 1968. Mon. Not. R. astr. Soc., 138, 137.

John, T.L. & Williams, R.J., 1976. Mon. Not. R. astr. Soc., 174, 253.

Johnson, H.L., 1966. A. Rev. Astron. Astrophys., 4, 193.

Johnson, H.L., 1965. Astrophys. J., 141, 923.

Johnson, H.L., Mitchell, R.I., Iriarte, B. & Wisniewski, W.Z., 1966. Comm. lunar planet. Lab., 4, 99.

Johnson, H.L., 1968. Stars and Stellar Systems, Vol. VII, 167.

Kalcofen, W. & Strom, S.E., 1966. J. Quant. Spectrosc.

Radiat. Trans., 6, 653.

Kalcofen, W., 1968. Astrophys. J., 151, 317.

Kalcofen, W., 1969. Theory and Observations of Normal Stellar Atmospheres, Ed. Owen Gingerich, M.I.T. Press, p. 225.

Kaplan, S.A. & Pikelner, S.B., 1970. The Interstellar Medium, Harvard University Press.

Klinglesmith, D.A., 1971. Hydrogen line Blanketed Model Stellar Atmospheres, NASA Sp. R., 3065.

Kontizas, E., Kontizas, M. & Smyth, M.J., 1976. Mon. Not. R. astr. Soc., 176, 79p.

Kudritzki, R.P., 1973. Astron. Astrophys., 28, 103.

Kudritzki, R.P., 1976. Astron. Astrophys., 52, 11.

Kurucz, R.L., 1969. Astrophys. J., 156, 235.

Kurucz, R.L., 1970. A complete Program for Calculating Model Stellar Atmospheres, Smithsonian Astrophys. Obs. Sp. R., 309.

Kurucz, R.L., 1973. Semi-empirical calculation of gf values, Smithsonian Astrophys. Obs. Sp. R., 351.

Kurucz, R.L., 1974a. Astrophys. J., 188, L21.

Kurucz, R.L., 1974b. Smithsonian Astrophys. Obs. Preprint, 234.

Kurucz, R.L., 1974c. Solar Phys., 34, 17.

Kurucz, R.L., 1974d. Semi-empirical calculation of gf values, Smithsonian Astrophys. Obs. Sp. R., 359.

Kurucz, R.L., Peytremann, E. & Avrett, E.H., 1974. Blanketed Model Atmospheres of Early-Type Stars, Smithsonian Institution, Washington, D.C.

Kurucz, R.L. & Peytremann, E., 1975. Tables of semi-empirical gf values, Vols. I, II, III, Smithsonian Astrophys. Obs. Sp. R., 362.

Kurucz, R.L., Private communication: 1976.

Laget, M., 1972. NASA Sp. R., 310, p. 283.

Lambert, D.L. & Pagel, B.E., 1968. Mon. Not. R. astr. Soc., 141, 299.

Lang, K.R., 1974. Astrophysical Formulae, Springer Verlag, Berlin - Heidelberg - New York.

Learner, R.C.M., 1972. ESO/CERN conference on Auxiliary Instruments for Large Telescopes, Ed. S. Laustsen & A. Reiz, p. 131.

Lesh, J.R., 1976. Astrophys. J., 208, 135.

Livingston, W.C., 1973. A. Rev. Astron. Astrophys., 11, 95.

Meaburn, J., 1970. Astrophys. Space Sci., 9, 206.

Menzel, D.H. & Pekeris, C.L., 1935. Mon. Not. R. astr. Soc., 96, 77.

Mihalas, D.M., 1964. Astrophys. J. Suppl., 9, 321.

Mihalas, D.M. & Morton, D.C., 1965. Astrophys. J., 142, 253.

Mihalas, D.M., 1965. Astrophys. J., 141, 564.

" " 1966. Astrophys. J. Suppl., 13, 1.

" " 1967a. " " 149, 169.

" " 1967b. " " 150, 909.

" " 1968. " " 153, 317.

Mihalas, D.M. & Stone, M.E., 1968. Astrophys. J., 151, 293.

Mihalas, D.M., 1969. Astrophys. J., 157, 1363.

" " 1970a. Astrophys. Space Sci., 8, 50.

" " 1970b. Stellar Atmospheres, Freeman Company, San Francisco.

Mihalas, D.M. & Auer, L.H., 1970a. Astrophys. J., 160, 1161.

Mihalas, D.M. & Auer, L.H., 1970b. Astrophys. J., 161, 1129.

Mihalas, D.M., Pagel, B. & Souffrin, P., 1971. Théorie des atmosphères stellaires, Ed. Observatoire de Genève 1920, Suisse.

Mihalas, D.M., 1972. Astrophys. J., 176, 139.

Mihalas, D.M., 1973. Sky Telesc., 46, 79.

Mihalas, D.M. & Athay, G.R., 1973. A. Rev. Astron. Astrophys., 11, 187.

Mihalas, D.M., 1974. Astrophys. J., 79, 1114.

Mihalas, D.M. & Hummer, D.G., 1974. Astrophys. J. Suppl., 28, 343.

Mitchell, R.I. & Johnson, H.L., 1969. Comm. lunar planet. Lab., 8, 1.

Morton, D.C. & Adams, T.F., 1968. Astrophys. J., 151, 611.

Morton, D.M., 1969. Theory and Observations of Normal Stellar Atmospheres, Ed. Owen Gingerich, M.I.T. Press, p. 253.

Nandy, K., 1966. Publ. R. Obs. Edinb., 5, 233.

Nandy, K., Thompson, G.I. & Humphries, C.M., 1974. Mon. Not. R. astr. Soc., 166, 297.

Nandy, K., Napier, W.McD. & Thompson, G.I., 1975a. Mon. Not. R. astr. Soc., 171, 259.

Nandy, K. & Schmidt, E.G., 1975b. Astrophys. J., 198, 119.

Nandy. K., Thompson, G.I., Jamar, C., Monfils, A. & Wilson, R., 1975c. Astron. Astrophys., 51, 63.

Nandy, K. & Kontizas, E., 1976a. Proc. IIIrd European Astronomical Meeting, Tbilisi, 1975, p. 82.

Nandy, K., Thompson, G.I., Jamar, C., Monfils, A. & Wilson, R., 1976b. Astron. Astrophys., 51, 63.

Nandy, K., 1976c. Highlights of Astronomy, I.A.U., XVIth General Assembly, Vol. 4, part II, 293.

Newall, H.F., 1896. Mon. Not. R. astr. Soc., 56, 98.

Novotny, E., 1973. Introduction to Stellar Atmospheres and Interiors, Oxford University Press.

Oke, J.B., 1964. Astrophys. J., 140, 689.

Oke, J.B. & Schild, R.E., 1970. Astrophys. J., 161, 1015.

Oliver, J.P., 1975. Publ. astron. Soc. Pacific, 87, 217.

Osmer, P.S. & Peterson, D.M., 1974. Astrophys. J., 187, 117.

Palmer, D.R & Gietzen, J.W., 1972. ESO/CERN Conference on Auxiliary Instruments for Large Telescopes, Ed. S. Laustsen & A. Reiz, p. 111.

Palmer, E., Hatley, M., Franks, A., Verrill, J. & Cale, B., 1975. Reports Progr. Phys., 38, 975.

Papathanasoglou, D., Deligiannis, J. & Kontizas, E., 1976. Observatory, 96, 158.

Pecker, J.C., 1965. A. Rev. Astron. Astrophys., 3, 135.

Peterson, D.M., 1969. Smithsonian Astrophys. Obs. Sp. R., 293.

Peterson, D.M., 1969. Theory and Observation of Normal Stellar Atmospheres, Ed. Owen Gingerich, M.I.T. Press, p. 137.

Peytrémann, E., 1970. Ph.D. Thesis, Universite de Genève.

Peytremann, E., 1972. Astron. Astrophys., 17, 76.

Peytremann, E., 1974. Astron. Astrophys., 33, 203.

Peytremann, E., 1974. Astron. Astrophys. Suppl., 18, 81.

Pottasch, S.R., Wesselius, P.R., Wu, C.-C. & van Duinen, R.J., 1977. Astron. Astrophys., 54, 442.

Purkins, T.E., 1972. UV Sky Scan experiment (S2/68) in TD-1A Satellite SRC.

Robinson, L.B. & Wampler, E.J., 1972. Publ. astron. Soc. Pacific, 84, 161.

Samson, J.A.R., 1967. Ultraviolet Spectroscopy Techniques of Vacuum, John Wiley & Sons Inc.

Schalén, C., 1975. Astron. Astrophys., 42, 251.

Schild, R.E., Peterson, D.M. & Oke, J.B., 1971. Astrophys. J., 166, 95.

Schild, R.E., 1977. Astron. J., 82, 337.

Schroeder, D.J., 1972. ESO/CERN Conference on Auxiliary Instruments for Large Telescopes, Ed. S. Laustsen & A. Reiz, p. 119.

Smith, M. & Strom, S.E., 1969. Astrophys. J., 158, 1161.

Smyth, M.J., 1973. Astrophysics III, Edinburgh University. (lecture notes).

Snijders, M.A.J. & Lamers, H.J.G., 1975. Astron. Astrophys., 41, 245.

Stalio, R., 1971. Proc. Third Colloquium on Astrophysics, Supergiant Stars, Ed. M. Hack, Trieste, 1971, p. 28.

Stecher, T.P., 1965. Astrophys. J., 142, 1683.

Stecher, T.P., 1969. Astrophys. J., 157, L125.

Stecher, T.P., 1970. Astrophys. J., 159, 543.

Stibbs, D.W.N., 1968. Astrophys. J., 168, 155.

Stilly, J.L. & Callaway, J., 1970. Astrophys. J., 160, 245.

Stothers, R., 1976. Astrophys. J., 209, 800.

Strom, S.E. & Avrett, E.M., 1965. Astrophys. J. Suppl., 12, 1.

Strom, S.E. & Kalcofen, W., 1967. Astrophys. J., 149, 191.

Strom, S.E. & Kurucz, R.L., 1966. Journ. Quart. Spectrosc. Rad. Transfer, Vol. 9, p. 591.

Strom, S.E., 1969. Theory and Observation of Normal Stellar Atmospheres, Ed. Owen Gingerich, M.I.T. Press, p. 99.

Tarafdar, S.P. & Vardya, M.S., 1973. Mon. Not. R. astr. Soc., 163, 35p.

Thompson, G.I., Humphries, C.M. & Nandy, K., 1974. Astrophys. J., 187, L81.

Travis, L.D. & Matsushima, S., 1968. Astrophys. J., 154, 689.

Turner, D.J., 1976. Astron. J., 81, 1125.

Underhill, A.B., 1966. Utrechtse Sterrekundige-Overdrukken, No. 19.

Underhill, A.B., 1966. The Early Type Stars, Astrophys. Space Science Libr., Vol. 6, D. Reidel Publishing Company, Dordrecht, Holland.

Underhill, A.B., 1969. Theory and Observation of Normal Stellar Atmospheres, Ed. Owen Gingerich, M.I.T. Press, P. 207.

Underhill, A.B., 1972. NASA SP-310, p. 367.

Underhill, A.B., Leckrone, D.S. & West, D.K., 1972. Astrophys. J., 171, 63.

Underhill, A.B., 1973. Stellar Chromospheres, I.A.U. Colloquium, Ed. S.D. Jordan & E.H. Avrett (NASA SP-317), p. 128.

Underhill, A.B., 1977. Discussion of paper by Henize et al. in Highlights of Astronomy, 4, pt.II, 315.

Unsöld, A., 1969. The New Cosmos, Longmans Springer Verlag, New York.

Van Citters, G.W. & Morton, D.C., 1970. Astrophys. J., 161, 695.

Van de Heuvel, E.P.J., 1965. Observatory, 85, 241.

Walker, A.R., 1976. Mon. Not. R. astr. Soc., 174, 555.

Wayne, G., Van Citters, G.W. & Morton, D.C., 1970. Astrophys. J., 161, 695.

Westerlund, B., 1957. Publ. Dom. Astrophys. Obs., 10, 425.

Whittet, D.C.B., 1977. Mon. Not. R. astr. Soc., 180, 29.

Wickramasinghe, N.C. & Nandy, K., 1972. Report Progress Phys., 35, 157.

Wickramasinghe, N.C. & Nandy, K., 1974. Astrophys. Space Sci., 26, 123.

Willis, A.J. & Wilson, R., 1975. Astron. Astrophys., 415, 205.

Wilson, R., 1964. Publ. Royal Obs. Edinb., 4, 67.

Wilson, R., Gardier, S., Jamar, C., Macau, J.P., Malaise, D., Monfils, A., Butler, H.E., Humphries, C.M., Nandy, K., Thompson, G.I., Barker, P.J., Wroe, H., Houziaux, L. & Boksenberg, A., 1972. Nature Phys. Sci., 238, 34.

Wilson, R.N. & Opitz, A., 1972. ESO/CERN Conference on Auxiliary Instruments for Large Telescopes, Ed. S. Laustsen & A. Reiz, p. 149.

Willstrop, R.W., 1965/66. Mem. R. astr. Soc., 69, 83.

Withbroe, G.L., 1971. Atomic Spectra and Gaseous Nebulae, Ed. by K.B. Gebbie, Nat. Bur. Standards Spec. Publ. 353 pp.

Wood, H.J., 1972. Auxiliary Instruments for Large Telescopes, Ed. S. Laustsen, A. Reiz, 165 pp.

Wood, H.J. & Albrecht, R., 1974. Astron. Astrophys., 34, 81.

Woolley, R.R. & Stibbs, D.W.N., 1953. The Outer Layers of a Star, Oxford at the Clarendon Press, London.

Wright, K.O., 1975. J. Roy. astron. Soc. Canada, 69, 265.

York, D.G., 1976. Transactions of the I.A.U., Vol. XVIA, p.123.